AD-A042 979 SHEFFIELD UNIV (ENGLAND) DEPT OF CHEMICAL ENGINEERIN--ETC F/G 21/2
POLLUTANT MINIMISATION BY BLUE FLAME STAGED COMBUSTION.(U)
1977 D S PRIOR AF-AFOSR-2682-74
UNCLASSIFIED AFOSR-TR-77-0843 NL

(1)

POLLUTANT MINIMISATION BY

BLUE FLAME STAGED

COMBUSTION.

AFOSR-TR- 77-0843

NOMENCLATURE

- SI Units, except where stated -

REPORT DOCUMENTATION PAGE

READ INSTRUCTIONS BEFORE COMPLETING FORM

1. REPORT NUMBER: AFOSR-TR-77-0843	2. GOVT ACCESSION NO.
3. RECIPIENT'S CATALOG NUMBER	
4. TITLE (and Subtitle): POLLUTANT MINIMISATION BY BLUE FLAME STAGED COMBUSTION,	5. TYPE OF REPORT & PERIOD COVERED: INTERIM rept.
6. PERFORMING ORG. REPORT NUMBER	
7. AUTHOR(s): DEREK S. PRIOR	8. CONTRACT OR GRANT NUMBER(s): AFOSR 74-2682
9. PERFORMING ORGANIZATION NAME AND ADDRESS: UNIVERSITY OF SHEFFIELD, CHEMICAL ENGINEERING & FUEL TECHNOLOGY DEPT, SHEFFIELD S1 3JD. ENGLAND	10. PROGRAM ELEMENT, PROJECT, TASK AREA & WORK UNIT NUMBERS: 2308A2, 61102F
11. CONTROLLING OFFICE NAME AND ADDRESS: AIR FORCE OFFICE OF SCIENTIFIC RESEARCH/NA, BLDG 410, BOLLING AIR FORCE BASE, D C 20332	12. REPORT DATE: 1977
	13. NUMBER OF PAGES: 215
14. MONITORING AGENCY NAME & ADDRESS (if different from Controlling Office): AF-AFOSR-2682-74	15. SECURITY CLASS. (of this report): UNCLASSIFIED
	15a. DECLASSIFICATION/DOWNGRADING SCHEDULE

16. DISTRIBUTION STATEMENT (of this Report)

2306 A2 18 p.

Approved for public release; distribution unlimited.

17. DISTRIBUTION STATEMENT (of the abstract entered in Block 20, if different from Report)

18. SUPPLEMENTARY NOTES

19. KEY WORDS (Continue on reverse side if necessary and identify by block number)

COMBUSTION
EVAPORATION
MATHEMATICAL MODELLING
STIRRED REACTORS
FUEL SPRAYS
CHEMICAL KINETICS

20. ABSTRACT (Continue on reverse side if necessary and identify by block number)

A general analysis for a steady state heterogeneous Well Stirred Reactor (WSR) is presented in which fuel evaporation, turbulent mixing and finite rate chemical kinetics are treated. A mathematical model for the BFB featuring a 17 step quasi global reaction mechanism, recirculation and a reactor network containing 2 WSR's is thus derived; a general modular computer program suitable for parametric evaluations was developed to facilitate this type of modelling. Convergence of the model solution scheme could be obtained for fuel lean and stoichiometric conditions only. Reasonably good agreement between measured and predicted values of BFB exit flow temperature, NO and CO pollutant emissions is apparent.

DD FORM 1 JAN 73 1473 EDITION OF 1 NOV 65 IS OBSOLETE

UNCLASSIFIED 400 047

Contract/Grant Number AFOSR - 74 - 2682

POLLUTANT MINIMISATION BY BLUE FLAME STAGED COMBUSTION.

DEREK S. PRIOR,

DEPARTMENT OF CHEMICAL ENGINEERING & FUEL TECHNOLOGY,

UNIVERSITY OF SHEFFIELD

SHEFFIELD S1 3JD

ENGLAND.

1977

INTERIM SCIENTIFIC REPORT.

Approved for public release;
distribution unlimited.

Prepared for

EUROPEAN OFFICE OF AEROSPACE RESEARCH AND DEVELOPMENT, LONDON ENGLAND.

and

AIRFORCE OFFICE OF SCIENTIFIC RESEARCH. BOLLING AIR FORCE,
WASHINGTON D.C. USA.

Approved for public release;
distribution unlimited.

AIR FORCE OFFICE OF SCIENTIFIC RESEARCH (AFSC)
NOTICE OF TRANSMITTAL TO DDC
This technical report has been reviewed and is approved for public release IAW AFR 190-12 (7b).
Distribution is unlimited.
A. D. BLOSE
Technical Information Officer

FRONTISPIECE BLUE FLAME BURNER OPERATION

Fuel lean, $\phi_{ov} \simeq 0.7$

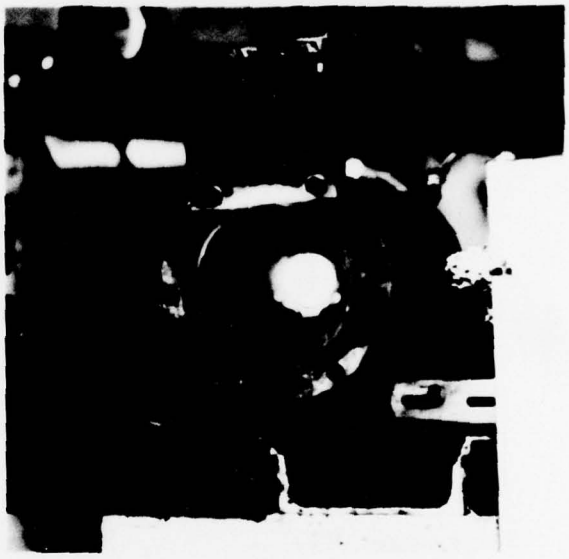

Stoichiometric, $\phi_{ov} \simeq 1.0$

Fuel rich, $\phi_{ov} \simeq 1.5$

SUMMARY

After discussing the fundamental processes which constitute liquid fuel (heterogeneous) combustion a number of techniques for the suppression of combustion generated air pollution are reviewed. In accordance with the need for new combustor concepts which is identified, a laboratory scale Blue Flame Burner (BFB) was designed and constructed which utilises a Coanda ejector to generate the internal recirculation of flame products to the spray formation region. Blue flame (soot free) conditions prevail in which the droplet wake mode of combustion is obtained. Experimental testing reveals that NO emissions for this device are very low under fuel rich conditions. Such operation of the BFB as the initial stage of a two stage configuration which uses interstage heat removal to inhibit further temperature rise should control NO emissions and burn out the CO and hydrocarbons formed in the first stage. Conceivable applications for this type of configuration could lie in the small to intermediate sized boiler range.

A general analysis for a steady state heterogeneous Well Stirred Reactor (WSR) is presented in which fuel evaporation, turbulent mixing and finite rate chemical kinetics are treated. A mathematical model for the BFB featuring a 17 step quasi global reaction mechanism, recirculation and a reactor network containing 2 WSR's is thus derived; a general modular computer program suitable for parametric evaluations was developed to facilitate this type of modelling. Convergence of the model solution scheme could be obtained for fuel lean and stoichiometric conditions only. Reasonably good agreement between measured and predicted values of BFB exit flow temperature, NO and CO pollutant emissions is apparent.

An on-line digital computer technique for autocorrelating hot wire anemometer signals to measure turbulence length scales is described, a method of correcting such data for the system time resolution error is also supplied.

ACKNOWLEDGEMENTS

The author would like to especially thank Professor J. Swithenbank for his stimulating supervision of this research project, and to acknowledge the financial support of the Science Research Council and USAF. In addition Dr. G.L. Wells is thanked for supplying the computer program PRIMER, from which development of program GRASP was possible; Phil. Felton is also thanked for co-development of the latter and for many helpful discussions.

The technicians at Buxton; Tony Jackson, John Collins, Jim French and Arthur Howe were most helpful in constructing experimental equipment and providing encouragement. Finally, grateful thanks to Mrs. Czerny for typing the thesis and to Dick and Mike for producing the photographs.

CONTENTS

List of Figures, Tables and Plates.

FIGURES (After Appendices)

FIGURES

FIGURES

NOMENCLATURE

- SI Units, except where stated -

(Note. The use of the same symbol to represent more than one variable was unavoidable.)

$< >$	Denotes the measured value of a correlation parameter.
a	Polynomial coefficient.
A	Area ; hot wire probe calibration constant (Ch.5.).
A_j	Pre-exponential coefficient (Arrhenius factor) in the jth reaction rate constant (cgs).
b_j	Back reaction rate constant of the jth reaction (cgs).
b_x	Cut-off frequency, angular.
B_{ev}	Evaporation transfer number, blue flame conditions.
B_j	Back reaction rate of the jth reaction (cgs).
c_i	Overall gaseous phase concentration of species i (eg gm/gm).
c_p	Gaseous phase specific heat.
c_B	$= C_p$ evaluated at region B conditions.
C_D	Droplet drag coefficient.
C_v	Discharge coefficient.
d_{ij}	Third body efficiency of species i in the jth reaction.
d_o	Atomiser orifice diameter.
D	Droplet diameter ; diffusivity.
E	Error (Ch.5.).
$E(k,t)$	Energy spectrum.
E_j	Activation energy in the jth reaction rate constant (cgs)
f	Frequency, cyclical.
f_j	Forward reaction rate constant of the jth reaction (cgs).
F_j	Forward reaction rate of the jth reaction (cgs).
F	Atomiser fuel flow number (imp).
FE	Total mass of fuel evaporated in a WSR (cgs).
$\dot{FE}$	Mean rate of fuel evaporation in a WSR (cgs).
F_i^o	Standard molar free energy change of species i (cgs).

ΔF_j	Change in free energy in the jth reaction (cgs).
F_v	View factor.
$F[\ ]$	Denotes a Fourier Transform.
g	Acceleration due to gravity.
G	Transfer function.
h	Manometer reading (imp).
h_i	Specific enthalpy of species i (cgs).
H_T	Specific enthalpy (cgs).
$\dot{H}_L$	Rate of enthalpy loss from a WSR(cgs).
i	Stoichiometric fuel/air mass ratio (Ch.4); base of complex number system (Ch.6).
k	Pressure jet atomiser correlation parameter; wavenumber (Ch.2).
$\hat{K}$	Correlation correction parameter.
K_j	Equilibrium constant for the jth reaction.
K_j^P	Equilibrium constant for the jth reaction, pressure units.
L, ℓ	Distance.
m	WSR gaseous phase mass (cgs).
$\dot{m}$	Gaseous phase mass flowrate (cgs).
$\dot{m}_E$	Mass evaporation rate (cgs).
$\dot{m}_{FUEL}$	Atomiser fuel mass flowrate (imp).
M	Spray size mass fraction (Ch.2).
MT	Total number of mixed gaseous phase species.
MV	Thermocouple emf, millivolts.
n	Rosin Rammler exponent; eddy frequency (Ch.2).
n_j	Temperature exponent in the jth reaction rate constant.
n_t	Total number of drops of size D in a spray.
Nu	Nusselt number.
NR	Number of chemical reactions.
NT	Total number of gaseous phase species.
p	Partial pressure.

$\dot{p}$	Rate of production/destruction of species i due to chemical reaction (cgs).
P	Total pressure.
P_f	Atomiser fuel injection pressure (psig).
ΔP	Combustor (air) pressure drop.
ΔP_D	Differential pressure across baffle (imp, Ch.5).
Pr	Prandtl number.
PU	Volume %age of spray remaining unevaporated.
q	Dynamic head; heat of combustion of fuel.
$\dot{Q}$	Volumetric flowrate.
$\dot{Q}_{COND}$	Rate of conductive heat transfer.
$\dot{Q}_{RAD}$	Rate of radiative heat transfer.
r	Radius.
R	Universal gas constant (thermal units); Rosin Rammler volume % oversize.
$R(\tau)$	Correlation function.
R'	Universal gas constant (pressure/volume units, cgs).
Re	Reynolds number.
R_{int}	Combustor internal recirculation level, %.
S	Coanda slit width (imp).
ΔS	Sampling line vacuum (Ch.5).
SC	Rotameter scale reading (Ch.5).
t	Elapsed time.
T	Temperature; turbulence intensity, % (Ch.5).
T_L	Droplet surface temperature.
u'	Fluctuating velocity component.
U	Velocity.
V	Reactor volume (cgs); velocity; hot wire anemometer bridge voltage (Ch.5).
V_{Rel}	Relative velocity.
W	Molecular weight.

$\bar{x}$	Rosin Rammler size parameter.
X_j	Third body in a dissociation reaction j.
$X(f)$	Frequency response function.
$Y_{O_2,\infty}$	Weight fraction of oxygen in ambient gas.
z	Gamma function independent variable.

Greek

α	Correlation correction weighting function.
α_{ij}	Stoichiometric coefficient of species i as a product in reaction j.
δ_{ij}	Stoichiometric coefficient of species i as a reactant in reaction j.
$\delta( )$	Delta function (Ch.6).
$\Gamma( )$	Gamma function.
β	Dimensionless ratio.
τ	Time displacement ; turbulence timescale.
τ_s	Reactor mean residence time.
τ_D	Specific mixing (turbulence dissipation) time.
τ_{SD}	$= \tau_s/\tau_D$, mixing parameter.
ϕ_{ov}	Overall burner estimated equivalence ratio.
ϕ_u	Proportion of reactor or stream gaseous phase which is unmixed (gm/gm).
ψ	Coanda unit mass entrainment ratio.
η	Entrainment efficiency factor relating theoretical value of ψ to the measured value.
γ_i	Concentration of species i in the mixed gaseous phase (gm/gm).
ω_i	Concentration of species i in the unmixed gaseous phase (gm/gm).
ε	Reactor liquid phase mass (cgs).
$\dot{\varepsilon}$	Liquid phase mass flow rate (cgs).
ρ	Density.
$\rho(\tau)$	Normalised autocorrelation function.

μ	Viscosity.
σ	Stefan Boltzman constant.
σ_j	Index which is zero for 1st/2nd order and unity for 3rd order reactions.
λ	Mean thermal conductivity of gaseous phase; skewness factor (Ch.4/5); turbulence length scale (Ch.6).
Δ	Increment.

Superscripts

'	Denotes feed stream conditions.
"	Denotes Laser measured value.
*	Denotes WSR intermediate variable, i.e. after evaporation and mixing but before chemical reaction in the steady state analysis; complex conjugation (Ch.6).
o	Denotes a Standard State value.
-	Mean value.
(n)	nth Derivative.

Subscripts

1	Reactor inlet conditions.
2	Reactor exit conditions.
A	Region A property.
B	Region B property.
c	Critical conditions.
cs	General combustion species (other than f, O_2 or N_2).
f	Fuel vapour species.
F	Forced convection conditions.
G	Gaseous phase.
i	General species; Coanda inlet plane conditions (Ch.4,5).
I	Isokinetic sampling conditions.
j	General reaction number; Coanda slit (jet) conditions (Ch.4,5).
ℓ	General reactor.
L	Liquid phase.
mi	Microscale.
ma	Macroscale.

o	Coanda exit plane conditions.
x,xx,XX	Pertaining to autocorrelation.
∞	Ambient conditions.

Abbreviations.

BFB	Blue flame burner.
CLA	Chemiluminescent gas analyser.
ISD	Initial size distribution.
PFR	Plug flow reactor.
PSR	Perfectly stirred reactor.
RMS	Root mean square.
SMD	Sauter mean diameter.
NTP	Normal temperature and pressure.
WSR	Well stirred (partially stirred) reactor.
UHC	Unburned hydrocarbon.

CHAPTER 1.

INTRODUCTION

At the present time, approximately 80 - 90% of the various fuels employed in energy conversion processes are either of the liquid or solid type, this then explains why an increasing amount of combustion research is being directed at two phase flow systems. The minimisation of air pollution generated by practical liquid fuelled combustors constitutes the subject of this study, with the mathematical modelling of such devices from a pollution standpoint playing an important role.

The next Chapter introduces the subject more comprehensively and sets out broad objectives for this project, whilst Chapter 3 defines these objectives more fully in relation to a laboratory scale combustor. Chapter 4 provides the basic theory needed for the establishment of a model for this device, which is given in Chapter 7. Chapters 5 and 6 are concerned with various experimental measurements on the laboratory combustor and a comparison between model predictions and these measurements are made in Chapter 8. Conclusions drawn from the study, plus recommendations for future work, are finally discussed in Chapter 9.

CHAPTER 2.

HETEROGENEOUS COMBUSTION AND POLLUTION

2.1 Foreword.

Having briefly introduced the overall area of research with which this study is concerned it is convenient to identify three important aspects of two phase combustion; these are a) its actual mechanics, b) associated air pollution, and c) mathematical modelling. The function of this chapter is the introduction of each of these in greater depth, pertinent literature also being reviewed. As will be seen, much of this literature concerns the gas turbine device; this is due to the widespread attention which this combustor has received in response to increasingly demanding design requirements.

2.2 The Combustion Process.

At this stage it is convenient to distinguish between homogeneous and heterogeneous combustion with respect to this study. The former denotes combustion of gaseous i.e. single-phase reactants whilst the latter is defined as two phase combustion between gaseous phase oxidant and liquid phase fuel. The exact mechanism of such heterogeneous combustion is naturally extremely complex, involving simultaneous heat, mass and momentum transfer throughout chemically reacting, two-phase, three-dimensional flow fields which in addition are invariably highly turbulent. It is then, perhaps not too surprising that relatively little work has been done on the subject, even though combustion research has intrigued and captivated scientists for more than 5000 years.

In any combustion process fuel and oxidant (usually air) are mixed together on a molecular scale, they then react to liberate some of the chemical energy of the fuel as heat; this thermal energy is then either employed directly, or converted to a third type before being exploited to do some sort of work. In the case of carbonaceous fuels soots are formed by the chemical reaction under some conditions, in addition a broad spectrum of hundreds of gaseous species may be

formed as combustion products, depending on fuel molecular weight and again prevailing conditions.

Liquid fuels then have to be vapourised into the gaseous phase and intimately mixed with the oxidant before homogeneous chemical decomposition via numerous possible reactions, which constitute the flame phenomenon, can ensue. Now such a fuel may either be completely evaporated and subsequently mixed with oxidant in a predetermined proportion before reaching the flame reaction zone, alternatively the two components may be injected separately into the flame, fuel being admitted via an atomising device. Evaporation, mixing and chemical reaction then proceed simultaneously, although sequentially, in this case. The first type of flame is referred to as premixed and the second, as a diffusion flame, since the overall combustion rate is controlled by diffusion i.e. a mixing process. Practical flames are usually of the latter type although combinations of the two do arise.

Reactants are fed to and combustion occurs within a constraining combustion chamber, throughout which spatial variations of local species velocities, concentrations and temperatures completely characterise the combustion; these variables are largely determined by the prevalent flow pattern, which is usually a strong function of operating conditions and combustor geometry.

The flow pattern may be characteristically, 1-, 2- or 3-dimensional with corresponding increasing complexity from a fluid mechanics point of view, an additional aerodynamic complexity is provided by the fact that practical combustor flows encountered are invariably highly turbulent. An excellent introduction to turbulence theory is provided by Hinze (1) and the subject will be further discussed in 2.2(c).

The governing fluid mechanics relations for any flow pattern are the Navier Stokes equations which are analytically relatively simple but conversely extremely difficult to solve, due to their non-linearity, even without including chemical reaction and two phase effects. Hence comparatively few solutions have been obtained for these equations. Species mixing rates throughout the flowfield of a combustor operating at fixed volume and pressure, predominantly depend on local

transport properties which are a function largely of local velocities and temperatures, species chemical reaction rates though are mainly sensitive to local concentrations and temperatures.

Fig.2.1 (after Poll (2)) is included at this point to illustrate the interrelation between the principal physical and chemical processes occurring throughout a heterogeneous combusting flow field. Major links between two processes are represented by double lines and the flow is considered to be subsonic, i.e. no direct influence of bulk flow on the gas phase temperature. The diagram again shows the complexity of two phase combustion, it should be emphasised that it represents a simplification of the overall process but certain major interactions are evident. The four important processes of atomisation, evaporation, mixing and chemical reaction will now be treated separately in more detail.

2.2(a) Atomisation.

For two phase diffusion flames, the first process which must be achieved is that of fuel atomisation. Before evaporation can proceed the liquid fuel must be injected into the combustor via an atomising device and rapidly disintegrated into a spray of preferably very small droplets; the resulting drops are then projected and dispersed - usually in a preferred direction. A spray of very fine droplets burns in much the same way as a gaseous fuel so that local fuel/air distributions can be controlled relatively easily, in practice a cloud of thousands of droplets is formed whose size varies widely and may lie in the range 1 - 500 microns. The drops produced in the immediate vicinity of the atomiser are collectively referred to as the "initial spray" and their size diminishes in flight. Droplets are virtually always assumed to be of the same shape, i.e. spherical.

Atomisers are continuously supplied with liquid fuel and liquid disintegration usually occurs in stages, each stage is essentially a vibratory process so that the cloud of droplets enters the flame intermittently. For most atomisers a liquid sheet of decreasing thickness extends from the atomiser until the sheet thickness is of the order of the largest drop size, unstable threads of liquid may also be

formed as part of the sheet. The drops by themselves may be unstable, i.e. they may shatter or coalesce, the instability of sheets and drops is discussed by Eisenklam (3) but as yet no information exists concerning the possible effect of gaseous phase turbulence on such instabilities. It appears that the relative velocity between the droplet and gaseous phase is one of the more important variables affecting the existence of shatter or coalescence. Surface tension forces within the drop tend to resist the deformation which results from the influence of external dynamic forces. The actual balance of these forces is influenced by the liquid viscosity, surface tension and density and this explains the influence of fuel physical properties on the atomisation process. The gaseous phase flow pattern in the atomiser vicinity can also be appreciated as having a considerable effect on this force balance.

The principal characteristic of any atomiser is the initial droplet size distribution produced, this is invariably a function of the atomiser type and size, as well as the pressure differential experienced by the fluid, (or fluids in the case of a multi fluid atomizer). This characteristic is extremely important since, coupled with: i) droplet location, ii) vapourisation rates and iii) mixing rates, it determines combustor fuel/air distributions which significantly affect the overall system performance and stability limits. There are five average or mean diameters which may be calculated for a spray with a known drop size distribution, these are:

1) Average Diameter $= \sum n_t D / n_t$ ..... (2.1)

2) Mean Diameter $= \sum n_t D^2 / \sum n_t D$ ..... (2.2)

3) Mean Volume Diameter $= \left(\sum n_t D^3 / \sum n_t \right)^{1/3}$ ..... (2.3)

4) Mean Surface Diameter $= \left(\sum n_t D^3 / \sum n_t D^2 \right)^{1/2}$ .... (2.4)

5) Sauter Mean Diameter $= \sum n_t D^3 / \sum n_t D^2$ ..... (2.5)

The most frequently used mean size is the Sauter Mean Diameter (SMD) because of its importance in mass transfer calculations; a droplet with diameter equal to the SMD has the same surface area to volume ratio as the entire spray. Various empirical correlations have been developed for prediction of a mean diameter for specific atomising devices, because of the number of variables influencing such expressions they are naturally expensive to determine and highly specific as already mentioned. Extensive use of droplet means for representing entire sprays has been made by combustion researchers, however, the practice is considered extremely inaccurate due to (i) the two orders of magnitude of drop size which are possible, (ii) the fact that small droplets behave in a very different way to large droplets in a combustor environment (iii) there being no indication of the distribution of drop sizes.

A number of mathematical functions have been developed for describing size distributions in order to incorporate droplet spray effects into heterogeneous combustion models. Mugele and Evans (4) have discussed a number of such distribution functions of which the Rosin-Rammler (5) expression was one of the earliest, it was originally developed for application to powdered materials, in cumulative volume form this function is:

$$R = 100\, e^{-(x/\bar{x})^n} \qquad \ldots\ldots\ldots \qquad (2.6)$$

where R = percentage of spray by volume whose diameter is greater than a given diameter x.

x = droplet diameter, microns.

$\bar{x}$ = a size parameter, microns.

n = an exponent which is a distribution parameter.

It can be seen that this distribution function has two fit parameters. Mugele and Evans also describe the Nukiyama and Tanasawa, Log Probability and Upper Limit distribution functions. The Upper Limit expression utilises a third fit parameter to provide a cut-off at the spray maximum drop size present, it is based on the differential equation of the Normal or Gaussian distribution.

Atomisers can conveniently be classified according to the primary source of energy which is employed to obtain liquid disintegration, a brief description of

various devices is now presented. Relations applicable to each device are also included.

The Pressure Jet Atomiser utilises fuel pressure energy for sheet disintegration to usually produce a conical spray; liquid fuel is tangentially injected into a conical chamber upstream of the exit orifice so that a swirling spray motion is induced. An example is shown diagrammatically in Fig.2.2(i). The spray may be hollow and have an appreciable cone angle within which contacting with a recirculating gas flow may be achieved. Alternatively the conical spray may be of the narrow angle type and have no real gaseous core. The pressure jet atomiser was one of the earliest fuel injection devices to be developed and usually produces a wide distribution of drop sizes, this is an inherent disadvantage from a combustion performance standpoint if significant numbers of large drops are formed.

The basic single orifice pressure jet atomiser design is frequently referred to as a simplex type, modification to this basic design in the form of spill, duplex, variable port and multiple orifice varieties have also been made for handling larger fuel flow ranges. From the equation of conservation of energy it follows that, over a wide range of pressures, the liquid flow rate is proportional to the square root of the pressure drop across the atomiser; the proportionality has been termed "Flow Number" and is usually given in dimensionally inconsistent units:

$$\text{Flow Number} = F = \frac{\text{Flow-rate (gallons per hour)}}{\sqrt{\text{Pressure differential across orifice (psi)}}} \quad \ldots\ldots \quad (2.7$$

$$= \frac{\text{Flow-rate (gallons per hour)}}{\sqrt{P_f}}$$

for an atomiser injecting fuel at P_f psi into a combustion chamber operating at atmospheric pressure. High injection pressures generally produce small droplets although little effect on drop size is observed as P_f is increased above about 200 psi.

Bowen and Joyce (6) obtained a convenient set of empirical correlations for the pressure jet atomiser which predict the two Rosin Rammler fit parameters as a function of P_f for $0.5 \leq F \leq 4.0$ gals/hr$(\text{psi})^{\frac{1}{2}}$. They were obtained by the so-called "substitute method" whereby the fuel properties are simulated by wax which is sprayed

as a liquid and solidifies in transit through a cool atmosphere. The particulate end product can then be conveniently analysed for size by sieving. The correlations derived are discussed in 4.3. Watkins (7) formulated an expression for calculating SMD that is applicable to both simplex and dual orifice nozzles:

$$SMD = \frac{490\ N^{0.215}}{\bar{p}^{0.442}} \left(\frac{W_f}{\rho_L} \right)^{0.209} \quad \ldots\ldots\ldots \quad (2.8)$$

where, W_f = total fuel flowrate, lb/hr.

ρ_L = density, lb/ft^3.

N = kinematic viscosity, centistokes.

$\bar{p}$ = mass weighted pressure differential, psid

$$= \left(\frac{W_{f\ pri}\sqrt{\Delta P_{pri}} + W_{f\ sec}\sqrt{\Delta P_{sec}}}{W_f} \right)^2$$

For pressure jet atomisers an expression for V, the initial velocity with which the drops are projected into the flame from the atomiser sheet, is included in the interests of completeness:

$$V = C_v \left(\frac{2g\ P_f}{\rho_L} \right)^{\frac{1}{2}} \quad \ldots\ldots\ldots \quad (2.9)$$

This crude expression assumes that all droplets have the same initial velocity and that the sheet velocity is constant in the direction of flow. The discharge coefficient C_v in practice is not a constant but a function of exit orifice diameter and P_f. At present no refinements to this method exist which can account for three dimensional and gaseous phase turbulence effects. However, it is possible to compute droplet trajectories for two-dimensional flows, Fig.2.3 shows the results of one such set of calculations (due to Mellor (12)) for a range of drop sizes.

The Rotary Atomiser invariably consists of a spinning cup into which the liquid is introduced on the inside surface near the axis, this results in a liquid sheet flowing inside the cup and leaving at the periphary. The centrifugal energy

thus imparted to the fluid is exploited to shatter the sheet, it can be shown (3) that it is essential for the operating conditions to be such that the fluid at the rim of the cup is in the form of a sheet (not as threads), in order to ensure fine atomisation. Macfarlane (8) presents characteristics for an atomiser of this type.

Twin Fluid Atomisers make use of a secondary fluid, e.g. steam or part of the combustion air, to impinge on the liquid sheet in order to employ the secondary fluid kinetic energy for:

a) promoting disintegration

b) controlling the spray angle

c) cooling and cleaning the injector.

The point of impingement may be either within or external to the atomiser, Fig.2.2(ii) portrays an example of the latter type. Secondary fluid may be introduced at low, medium or high pressure but an optimum flowrate in terms of atomisation efficiency exists. This class of atomiser has become widely favoured due to the fact that it is capable of producing inherently fine sprays. Felton and Swithenbank (9) have examined the characteristics of an air-blast atomiser with respect to gas turbine stability. Steam may also be usefully employed as a secondary fluid. Design of twin fluid atomisers also follows empirical lines since little is known of the aerodynamic behaviour of gas streams as they impact on mobile liquid surfaces. A typical expression for calculating spray SMD for an air blast atomiser is (7):

$$SMD = \frac{27779\ N^{0.215}}{\rho_L^{0.651}} \left(\frac{W_f^{0.209}}{\bar{V}^{0.884}} \right) \quad \ldots\ldots\ldots \quad (2.10)$$

where,

$$\bar{V} = \frac{W_a V_a}{W_a + W_f}$$

W_a = air flowrate, lb/hr.

V_a = air velocity, ft/sec.

An alternative more complicated expression for an internal impingement air blast design is given by Eisenklam (3), see also Hunter et al (10). It is important to

stress the fact that these correlations apply for specific atomiser geometries, further, no such correlations exist at present which enable prediction of size distribution data.

Other types of atomiser which may be used in combustion systems include Ultrasonic and Hartmann whistle devices, these exploit vibration and acoustic effects respectively. Fig.2.2(iii) shows an ultrasonic design in which a piezo-electric crystal is electrically excited to oscillate at 40 kHz in order to shatter fuel into small drops. A "jet whistle" device is shown in Fig.2.2(iv), a small convergent-divergent nozzle is featured, this accelerates a central air stream to supersonic speeds ($M \simeq 1.5$). A standing shock wave is thus induced when the flow impinges on an integral bluff body located at a distance $\lambda/4$ (λ = wavelength of flow oscillations) from the nozzle. The fuel is therefore forced to flow through very large velocity gradients across the shock wave and an extremely fine spray (mean diameter $\simeq$ 10-20μ) is formed. Fig.2.2(iv) shows the direction in which the atomised fuel leaves this twin fluid type atomiser, it is important to ensure that the spray droplets do not contact the combustor walls or quenching difficulties may arise. Locklin and Bolt (94) describe other similar acoustic atomisers. Vapouriser tubes are sometimes employed instead of an atomiser, these produce fuel droplets plus a little fuel vapour partly premixed with air.

Very little work has been done on the evaluation of atomisation times under combustion conditions, they are generally accepted as being small and of the order of 0.1 milliseconds. The most important characteristic for any atomiser is the spray initial size distribution, actual measurement of this parameter is discussed in 5.7.

2.2(b) Evaporation.

Evaporation is the important heterogeneous combustion process describing mass-transfer from the liquid phase to the bulk gaseous phase. As stated previously the rate of transfer is directly proportional to the interfacial contact area so that, for a monosize spray, it has a maximum value for the smallest droplet diameter. Clearly high evaporation rates are required for either high intensity or complete combustion.

Fuel injected into a combustor is usually cold so that droplets must undergo heating until they reach their boiling point before they can be vapourised by supply of their latent heat of vapourisation. Hence, evaporation is essentially a transient heat-transfer controlled process. Prakash and Sirignano (11) suggest that through a droplet's lifetime a gas-phase laminar boundary layer exists which gives rise to a shear on the droplet surface, hence a liquid-phase viscous boundary layer exists, consequently recirculating motion within the droplet is induced. Calculations show that the characteristic time for recirculation is usually less than the droplet lifetime, but not by several orders of magnitude, so that this internal motion and convection of heat from the surface to the interior could very likely be the most important mechanism for droplet heating. For a multi-component fuel internal motion will then continually bring the more volatile fractions from the interior of the droplet to the vicinity of the surface, where they may diffuse to the actual surface and vapourise. The least volatile fractions will vapourise last, if the droplet residence time is insufficient to permit evaporation of these components then they will probably "crack" to form lower hydrocarbons or soots. High molecular weight multicomponent fuels are in fact more susceptible to such liquid phase decomposition reactions.

Very small droplets are rapidly heated and vapourised whereas the heating and vapourisation processes are far slower for larger drops, hence, for a spray of droplets in which a large range of droplets exists it can be appreciated that the net evaporation rate is largely controlled by the fraction present and vapourisation rate of the larger drops. Hence the proportion of fuel evaporated initially increases with time and later slows down, the spray mean drop size also increases during evaporation and overall combustion, even though all droplet diameters diminish with time.

In considering droplet trajectories under combustion conditions it is usual to assume that all droplets possess the same injection velocity for any given fuel atomiser. Mellor (12) concluded from his investigations of droplet velocities in a spray that not all droplets move with the same velocity, in fact the initial velocity of the droplets increases with diameter. At droplet sizes above about

100μ all droplets tend to move at the same velocity for any atomiser injection pressure. Hence, the error in assuming that all droplets possess the same initial velocity is likely to be small in view of the fact that the overall rate of evaporation from a spray is largely controlled by the larger drops. The momentum of larger drops is far greater than the smaller droplets and they usually continue on a trajectory relatively undeterred by the local gas flow but determined by the atomiser spray angle, on the other hand the smaller droplets follow the gas streamline more or less completely. It is interesting to note that for relatively non-luminous flames it is sometimes possible to actually observe the trajectories of the larger drops by shining a powerful light source into the spray zone. Eisenklam (3), Mellor (12) and Hunter et al (10) present details of droplet trajectory calculations for various sized droplets, see also Fig.2.3. Now local gas velocities $V_G(0)$ in the spray region depend primarily on the prevalent flow pattern and hence the combustor geometry. Clearly a relative velocity $V_{Rel}(t)$ exists between the gaseous phase and the evaporating droplets, which will rarely be constant but a function of distance from the fuel injector and hence a function of time. The initial relative velocity $V_{Rel}(0)$ between the gaseous flow and the liquid droplets may be expressed:

$$V_{Rel}(0) = V_G(0) - V_S(0) \quad \ldots\ldots\ldots \quad (2.11)$$

where $V_S(0)$ is the atomiser droplet velocity which, as previously explained, is assumed the same for all drops in the spray when they leave the fuel injector. This initial velocity is very dependent on the type of fuel injector and is naturally much greater for an air assist atomiser, for example, than a pressure jet atomiser. It is clear then that $V_{Rel}(0)$ can be positive or negative, depending on the atomiser/flow pattern configuration. $V_S(0)$ is also dependent on orifice size for the two types of atomiser just mentioned, and is reduced for small orifice diameter.

Since a relative velocity exists between the gas stream and each droplet, viscous drag forces exist which will either accelerate or retard the droplet depending on which of the two velocities is largest at any instant in time.

In a subsequent section it will be shown that the drag forces, which act to reduce the gas-droplet relative velocity, have a large influence on evaporation rate and are i) a function of Reynolds number ii) inversely proportional to droplet diameter. Hence, small droplets rapidly assume the local gas velocity whereas larger drops tend to retain their own velocity relative to the gas stream. Gaseous phase turbulent velocity fluctuations will clearly affect $V_{Rel}(t)$ also.

Having introduced the concept of relative velocity between the two phases it is now convenient to distinguish between the two modes of combustion possible for an evaporating fuel droplet in a typical combustor environment. These are a) droplet Diffusion flames and b) droplet Wake flames. Under completely stagnant conditions an evaporating spherical drop is concentrically surrounded by a fuel vapour film, this is bounded by a thin flame zone, where fuel vapour and oxidant combine, the vapour plus flame region being referred to as the Reaction Zone. This type of combustion is known as a Diffusion flame since the overall rate of combustion is diffusion controlled. If the relative velocity between the surrounding gaseous phase and the droplet is increased, as under natural convection conditions, the reaction zone distorts as shown in Fig.2.5(b). When V_{Rel} is increased further, as under forced convection conditions, distortion of the reaction zone increases, Fig.2.5(c), (d). Assuming $V_G > V_S$ then the reaction zone is now entirely in the forward half of the drop, where due to gaseous flow over the droplet surface, a low pressure region of recirculating flow is created, and heat transfer rates are high in this region. Under these conditions some or all of the vapourised fuel burns in the wake of the droplet and a degree of premixing with gaseous oxidant due possibly to entrainment into this low pressure region prior to combustion, is possible. This mode of combustion is suitably referred to as a Wake flame, if the relative velocity is increased still further the wake flame is extinguished when a critical velocity is reached, this is the Extinction Velocity, Sjögren (13). Diffusion flames are characteristically yellow due to the soots which are always formed, the reaction zone is at high temperature due to the fact that fuel vapour and soot combine in locally

stoichiometric proportions. There exists a minimum droplet diameter, approximately 5 microns (μ), below which a single droplet cannot support its own individual diffusion flame, (14), it is widely appreciated that combustion of very small droplets resembles homogeneous combustion. When the flame adjacent to the droplet is completely blown off then the vapourised fuel can almost completely mix with oxidant before near-homogeneous combustion occurs in a flame zone away from the evaporating droplets. For convenience this form of combustion is also referred to as a Wake flame - due to the fact that premixing occurs in both forms. Wake flames are therefore blue and relatively non luminous, this type of combustion is frequently referred to as Blue Flame Combustion.

Naturally if $V_S > V_G$, as is frequently the case for fuel injectors in gas turbine combustors, then the low pressure wake region is situated behind, instead of in front of, the droplet. Due to velocity fluctuations, the effect of turbulence on reaction zone shape is to cause a continuous wrinkling and irregular motion of the zone boundary, Ohta et al (16). Such velocity fluctuations also tend to reduce the mean value of the extinction velocity. Emmons (17) has pointed out that at relative velocities between that corresponding to Fig.2.5(d) and actual extinction, the wake flame may re-attach itself to the forward droplet surface.

Sjögren (13) demonstrated that the critical extinction velocity required to force a transition from diffusion to wake flame burning is a strong function of the local oxygen concentration. He used wicks which were continuously fed with fuel to simulate droplet combustion. Fig.2.4 shows the results which were obtained, the most remarkable feature of which was the fact that the extinction velocity falls to zero when the oxygen concentration is diluted to 14-16% with nitrogen, i.e. effectively combustion gases. This means that, for an unspecified fuel, it is impossible for droplet diffusion flames to exist at this oxygen concentration since a relative velocity between an evaporating droplet and the surrounding gaseous phase will always occur. Sjögren also investigated the effect of using carbon dioxide as diluent, in addition, he found that the extinction velocity was proportional to the square root of the wick diameter.

There are three basic mechanisms of heat transfer which may be responsible for droplet heating under flame conditions, these are:

1. Convective transfer. This is a function of droplet diameter, V_{Rel} and gaseous phase temperature: convective heat transfer expressions will be discussed a little later.

2. Conductive transfer. This form of heat transfer occurs through the vapour film surrounding a diffusion type flame. Rate of transfer may be given by (15):

$$\dot{Q}_{COND} = 12 \lambda \frac{M}{\rho_L r_L^2} \Delta T \quad \ldots\ldots\ldots \quad (2.12)$$

where, $\lambda = \lambda(T_{film})$ = film coefficient of conduction.

T_{film} = film temperature $\simeq \frac{1}{2}(T_L + T_G)$

$\Delta T = T_G - T_L$

M = mass size fraction of spray with diameter d.

3. Radiative transfer. It may be shown (14) that radiative heat transfer from the flame is inadequate to heat the droplets to give the required vapourisation, especially under blue flame conditions. It is largely a function of gaseous temperature, gas emissivity and droplet surface area. Rate of transfer may be expressed (16):

$$\dot{Q}_{RAD} = 6 F_v \varepsilon \sigma \frac{M}{\rho_L r_L} (T_G^4 - T_L^4) \quad \ldots\ldots\ldots \quad (2.13)$$

where, for black-body radiation to the drops and a view factor (F_V) = 1 (no drop/drop interference assumed):

$$F_V . \varepsilon . \sigma \simeq 1.355 \times 10^{-12} \text{ W/m}^2\text{K}^4 \text{ Ref.(2)}$$

The flue dynamic processes of turbulent mixing and recirculation also influence droplet heating rates.

Most of the research on droplet combustion has been devoted to studies of the combustion of stationary isolated single droplets since it is generally held to be a precursor to the description of more complex spray combustion. Such research has usually treated the overall process of droplet combustion rather than considering

the evaporation process separately, in doing so a very crude chemical reaction model is incorporated due to analytical complexity. The calculation of evaporation rates for single drops is discussed in some detail in 4.4.

In practical heterogeneous combustion systems an atomising device is normally used to derive a spray of droplets of characteristic initial size distribution for a given device, see section 2.2(a). Evaporation from sprays is much more complex than single droplet evaporation since spatial distributions of both phases and droplet collision processes have to be considered. Local temperatures in a spray are additionally affected by such spatial distributions. It has been shown above that droplet dynamic effects and evaporation rates are very dependent on droplet diameter and size distribution functions are necessary for describing sprays. Nuruzzaman et al (36) employed a model based on a Rosin-Rammler distribution function to calculate the relative charge in combustion efficiency in a turbojet with oxygen content, they concluded that the use of mean drop sizes in such considerations was inadequate. For a review of theories which have been evolved for spray combustion under rocket chamber conditions see the excellent general droplet combustion review of Williams (20).

2.2(c) Mixing.

Before vapourised fuel and oxidant gaseous species can chemically react the respective molecules, which are initially separate, must be brought together in close contact, the physical process is designated mixing and possesses a finite rate. High mixing rates in heterogeneous combustion are sought in order to maximise combustion performance. The process is important under combustion conditions since it is usually the rate-limiting step, it is also one of the most difficult processes to mathematically characterise since it is beyond the present scope of science to compute the motion of individual molecules.

Species mixing is a strong function of gaseous phase fluid mechanics and molecular diffusion, which both result in spatial variation of local gaseous transport properties, hence it is also intimately related to combustor flow pattern.

Turbulent fluid motion, which is undesirable in ducted flows due to the high associated pressure drop, is extremely desirable from a combustion standpoint since its irregular random nature tends to give very high mixing rates, in fact virtually all flames of technological importance are turbulent. A turbulent flow is classically regarded as being composed of a large number of distinct fluid masses, or eddies, which are each small and fluctuate randomly, their motion being superimposed on the mean flow of the fluid. Because of the random nature of turbulence statistical expressions are employed to describe it, it can also be deduced (1) that transport of a transferable quantity by such random fluid motion is diffusive in nature; for an introduction and comprehensive treatment of turbulent behaviour refer to Hinze (1). It can be shown (38) that the energy spectrum, intensity and scale are the most important turbulence parameters with respect to mixing. The turbulence intensity is defined as the ratio of the root-mean-square value of the fluctuation to the flow mean velocity, and is usually in the range $0.1 \rightarrow 0.4$ for practical flows.

When viscous streams of different velocity impinge a shear flow is produced where predominantly large eddies are formed which then interact inertially to give a complete size range of eddies, each of defined wave number k at any instant in time t, where:

$$k = \frac{2\pi n}{\bar{U}} \quad \ldots\ldots\ldots \quad (2.14)$$

and n = eddy frequency ($\propto$ (eddy size)$^{-1}$)

$\bar{U}$ = mean flow velocity.

Hence an energy spectrum E(k,t) can be envisaged for any turbulent flow, Fig.2.6 illustrates the general form of such a spectrum; it can be shown (38) that the area under the curve is equal to the kinetic energy of turbulence, and that the maximum possible value of the area can be calculated from an energy balance across the turbulence generation system. The smallest eddies present, which possess the highest frequencies and wave numbers, are frequently referred to as dissipation eddies since they viscously dissipate the turbulence to heat (the effect on actual gas temperature is negligible though). This range of eddies actually mix on the

molecular scale, their size is two or three orders of magnitude greater than the molecular mean free path and varies inversely with $\bar{U}$. A limit to this trend is imposed by the fluid viscosity and, as for any fluid-dynamic process, the nature of the flow is determined by the ratio between the inertial and viscous forces, i.e. the Reynolds number. Energy is transferred to these dissipation eddies from the larger eddies by means of a continuous flux through the wavenumber range, dissipation increasing simultaneously. The size of the largest eddies is initially of the order of the dimension of the turbulence generator and although formation of, and transfer of energy to, smaller eddies progressively occurs the remaining largest eddies can grow in size until they are of the order of the distance between the flowfield constraining boundaries. It is interesting to note that it is not the largest eddies which have the maximum kinetic energy but the eddies in a slightly higher wavenumber range as Fig.2.6 shows, this wave number range is referred to as the "energy containing eddies". An intermediate range also exists, the inertial eddies, where the decay process is relatively slow; the high wave number eddies are independent of the external conditions producing the forces which generate the initial largest eddies. For a discussion of the properties of and defining functions for E(k,t) refer to (1), (38) discusses the effects of temperature and pressure on the energy spectrum.

It is convenient to distinguish between two types of fluid mixing; these are the molecular scale (or micro-) mixing, which, as just mentioned, governs the actual species chemical reaction, and large scale (or macro-) mixing which leads to mean concentration of species.

It can be appreciated then, that in order to fully describe mixing effects, a detailed knowledge of transport processes throughout the combustor flowfield is demanded, which in turn implies use of the Navier-Stokes equations governing the fluid dynamics for turbulent, unsteady and possibly 3-dimensional flow. This system of equations cannot be solved at present. However, Spalding et al (39) have developed an approach for 2-dimensional, steady state recirculating flows which treat turbulent flows as though they were laminar ones with transport

properties which vary from place to place. Such a flow is considered to have "effective" values for viscosity, thermal conductivity and diffusion coefficient, which are all spatial functions. Spalding et al discuss various methods of specifying these effective values including Prandtl's so called mixing length hypothesis which asserts that the effective viscosity is a function of:

i) local fluid density,

ii) a "mixing length",

iii) the normal velocity gradient.

The mixing length was considered as being more easily estimated, and perhaps amenable to more satisfactory description by an additional differential equation. The overall technique used will be further discussed in Section 2.6(b).

Harsha (40) developed a general method for analysing turbulent mixing phenomena that was limited to free, i.e. unconfined, flows. The mixing field was assumed to exist in a constant pressure environment remote from walls and to be due to the interaction of two streams only. These two approaches are both dependent on empirical input information, which is considered to be unsatisfactory, although both obtained reasonable results. Much expertise needs to be gained before the analysis of three dimensional turbulent mixing effects can be approached with confidence.

Three other types of technique, which are mainly concerned with describing micro-mixing processes, will now be considered, the feature that they have in common is the fact that local shear stresses, velocities and transport properties are not evaluated. They all therefore require considerably less effort to predict the same effects but have enjoyed varying degrees of success.

The first such approach involves the use of an assumed homogeneous fuel distribution pattern within a given flowfield. Heywood (41) applied the technique to predict pollutant emissions and employed an assumed Gaussian distribution of fuel/air equivalence ratio, thus he only treated macro-mixing effects. Gouldin (42) formulated a similar approach to treat micro-mixing phenomena. Both of these analyses, however, are non-fundamental in that they require experimental information to set a "ground" value for a mixing parameter.

The third class of mixing theory has been termed deterministic since such analyses seek to derive turbulence decay expressions from turbulence theory and combustor geometry. An introduction to this type of model is provided by Poll (2) and Rosenweig (44). The decay of instantaneous fluctuations in a scalar quantity, such as concentration or temperature, about its mean value is related to the turbulence field through the micro-scale at high Reynolds numbers. The determination and properties of turbulence scales is elaborated in Chapter 6. For stationary isotropic turbulence, in which the statistical features have no directional preference, Rosenweig obtained an expression for scalar dissipation ε_s by means of the scalar energy spectrum function $E_s(k)$:

$$E_s(k) = c \cdot \varepsilon_s \varepsilon^{-1/3} k^{-5/3} \quad \ldots\ldots\ldots \quad (2.15)$$

where, c = a constant,

ε = turbulent kinetic energy dissipation.

and

$$\varepsilon_s = \bar{b}^2 \left(\frac{\varepsilon}{L_s^2} \right)^{1/3} \quad \ldots\ldots\ldots \quad (2.16)$$

where b = fluctuation of scalar quantity (e.g. concentration or temperature) about its mean,

L_s = scalar microscale.

When combined with a conservation equation for the scalar quantity over an elemental volume of the flowfield the above two relations yield, for the characteristic decay time τ_m:

$$\tau_m = \frac{L_s^{2\,1/3}}{\varepsilon} \quad \ldots\ldots\ldots \quad (2.17)$$

i.e. a function of turbulence parameters only.

Swithenbank (35,38,45) also utilised isotropic turbulence dissipation functions to develop a deterministic approach in which the microscales are further related to the available energy for turbulence generation, and combustor geometry. In combustion systems this energy results from the pressure loss across the turbulence generator. An outline of the method used is given below.

Since velocity and concentration fluctuations decay simultaneously (Reynolds Analogy), it is first hypotherized that the degree of mixing achieved is equal to the degree of turbulent dissipation, within any given flow system. An energy balance is now performed (45):

Pressure drop across baffle or other type of stabiliser i.e. turbulence generator.	=	Energy "held" in flow velocity profile.	+	Turbulence kinetic energy.	+	Dissipation energy.

Algebraically:

$$\frac{P}{q} = \frac{KE_{av}}{q} + 3\left(\frac{u'}{\bar{U}}\right)^2 + \frac{D}{q} \quad \ldots\ldots\ldots \quad (2.18)$$

where q = dynamic head = $\frac{1}{2}\rho_G \bar{U}^2$

For a typical baffle the terms in (2.18) are plotted as a function of non-dimensional distance from the baffle, Fig.2.7. A characteristic dissipation time τ_D is now postulated, note that Dissipation and not Diffusion is the process concerned:

$$\tau_S = C^* \frac{\ell_e}{u'_{max}} \quad \ldots\ldots\ldots \quad (2.19)$$

where, C^* = a constant (estimated by Swithenbank to be of the order unity).

ℓ_e = mean size of the energy-containing eddies $\simeq 0.2\lambda$ (38).

u'_{max} = maximum value of the r.m.s. turbulent velocity fluctuations.

For a constant mean velocity system the characteristic stay time is given by

$$\tau_S = \frac{X}{\bar{U}}$$

where, X = system length

$\simeq 10\lambda$ (Fig.2.7).

Hence,

$$\tau_S/\tau_D = \tau_{SD} \frac{X}{\ell_e} \left(\frac{u'}{\bar{U}}\right)_{max}$$

$$\therefore \quad \tau_{SD} \simeq 50 \left(\frac{u'}{\bar{U}}\right)_{max} \quad \ldots\ldots\ldots \quad (2.21)$$

The factor τ_{SD} is termed unmixedness since high values of this parameter indicate good mixing, or stirring, and vice versa. The flow energy balance (2.18) can then be combined with equation (2.21) to eliminate the maximum turbulence intensity

term which, although a function of system geometry is difficult to determine to any accuracy:

$$\tau_{SD} = 50 \left(\frac{\Delta P}{3q}\right)^{\frac{1}{2}} \quad \ldots\ldots\ldots \quad (2.22)$$

This mixing parameter is particularly applicable to the partially-mixed reactor theory originally formulated by Vulis (46), as will be demonstrated in Section 2.6(a).

The testing of these various theories for mixing by experimental means is extremely difficult for heterogeneous combustion because of the obvious difficulty in isolating the mixing process. For homogeneous combustion tracer tests may be performed by injecting an inert compound, such as He or Ar, into the combustor and analysing local combustion gases at points downstream from where the tracer was injected. The method is subject to sampling errors although useful information can be gained under carefully controlled conditions.

2.2(d) Chemical Reaction.

Chemical Reaction is arguably the most fundamental of the processes which constitute a flame since:

i) it is the step responsible for the actual heat release i.e. conversion of fuel chemical energy into thermal energy,

ii) it is the process whereby oxidation of the fuel vapour actually generates the many "new" chemical species, referred to collectively as combustion products,

iii) it takes place in the gaseous phase and is common to both single and two-phase combustion.

The chemical decomposition of the fuel takes place by a number of individual steps, or reactions, each of which may be exothermic or endothermic and each of which involve molecular rearrangement but conservation of mass. The number of different reactions and species involved increases rapidly with fuel molecular weight, and particulate material (soots) as well as gaseous products may result under certain conditions. The complexity of the situation is also hampered by the fact that, even for hydrocarbon fuels of moderate molecular weight, many of the initial reactions between fuel and oxidant are not known with any certainty. The succeeding

reactions are however well known and for any hydrocarbon fuel the final products, under complete combustion conditions, are predominantly water vapour and carbon dioxide.

Each chemical reaction may proceed in a forward and a backward direction and the characteristic "kinetic rate" of the forward reaction may be generally expressed, for a bimolecular reaction as:

$$a\,A + b\,B \underset{b_j}{\overset{f_j}{\rightleftharpoons}} c\,C + d\,D \qquad \ldots\ldots\ldots \qquad (2.23)$$

Forward reaction rate = $f_j [A]^a [B]^b$ (Similar for uni- and ter-molecular classes of reaction)

where, $[\ ]$ denotes concentration of species A, B, C, D and a, b, c, d are the corresponding species stoichiometric coefficients.

f_j = forward reaction rate "constant"

$$= A_j T^{nj} \exp(-E_j/RT) \qquad \ldots\ldots\ldots \qquad (2.24)$$

A similar expression can be written for the reverse reaction and it should be noted that a) f_j is not a true constant, b) the overall rate is very sensitive to both reactant concentration and temperature, c) the rate is independent of any species velocity terms. When a sufficiently large amount of time is available dynamic equilibrium prevails in which the forward and backward rates of reaction are equal, an equilibrium constant K_j may be defined:

$$K_j = \frac{f_j}{b_j} \qquad \ldots\ldots\ldots \qquad (2.25)$$

Under combustion conditions species mean residence times in the flame are invariably much smaller than the time required to reach equilibrium and most chemical reactions are kinetically rate-limited; compared to the other processes of atomisation, evaporation and mixing, chemical reaction rates are considered to be very high (27) under most conditions.

Due to the large ranges of temperature and pressure over which a kinetic rate expression is required to be valid such kinetic data can be subject to significant inaccuracies, in some cases order of magnitude estimates only can be made. Golden (47) reviewed several methods of estimating such rate data whilst Baulch et al (48) have compiled an invaluable source of kinetic data for high temperature chemical reactions, recommended rate constant and equilibrium data are presented (for specified ranges of application) for each reaction after a critical evaluation of available data.

At flame temperatures vapourised hydrocarbons decompose or "crack" into smaller hydrocarbon molecules and radicals but the exact mechanism and associated kinetics by which even the simplest hydrocarbon disintegrates into other components is far from understood and is extremely complex. Such thermal decomposition is termed pyrolysis and is very important in the study of soot formation rates. Soots are particulates formed from the pyrolysis of hydrocarbon or other organic molecules in which many thousands of atoms, in a much higher carbon/hydrogen ratio than in the fuel molecule, have solidified together. Hence the processes of dehydrogenation, condensation, chain reactions and polymerisation may be involved in pyrolysis but very many intermediate routes between these processes appear plausible.

Such mechanisms may be a function of local temperature,pressure, species concentration plus the fuel chemical constitution and flame residence time. Free radicals and reactive intermediate species are generally recognized as being important participants in such mechanisms. It is known (14) that primary pyrolysis products are H_2, CH_4, C_2H_2, C_2H_4, with significant quantities of C_3 and C_4 hydrocarbons. Green and Toennies (49) give estimates for the characteristic pyrolysis times of several hydrocarbons. Poll (2) also presents suitable references in his review for the rates of splitting and hydrogen extraction reactions. Due to the complication of pyrolysis reactions many investigators have expressed fuel decomposition by overall partial oxidation reactions, some of these have been assumed to be infinitely fast whilst others have more realistically been

rate limited. These overall reactions have frequently been termed "quasi-global", a selection of such reactions are:

(i) For the two-step decomposition of methane (50)

$$\left.\begin{aligned} CH_4 + \tfrac{3}{2} O_2 &\rightarrow CO + 2 H_2O \\ CO + \tfrac{1}{2} O_2 &\rightarrow CO_2 \end{aligned}\right\} \quad \ldots\ldots\ldots \quad (2.26)$$

Overall rate expressions:

$$\frac{dX}{dt} = A_x \exp(-E_x/RT)\, f_x\, f_{O_2}^{\frac{1}{2}}\, f_{H_2O}^{\frac{1}{2}}\, (P/RT)^2$$

where, $X = CH_4$, $A_x = 5.3 \times 10^{15}$ litres/gm mole sec. $E_x = 57 \pm 5$ kcal.

$X = CO$, $A_x = 1.8 \times 10^{10}$ litres/gm mole sec. $E_x = 25 \pm 5$ kcal.

(ii) $$C_n H_m + \tfrac{n}{2} O_2 \rightarrow n\,CO + \tfrac{m}{2} H_2 \quad \ldots\ldots\ldots \quad (2.27)$$

$$\text{Reaction rate (51)} = A_j\, T\, e^{(-12,900/T)} \left[C_n H_m\right]^{\frac{1}{2}} \left[O_2\right] (P)^{-0.825}$$

where $A_j = 5.52 \times 10^8$

Edelman derived this expression after considering the results of an extremely detailed investigation of hydrocarbon oxidation conducted by Chinitz and Bawer (81) in which fuel breakdown was modelled using 69 reactions and 31 species.

(iii) $$C_8H_{16} + O_2 \rightleftharpoons 2\,C_4H_8O \quad \ldots\ldots\ldots \quad (2.28)$$

$$\text{Forward rate constant (100)}, f_j = 5 \times 10^7\, T^{1.5}\, e^{(-7900/T)}$$

$$2\,C_4H_8O + 3O_2 \rightleftharpoons 8CO + 8H_2 \quad \ldots\ldots\ldots \quad (2.29)$$

$$\text{Forward rate constant}, f_j = 1 \times 10^{11}\, T^{4.5}$$

The above rate constant expressions are for the forward reactions, the reverse reactions are usually assumed negligible. Other investigators have produced completely global kinetic rate expressions, these are unfortunately specific to the combustor concerned, eg Odgers (52).

A selection of more fundamental chemical reactions which may occur under combustion conditions is now presented, rate expressions for these reactions are generally available from reference (48).

Methane decomposition reactions, where M signifies a general third body:

$$CH_4 + M \rightleftharpoons CH_3 + H + M \quad \ldots\ldots\ldots \quad (2.30)$$

$$CH_4 + H \rightleftharpoons CH_3 + H_2 \quad \ldots\ldots\ldots \quad (2.31)$$

$$CH_4 + OH \rightleftharpoons CH_3 + H_2O \quad \ldots\ldots\ldots \quad (2.32)$$

$$CH_4 + O \rightleftharpoons CH_3 + OH \quad \ldots\ldots\ldots \quad (2.33)$$

$$CH_3 + O_2 \rightleftharpoons HCO + H_2O \quad \ldots\ldots\ldots \quad (2.34)$$

$$HCO + OH \rightleftharpoons CO + H_2O \quad \ldots\ldots\ldots \quad (2.35)$$

$$HCO + M \rightleftharpoons H + CO + M \quad \ldots\ldots\ldots \quad (2.36)$$

Carbon monoxide decomposition reactions:

$$CO + OH \rightleftharpoons H + CO_2 \quad \ldots\ldots\ldots \quad (2.37)$$

$$CO + O + M \rightleftharpoons CO_2 + M \quad \ldots\ldots\ldots \quad (2.38)$$

$$CO_2 + O \rightleftharpoons CO + O_2 \quad \ldots\ldots\ldots \quad (2.39)$$

Reaction (2.37) being the most significant of these three.

Hydrogen combustion mechanism:

$$O_2 + H_2 \rightleftharpoons OH + OH \quad \ldots\ldots\ldots \quad (2.40)$$

$$OH + H_2 \rightleftharpoons H_2O + H \quad \ldots\ldots\ldots \quad (2.41)$$

$$O_2 + H \rightleftharpoons OH + O \quad \ldots\ldots\ldots \quad (2.42)$$

$$O + H_2 \rightleftharpoons OH + H \quad \ldots\ldots\ldots \quad (2.43)$$

$$O + H_2O \rightleftharpoons OH + OH \quad \ldots\ldots\ldots \quad (2.44)$$

$$H + H + M \rightleftharpoons H_2 + M \quad \ldots\ldots\ldots \quad (2.45)$$

$$O + H + M \rightleftharpoons OH + M \quad \ldots\ldots\ldots \quad (2.46)$$

$$H + OH + M \rightleftharpoons H_2O + M \quad \ldots\ldots\ldots \quad (2.47)$$

$$O + O + M \rightleftharpoons O_2 + M \quad \ldots\ldots\ldots \quad (2.48)$$

The Zeldovich (53) reactions for describing nitric oxide formation are:

$$O + N_2 \rightleftharpoons NO + N \quad \ldots\ldots\ldots \quad (2.49)$$

$$N + O_2 \rightleftharpoons NO + O \quad \ldots\ldots\ldots \quad (2.50)$$

Further reactions involving NO are:

$$N + OH \rightleftharpoons NO + H \quad \ldots\ldots\ldots \quad (2.51)$$

$$N_2 + OH \rightleftharpoons NO + NH \quad \ldots\ldots\ldots \quad (2.52)$$

Whilst Fenimore (54) proposed the following reactions which are significant under fuel rich conditions in affecting NO formation:

$$CH + N_2 \rightleftharpoons HC + N \quad \ldots\ldots\ldots \quad (2.53)$$

$$C_2 + N_2 \rightleftharpoons 2CN \quad \ldots\ldots\ldots \quad (2.54)$$

$$C + N_2 \rightleftharpoons CN + N \quad \ldots\ldots\ldots \quad (2.55)$$

Pratt (55) has suggested that, under various flame conditions, the other oxides of nitrogen nitrous oxide N_2O and nitrogen dioxide NO_2 can directly affect production of NO.

Nitrous oxide mechanism (55):

$$N_2 + O + M \rightleftharpoons N_2O + M \quad \ldots\ldots\ldots \quad (2.56)$$

$$N_2O + O \rightleftharpoons NO + NO \quad \ldots\ldots\ldots \quad (2.57)$$

$$N_2O + O \rightleftharpoons N_2 + O_2 \quad \ldots\ldots\ldots \quad (2.58)$$

$$N_2O + H \rightleftharpoons N_2 + OH \quad \ldots\ldots\ldots \quad (2.59)$$

Nitrogen dioxide mechanism (55):

$$NO + O + M \rightleftharpoons NO_2 + M \quad \ldots\ldots\ldots \quad (2.60)$$

$$O + NO_2 \rightleftharpoons NO + O_2 \quad \ldots\ldots\ldots \quad (2.61)$$

$$H + NO_2 \rightleftharpoons NO + OH \quad \ldots\ldots\ldots \quad (2.62)$$

Chemical reactions involving the oxidation of sulphur to sulphur dioxide SO_2 and sulphur trioxide SO_3 are given by Levy (56), those not involving hydrogen sulphide H_2S are:

$$S + O \rightleftharpoons SO \quad \ldots\ldots\ldots \quad (2.63)$$

$$S + S \rightleftharpoons S_2 \quad \ldots\ldots\ldots \quad (2.64)$$

$$SO + O \rightleftharpoons SO_2 \quad \ldots\ldots\ldots \quad (2.65)$$

$$SO + SO \rightleftharpoons S_2O_2 \quad \ldots\ldots\ldots \quad (2.66)$$

$$SO_2 + O + M \rightleftharpoons SO_3 + M \quad \ldots\ldots\ldots \quad (2.67)$$

$$SO + O_2 + M \rightleftharpoons SO_3 + M \quad \ldots\ldots\ldots \quad (2.68)$$

$$SO_3 + H_2 \rightleftharpoons SO_2 + H_2O \quad \ldots\ldots\ldots \quad (2.69)$$

$$SO_2 + O \rightleftharpoons SO_3 \quad \ldots\ldots\ldots \quad (2.70)$$

$$SO_3 + CO \rightleftharpoons CO_2 + SO_2 \quad \ldots\ldots\ldots \quad (2.71)$$

Other reactions involving SO_x, NO_x and H_2S interactions, plus hydrocarbon interactions and metallic surface reactions may also occur in heterogeneous two phase combustion. However, these are very complex and the kinetics of such reactions is generally not known so that they are excluded from this discussion.

Due to the very many physical processes involved the kinetics and exact mechanism of soot formation are largely unknown. As mentioned above, pyrolysis chemical reactions play an important role whilst the diffusion mode of droplet combustion is known to produce very much more soot than the wake mode of combustion. This is probably due to the cracking of the fuel vapour in the locally high temperature (stoichiometric) flame surrounding each drop, in the former mode. The oxidation of soots is known to be slower than their rate of formation (14) so that once formed the particles tend to remain, and even coagulate further to produce smoke.

For a homologous series of hydrocarbons the tendency to smoke increases with molecular weight, but the reverse is true for olefinic and some aromatic compounds. The tendency to smoke is also known to be higher for branched chain and unsaturated hydrocarbon fuels. The luminosity of a flame is related to the rate of carbon formation. High pressure seems to favour soot formation, but there is no simple relation between temperature and soot formation. For a discussion of the effects of physical processes on soot formation in flames refer to (14).

In premixed flames one would not expect carbon formation from mixtures in which there is more than sufficient oxygen to burn the fuel carbon to carbon monoxide, hence carbon formation can be avoided in this class of flame, i.e. also in the wake mode of two phase combustion.

2.3 Heterogeneous Combustor Devices.

Four different classes of liquid fuelled combustor can be identified, before each of these is described it is important to bear in mind that steady or continuous combustor devices only are the subject of this study. Hence the exclusion of reciprocating types.

2.3(a) The Gas Turbine.

The gas turbine device has been applied to both mobile and stationary power

generation, by far their most important application though is the powering of commercial and military aircraft. The gas turbine is also increasingly being used for both automobile propulsion and as a component in stationary power generation cycles for industry.

Fig.2.8 shows a schematic of the internal flowfield of a typical gas turbine combustor. The primary zone, which is just downstream of the fuel injector, is a region of intense turbulent mixing and strong recirculation which serves to stabilise the combustion. The recirculation is induced by the swirler air fraction plus the entrainment property of the first row of liner penetration jets and results in the mixing of hot combustion products and fuel droplets/vapour. Combustion is largely completed in the secondary zone and the dilution zone cools the combustion gases with a fraction of the air to a temperature which the actual turbine blades can tolerate with acceptable stress. A further fraction of the total air feed is frequently used for cooling the combustor liner so that as the diagram shows, the overall turbulent flowfield is highly complex. The fuel injector device was initially a pressure jet atomiser or vapouriser tube although the present trend is towards airblast atomisers which generate very fine sprays.

For aviation use the gas turbine combustor is required to be compact, in order to minimise the engine overall weight, and to give high performance in order to maximise both power output and fuel economy. These requirements then imply high combustion intensity and efficiency, which is why large can air pressure drops are used to maximise turbulent mixing rates. High engine reliability is naturally vital, in addition, gas turbines are expected to ignite easily and operate efficiently over wide ranges of temperature and pressure for long periods. In view of these stringent demands good quality fuels such as kerosine are normally used, fuel costs in general are regarded as being of only secondary importance.

Due to the large numbers of gas turbine combustors which are in use, and their design requirements, a large amount of empirical and fundamental research work has been concentrated on this device. The remaining heterogeneous combustor devices are all of the stationary type.

2.3(b) Power Generation Boilers.

These are sometimes termed utility boilers and are normally large scale installations for the generation of power, they are also wide spread throughout the world, a large range of fuels being used. Liquid fuels used are of lower grade than aviation gas turbine types, e.g., residual fuel oil, which can contain significant amounts of chemically bound sulphur/nitrogen. The fuel is usually introduced into the combustor by means of a matrix of burners which employ pressure jet, rotary cup or twin fluid atomisers to actually inject the fuel. Unlike gas turbine combustors which are largely blue flame, these burners produce turbulent diffusion mode droplet flames which are yellow, i.e., luminous. Hence high radiative heat transfer rates within the boiler section are realised. Peak temperatures throughout the boiler are lower than those found in the gas turbine and design types vary widely.

The complete combustion of the fuel with the minimum of excess air under stable, hence easily controllable, conditions is the chief requirement of the power generation boiler. Increasing the excess air supplied to the burners is unacceptable since large flue gas heat losses and high air supply costs would result.

The fluidised bed combustion concept may be applied to this combustor device for either direct combustion or gasification of the liquid fuel, in order to obtain high heat transfer rates plus intense combustion at low temperatures.

Compared to the gas turbine the power generation boiler has received considerably less attention in the way of research and development.

2.3(c) Industrial Furnaces and Flare stacks.

Liquid fuels are employed in chemical engineering and many other industrial processes for combustion in furnaces which may be used for small scale steam raising, evaporators and the heating of various solids etc. Again, yellow turbulent diffusion mode of droplet combustion generally prevails and high heat transfer rates are the main requirement. Low grade dirty fuels frequently have to be burnt as economically as possible under stable conditions.

In some refinery processes a situation is often encountered where the storage costs of certain low grade liquid fuels, although more often gaseous fuels perhaps,

may be prohibitive. In these circumstances it is more economical to simply burn the fuel in the open atmosphere using a device known as a flarestack, the turbulent diffusion flame is then required to entrain its own combustion air. Both these kinds of combustor are by necessity in a relatively crude state of development, empirical techniques generally being accepted.

2.3(d) Domestic Boiler Appliances.

This last class of heterogeneous combustor is used for household heating and includes building heating devices in general. These combustors are small scale and are required to handle low flowrates of relatively low grade fuels such as distillate oils; pressure jet atomisers often being used. They are also desired to be compact, quiet, clean, easily controllable and again economic to purchase and run. The design of this type of combustor generally proceeds along empirical lines. Fuels are invariably injected at pressures in the 100 psig range and at flowrates of around 0.8 gph, problems of nozzle duct blockage are often experienced at fuel throughputs less than this figure (94).

2.4 Combustion generated Air Pollution.

The field of combustion research has expanded in recent years to encompass the study of air pollutant formation as an integral part of combustor performance. This development has perhaps been spurred by public awareness and accelerated greatly by the widespread introduction of generally stringent legislation. Much heated discussion on the subject has been provoked as a result, the consequences and economic losses attributable to air pollution therefore, are considered well known (62-65).

Which species discharged into the atmosphere may be considered to be pollutants? The answer to this question is conveniently expressed in the form of Table I below, the major annoyances generally associated with each species is also presented.

TABLE I. AIR POLLUTANTS.

	Pollutant species.	Associated major annoyances.
a)	Carbon Monoxide (CO)	Toxic (reduces oxygen capacity of blood).
b)	Oxides of Nitrogen (NO, NO_2)	Toxic (basic constituent for photochemical smog formation).
c)	Hydrocarbons (UHC)	Toxic, irritant or inert - depending on fuel chemical composition (basic constituent for photochemical smog formation).
d)	Oxides of Sulphur (SO_2, SO_3)	Toxic, readily forms sulphuric acid, irritant, aerosol formation. Corrosion.
e)	Hydrocarbon organic derivatives (e.g., aldehydes)	Irritants, odourants (basic constituent for photochemical smog formation).
f)	Smoke, particulates.	Numerous e.g., visibility reduction, nucleation sites.
g)	Sulphur compounds (e.g., H_2S)	Toxic, odourants.
h)	Lead (Pb)	Toxic.
i)	Other metals (e.g., V, Mn, P)	Toxic, atmospheric reactions.

The table lists the primary air pollutant species (hereafter referred to as pollutants), and the first six are almost universally recognized as being the most serious. It should be noted that possible weather interference has been largely ignored, so that carbon dioxide and water vapour have not been considered pollutant entities. Metallic lead can be neglected in this study since it is a consequence of internal combustion engine operation, i.e., not of the continuous combustor type. Nitric oxide, NO and nitrogen dioxide, NO_2 are the major oxides of nitrogen of interest and are collectively referred to as NO_x, similarly the oxides of sulphur are collectively termed SO_x. Hydrocarbon emissions are the result of inefficient combustion or incomplete fuel utilisation, hence they are collectively termed Unburnt Hydrocarbons (UHC for convenience).

The scale of any individual air pollution problem is naturally very complex and a function of many factors such as emission frequency, combustor type and size, etc. Sawyer (66) has made an appraisal of the scale of problem presented by aircraft pollutant emissions, major problem areas were then highlighted.

Energy conversion combustion processes as a whole account for extremely large proportions of the artificial emission of all major pollutant species, for example

TABLE II. BREAKDOWN OF SOURCES OF THE MAJOR AIR POLLUTANTS IN THE UNITED STATES; 1968.

Species	Total Emission 10^6 Tons/Year	COMBUSTION			PARTIALLY COMBUSTION	
		Vehicles %	Stationary Plant %	Miscellaneous %	Industrial Processes %	Solid Waste Disposal %
NO_x	20.6	39.3	48.5	8.3	1.0	3.9
SO_x	14.6	2.4	73.5	1.8	22.0	0.3
CO	100.4	63.8	1.9	16.9	9.6	7.8
UHC	32	55.6	2.2	13.1	24.1	5.0
Particulates	28.3	4.3	31.4	33.9	26.5	3.9

Source of data = Reference (95).

during 1968 and in the United States, this proportion was 95% for NO_x as Table II shows. The Table also presents a breakdown of the contributing primary sources of emission for SO_x, CO, UHC and Particulates for that year in the U.S. In each case the most significant source is underlined, so that it can be immediately appreciated that stationary plant was responsible during 1968 for the highest emissions of NO_x and SO_x, whilst vehicles in general produced the greatest CO and UHC pollutant emissions. Production of particulates was more evenly distributed. The natural rate of generation of NO_x has been estimated as being about 15 times greater than the corresponding manmade NO_x production rate, however, the latter is concentrated in urban areas where actual levels are higher. Even so these levels rarely exceed toxic thresholds, the reasons for limiting their emission into the atmosphere are mainly that they form secondary pollutants by further atmospheric reactions.

With the possible exception of particulates, it is widely accepted that emissions of pollutants have been and are increasing with time. Thus Derwent and Stewart (96) have presented NO_x emissions data for the U.K. which correspond to the period 1965-1970, while Bartok et al (67) estimated future emissions of NO_x in the U.S. up to the year 2000, based on the continuation of current trends. Information on particulates and SO_2 emissions in the U.K. from 1950 - 1968 is also available (63).

Legislation introduced to control air quality has been considerably more stringent in the U.S., moreover, the proposed standards for manmade NO_x emissions have provided the toughest goal. For an example of such U.S. Federal Standards refer to (66,67). European air pollution problems at present are more localised and less acute so that existing European legislation is not so rigid.

Having considered future trends in, and the existing legislation for control of, air pollution, it can be concluded that there definitely exists a need for the application of further related combustion research if the demands for an overall reduction in pollutant emissions in the future are to be met. Now such a research effort can clearly be directed at one or all of three possible phases of control, these are:

1. FUEL TREATMENT. This involves refinement of the existing fuel to remove impurities. Removal of sulphur containing compounds ensures that SO_x and other sulphur containing pollutants are not formed in the combustor, hence corrosion risk is also averted. Processing to reduce fuel bound nitrogen content helps reduce NO_x but is more significant for solid fuels. To a lesser extent still, metal-containing emissions can be obviated through fuel processing. The other major pollutants listed in Table I. however are not affected by this phase of control, and fuel chemical processing operations in general are expensive.

2. COMBUSTION MODIFICATION. The next phase of control corresponds to refinement of the actual combustion process and can be implemented in either of two ways. Firstly by a relatively minor modification to the emitting combustor, this type of approach is often successful in reducing one or two of the major pollutants only, and usually at the expense of increased emission of one of the other pollutants. The second approach involves either a major modification to the combustor, or the application of new design principles to generate completely new combustor concepts. Naturally the extent to which a successful new heterogeneous device can be created is a function of combustor type but the advantage gained (or perhaps the goal) is the suppression of all pollutant formation in the device.

3. EFFLUENT PROCESSING. The third phase or mode of control, as for the first, utilises chemical processing. Combustion effluents can be "cleaned up" by various chemical engineering unit operations in order to actually remove the pollutant species from the bulk gases after they have been formed. Again, although such techniques already exist to enable the extraction of any pollutant, they are extremely costly. Obviously they are only applicable to stationary large scale combustor types, for which large volumes of flue gases have to be handled. This mode of control is frequently applied to Power Station boiler effluents, particulates being removed by electrostatic precipitation. Cyclones and settling chambers are examples of other kinds of particulate extraction equipment; all three such devices however possess inherent disadvantages, such as high initial cost, long separation time, additional running and maintenance costs. Examples

of gaseous pollutant processing operations include adsorption onto solids, absorption into liquids, e.g. by scrubbing and catalytic removal. The former operations are more applicable to SO_x and NO_x, as discussed by Bartok et al (67), whilst Solymosi & Kiss (68) have considered NO_x reduction by catalytic reaction with CO.

From the foregoing it can be appreciated that the second phase of control, that of combustion modification, constitutes the most satisfactory solution to the problem on a long term basis, this opinion is shared by others e.g. (69). As would be expected adoption of these methods of control requires the most research effort. Hence in the remainder of this section attention will be focussed upon pollutant suppression techniques which involve combustion modification, factors affecting the formation of the more important pollutant species though will be first considered.

2.4(a) Factors Affecting Emission of the more important Pollutants.

The complexity of pollutant minimisation technology is borne out by the fact that various species emissions are frequently conflicting functions of combustion conditions. Faced with this situation, many investigators have carried out fundamental studies on individual pollutants under carefully controlled conditions.

The rate of emission of all pollutants from a heterogeneous combustor depends on the prevalent rates of atomisation, evaporation and turbulent mixing, but usually to a greater extent on chemical reaction kinetics. Emission rates are thus dependent on the profiles of concentration, temperature and velocity throughout the combustor flowfield. The parameters to which the emission rates of individual major pollutant species are predominantly sensitive will now be discussed.

Historically, soots were the first such species to receive attention, this being understandably due to their visual prominence. The kinetics of formation and destruction of carbonaceous solids in flames has been described in outline in 2.2(d). It was shown that carbon formation in any basically premixed type of flame can be controlled by the amount of available oxygen, i.e. the combustor

air feedrate, so that significant formation would only be expected under fuel rich conditions. This is not true for the diffusion mode of droplet combustion since locally stoichiometric, i.e. high temperature flames around the drop always exist, pyrolysis of fuel vapour takes place in these flames with significant carbon being formed. For this mode of droplet combustion then the emission rate of particulates is insensitive to air feedrate or species concentrations because, once formed particulates tend to remain, destruction rates being very low indeed (14).

The sensitivity of soot formation to droplet ballistics and dynamics is reflected in the dependence of droplet mode of combustion on gas-drop relative velocity as previously explained in 2.2.(b). Sjögren (13) found that the extinction velocity of small droplets is very low so that, coupled with superior evaporation rates, this explains why the wake mode of droplet combustion and minimal soot formation is obtained from efficient atomisers which produce initial size distribution of droplets which are weighted in the lower range.

It has been found that soot formation rates are dependent on the strength of applied electrical fields (70), and also upon fuel additives (usually based on borium or manganese) (71).

Clearly more fundamental information on hydrocarbon breakdown mechanisms and kinetics; plus identification of particulate emissions in terms of particle size distributions and chemical composition, is required before a complete understanding of all the factors which influence soot emission rates is obtained. However, empirical methods have had some success in substantially reducing such emissions from gas turbine combustors.

Emission of carbon monoxide, and unburned hydrocarbons usually reflect inefficient or incomplete combustion, they both decrease with increasing flame residence time. In order to promote complete combustion rapid atomisation, evaporation and mixing are required since this assures that all fuel has sufficient time to chemically react in the flame. Homogeneous fuel/oxidant distributions throughout a heterogeneous combustor flowfield is the other important factor, under fuel lean, i.e., excess oxidant conditions extremely low emission rates of CO and UHC result. It is important to ensure that temperatures are high enough

in all parts of the combustor so that thermal quenching of hydrocarbon and carbon monoxide oxidation reactions does not occur. The effect of increasing either combustor inlet air temperature or operating pressure is to increase burning rates and hence reduce CO and UHC emissions. Probably the most important parameter is the atomiser initial size distribution since this largely governs the evaporation process and therefore fuel availability. The importance of mixing on CO emissions from a kerosine-fuelled tubular burner was demonstrated by Pompeii and Heywood (72) by means of a stochastic mixing model for the burner.

The most difficult pollutant to minimise from any combustor is nitric oxide, NO, NO_2 the other important oxide of nitrogen, is formed in only negligible proportions at temperatures above 1000 K and so will not be considered any further. Now NO is formed by the oxidation of either fuel-bound nitrogen or atmospheric free nitrogen, air being the oxidant generally used in any combustor. The chief difficulty in controlling NO is that it can be formed as a result of very efficient combustion, which is required to suppress emission of soots, CO and UHC's! The rate of formation of NO is extremely sensitive to temperature, so that it reaches a maximum under near stoichiometric fuel/oxidant proportions, and decreases under fuel lean or fuel rich conditions. As has been previously explained the rate of release of chemical energy in most flames is turbulent mixing controlled, NO production is predominantly controlled by chemical kinetics though. NO formation also increases with residence time at flame temperatures, and is dependent on local oxygen atom and molecule concentrations as examination of equations (2.49-52, 2.56-62) will verify. Very many fundamental and applied studies of NO_x formation have been made, this being no doubt attributable to the fact that its requirements for minimising usually conflict with the requirements for suppressing other pollutants.

On a fundamental level Pratt and Malte (55) investigated chemically rate-limited, fuel lean gaseous combustion of CO with moist air in a jet stirred reactor, this is a device in which extremely high turbulence mixing rates are produced by an air jet issuing into a small volume. They found that under conditions of intense turbulence and backmixing super-equilibrium concentrations of O atoms and

other reaction intermediates cause nitrous oxide N_2O to act as an important intermediate in NO_x formation, via reactions (2.56-59), for fuel-lean combustion, this mechanism being important at temperatures less than about 1800 K. Pratt and Malte found that the effect of turbulent fluctuations was to produce higher peak temperatures and hence higher NO_x levels, the maximum NO_x concentration measured in this system was 32 ppm. The study was very useful since it isolated the effects of reaction kinetics, the processes of atomisation, evaporation and mixing being absent. The energy releasing and pollutant formation reactions, unlike in one-dimensional flow systems, could not be separated because the highly stirred reactor tested was found to generate such super-equilibrium O, H and OH species concentrations. These species provided an important coupling effect because the reactor was so well mixed. Pratt and Malte (73) also succeeded in measuring O atom concentrations in such a system by direct spectroscopic techniques. Bowman et al (74) investigated the relative effects of finite turbulent mixing in a similar reactor fuelled with methane, maximum measured NO was of the order of 100 ppm. Eberius and Just (75) investigated the influence of hydrocarbon fuel structure on NO for premixed propane, ethylene and acetylene flames. They found large "overconcentrations" of NO in very fuel rich flames. In addition they found that NO formation could be reasonably separated into three classes, a) Zeldovich mechanism with equilibrium O atom concentration, b) Zeldovich mechanism with the remaining excess O atom concentration, c) other reactions involving such radicals as CH, C and C_2. Myerson (76) carried out an experimental investigation into the reduction of NO by hydrocarbon/O_2 mixtures in a flowing system of simulated combustion effluents. It was suggested that O_2 could produce free radicals such as CH and CH_2 by hydrogen abstraction of the hydrocarbon, this could then reduce the NO through reactions typified by the exothermic step:

$$CH + NO \rightleftharpoons CHO + N \quad \ldots\ldots\ldots \quad (2.73)$$

Clearly more investigations of this type are needed. All the above fundamental studies pertained to homogeneous combustion, similar studies for heterogeneous combustion have also been made. Thus Kollrack and Aceto (77) theoretically analysed a gas turbine combustor with respect to NO formation and predicted that NO levels resulting from liquid fuel combustion, as characterised by a monosized

spray (defined by SMD), were up to two orders of magnitude larger than NO levels for premixed combustion. They postulated that slower mixing could prolong radical concentration overshoots and produce temperature overshoots, thereby increasing NO production. Bracco (77) used an analysis of single droplet quasi-steady state combustion with a simple chemical reaction expression to determine rates of NO formation for hydrocarbon fuels. Larger NO formation rates are expected for the diffusion mode of droplet combustion than for the wake mode since the former flames burn at locally stoichiometric proportions i.e., high temperature, whereas the air/fuel ratio in the latter can be varied.

The last major pollutant species to be briefly considered in relation to primary variables are the oxides of sulphur SO_x. It can be appreciated from equations (2.63-71) that SO_x production rates are also dependent on oxygen atom and molecule concentrations. It appears that these two species concentrations predominantly influence SO_x formation, with residence time and flame temperatures being of less importance (79). However, when the temperature of the flame gases falls below the dewpoint of water and sulphuric acid, then corrosion occurs. Banchero and Verhoff (80) describe prediction of dewpoints from fuel gas composition and temperature by means of vapour-liquid equilibria. SO_x production is also a function of the sulphur content of the fuel and is zero for a sulphur-free fuel. Low oxygen concentrations, i.e. fuel rich combustion favours minimal SO_x formation from a sulphur containing liquid fuel.

2.4(b) Minor Combustion Modifications aimed at Suppression of Emissions.

A large number of relatively minor modifications to existing heterogeneous combustors have been proposed which attempt to reduce pollutant emissions, often with respect to only one or a few major pollutant species. Table III. summarises these modifications and indicates which pollutants are favourably affected, it is worthwhile emphasizing the fact that the effects of such modifications are not always clearly defined.

TABLE III. MINOR HETEROGENEOUS COMBUSTOR MODIFICATIONS.

Modification	Pollutant species reduced	Pollutant species increased
a) Overall fuel rich or low excess air operation.	NO_x if temperature is reduced, SO_x also.	Particulates under certain conditions, CO, UHC.
b) Overall fuel lean or high excess air operation.	NO_x if temperature is reduced, soots, CO and UHC.	SO_x
c) Change atomiser.	Possibly all species for a very fine spray.	Soots for some very fine sprays.
d) Multiple atomiser configurations, modify fuel distribution to the atomisers.	Possibly all species for very fine sprays.	
e) Water injection	Can reduce smoke, also NO_x if temperature is reduced.	CO and UHC if combustion reactions quenched.
f) Redistribute airflow in gas turbine combustors.	Difficult to assess.	Difficult to assess.
g) Increase air feed temperature.	CO and UHC.	
h) Increase operating pressure.	Usually CO and UHC.	Usually NO_x.

The effects for these minor combustion modifications then are not consistent for all species and are also a function of combustor type, there is general agreement that these modifications are inadequate if realistic reductions in pollutant emissions are to be made (82).

2.4(c) Emission Suppression by Combustor Redesign.

Various major combustion modifications, which either involve combustor redesign or new concepts altogether, have also been proposed for suppressing pollutant formation. The principles involved and potential emission performance of each of the following four different heterogeneous combustor concepts will now be discussed:

i) Recirculation combustors.

ii) Fuel prevapourizing and premixing combustors.

iii) Variable geometry combustor designs.

iv) Staged combustion configurations.

In the first class of these concepts a portion of the combustion products is transferred back to the initial spray formation region of the combustor flowfield, the process is termed recirculation and results in a dilution of the gaseous phase species. Actual definitions of the recirculation ratio parameter vary widely. The effects of recirculation on liquid phase fuel depends on the temperature of the recirculated gases, if the gases are at relatively high temperature they increase heat transfer to, and hence the evaporation rate of, the fuel droplets. Naturally, all recirculated gases will have an additional fluid dynamic effect on the liquid phase in that they will modify droplet concentrations and trajectories since the gaseous phase flow pattern will be strongly affected. Increases in flame stability and combustion performance are generally associated with the introduction of hot recirculated gases into the spray formation zone, because the preheating/"premixing" obtained results in the stable ignition of fuel and oxidant over a wider range of combustor operating conditions. Considering the process on a smaller scale, eddies of hot combustion products will promote the dispersal of, and mixing between, cool fuel vapour and oxidant eddies, in doing so the temperatures of these reactant eddies will also be raised. The net effect then is that eddies of reactant species are very rapidly prepared for ignition and subsequent combustion.

An important consequence of recirculation is that the residence time of the actual recycled gases is increased although the mean gaseous residence time is in fact reduced. Oxygen concentrations in the flame zone are also reduced by dilution due to recycled combustion products. Recirculation would also be expected to increase radical concentrations although it is extremely difficult to predict the net effects on any species with any certainty.

It has long been known that recirculation reduces flame luminosity (83) and the primary reason for this is the reduction in oxygen concentration which results. As explained in 2.2(b) the extinction velocity is a strong function of oxygen concentration and for diluent gases predominantly composed of nitrogen, i.e. combustion products, this critical velocity falls to zero at oxygen concentrations less than about 14% (13) for an unspecified fuel. Hence blue flame combustion, due to the wake mode of droplet combustion, is obtained at recirculation levels which

produce mean dilutions of oxygen corresponding to this concentration. Soot formation rates under blue flame conditions are extremely low so that recirculation has a strong effect on emission of this pollutant. Thus Kamo et al (83) noticed a critical recirculation level for their oil burner at which flame colour changed from yellow to blue and combustion noise was reduced. The effect of excess air, as well as recirculation, on smoke emissions was also studied, Fig.2.9 shows the results that were obtained for this particular burner. Another factor contributing towards the reduction in soot emissions by recirculation may well be the increased combustion radical concentrations obtained (15), clearly a more detailed understanding of hydrocarbon pyrolysis mechanisms is required.

The effect of recirculation on other gaseous pollutants will be discussed for specific heterogeneous combustor designs after the various techniques for producing recirculation have been first described. These fall into two categories, external and internally generated recirculation (with respect to the combustor casing).

The former category involves the use of external ducting and a pump to transfer combustion products from the exit to the inlet planes of the combustor. Cooling of the gases, which is undesirable, is inevitable to some extent and, due to the periphery equipment required, the combustor becomes both cumbersome and expensive to operate. Hazard (84) investigated the effects of externally-generated recirculation (EGR) on two kerosine-fuelled burners which were both swirl stabilised and water cooled, one was operated fuel rich and the other fuel lean. It was found that EGR was considerably more effective than excess air in suppressing NO formation due to the reduction in local peak temperatures obtained. Blue flame combustion was usually obtained, CO emissions were generally below 3 gm/kg fuel at firing rates above 20 lb.fuel/hr. but were approximately independent of EGR level. Unfortunately the sensitivity of NO emission to burner cooling rate was not investigated.

In the second category, recirculation within the combustion chamber is accomplished through the exploitation of fluid dynamic phenomena to generate a region of reverse flow. An obvious advantage to this approach is the high temperature of the recirculated gases which favourably increases fuel evaporation rates.

One of the earliest oil-fired burners developed to operate in the blue flame regime was the Ventres blue-flame burner (85); this was equipped with a low pressure air/oil atomiser and featured fuel evaporation within a horizontal vapouriser tube. Combustion products recirculation into the inlet of this tube was promoted by an eductor effect, and secondary air was added at various points throughout the combustor to complete the combustion. After startup, which was achieved by conventional high voltage ignition, quiet and stable blue flame operation was obtained at firing rates of 0.1 - 0.35 gph on a variety of fuels ranging from kerosine to heavy oils. Stack gas analyses of 12-14% CO_2 content, with no smoke, were consistently obtained, emission of other species was not studied. Another early, high intensity, combustor designed to run on a variety of liquid fuels under blue flame conditions is described by Reman & Verkoren (86). Feed air entered the combustion chamber via a swirl-inducing air register which, together with combustor geometry, was responsible for the establishment of a double vortex flow that generated intense recirculation in the central low pressure region of the flowfield. A wide range of fuels was again used, each was injected by means of a pressure jet atomiser, at a high injection pressure of 400 psi. High flue gas CO_2 levels were measured and no smoke formed, although high air pressure drops (≈ 20" W.G.) were required to drive the recirculation region. Heavier fuels were preheated before atomisation to keep their viscosity at or below 200cS. Pollutant emissions were not investigated for this burner.

Cooper and Marek (87) investigated two methods of achieving controlled internal recirculation by exploiting fluid dynamic properties, these were a) reverse flow within a vortex, b) attached jet entrainment. Prototype blue-flame burners were designed and constructed using each method but tests revealed that satisfactory blue flame combustion over a wide range of operating conditions could not be obtained for the vortex flow design. However, smokefree, quiet blue flame combustion was successfully demonstrated at excess air levels varying from stoichiometric to 30% and at inlet air pressures as low as 2" W.G. for the attached jet burner. Fig.2.10 shows a sectional view through this burner, it can be seen that the inlet air is deflected by a solid surface after flowing

through a slit. As a result the air jet stream is attached to the solid surface and a pressure drop across the jet layer generates entrainment of ambient gases, the phenomenon is known as the Coanda effect and was used to cause internal recirculation of combustion products. The slit width was 1/16" so that excessive inlet air pressure drops were avoided, although relatively low mixing rates were inevitable. Examination of Fig.2.10 reveals that this combustor device features a degree of both fuel prevapourisation and fuel vapour/primary air premixing before the reaction zone, combustor walls are also convection-cooled. Fuel oils were injected at firing rates of 0.65 - 1.1 gph by means of pressure jet atomiser (100 psig) and up to 75% recirculation was deduced by gas analysis. CO emissions were less than 20 ppm although fuel rich operation and other pollutant emissions were unfortunately not investigated. Instability and blow off was erratically detected at excess air levels above 30%. Two other problems encountered were cooling of the oil nozzle and slit mis-orientation due to thermal expansion, although both of these could be overcome to some extent by slight redesign. Torborg and Janssen (88) obtained further experimental performance data for this burner and in addition measured the spectral radiation characteristics of the device in the range 0.3 μ ultraviolet → 3.0 μ infra red. The relatively high background radiation detected indicated that the ultraviolet region was best suited to flame sensing. The radiation intensity was observed to decrease when either air/fuel ratio or the recirculation rate were increased. Nagey et al (89) modified Cooper and Marek's basic design and experimentally deduced the effect of recirculation ratio on NO_x and CO pollutant emissions although the fuel used was not specified. Presumably due to the resulting reduced oxygen-concentration, increased recirculation significantly reduced NO_x emissions but increased CO emissions. In terms of net pollutant emissions the optimum recirculation level was 50%, at which NO_x and CO emissions were 4 and 8 ppm respectively i.e., very low. Reeve (90) tested a prototype blue flame burner which utilised a coaxial Coanda ejector device to generate internal recirculation of combustion products, the air jet was attached to the curved surface of the ejector throat, as shown in Fig.2.11. Pressure jet atomisation of residual

fuel oil was employed and soot-free blue flame combustion was obtained over a range of air/fuel ratios; relatively high inlet air pressure losses of the order of 3 psig were needed to drive the recirculation region. Burner operating limits and radiation levels (2μ spectral region) were measured with the burner actually installed in a furnace. Initial startup invariably constitutes a transient operation problem for all recirculating type burners, preheating of the complete burner using a gaseous fuel such as propane is the solution to this difficulty which is usually adopted.

Hedley (91) investigated the influence of recirculation ratio on the volumetric combustion rate, i.e., combustion intensity, for an idealised oil fired system and concluded that:

i) For adiabatic combustion products recirculation the combustion rate is increased, optimum levels depending on extent of fuel burn out.

ii) Recirculation of non-adiabatic combustion products may increase or decrease reaction rates, depending on the extent to which they have been cooled.

In the second class of heterogeneous combustor concepts an attempt is made to transform the problem from the two phase regime to the single phase, homogeneous combustion, domain. To achieve this desirable aim the liquid fuel is invariably injected with some or all of the combustion air into a separate initial section of the combustor, where it is atomised, evaporated and mixed with oxidant as completely as possible. The reactant mixture then flows into the combustion zone of the chamber where it is burnt completely in the wake mode in a premixed, i.e., easily controlled flame. Since the air/fuel distributions are then adjustable it follows that conditions may be theoretically optimised for minimal net pollutants emission. In practice the inlet air temperatures are usually insufficient to give complete fuel prevapourisation unless the air can be preheated in some way.

It has already been mentioned, 2.4(a), that NO_x formation is a strong function of local peak temperatures. Hence, in some local flowfield region where turbulent eddies of fuel rich and fuel lean composition exist, temperature gradients will necessarily also exist. Peak temperatures along these gradients can then

correspond to the stoichiometric mixture, i.e.,maximum value. Under these peak temperature conditions NO_x formation will similarly be extremely high, and considerably greater than that for the average temperature of the overall mixture. In a prevapourising/premixing combustor configuration this situation is avoided and NO_x emissions are controllable. Emission of soots should be also avoidable and suppression of other pollutants possible. No detailed investigation of the emission characteristics of a prevapourising/premixing type of combustor appears to have been reported to date. This may be partially attributable to the fact that such combustors possess two inherent disadvantages. Firstly combustor volumes are increased, and secondly there are risks of fuel preignition, or flashback, under certain flow conditions. For gas turbine combustors these possibilities are extremely unacceptable, the occurrence of flashback in aviation types is very difficult to avoid due to the large range in both inlet temperatures and operating pressure over which they are required to function.

The aim in designing a liquid fuelled combustor to utilise variable geometry, the third concept, is to be able to vary part or all of the two phase flow pattern. If this is possible, then distributions of concentration, temperature and velocity for both phases may be also varied, hence pollutant emissions may be radically changed and possibly controlled. Varying the feed air distribution throughout the combustor is obviously one such way in which variable geometry could be used. For example, in a gas turbine combustor the amount of air supplied to the dilution zone could possibly be varied, in this way the degree of quenching achieved and hence the ratio of CO plus UHC to NO_x could be similarly varied. Nagey et al (89) postulate that variable geometry will probably be necessary to control combustor temperatures within narrow limits if their recirculation combustor (based on the work of Cooper & Marek (87)) was to be able to power vehicles which could satisfy the United States 1976 Federal Emission requirements. The use of variable geometry in practical combustors is nowever, greatly hampered by mechanical complexities, the number of combustor moving parts would be greatly increased so that reliability, not to mention costs, would inevitably suffer. Sophisticated control loops would in some cases be demanded to actuate the variable geometry, additional

components would then be required to sense the controlling parameters. Another problem that can be envisaged concerns the materials of which additional parts in general should be made in order to withstand highly turbulent, high temperature combustor environments for large periods of time. Yet another unknown is the response rate which would be expected of an actuating control system for effecting geometry modifications to combustor operation.

The fourth important concept which may be applied to design low emissions heterogeneous combustors is that of multi stage combustion, in which the heat release from the fuel is designed to take place in more than one distinct stage. Clearly many such configurations could be envisaged, of varying complexity, although relatively little attention has been focussed on this area. Low NO_x emissions can theoretically be achieved from a 2 stage combustor in which the 1st stage is operated fuel rich to control temperature and therefore NO_x formation, and in which combustion of the CO/UHC generated in the 1st stage is completed in the 2nd stage. Interstage heat removal should ensure that temperatures in the second stage do not rise to a level where significant further NO_x formation occurs. The problem with this scheme is that soots would form in the 1st stage which take extremely long residence times to burn out. Wendt et al (92) discuss a burner which utilises 2 stage heat release to minimise SO_x and NO_x. The burner is designed to run stably on gaseous fuels, part of the fuel is burnt at "moderate" excess air to avoid soot formation and the remaining fuel is injected downstream of this primary zone. A reversal of the normal pollutant formation reactions is claimed, resulting in low SO_x and NO_x emissions for clean fuels. Yamagishi et al (93) investigated a gaseous combustion scheme in which 2 stage air addition and NO fuel doping were featured.

Four combustor design techniques which could show considerable promise in progressing towards the goal of two phase combustion with minimal emissions of each major pollutant species have been discussed, it is evident though that new, improved methods of emission control will also have to be developed to reach this goal.

2.5 Combustor Modelling.

The design of heterogeneous combustion equipment in the past has generally proceeded along empirical lines, with a great deal of emphasis placed upon rigorous experimental testing that can be both excessively time consuming and expensive. More fundamental design techniques, which as a rule are employed for other types of engineering calculations, have not been developed for heterogeneous combustors because of their inherent complexity which was outlined in Section 2.2. In recent years, however, a great deal of interest has been aroused in the analytical description, or mathematical modelling, of both single and two phase combustors. Such modelling seeks to predict combustor performance parameters, from theoretical considerations, in order to aid the design process and reduce purely empirical development to a minimum. The current requirement for low pollutant emissions from combustion processes has added another dimension of complexity to combustor design. As discussed in Section 2.4 various minor and gross combustor modifications have been proposed for suppressing the amount of pollutant species emitted in the exhaust stream from various combustion chambers. The value of a mathematical model for predicting pollution characteristics, in addition to general combustion performance, can therefore be appreciated. A suitable model should aim to be capable of parametric evaluation of a particular combustion modification, with respect to the net emission of all major pollutant species, in this way optimum configurations could be quickly arrived at. An advantage to this approach is that sets of species whose respective emission indexes (kg pollutant/kg fuel) vary in conflicting manners with operating conditions could be effectively studied, provided that the model adequately described the various chemical and physical processes that were introduced in 2.2.

Ideally then an analytical model should be capable of predicting the following primary performance variables under a wide range of combustor operating conditions:

i) All major pollutant species production rates.

ii) Overall combustion efficiency.

iii) Combustor heat release rates.

iv) Combustor blowoff stability limits.

v) Combustion intensity.

vi) Overall pressure losses.

No such model exists at present which is capable of predicting all this data! However, various attempts have been made to predict one or two of these variables, in each case it was necessary to simplify the situation somewhat by identifying the processes which the relevant variable(s) depended most strongly on. These processes were then treated mathematically as accurately as possible, with varying degrees of success.

Two distinct types of modelling have emerged to date, each of which will now be discussed.

2.5(a) Chemical Reactor Models.

The underlying assumption on which this modelling technique is based is that a combustor internal flow can be approximated by a suitable network of chemical "reactors". The mean combustor flow pattern, plus variation of mixing rates throughout the flowfield, predominantly control the sequencing of the reactors in the network. As will be seen shortly the reactors normally used in any particular network are of two types, each of these represent discrete microsystems in which heat, mass and momentum are conserved.

The first type of reactor is termed stirred or zero-dimensional. Chemical and physical properties at every point throughout the reactor and within the exit stream are identical for a Perfectly Stirred Reactor (PSR). The PSR constitutes a theoretical ideal since infinitely high turbulent mixing rates are required to realise such homogeneity, typical combustor pressure losses, however, result in finite mixing rates so that a Well Stirred Reactor (WSR) is defined in which a degree of unmixedness exists. Highly stirred WSR's have characteristically good continuous ignition of fresh reactants (wide turndown) but poor burnout.

The second type of reactor is referred to as a plug-flow or one-dimensional reactor (PFR). In this device system properties are a function of one space coordinate, which is usually the mean flow direction in a continuous flow system, no cross-mixing being permitted in such a system. PFR's understandably produce

good burnout (referring again to reactors in which combustion is present) but on the other hand poor turndown, since fluid mixing rates are very low by definition.

The properties of these two extreme concepts could be illustrated by a hypothetical tracer experiment, in which a step-function concentration of a tracer substance is introduced into the feed stream to each system at some instant. The system response, i.e., subsequent tracer concentration in the system exit stream, for an ideal PSR would be an immediate exponential rise with elapsed time. The corresponding PFR response would simply be the appearance of the same step input at the exit, precisely one mean residence time later. The residence time distribution function for a reactor is the negative of the response function time derivative and can be used to estimate reactor volumes, as demonstrated for a pulverised anthracite flame by Beer and Lee (98).

It should be noted that additional classes of two, three and four (including time) dimensional reactors could also be defined, but their analysis rapidly increases in complexity.

It is considerably easier to mathematically describe chemical processes within combusting reactors of either type, than it is to similarly treat two phase fluid dynamics and other physical processes, unless of course the reactor volume in a particular network is made differentially small. An important consequence of this situation is that the chemical reactor modelling of combustion systems has inherently greater potential for predictions of the type i), ii) and iv) mentioned in the above section. More specifically, it is especially suited to the prediction of major pollutant species emission rates, since these rely heavily on the incorporation of complex chemical reaction kinetics as discussed in Section 2.2(d). Physical combustion processes are also important in this context, but to a lesser extent.

Now the species and energy balances for a stirred reactor result in a set of non-linear simultaneous equations, solution of these gives species concentrations and temperature within that reactor. In a plug flow type reactor the conventional analytical technique involves a stepwise numerical integration of the chemical

reaction rate equations along the flow path; associated problems of internal size, solution stability and computation time may be overcome by treating a PFR as a series of differentially small (ideally)WSR's. Solution of these species and energy analytical conservation expressions for each reactor in the network yields the primary model results of combustor exit flow composition and temperature. Realistic flowfield spatial species and temperature distributions are not obtained, unless of course a large number of again differentially small reactors constitute the network.

Turning now to the chemical reactor modelling of actual combustion devices, examination of available literature shows that the gas turbine has received by far the greatest attention (2). Swithenbank and Poll et al (45) developed a homogeneous model which used Odgers global kinetic rate expression (52) to enable predictions of combustion efficiency and stability limits for a 5 reactor network (2) to be made. The agreement between these predictions and corresponding experimental measurements was certainly encouraging, although the model was not capable of realistic pollutant emissions predictions. Hammond and Mellor (99) used a quasiglobal reaction kinetics scheme for predicting NO and CO emissions plus certain performance variables for a liquid hydrocarbon fuelled gas turbine; atomisation, evaporation and mixing effects were not considered and no comparison with actual measurements made. Roberts et al (100) produced a gas turbine model which included monosized spray evaporation calculations for similar predictions whilst Edelman and Economos (101) developed a considerably more detailed model formulation for emissions predictions, again for the gas turbine device. Quasi-global kinetics and turbulent mixing processes were treated for two phase flow with swirl, a comprehensive range of predictions was therefore produced. For a more detailed discussion of these and other models, for gas turbine combustors, see Poll (2).

Very little chemical reactor modelling work for other types of heterogeneous combustors has been attempted, this is surprising in view of the fact that the flowfield in some of these devices is considerably less complex than that of the gas

turbine. Bartok et al (102) considered the prediction of NO levels from a utility boiler type burner which was fired with gaseous methane. The model incorporated convective and radiative heat transfer within a simplified plug flow reactor and global combustion. Predicted trends were shown to be of the correct form. Breen, Bagwell et al (103) developed a model of NO formation in power station boilers, again for homogeneous combustion. Turbulent mixing and detailed isothermal reaction kinetics were considered for assumed flame residence times.

Two main problems are invariably encountered in stirred reactor modelling, these are:

a) The determination of a representative reactor sequence for a particular combustor flowfield.

b) The incorporation of all chemical and physical processes within each reactor. More specifically it is apparent that a rigorous analysis of a heterogeneous WSR has not been available to date.

2.5(b) Continuum Models.

The second approach to combustor modelling does not attempt to subdivide the flowfield into a series of finite zones but rather to deduce concentrations, velocities and temperatures at every point throughout the flow, hence the term continuum modelling. The analytical task then, is to solve the governing fluid dynamic (Navier Stokes, 2.2/2.2(c)) equations for turbulent, chemically reacting flows. Much useful work has been done in this field by Spalding et al (39) who have developed a technique based on the assumption that the time dependent character of turbulence may be ignored, this allows such flows to be treated in the same way as laminar ones which have spatially dependent transport properties. The differential equations to be solved are then rewritten in finite difference form for a grid of points usually non-uniformly distributed throughout the flowfield, values for velocity, temperature, etc. are computed at each point. Characteristically two-dimensional flows have been considered to date, these have been either with or without recirculation, i.e. described by partial differential equations which are mathematically parabolic or elliptic respectively. Three dimensional flows are analytically considerably more complex and the modelling of such flows

has not been attempted to date. Since the solution of two-dimensional problems by finite difference techniques requires very large amounts of computer storage and processing time, it is extremely difficult to incorporate realistic chemical reaction kinetics, as this would increase the number and complexity of governing non-linear equations. Continuum modelling then is, at present, potentially more applicable to predictions of the type iii), v) and vi) in Section 2.5 above, rather than to the prediction of pollutant emission rates. A basic problem encountered with this modelling technique concerns the grid size, which determines the number of points in the flowfield at which the finite difference equations must be solved. Clearly a minimum number in terms of adequate flow description (in relation to turbulent eddy sizes) exists, at the same time an upper limit is imposed by the available computer storage space and running time, so that an optimum must be sought.

Anasoulis et al (102) succeeded in obtaining axisymmetric solutions of the time-averaged Navier Stokes equations for two dimensional flow fields in which heterogeneous effects were included. A simple equilibrium chemical kinetics scheme was employed to characterise hydrocarbon oxidation whilst NO formation was rate-limited, to speed calculations a simple turbulence model together with a field relaxation technique was used. Predominantly aerodynamic predictions were presented, as would be expected, and limited comparison with actual experimental results made.

Continuum modelling then is primarily a fluid dynamic research tool at present, indeed it is also true that a considerable amount of time and effort is required to become familiar with the many mathematical techniques employed in such models. In the future however, one can envisage that continuum type models will provide superior combustor predictions of all kinds when more sophisticated mathematical methods and more powerful computers have been developed. The accurate description of two phase, three dimensional aerodynamic effects, with combustion reaction kinetics, should then be more feasible.

2.6 Summary.

The three important subjects of heterogeneous combustion mechanism, air pollution and mathematical modelling have then been introduced and interrelated From this discussion the following important points emerged:

1) The major variables influencing the processes of atomisation, evaporation,mixing and chemical reaction were identified.

2) Techniques for suppressing pollutants emissions were reviewed.

3) The need for a mathematical model for predicting emissions of the major pollutants from two phase combustors was emphasized.

4) Such a model should be of the chemical reactor type and include the four processes mentioned in 1), reaction kinetics being the most important.

5) No rigorous analysis of a heterogeneous WSR is available.

6) Much research work has been concentrated on the gas turbine, other devices having received relatively little attention.

CHAPTER 3.

THE BLUE FLAME HETEROGENEOUS COMBUSTOR

3.1 Introduction.

As emphasised in 2.4, 5 and 7 the gas turbine is the only heterogeneous, i.e., liquid fuelled, combustor type to have received any real attention in the way of pollutant emissions suppression or modelling. Prompted by these observations a low pollution combustor, of medium intensity and hence direct application to intermediate sized boiler equipment, was designed to enable studies of emission performance optimisation to be carried out. To eliminate the formation of particulate effluent this burner promoted blue flame combustion through the use of internal recirculation of combustion products. Using these design principles a prototype burner was constructed for actual laboratory testing; this Chapter describes the burner and fully identifies the experimental and theoretical project aims in relation to this device.

3.2 Design of the prototype Blue Flame Burner.

It was shown in 2.5(c) that recirculation of combustion products to the spray formation region of a liquid fuelled combustor not only enhances flame stability but is also responsible for the establishment of blue flame conditions in which fuel/air ratios are controllable, i.e. , Droplet Wake Mode of combustion. Sjögren has suggested that this is due to the oxygen dilution effect, which decreases the critical velocity (2.2(b)) to zero effectively (13). In order to derive blue flame conditions a burner was designed, for operation at atmospheric pressures, which featured a Coanda ejector device for the generation of a controlled amount of recirculation. The design requirements for this device were:

i) good mixing between the hot recirculated combustion products and the fuel spray and good subsequent mixing between this mixture and the feed air. The former is required for the promotion of prevapourisation and premixing, plus flame stability, whilst high species mixing rates result from the latter. Hence large turbulence dissipation rates are required, so that maximum use of the inlet air pressure energy is made.

ii) a means of controlling the degree of internal recirculation.

iii) the device should be compact to enable easy accommodation into the burner combustion chamber.

iv) physical robustness and capability of withstanding high temperatures.

Fig.3.1 shows a scaled longitudinal section through the prototype blue flame burner, which was of tubular construction. The Coanda ejector consisted of a narrow annular slit adjacent to a curved surface, the ejector throat, and was positioned in the combustion chamber as shown in Fig.3.2(i). Air is introduced to the chamber via the coanda slit and is attached in the form of a jet layer to the curved surface, attachment occurring by virtue of the Coanda effect. Since there is a pressure drop across this layer (see Fig.3.2(ii)), the jet flow has a finite entrainment appetite, this is satisfied by the internal recirculation of combustion products around the periphery of the coanda unit, as shown in Fig.3.2(i). The expected gaseous flow pattern in the remainder of the burner is also illustrated in this diagram, as is the main flame zone. Fig.3.3 presents details of the actual construction of the coanda unit, note that accurate machining of the two principal components A and B was demanded. These two components were spaced apart at a distance corresponding to the slit width S which was determined by the thickness of the brass shim interposed between the two; as will be seen in 4.5 the slit width controls the ejector entrainment ratio and hence the internal recirculation ratio. A and B were machined from mild steel and locked together by three screws; the complete ejector was held in position by two brass bushes, plus two mild steel spacing sleeves, Fig.3.1. Now there is a design criterion for the actual attachment of the air jet to the curved surface, this is (90) that the ratio of the curved surface radius to the slit width should be at least 25. Air was fed to the ejector unit from the air manifold formed by the burner head-plate, tailplate and inner/outer casings; note also that a small "reservoir" exists behind the slit for cooling purposes plus the damping of inlet air pressure fluctuations.

Fuel was injected into the combustion chamber by means of a simple pressure jet atomiser, nominally 0.05 gal/hr(psi)$^{\frac{1}{2}}$ Flow Number (0.6 gal/hr at P_f = 160 psi),

which is shown in detail in Fig.3.4. The atomiser was of relatively low fuel throughput but was used so that good atomisation, i.e. a relatively fine initial size distribution, would be achieved. Its spray angle was only 45^{o}, this minimised the undesired impingement of the spray onto metal surfaces. The atomiser was mounted on the end of a water-cooled copper fuel gun so that it would not overheat, in addition a sintered bronze fuel filter was used as a blockage-preventing precaution. The atomiser seated onto an annealed copper washer, Fig.3.4. The resulting fuel spray is first mixed with combustion products, to prepare it for ignition, and then progressively with feed air through the coanda ejector throat. In this way blue flame conditions plus a degree of prevaporisation and premixing (2.5(c)), prior to the main reaction zone downstream of the ejector, are both obtained.

It can be appreciated, from Fig.3.1, that the feed air is preheated in its passage through the air manifold, this again promotes rapid vapourisation of the fuel spray. The most important feature of the burner is the ability to control the overall flame fuel/air distributions and hence mean flame temperatures, due to the design requirement of Wake Mode droplet combustion.

Except where previously described the burner was constructed throughout of mild steel since a very large prototype lifetime was not essential. As detailed in Fig.3.1, the larger sections of the burner were fastened together by means of $\frac{3}{8}$" BSW nuts and bolts, thin asbestos sealing gaskets being interposed between each section.

3.3 A Two Stage Combustor Configuration for Minimal Emission of Pollutants.

The blue flame burner unit described in 3.2 is intended to form the first stage of a 2 stage combustor configuration for liquid fuels which is potentially capable of minimal emission of all major pollutant species. It should be possible to operate this first stage fuel-rich, as explained in 3.2, so that prevailing temperatures in this unit could be substantially reduced, without the usual formation of soots, due to the blue flame operation. Since NO_x formation is so strongly dependent on peak temperature, see 2.5(a), the emissions of this pollutant species from the first stage should be low. SO_x should be similarly controlled

because it is predominantly sensitive to local oxygen concentration. Combustion is then completed in the second stage with secondary air where the CO and UHC, evolved as a result of the first stage fuel-rich operation, are burned off. Intermediate heat removal between the two stages is employed to reduce the second stage flame temperature to levels where further NO_x formation is small. Emissions of all the major pollutant species from the 2 stage combustor should then be suppressed, provided that complete combustion of UHC's etc. is obtainable in the second stage. As explained in 2.5(c) the 2 stage combustion idea is certainly not new, although the concept of using a blue flame burner for the first stage perhaps is. The 2 stage combustor described above is illustrated schematically in Fig.3.5, it is anticipated that control of the 2 stage device could be effected by means of a peak-seeking control system with an infra red detector on the second stage to sense overall stoichiometric operation.

This project focusses its attention upon the blue flame burner, i.e., the first stage unit, since the characteristics of this device largely control the overall combustor performance with respect to pollutant formation. The succeeding stages of heat removal and final burnout are considered to be relatively conventional operations and to require less attention at present.

3.4 Modelling of the Blue Flame Burner (BFB).

The value of an analytical model for predicting the emission performance of heterogeneous combustors was clearly demonstrated in section 2.6. For the actual optimisation of the BFB emission performance it was therefore decided to develop such a mathematical model. The model was required to be applicable to this particular combustor, but to proceed preferably along general lines to enable application to other liquid fuelled combustor types.

The prediction of soot formation for the BFB is conveniently not required by definition. As mentioned in 2.2.(d) the reaction kinetics for CO and NO_x formation are reasonably well known, hence a primary requirement of the model was that it should be capable of prediction of these two species; since the emission index of each of these species frequently vary in a conflicting manner (2.5(a)), this should provide a good test for the model. The reaction kinetics describing SO_x formation

are not widely agreed upon, so that the burner was run on kerosine since this fuel is usually relatively sulphur-free.

The BFB should also be a convenient device to model since its expected flow pattern, 3.2, is relatively simple; this is certainly true when compared with that of a gas turbine, 2.4(a). The BFB flow pattern in fact is largely two-dimensional.

As concluded in 2.7, a WSR submodel in which evaporation, turbulent mixing and complex reaction kinetics are all incorporated is required. The stirred reactor network should also include internal recirculation effects, hence a submodel for the coanda ejector unit entrainment parameter is needed.

3.5 Experimental Measurements Required.

Kerosine, then, has been selected as a test fuel for the BFB due to modelling considerations, use of this fuel has a second advantage in that it can be atomised extremely efficiently, this being due to its favourable physical properties. Hence sprays of relatively fine initial size distribution should be produced by the pressure jet atomiser, this is desirable from a blue flame combustion standpoint due to superior evaporation rates plus lower extinction velocities, 2.2(b). Testing of the prototype burner, with kerosine as the fuel, is hence required in order to ascertain practical blue flame operating limits; in addition, the necessary air pressure drop to drive the burner needs determining. Clearly the prototype should also be test-run on lower grade fuels.

In order to test the emission performance of the BFB it was decided to measure the composition of its exit flow with respect to CO and NO_x over a range of operating conditions. It would then be possible to directly compare the experimentally-determined values for emission of these two major pollutant species, with the corresponding predictions of the mathematical model for these species. This type of critical comparison is considered to be essential to the development of realistic models.

A second type of experimental measurement is clearly necessitated, this being that of model input information. Firstly, the burner flow pattern requires detailed experimental investigation, so that the suitable stirred reactor network

can be confirmed for this flowfield. Further to this it is apparent that any measurements which could assist the characterisation of flowfield turbulent mixing rates would be extremely valuable, 2.2(c), this would certainly aid the selection of reactor types (i.e. WSR or PFR) needed throughout the network. Secondly the entrainment characteristic of the Coanda ejector unit, and hence the combustor internal recirculation characteristic, requires actual measurement. Also the atomiser fuel mass flow/injection pressure calibration requires determination. The other important atomiser characteristic to be measured, for a range of operating conditions, is the initial droplet size distribution produced.

3.6 Summary.

1. A blue flame burner (BFB) has been designed and constructed.
2. The BFB is intended to form the first stage of a 2 stage heat release combustor which is potentially capable of minimal emission of all major pollutant species.
3. The BFB stage forms the subject of this study since the characteristics of this device largely control the overall emission performance of the 2 stage configuration.
4. It is proposed to develop a mathematical model, of the chemical reactor type, for this burner. Primary predictions required are BFB CO and NO_x emissions.
5. The experimental characterisation of BFB exit flow composition, with respect to CO and NO_x, is required.
6. It is intended to compare the results of 4. and 5.
7. Various additional experimental measurements are required as model input information, these have been identified.

Project objectives have thus been defined more fully.

CHAPTER 4.

THEORY.

4.1 Introduction.

This Chapter presents the basic stirred reactor theory which, as outlined in 2.6(b) and 3.4, is required for the construction of a mathematical model of any heterogeneous combustor to enable the prediction of pollutant emission performance. Whilst this analysis, given in 4.2, is of completely general application, the succeeding analyses for the blue flame burner (BFB) spray atomisation and evaporation processes are unavoidably more specific, 4.3 and 4.4 respectively. In addition, a simple model for the coanda ejector entrainment performance is given 4.5, this enables the prediction of burner internal recirculation levels to be made.

4.2 Heterogeneous Well Stirred Reactor Analysis.

In the WSR analysis the liquid phase is considered as being present in the reactor in the form of a spray of fuel droplets, around which the bulk gaseous phase coexists. Contrary to usual practice the volume of the reactor occupied by the liquid phase is assumed to be finite even though it is small due to relative densities. This allows the development of a more rigorous analysis which is capable of general application, and in particular to the case of a heterogeneous combustor primary WSR, in which very dense fuel sprays may be present. It should be appreciated that for most reactors the ratio of gaseous phase to liquid phase volume is very high indeed.

Although the three processes of evaporation, mixing and chemical reaction usually proceed more or less simultaneously in any combustor, 2.2, it is convenient to formulate the analysis so that they are considered to occur in any STEADY STATE reactor in series, which seems reasonable physically. This starting point enables the evaluation of reactor gaseous phase species concentrations after the evaporation and mixing processes, these "Intermediate Concentrations" then effectively define the homogeneous 'feed' to the chemical reaction process, i.e. PSR type calculations. The combustion scheme is shown in Table IV below, the oxidant being assumed to

TABLE IV. WSR COMBUSTION SCHEME

(1)	Liquid fuel	→	Evaporated fuel (unmixed)	EVAPORATION
(2)	Evaporated fuel (unmixed)	→	Evaporated fuel (mixed)	MIXING
	Oxygen (unmixed)	→	Oxygen (mixed)	
	Nitrogen (unmixed)	→	Nitrogen (mixed)	
(3)	Evaporated fuel (mixed) + Oxygen (mixed)	→	Combustion products	CHEMICAL REACTION
	Oxygen (mixed) + Nitrogen (mixed)			

to consist of oxygen and nitrogen i.e., air. It is important to consider the mixing between these two components of air since NO_x pollutant predictions are required; the intimate mixing of the oxygen and vapourised fuel species on a molecular scale is a prerequisite of combustion.

The feedstream to, or product stream from, any reactor is assumed to be composed of any or all of the eight general species in the above scheme - with only fuel existing in the liquid phase. This is important as the analysis then becomes completely general, enabling application to any reactor in a particular network. Fig.4.1 shows the composition of the general two phase steady state reactor, note that the liquid phase is drawn coalesced in the interests of simplicity. Transfer from the liquid phase to the gaseous phase is provided by a mean fuel evaporation rate $\dot{F}E$; the rest of the variables to be used are fully explained in the Nomenclature The analysis also assumes that the product stream conditions are identical with those in the reactor and that the mean residence time of each phase in the reactor is the same. The latter assumption is theoretically incompatible with the existence of a relative velocity between the bulk gases and the fuel droplets, although it greatly simplifies both the WSR analysis and the calculation of fuel distribution around any particular reactor network. This assumption is employed as a first approximation in this study but a refinement could be made to incorporate unequal phase residence time effects.

The other assumption made is:

Rate of formation of mixed fluid = (mass of unmixed fluid)/τ_D,

this rate being considered to be the same for each of the three species in (2) listed in Table IV. τ_D is the characteristic turbulence dissipation time, which may be shown (2.2(c)), to be related to the system geometry and operating conditions.

$$\text{Total reactor mass} = m + \varepsilon \quad \ldots\ldots\ldots \quad (4.1)$$

$$\therefore \text{Total reactor volume} = \frac{m}{\rho_G} + \frac{\varepsilon}{\rho_L} = V_G + V_L = V$$

The reactor mean residence time is defined using exit conditions, since these are representative of reactor conditions, as:

$$\tau_S = \frac{m}{\dot{m}_2} = \frac{\varepsilon}{\dot{\varepsilon}_2} \quad \ldots\ldots\ldots \quad (4.2)$$

Using (4.1)

$$\tau_S = \frac{V}{\left(\frac{\dot{m}_2}{\rho_G} + \frac{\dot{\varepsilon}_2}{\rho_L}\right)} \quad \ldots\ldots\ldots \quad (4.3)$$

Gaseous phase mass balance.

$$\dot{m}_1 - \dot{m}_2 + \dot{FE} = \frac{dm}{dt} \quad \ldots\ldots\ldots \quad (4.4)$$

Liquid phase mass balance.

$$\dot{\varepsilon}_1 - \dot{\varepsilon}_2 - \dot{FE} = \frac{d\varepsilon}{dt} \quad \ldots\ldots\ldots \quad (4.5)$$

Note: $\dot{m}_1 < \dot{m}_2$, $\dot{\varepsilon}_1 > \dot{\varepsilon}_2$

Mass balance on unmixed fluid in the gaseous phase.

$$\frac{d(m\phi_u)}{dt} = \dot{m}_1 \phi_u' - \dot{m}_2 \phi_u - \frac{m\phi_u}{\tau_D} + \dot{FE}$$

i.e. all evaporated liquid enters the unmixed fluid before mixing.

$$\therefore m\frac{d\phi_u}{dt} + \phi_u \frac{dm}{dt} = \dot{m}_1 \phi_u' - \dot{m}_2 \phi_u - \frac{m\phi_u}{\tau_D} + \dot{FE} \quad \ldots\ldots\ldots \quad (4.6)$$

Subtracting ϕ_ux(4.4) from (4.6):

$$m\frac{d\phi_u}{dt} = \dot{m}_1(\phi_u' - \phi_u) - \frac{m\phi_u}{\tau_D} + \dot{FE}(1 - \phi_u)$$

Now, at steady state $\frac{dm}{dt} = \frac{d\phi_u}{dt} = 0$ so that:

$$\frac{m}{\dot{m}_1} = \frac{m}{\dot{m}_2 - F\dot{E}} = \frac{m/\dot{m}_2}{1 - F\dot{E}/\dot{m}_2} = \frac{\tau_S}{(1-\beta)} \qquad \ldots\ldots\ldots \quad (4.7)$$

where, $\beta = F\dot{E}/\dot{m}_2$ (dimensionless) $\qquad \ldots\ldots\ldots \quad (4.8)$

Hence:

$$0 = \frac{(\phi_u'-\phi_u)(1-\beta)}{\tau_S} - \frac{\phi_u}{\tau_D} + \frac{\beta}{\tau_S}(1 - \phi_u)$$

$$\therefore \quad \phi_u = \frac{\phi_u'(1-\beta) + \beta}{1 + \tau_{SD}} \qquad \ldots\ldots\ldots \quad (4.9)$$

where,

$\tau_{SD} = \tau_S/\tau_D$ = unmixedness parameter (2.2(c)).

For given τ_{SD}, $F\dot{E}$ and feed conditions then, (4.9) and (2.22) define the proportion of the steady state reactor gaseous phase which is unmixed (final reactor value), in practice this will be small for all but inefficient reactors.

Composition of feed stream for fuel vapour reactant:

$$\dot{m}_1 C_f' = \dot{m}_1\phi_u'\omega_f' + \dot{m}_1(1 - \phi_u')\gamma_f'$$

$$\therefore \quad C_f' = \phi_u'\omega_f' + (1-\phi_u')\gamma_f' \qquad \ldots\ldots\ldots \quad (4.10)$$

Similarly for feed stream oxygen, nitrogen and also for any other general combustion species (subscript cs and only existing in the mixed gaseous phase):

$$C'_{O_2} = \phi_u'\omega'_{O_2} + (1 - \phi_u')\gamma'_{O_2} \qquad \ldots\ldots\ldots \quad (4.11)$$

$$C'_{N_2} = \phi_u'\omega'_{N_2} + (1 - \phi_u')\gamma'_{N_2} \qquad \ldots\ldots\ldots \quad (4.12)$$

$$C'_{cs} = (1 - \phi_u')\gamma'_{cs} \qquad \ldots\ldots\ldots \quad (4.13)$$

Analogously the reactor composition may be expressed:

$$\left.\begin{aligned} C_f^* &= \phi_u\omega_f + (1 - \phi_u)\gamma_f^* \\ C^*_{O_2} &= \phi_u\omega_{O_2} + (1 - \phi_u)\gamma^*_{O_2} \\ C^*_{N_2} &= \phi_u\omega_{N_2} + (1 - \phi_u)\gamma^*_{N_2} \\ C^*_{cs} &= (1 - \phi_u)\gamma^*_{cs} \end{aligned}\right\} \qquad \ldots\ldots\ldots \quad (4.14)$$

[NB (i) the superscript * denotes intermediate values i.e. before chemical reaction.

(ii) $\omega'_f + \omega'_{O_2} + \omega'_{N_2} = \omega_f + \omega_{O_2} + \omega_{N_2} = 1$]

Unmixed fuel vapour mass balance.

$$\frac{d(m\phi_u \omega_f)}{dt} = \dot{m}_1 \phi_u' \omega_f' - \dot{m}_2 \phi_u \omega_f + \dot{FE} - \frac{m\phi_u \omega_f}{\tau_D} \quad \ldots\ldots\ldots \quad (4.15)$$

But, L.H.S. of (4.15)

$$= m\phi_u \frac{d\omega_f}{dt} + m\omega_f \frac{d\phi_u}{dt} + \phi_u \omega_f \frac{dm}{dt} = 0$$

since $\frac{d\omega_f}{dt} = 0$ also.

$$\therefore \quad 0 = (1-\beta)\,\phi_u'\omega_f' - \phi_u\omega_f + \beta - \phi_u\omega_f\,\tau_{SD}$$

$$\therefore \quad \omega_f = \frac{\phi_u'(1-\beta)\,\omega_f' + \beta}{\phi_u(1+\tau_{SD})} = \frac{\phi_u'(1-\beta)\,\omega_f' + \beta}{\phi_u'(1-\beta) + \beta} \quad \ldots\ldots\ldots \quad (4.16)$$

using (4.9)

Unmixed oxygen mass balance.

$$\frac{d(m\phi_u \omega_{O_2})}{dt} = \dot{m}_1 \phi_u' \omega_{O_2}' - \dot{m}_2 \phi_u \omega_{O_2} - \frac{m\phi_u \omega_{O_2}}{\tau_D} \quad \ldots\ldots\ldots \quad (4.17)$$

Hence using the above technique and $\frac{d\omega_{O_2}}{dt} = 0$:

$$\omega_{O_2} = \frac{\phi_u'(1-\beta)\,\omega_{O_2}'}{\phi_u'(1-\beta) + \beta} \quad \ldots\ldots\ldots \quad (4.18)$$

Unmixed nitrogen mass balance

$$\frac{d(m\phi_u \omega_{N_2})}{dt} = \dot{m}_1\phi_u'\omega_{N_2}' - \dot{m}_2\phi_u\omega_{N_2} - \frac{m\phi_u \omega_{N_2}}{\tau_D} \quad \ldots\ldots\ldots \quad (4.19)$$

So that:

$$\omega_{N_2} = \frac{\phi_u'(1-\beta)\,\omega_{N_2}'}{\phi_u'(1-\beta) + \beta} \quad \ldots\ldots\ldots \quad (4.20)$$

In order to derive the required expressions for the intermediate concentrations of the mixed reactants and other combustion species, mass balances are now performed on the mixed portion of the reactor gaseous phase.

Mixed fuel vapour mass balance.

$$\frac{d(m(1-\phi_u)\gamma_f^*)}{dt} = \dot{m}_1(1-\phi_u')\gamma_f' - \dot{m}_2(1-\phi_u)\gamma_f^* + \frac{m\phi_u\omega_f}{\tau_D} \quad \ldots\ldots\ldots \quad (4.21)$$

Expanding the L.H.S. of (4.21) and using $\frac{d\gamma_f^*}{dt} = 0$:

$$0 = (1-\beta)(1-\phi_u')\gamma_f' - (1-\phi_u)\gamma_f^* + \phi_u\omega_f\tau_{SD}$$

$$\therefore \quad \gamma_f^* = \frac{(1-\beta)(1-\phi_u')\gamma_f' + \phi_u\omega_f\tau_{SD}}{(1-\phi_u)}$$

Hence, using (4.9) and (4.16) :

$$\gamma_f^* = \frac{(1-\beta)(1-\phi_u')(1+\tau_{SD})\gamma_f' + (\phi_u'(1-\beta)+\beta)\left[\frac{\phi_u'(1-\beta)\omega_f'+\beta}{\phi_u'(1-\beta)+\beta}\right]\tau_{SD}}{(1+\tau_{SD}) - \phi_u'(1-\beta) - \beta}$$

$$\therefore \quad \gamma_f^* = \frac{(1-\beta)(1-\phi_u')(1+\tau_{SD})\gamma_f' + \tau_{SD}(\phi_u'(1-\beta)\omega_f' + \beta)}{(1-\beta)(1-\phi_u') + \tau_{SD}} \quad \ldots\ldots\ldots \quad (4.22)$$

Mixed oxygen mass balance.

$$\frac{d(m(1-\phi_u)\gamma^*_{O_2})}{dt} = \dot{m}_1(1-\phi_u')\gamma'_{O_2} - \dot{m}_2(1-\phi_u)\gamma^*_{O_2} + \frac{m\phi_u\omega_{O_2}}{\tau_D} \quad \ldots\ldots \quad (4.23)$$

Using $\frac{d\gamma^*_{O_2}}{dt} = 0$, a similar expression is obtained:

$$\gamma^*_{O_2} = \frac{(1-\beta)(1-\phi_u')(1+\tau_{SD})\gamma'_{O_2} + \tau_{SD}\phi_u'(1-\beta)\omega'_{O_2}}{(1-\beta)(1-\phi_u') + \tau_{SD}} \quad \ldots\ldots \quad (4.24)$$

Mixed nitrogen mass balance.

$$\frac{d(m(1-\phi_u)\gamma^*_{N_2})}{dt} = \dot{m}_1(1-\phi_u')\gamma'_{N_2} - \dot{m}_2(1-\phi_u)\gamma^*_{N_2} + \frac{m\phi_u\omega_{N_2}}{\tau_D} \quad \ldots\ldots \quad (4.25)$$

So that:

$$\gamma^*_{N_2} = \frac{(1-\beta)(1-\phi_u')(1+\tau_{SD})\gamma'_{N_2} + \tau_{SD}\phi_u(1-\beta)\omega'_{N_2}}{(1-\beta)(1-\phi_u') + \tau_{SD}} \quad \ldots\ldots \quad (4.26)$$

General combustion (non reactant) species mass balance.

$$\frac{d(m(1-\phi_u)\gamma_{cs}^*)}{dt} = \dot{m}_1(1-\phi_u')\gamma'_{cs} - \dot{m}_2(1-\phi_u)\gamma_{cs}^* \quad \ldots\ldots\ldots \quad (4.27)$$

$$\therefore \quad \gamma_{cs}^* = \frac{(1-\beta)(1-\phi_u')(1+\tau_{SD})\gamma'_{cs}}{(1-\beta)(1-\phi_u') + \tau_{SD}} \quad \ldots\ldots\ldots \quad (4.28)$$

Equations (4.22,24,26,28) thus define the required homogeneous feed prior to chemical reaction. Examining these:

A - For $\phi_u' = 1$

i.e. a feed of unmixed reactants only.

$$\gamma_f^* = (1-\beta)\omega_f' + \beta$$

$$\gamma^*_{O_2} = (1-\beta)\omega_{O_2}' \qquad \text{and} \qquad \gamma^*_{N_2} = (1-\beta)\omega_{N_2}'$$

$$\gamma^*_{cs} = 0$$

B - For $\phi_u' < 1$

i.e. As; $\tau_{SD} \to 0$, $\therefore$ $\left|\begin{array}{l}\tau_S \to 0\\ \tau_D \to \infty\end{array}\right.$:

$$\gamma^*_f \to \gamma_f'$$

$$\gamma^*_{O_2} \to \gamma'_{O_2}, \quad \gamma^*_{N_2} \to \gamma'_{N_2}$$

$$\gamma^*_{cs} \to \gamma'_{cs}$$

or ; $\tau_{SD} \to \infty$, $\therefore$ $\left|\begin{array}{l}\tau_S \to \infty\\ \tau_D \to 0\end{array}\right.$:

$$\gamma^*_f \to (1-\beta)C_f' + \beta$$

$$\gamma^*_{O_2} \to (1-\beta)C'_{O_2},$$

$$\gamma^*_{N_2} \to (1-\beta)C'_{N_2}$$

$$\gamma^*_{cs} \to (1-\beta)C'_{cs}$$

Having defined the 'intermediate' composition of the gaseous phase, i.e. after the evaporation and mixing processes, two further balances can be made in order to characterise the reactor gaseous phase final composition, i.e. after the final chemical reaction process. These balances are the familiar rate-

limited PSR governing equations, in modified form, although again for steady state. During the chemical reaction process the mixed gaseous phase concentrations γ^* change to give the final values γ; the unmixed gaseous phase concentrations ω naturally are unaltered although these species do contribute to the mean gaseous physical properties of i) enthalpy, ii) specific heat, iii) density and iv) molecular weight.

Chemical reaction, mixed species mass balance.

$$\frac{\dot{m}_2}{\rho_G V W_i}(\gamma_i^* - \gamma_i)(1 - \phi_u) + \dot{p}_i = 0 \quad \ldots\ldots\ldots \quad (4.29)$$

for i = 1, MT . MT = Total number of mixed gaseous species.

Chemical reaction, gaseous phase energy balance.

$$\frac{\dot{m}_2}{\rho_G V W_i} \sum_{i=1}^{MT} (\gamma^*_i h^*_i - \gamma_i h_i)(1-\phi_u) + \frac{\dot{m}_2}{\rho_G V W_i} \sum_{i=MT+1}^{NT} \omega_i (h^*_i - h_i)\phi_u = \dot{H}_L \quad (4.30)$$

$\dot{H}_L$ = 0 for adiabatic operation.

The species chemical kinetic production/destruction rate is:

$$\dot{p}_i = \sum_{j=1}^{NR} (\alpha_{ij} - \delta_{ij})(F_j - B_j) \quad \ldots\ldots\ldots \quad (4.31)$$

Now the forward and backward (respectively) reaction rates are related to the reactor gaseous phase (mixed) species concentrations by the expressions:

$$F_j = f_j X_j^{\sigma_j} \prod_{i=1}^{MT} \left(\frac{\rho_G}{W_i}(1-\phi_u)\gamma_i\right)^{\delta_{ij}} \quad \ldots\ldots\ldots \quad (4.32)$$

$$B_j = b_j X_j^{\sigma_j} \prod_{i=1}^{MT} \left(\frac{\rho_G}{W_i}(1-\phi_u)\gamma_i\right)^{\alpha_{ij}} \quad \ldots\ldots\ldots \quad (4.33)$$

where X_j is a third body in a dissociation reaction:

$$X_j = \sum_{i=1}^{MT} d_{ij} \left((1-\phi_u) \frac{\gamma_i}{W_i} \right) \quad \ldots\ldots\ldots \quad (4.34)$$

The forward reaction rate constants are defined as:

$$f_j = A_j T^{n_j} \exp(-E_j/RT_2) \quad \ldots\ldots\ldots \quad (4.35)$$

The backward reaction rate constants are simultaneously fixed by means of the reaction equilibrium constants:

$$b_j = f_j K_j \sum_{i=1}^{MT} (\delta_{ij} - \alpha_{ij}) \quad \ldots\ldots\ldots \quad (4.36)$$

$$K_j = K_j^p (R'T_2) \quad \ldots\ldots\ldots \quad (4.37)$$

$$K_j^p = \exp(-\Delta F_j/RT_2) \quad \ldots\ldots\ldots \quad (4.38)$$

$$= \exp\left[- \sum_{i=1}^{MT} (\alpha_{ij} - \delta_{ij}) F_i^o/RT_2 \right] \quad \ldots\ldots\ldots \quad (4.39)$$

The system of equations is completed with the equation of state:

$$P = \rho_G \frac{R'}{W} T_2 = \rho_G R'T_2 \sum_{i=1}^{MT} \left((1-\phi_u) \frac{\gamma_i}{W_i} \right) + \rho_G R'T_2 \sum_{i=MT+1}^{NT} \left(\phi_u \frac{\omega_i}{W_i} \right) \ldots\ldots \quad (4.40)$$

Now the thermal properties of each species are described by means of the general polynomials:

$$C_p/R = a_1 + a_2 T + a_3 T^2 + a_4 T^3 + a_5 T^4 \quad \ldots\ldots\ldots \quad (4.41)$$

$$H_T/RT = a_1 + \frac{a_2}{2} T + \frac{a_3}{3} T^2 + \frac{a_4}{4} T^3 + \frac{a_5}{5} T^4 + \frac{a_6}{T} \quad \ldots\ldots\ldots \quad (4.42)$$

$$F_T/RT = a_1(1-\ln T) - \frac{a_2}{2} T - \frac{a_3}{6} T^2 - \frac{a_4}{12} T^3 - \frac{a_5}{20} T^4 + \frac{a_6}{T} - a_7 \ldots\ldots \quad (4.43)$$

, the coefficients for a large range of species are presented by McBride et al (110), $a_{1\to7}$ for each species being given for each of the two temperature ranges 300→1000K and 1000→5000K.

The final reactor gaseous phase composition has thus been defined, this may also be expressed in terms of final overall concentrations:

$$C_f = \phi_u \omega_f + (1 - \phi_u)\gamma_f \quad \ldots\ldots\ldots \quad (4.44)$$

$$C_{O_2} = \phi_u \omega_{O_2} + (1 - \phi_u)\gamma_{O_2} \quad \ldots\ldots\ldots \quad (4.45)$$

$$C_{N_2} = \phi_u \omega_{N_2} + (1 - \phi_u)\gamma_{N_2} \quad \ldots\ldots\ldots \quad (4.46)$$

$$C_{cs} = (1 - \phi_u)\gamma_{cs} \quad \ldots\ldots\ldots \quad (4.47)$$

The complete system of equations (4.1→47) characterises the general heterogeneous partially stirred reactor, WSR, for steady state operation. Application is readily extended to the homogeneous case by specifying:

$$\dot{\varepsilon}_1 = \dot{\varepsilon}_2 = \beta = 0$$

$$V = V_G$$

4.2(a) WSR Solution Technique.

Equations (4.1-47) constitute a highly non linear set of equations, due very largely to the exponential dependence of chemical reaction rates upon temperature, (4.35,38). In addition $\dot{F}E$ is a complex function of temperature T_2 and staytime τ_S, as will be shown in 4.4. Hence the WSR governing equations have to be solved iteratively, as Fig.4.2 illustrates. This technique is based on the numerical method of PSR solution developed by Osgerby (115), in which a Newton Raphson correction procedure is employed to converge on the PSR system solution, from an initial guess. Before this WSR solution technique can be used it is necessary to supply a reaction kinetic scheme, rate data, thermodynamic data plus the prevailing feed conditions. Fig.4.2 also shows the initialisation steps required by the technique, note also that an equilibrium composition calculation constitutes the initial guess. Details of the equilibrium calculation are given in Appendix E.

An inherent advantage of the WSR formulation presented above, 4.2, is that the already developed Newton Raphson mathematical procedure of Osgerby can be incorporated, after a certain amount of modification which is outlined in Chapter 7. Further details of the actual Newton Raphson procedure are given in Reference (115).

4.2(b) PFR Formulation.

As described in 2.5(a) a PFR may be reasonably approximated by a series of 10 WSRs in order to simulate the characteristic burnout produced by this type of reactor. The first WSR "subvolume" may be solved using the iteration technique just described whilst the second and subsequent subvolumes may be solved in the same way but with a modified initial guess. The new initial guess is provided by a linear extrapolation for T and γ_i from the previous subvolume converged values.

4.3 Pressure Jet Atomiser Characteristics.

As explained in 2.2(a), Bowen and Joyce (6) obtained a set of empirical correlations for describing the Rosin Rammler Initial Size Distribution (ISD) characteristic for any given pressure jet atomiser and injection pressure P_f. A modified version of these correlations was employed for the prediction of atomiser ISD in the blue flame burner mathematical model.

Using the same notation as in 2.2(a) :

$$\bar{x} = \frac{k}{P_f^{(0.3358 - 0.02427\ F)}} \quad \ldots\ldots\ldots \quad (4.48)$$

$$\log_{10} k = 2.7008 + 0.2162\ F \quad \ldots\ldots\ldots \quad (4.49)$$

$$SMD = \frac{k}{P_f^{(0.3712 - 0.02589\ F)}} \quad \ldots\ldots\ldots \quad (4.50)$$

As discussed in Chapter 7 the values of $\bar{x}$ predicted by (4.48) did not correspond to the experimentally determined, (5.7), value. The value of the ratio $(\bar{x}/SMD)$ as predicted by(4.48-50) did correspond to the experimentally-deduced value however. In view of this, the above correlations were adjusted so that they predicted the measured Rosin Rammler parameters (superscripted variables):

$$\left.\begin{aligned} \bar{x}'' &= \bar{x}\ (0.6119 - 0.011\ P_f) \\ SMD'' &= SMD(0.6119 - 0.011\ P_f) \end{aligned}\right\} \quad \ldots\ldots\ldots \quad (4.51)$$

Now, the Rosin Rammler exponent is given by the equation:

$$\frac{\bar{x}''}{SMD''} = \frac{\bar{x}}{SMD} = \Gamma(1 - 1/n) = \frac{\Gamma(2-1/n)}{(1-1/n)} \quad \ldots\ldots\ldots \quad (4.52)$$

since the Gamma Function $\Gamma(z)$, which is defined mathematically;

$$\Gamma(z) \qquad \int_0^\infty t^{z-1} e^{-t} dt \qquad \ldots\ldots\ldots \qquad (4.53)$$

has the following recurrence relation:

$$\Gamma(z+1) = z\Gamma(z) = z! \qquad (z > 0) \qquad \ldots\ldots\ldots \qquad (4.54)$$

Now, for the following range of z and hence n, the Gamma Function may be conveniently fitted by the polynomial:

$$\Gamma(z+1) = 1 + a_1 z + a_2 z^2 + a_3 z^3 + a_4 z^4 + a_5 z^5 \quad \ldots\ldots\ldots \qquad (4.55)$$

$$a_1 = -0.5749$$
$$a_2 = 0.9512$$
$$a_3 = -0.6999$$
$$a_4 = 0.4246$$
$$a_5 = -0.1011$$

for $z = (1 - 1/n)$ and $0 \leq z \leq 1$ i.e. $n \geq 1$

the polynomial being obtained from Hastings (118). For given $\bar{x}$", SMD" then, equation (4.52) may be iteratively solved for n.

Before the above correlations can be used it is first necessary to know F as $f(P_f)$ as accurately as possible for the BFB atomiser, the experimental determination of this function is fully covered in (5.6).

Fig. 4.3 shows the ISD characteristic for this atomiser which is predicted using equations (4.48-55); the volume fraction of the spray in each of 20 size intervals of 12μ is given for a range of fuel injection pressures. Thus the size distribution of the fuel spray generated by the burner atomiser can be directly computed and used as input to the evaporation calculations.

4.3(a) Spray Initial Mean Velocity.

Equation (2.9) may be used to calculate $V_s(o)$, the spray initial mean velocity, for a pressure jet atomiser providing that C_v the coefficient of discharge at any P_f is known. Tipler (119) made a series of measurements of C_v for a range of these atomisers with various orifice diameters d_o, Fig.4.4. Now d_o for the blue

flame burner atomiser is 0.008 inches, i.e. outside the range of Tipler's data, as Fig.4.4 shows this data was extrapolated (by means of a crossplot) to this value of d_o. The extrapolated curve was fitted by the simple expression:

$$C_v = 0.0564 + 0.0117\, P_f^{\frac{1}{2}} + 0.00312\, P_f \quad \ldots\ldots\ldots \quad (4.56)$$

$$(0 \leq P_f \leq 200 \text{ psig})$$

For kerosine fuel of density 790 kg/m^3, equation (2.9) becomes:

$$V_s(o) = 4.179\, C_v (P_f)^{\frac{1}{2}}$$

Now the cone angle of the atomiser is 45^o, as illustrated in Fig.4.5, so that the mean droplet trajectory angle θ is equal to 11.25^o. Hence the final expression for $V_s(o)$:

$$V_s(o) = 4.179\, C_v (P_f)^{\frac{1}{2}} \cos\theta = 4.098\, C_v (P_f)^{\frac{1}{2}} \quad \ldots\ldots\ldots \quad (4.57)$$

Hence for any P_f the corresponding $V_s(o)$ is readily computed for use in the time dependent evaporation calculations. The actual atomisation process is assumed to be instantaneous.

4.4 Evaporation Theory.

The basic requirement of any theory which attempts to describe the evaporation rate of a multisize fuel spray is for an expression which describes the evaporation rate of a droplet of given diameter. Virtually all the expressions proposed to date have been for the Diffusion Mode rather than the Wake Mode of droplet combustion.

Probert (18) was the first investigator to assume that the evaporation rate $\dot{m}_E$ is proportional to droplet diameter, he derived the well known d^2 law which has been widely employed in combustion models for monosize sprays and frequently validated experimentally, e.g. (19). Many of the droplet combustion models that have been formulated to date have been based on the spherico-symmetric approach for steady state isobaric conditions and single component spherical fuel droplets, these models have been reviewed by Williams (20). Fig.4.6 illustrates the gaseous/liquid phase transfer processes considered in such an approach. The droplet evaporates and acts as a source of vapour, since the oxidant and fuel are initially separate the fuel vapour and oxidant burn in a molecular diffusion-

controlled flame surrounding the vapour film. Heat is transferred by conduction from the flame zone to the droplet to provide the latent heat of vapourisation of the fuel droplet. The following simplifying assumptions are usually made:

i) exothermic chemical reaction between the fuel vapour and oxidant occurs in the flame zone, where they combine in stoichiometric proportions.

ii) chemical reaction occurs instantaneously so that the flame zone is infinitely thin, the partial pressures of both fuel vapour and oxidant are zero at this point.

iii) chemical reaction proceeds to completion, so that it requires no activation energy.

iv) the droplet temperature is uniform and equal to the fuel boiling point.

v) radiation and thermal diffusion effects are negligible.

vi) the Lewis number is unity.

Godsave (21) obtained an expression for $\dot{m}_E$ which was a function of flame radius, this suffers the drawback that this radius is extremely difficult to estimate since, as has already been demonstrated (Fig.2.5), the reaction zone distorts under the smallest relative velocity - even without taking turbulence effects into account. Other examples of solutions to the spherico-symmetric model governing mass and energy balances are provided in references (22-26). All of these are naturally applicable to the diffusion mode of droplet combustion and all assume constant transport properties in order to simplify the derived expressions for practical use. The latter is a drastic assumption since transport properties are a strong function of both chemical composition and temperature.

More sophisticated analyses of evaporation effects have been developed with varying degrees of success, for a review of these see Williams (20).

For the WSR model and blue flame conditions, i.e. droplet wake mode of combustion, an expression for droplet evaporation rate only is required since the burning process, which is integral to the spherico-symmetric type model, is described by separate reaction kinetics. The vapourised fuel in the wake mode of combustion is considered to mix and subsequently react with oxidant downstream from the droplet of origin, as discussed in 2.2(b).

AD-A042 979 SHEFFIELD UNIV (ENGLAND) DEPT OF CHEMICAL ENGINEERIN--ETC F/G 21/2
POLLUTANT MINIMISATION BY BLUE FLAME STAGED COMBUSTION.(U)
1977 D S PRIOR AF-AFOSR-2682-74

UNCLASSIFIED AFOSR-TR-77-0843 NL

2 OF 3
AD A042979

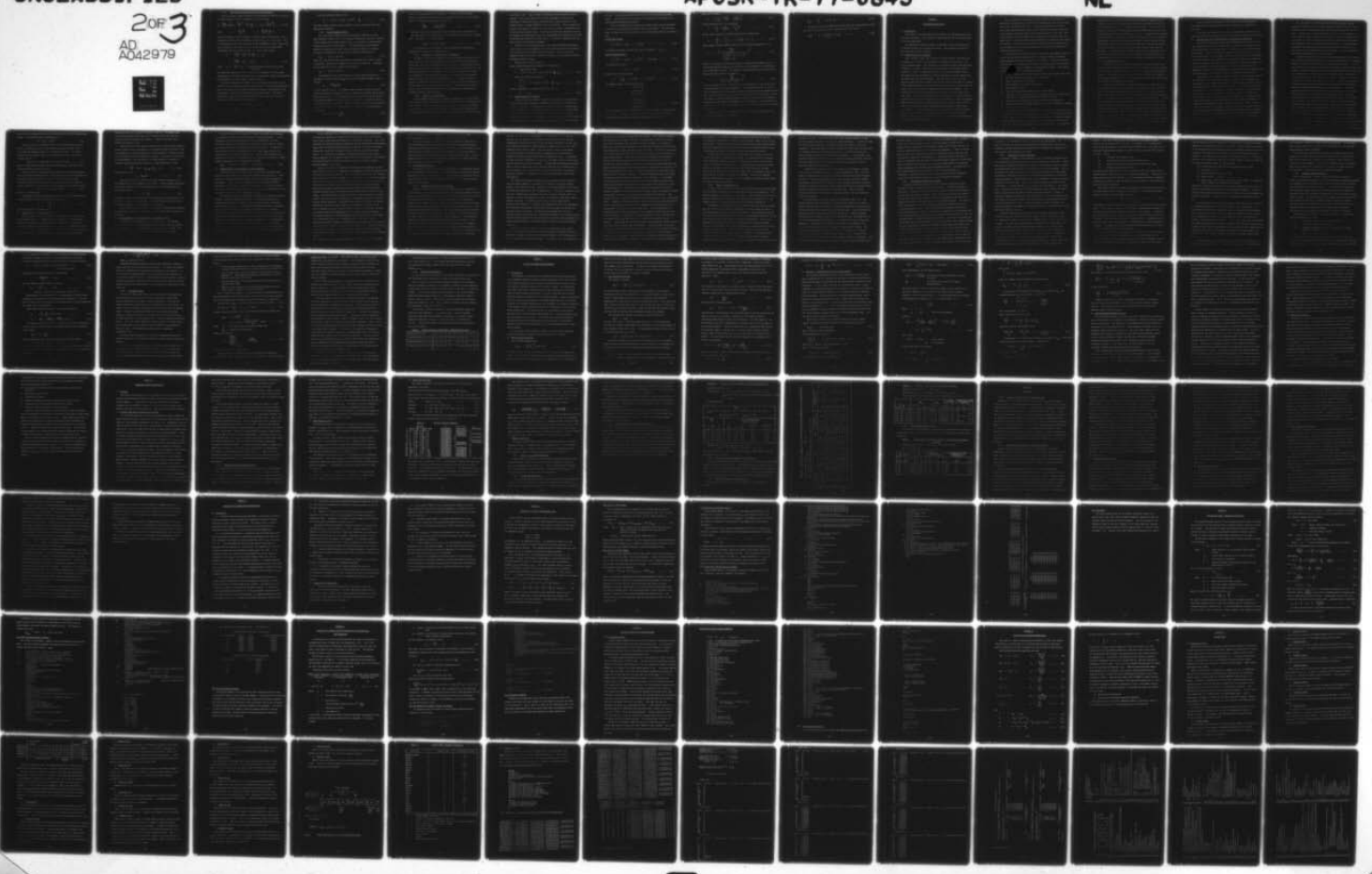

4.4(a) Blue Flame Combustion, Evaporation Rate Expression.

Now in the general spherico-symmetric evaporation model of Wise et al (120) the following equation for static evaporation rate $\dot{m}_E$ is derived:

$$\dot{m}_E = \frac{4\pi\lambda_B r_L}{C_B} \ln\left[\frac{q}{L}\left(1 + \frac{Y_{O_2,\infty}}{i}\right)^{\alpha_1} - \frac{C_B}{L}\left(\frac{q-L}{C_B} + T_L - T_\infty\right)\left(1 + \frac{Y_{O_2,\infty}}{i}\right)^{\alpha_2}\right] \quad \ldots\ldots\ldots \quad (4.58)$$

where, $\alpha_1 = \dfrac{C_B \rho D_B}{\lambda_A}$ $\qquad$ $\alpha_2 = \dfrac{C_B \rho D_B}{\lambda_B}\left(\dfrac{\lambda_B}{\lambda_A} - 1\right)$

Instead of making the common assumption of constant thermal properties it is now assumed that, for blue flame conditions, the ratio of $Y_{O_2,\infty}/i$ is very small. This is justified by the fact that the gaseous oxygen concentration is sma_ anyway under these conditions, 2.2(b) and 2.5(c), also by the fact that the stoichiometric oxidant/fuel ratio for kerosine is about 14. Hence (4.58) becomes:

$$\dot{m}_E = \frac{4\pi\lambda_B r_L}{C_B} \ln\left[\frac{q}{L} - \frac{C_B}{L}\left(\frac{q-L}{C_B} + T_L - T_\infty\right)\right]$$

$$= \frac{4\pi\lambda_B r_L}{C_B} \ln\left[1 + B_{ev}\right] \quad \ldots\ldots\ldots \quad (4.59)$$

where, $B_{ev} = \dfrac{C_B}{L}(T_\infty - T_L)$ = Evaporation transfer number for blue flame conditions.

The evaporation expression (4.59) is realistically independent of either oxygen concentration or stoichiometric mixture ratio, the expression reflects the observation that evaporation is a heat transfer controlled process.

The region B properties of specific heat C_B and thermal conductivity λ_B are considered to be approximately those of nitrogen, and to be functions of temperature. Specific heat C_B as a f(T) is easily calculated by means of the polynomial (4.41), the appropriate coefficients being obtained from McBride (110). The thermal conductivity λ_B may be described by the modified Eucken method due to Misic and Thodos (121), which employs critical properties:

$$\frac{\lambda\psi}{C_p} = 10^{-6}\left(14.52(T/T_c) - 5.14\right)^{2/3}$$

where, $\psi = \dfrac{T_c^{1/6} M^{1/2}}{P_c^{2/3}}$, $\qquad T = \dfrac{1}{2}(T_L + T_\infty)$

Inserting nitrogen properties gives:

$$\lambda_B = 1.432 \times 10^{-5} C_B (T - 44.67)^{2/3} \cdot \frac{W}{mk} \quad \ldots\ldots\ldots \quad (4.60)$$

Both these thermal properties were evaluated at the mean of droplet (B.Pt) and ambient gas temperature.

4.4(b) Droplet Dynamics Effects

Up to this point evaporation rates under stagnant conditions only have been considered, however since in all practical heterogeneous combustors a relative velocity between the two phases always exists, it is necessary to include droplet dynamics and forced convection effects. The normal method of describing the increase in evaporation rate which accompanies forced convection is to apply an empirical correlation of the type first postulated by Frössling (31):

$$\dot{m}_{E,F} = \dot{m}_E (1 + a\, Re^b\, Pr^c) \quad \ldots\ldots\ldots \quad (4.61)$$

where; a, b and c are constants of generally assumed (26) values 0.276, $\frac{1}{2}$ and $\frac{1}{3}$ respectively; the subscript F denotes forced convection conditions. Inserting typical values for Pr (26), equation (4.61) becomes:

$$\dot{m}_{E,F} = \dot{m}_E (1 + 0.244\, Re^{\frac{1}{2}}) \quad \ldots\ldots\ldots \quad (4.62)$$

As mentioned in 2.2(b) viscous drag forces cause either acceleration or retardation of droplets whenever $V_{Rel}(t) \neq 0$, hence the Reynolds number, which is defined:

$$Re = \frac{2\, V_{Rel}\, r_L\, \rho_G}{\mu_G} \quad \ldots\ldots\ldots \quad (4.63)$$

is also a function of time. Now droplet dynamics depend on gaseous phase and droplet phase physical properties, as well as combustor flow pattern and the droplet drag coefficient C_D. It is conventional (15,20) to compare the drag coefficient of evaporating droplets with those of smooth inert spheres, although the former is a small amount less than the latter. Fig.4.7 presents measured data due to Rosenhead (33) for C_D as f(Re), also plotted are Stokes' law and the following correlation due to Zahm:

$$C_D = 0.48 + \frac{28}{Re^{0.85}} \quad \ldots\ldots\ldots \quad (4.64)$$

which fits the data reasonably successfully. In order to incorporate drag effects an expression is required for the acceleration experienced by an individual droplet. Vincent (26) derived such an expression:

$$\frac{dV_{Rel}}{dt} = \frac{3\ C_D\ \rho_G\ V_{Rel}^2}{8\ r_L\ \rho_L} \qquad \ldots\ldots\ldots \qquad (4.65)$$

In general it can be appreciated that forced convection is more significant for larger drops whose Re is initially high, and as discussed in 2.2(b), tends to remain high. The relative velocity is defined:

$$V_{Rel}(t) = |V_G(t) - V_S(t)| \qquad \ldots\ldots\ldots \qquad (4.66)$$

For a discussion of the effects of natural convection and turbulence on evaporation rates refer to (20,16) respectively.

4.4(c) Evaporation Timestep Calculation Technique.

In order to calculate fuel evaporation rates under typical conditions in the blue flame burner a timestep technique was devised (similar to that described by Vincent (26)) in which one dimensional flow is assumed. Initial atomiser relative velocities and the ISD were computed using the above equations, drag forces etc. were recalculated after each time increment. 21 spray size intervals, each of which were represented by the interval mean diameter, were considered and the complete timestep procedure is given in the flowchart Fig.4.8. A computer program was written to handle these calculations, this was modified to enable incorporation in the BFB model, and is fully described in Chapter 7. This Chapter also presents a separate set of evaporation characteristics for the blue flame burner that were obtained using this timestep technique.

4.4(d) WSR Mean Evaporation Rates.

The WSR analysis presented in 4.2 requires an expression for $\dot{F}E$, the reactor mean evaporation rate, which defines the rate of mass transfer from the liquid to the gaseous phase. Now as Fig.4.9 shows, the percentage of the fuel spray remaining unevaporated PU at any elapsed time t decreases non-linearly, it follows that the evaporation rate of the spray is not constant throughout any particular WSR in which

fuel droplets exist. Hence a means of estimating the mean evaporation rate is required. Now it can be shown, Poll (2), that although it is not strictly permissible to analyse any process occurring within a stirred reactor in a non-integral manner, a separate PHASE may in fact be so treated. Thus the evaporation process is envisaged as proceeding in a plug flow "sub reactor", surrounded by the stirred reacting (gaseous) phase. In this way the spray mean evaporation rate may be estimated by calculating the total fuel evaporated for the elapsed time in the WSR, and dividing this quantity by the stay time τ_s. It should be emphasised that this forms only one of the possible approaches.

Now PU(t) can be evaluated by means of the timestep technique described in 4.4(c) above, it is also assumed that all of the fuel spray remains in the reactor for the stay time τ_s as required by the WSR analysis. Again, it should be emphasised that it is possible to modify the analysis to incorporate more realistic differential phase stay times.

Consider time t shown in Fig.4.9:

Amount evaporated during time increment Δt at elapsed time t

$$= \text{area of shaded region}$$

$$= \tfrac{1}{2}\left[(100 - PU(t-\Delta t)) + (100 - PU(t))\right] \frac{\Delta t}{100} \dot{m}_{FUEL} \quad \ldots\ldots\ldots \quad (4.67)$$

$\therefore$ Total fuel evaporated in reactor ℓ

$$= \sum_{t = t_\ell}^{t_\ell + \tau_s} \tfrac{1}{2}\left[200 - PU(t-\Delta t) - PU(t)\right] \frac{\Delta t}{100} \dot{m}_{FUEL} \quad \ldots\ldots\ldots \quad (4.68)$$

Hence the required mean evaporation rate for reactor ℓ:

$$\dot{FE} = FE/\tau_s \quad \ldots\ldots\ldots \quad (4.69)$$

4.5 Internal Recirculation Model.

Clearly a theoretical model is required for the prediction of the degree of internal recirculation generated in the BFB by the Coanda ejector device, plus $V_G(0)$ the initial gaseous phase mean flow velocity in the spray formation region. Now as described in 3.2 the fluid flow through the Coanda unit is strictly three dimensional and highly turbulent, i.e., of a complex nature. No rigorous theoretical treatment of such a flowfield is available to date, possibly the nearest attempt was that of Mon and Pao (122) who considered two dimensional curved wall

jet flow. The governing equations were found to be very nonlinear and highly complex. Hence the theoretical treatment of the Coanda flow was limited to the simpler momentum exchange type analysis.

Fig.4.10 illustrates the two dimensional Coanda geometry and the nomenclature to be used, the two dimensional idealised flows are also shown. The theoretical model for steady state ejector operation is due to Swithenbank (38) and is presented here.

Ejector mass balance.

$$\rho_i \int V_i dA_i + \rho_j V_j A_j - \rho_o \int V_o dA_o = 0 \quad \ldots\ldots\ldots \quad (4.70)$$

To simplify the analysis constant area mixing is assumed, $\therefore A_i = A_o$

Ejector momentum balance.

$$\rho_i \int V_i^2 dA + \rho_j V_j^2 A_j - \rho_o \int V_o^2 dA = \int (P_o - P_i) dA \quad \ldots\ldots\ldots \quad (4.71)$$

By the Bernoulli relation:

$$(P_o - P_i) \approx \tfrac{1}{2} \rho_i V_i^2 \quad \ldots\ldots\ldots \quad (4.72)$$

Hence (4.71) may be reexpressed:

$$V_j = \left[\frac{1}{\rho_j A_j} \left(\rho_o \int V_o^2 dA - \tfrac{1}{2} \rho_i \int V_i^2 dA \right) \right]^{\frac{1}{2}} \quad \ldots\ldots\ldots \quad (4.73)$$

The skewness factor λ may be defined as (38):

$$= \frac{\rho^2 / A \int V^2 \, dA}{\left(\rho / A \int V \, dA \right)^2}$$

$$= \frac{r^2 \int V^2(r) r \, dr}{2 \left(\int V(r) r \, dr \right)^2} \quad \ldots\ldots\ldots \quad (4.74)$$

for flow through a circular cross section of radius r in which a velocity profile V(r) exists. The skewness factor is a measure of the flow non uniformity or departure from a flat profile, for which it has the value of unity.

Hence (4.73) becomes:

$$V_j = \left[\frac{1}{\rho_j A_j} \left(\frac{\lambda_o \dot{m}_o^2}{\rho_o A} - \frac{\lambda_i \dot{m}_i^2}{2 \rho_i A} \right) \right]^{\frac{1}{2}} \quad \ldots\ldots\ldots \quad (4.75)$$

A mass entrainment ratio ψ is now defined:

$$\psi = \frac{\dot{m}_o}{\dot{m}_j} = \frac{\dot{m}_o}{V_j A_j \rho_j} = \frac{\dot{m}_i + \dot{m}_j}{\dot{m}_j} \quad \ldots\ldots\ldots \quad (4.76)$$

Now for perfect mixing, the following relation can be deduced (38):

$$\rho_o = \frac{\dot{m}_j}{\dot{m}_o} \rho_j + \frac{\dot{m}_i}{\dot{m}_o} \rho_i = \rho_i \left[\frac{1}{\psi} \left(\frac{\rho_j}{\rho_i} - 1 \right) + 1 \right] \quad \ldots\ldots\ldots \quad (4.77)$$

Substituting (4.77) and (4.75) into (4.76) then yields the desired expression for ψ:

$$\psi = \eta \left(\frac{\frac{2\rho_i A}{\rho_j A_j}}{\frac{2 \lambda_o}{\left[\frac{1}{\psi} \left(\frac{\rho_j}{\rho_i} - 1 \right) + 1 \right]} - \lambda_i \left(1 - \frac{1}{\psi} \right)^2} \right)^{\frac{1}{2}} \quad \ldots\ldots\ldots \quad (4.78)$$

where η is an efficiency factor which relates the theoretical entrainment ratio to a corresponding measured quantity, the estimation of this parameter for the BFB Coanda unit is described in 7.2(a). For isothermal (non-combusting) flow, constant density prevails so that (4.78) may be reduced to:

$$\psi = \eta \left(\frac{\frac{2A}{A_j}}{2 \lambda_o - \lambda_i (1 - 1/\psi)^2} \right)^{\frac{1}{2}} \quad \ldots\ldots\ldots \quad (4.79)$$

which is of quadratic form. However for the combustion case equation (4.78) is not so simple and has to be solved iteratively. The entrainment ratio of the ejector then is a function of area and density ratios, plus the inlet and exit skewness factors. Due to the high velocity air jet the inlet skewness factor would be expected to depart from unity, the exit plane skewness would be expected to be related to the turbulent mixing rate and the Coanda throat length, but not so strongly. Fig.4.11 depicts the variation of ψ with area ratio for various values of the skewness factors, η is assumed to be unity.

The level of internal recirculation R_{int} generated by the Coanda ejector may now be defined, again on a mass basis:

$$R_{int} = \frac{\dot{m}_i}{\dot{m}_o} = 100\ (1 - \frac{1}{\psi})\ \% \quad \ldots\ldots\ldots \quad (4.80)$$

The initial mean gaseous phase flow velocity $V_G(0)$ may be approximated as being that gaseous velocity which exists at the Coanda unit inlet plane:

$$V_G(0) = V_i = \frac{4}{\rho_i\ \pi\ d_i^{\ 2}} (\psi - 1) \rho_j \dot{Q}_j \quad \ldots\ldots\ldots \quad (4.81)$$

CHAPTER 5.

EXPERIMENTAL MEASUREMENTS.

5.1 Introduction.

This Chapter is concerned with the acquisition of the experimental data which, as outlined in Chapter 3, was necessary for model input and actual characterisation of the blue flame burner.

The experimental system was housed in a laboratory located at the University of Sheffield research site, Harpur Hill, Buxton. Mean atmospheric pressure at this laboratory was about 730 mm Hg.

5.2 Burner Facility and Operation.

Plate 1 depicts a front view of the overall burner facility, the burner exit is rigged with a sampling stage unit which is equipped with thermocouple, pitot and gas sampling probes. The construction of the burner itself has been described in Chapter 3; as Plate 2 shows it was rigidly mounted in a horizontal position by means of a stand. A fume ejector, which is not visible in either of these photographs, was also assembled to the rig for the purpose of rapidly removing the hot burner exit flow from the building. The ejector was of the 0.22 m Olin Matheson Coanda type and was driven by the main air supply system, Fig.5.1. A Reavell rotary compressor driven by a 67.5 kW electric motor was used to derive the main air supply, up to 0.3 kg/s of air at 250 kN/m^2 gauge pressure was available. The compressor was lubricated under pressure and cooled by a continuous flow of cold mains water. The air was passed through a 9 m^3 receiver vessel which removed any compressor oil from the air, it also removed any low frequency pressure fluctuations. Before reaching the burner or fume ejector the air was passed through a filter to remove any remaining oil drops or condensation which may have occurred in the supply lines. After passing through a control valve the air volumetric flowrate, about 600 lit/min maximum, was measured with a rotameter (calibrated at 15° C, 760 mm Hg) before entering the burner air manifold. A mercury manometer monitored the air pressure in this manifold.

Fig.5.2 illustrates the fuel supply system, throughout the majority of experimental runs kerosine was used as the fuel although some tests were performed using a light residual fuel oil, 5.3. Kerosine was supplied from a pressure vessel (approximately internal volume 0.11 m^3) which was pressurised to 180 psig using nitrogen, the maximum atomiser fuel injection pressure was 160 psig. After passing through a filter to remove physical impurities the kerosine flowed, via a needle valve, to the actual water cooled copper fuel gun and thence to the pressure jet atomiser. The needle valve regulated the kerosine injection pressure, which was registered on a Bourdon pressure gauge whose calibration was checked with a Budenberg dead weight tester.

The blue flame recirculating burner was "warmed up" using gaseous propane as a fuel, this was injected into the Coanda unit throat by means of an ignition probe inserted into the burner through the exit orifice. Practice was required before trouble free lighting up of the burner was obtained, under some conditions the propane flame tended to stabilise at the burner exit orifice. The following procedure was employed for lighting up the burner:

1. Turn on propane supply to pilot light and ignition probe, ignite pilot light.
2. Fill fuel vessel and pressurise to 180 psig with N_2.
3. Turn on cooling water to fuel gun.
4. Check compressor oil, turn on cooling water.
5. Start compressor motor.
6. Insert the lighted propane ignition probe into the burner.
7. Open main air valve slowly until stable combustion (blue) of propane and air takes place. Allow five minutes for the burner to warm up.
8. Open fuel injection needle valve until about 40 psig is indicated.
9. Increase fuel and air flowrates gradually until steady combustion is obtained.
10. Withdraw the ignition probe.

Under most conditions the kerosine flame was observed to be completely blue, as required, see the Frontispiece colour plates which are views into the burner exit orifice. When the burner was at steady state temperature the combustion chamber walls, but not the Coanda unit, glowed red - the Frontispiece was taken before steady state was reached so that flame colour could be observed. The flame was

completely blue under fuel lean and stoichiometric conditions, under fuel rich conditions this was also the case although the flame outer edges were yellow at overall equivalences, $\phi_{ov} > \approx 0.6$ (ϕ_{ov} defined in 5.8(f)). Close to fuel rich blowout the flame became completely yellow and mean temperatures in the exit flow dropped rapidly, under these conditions ϕ_{ov} was ≈ 2.0. Combustion noise increased as the throughput was increased. Flame length increased as ϕ_{ov} was increased, at stoichiometric conditions the flame protruded about 5 cm out of the exit orifice. The burner was observed to be extremely stable and easy to control, the stability loop was not determined since the mode of operation changed as the limits were approached. A "scaling" of the combustion chamber walls was apparent after many runs had been performed, this was to be expected since the complete burner was constructed of mild steel which oxidises at relatively low temperatures, 5.8(g).

5.3 Residual Fuel Oil Tests.

Clearly fuels of lower grade than kerosine are of practical interest, such fuels may contain substantial amounts of sulphur and nitrogen containing compounds, also free carbon. The reasons for using kerosine as a test fuel were presented in Chapter 3. Industrial fuels can also contain very many hydrocarbon components of high molecular weight and may be extremely viscous, in some cases emulsification is necessary for satisfactory fuel injection.

A brief test was conducted to determine how easily such lower grade fuels could be handled by the blue flame burner. Light residual fuel oil was used to fire the burner after it had been preheated by passing it through two separate heating coils immersed in a heating bath, which was thermostatically maintained at 80^{o} C. This lowered the fuel's viscosity and thus promoted atomisation. The fuel oil could have been preheated far more efficiently but it was still found that stable combustion could be obtained, under a wide range of fuel/air ratios, using a pressure jet atomiser. The presence of sulphurous fumes was detected and the burner was a little more difficult to light up using residual fuel oil rather than kerosine. The resulting flame was largely blue although yellow streaks were abundant, these were due to the formation and trajectories of large drops of fuel. Some soot was also liberated, but only in small quantities, under overall fuel rich operation only.

It was concluded that the burner could be modified to handle commercial lower grade fuel oils although much more work is required on the combustion of such fuels.

In the next four sections, 5.4-7, a series of measurements conducted on the burner and its fuel atomiser under cold i.e. non combusting conditions are described.

5.4 Quantification of the Burner Internal Recirculation Characteristic.

The stirred reactor model network requires knowledge of the fraction of the flow leaving the Coanda unit exit plane which, at some distance downstream of this point, recirculates around the unit back to the inlet plane. This recirculation was necessary to satisfy the entrainment appetite of the attached jet, 3.2. The actual quantification of the internal recirculation characteristic was accomplished by a novel technique which necessitated a baffle being inserted in the combustion chamber to completely block off the recirculation path. Hence the technique could not be applied under combustion conditions. In these measurements hot wire anemometry was employed to actually measure velocity profiles of air passing through the ejector unit, use of a hot wire probe also required cold flow conditions.

The aluminium baffle ring was secured to the rear of the Coanda unit by means of three screws, two O rings made of rubber also ensured that a reasonably gas tight seal, as Fig.5.3 shows, was obtained. Pressure tappings A and B were set up and connected to an inclined 1.5" water manometer. The fuel gun was removed and an air inlet tube plus circular flow distributor assembled to the combustor head plate as Fig.5.2 shows, a secondary air source was introduced into this tube. The flow distributor deflected this air stream to simulate the recirculated flow through the annular gap between the Coanda unit and the combustion chamber; the radius of the distributor was equal to the Coanda unit outer radius. At any Coanda flow setting $\dot{Q}_j$ the secondary flowrate $\dot{Q}_i$ could be varied until zero differential pressure across the baffle, as read on the water manometer, was obtained. The particular value of $\dot{Q}_i$ which produced zero differential pressure was then the value of the internal recirculation flowrate which satisfied the Coanda unit entrainment appetite.

For a slit width S of 0.020" the baffle differential pressure ΔP_D was measured as a function of $\dot{Q}_i$ for various settings of Coanda jet flow $\dot{Q}_j$. Fig.5.5 presents the set of characteristic curves that were thus obtained for this slit width. Similar sets of curves were derived for values of S corresponding to 0.015" and 0.010", Figs. 5.6 and 5.7 respectively. Curves of entrainment ratio as a function of Coanda jet throughput $\dot{Q}_j$ using this measurement technique were also constructed, Fig.5.8, these are discussed in Chapter 7. The data enables evaluation of the simple Coanda ejector entrainment analysis presented in 4.5 after values for the skewness factors have been derived. Values for these were measured experimentally using hot wire anemometry.

The blue flame burner was turned through 180^o and remounted on its stand so that a DISA 55P11 miniature hot wire probe could be traversed inside the combustion chamber, the baffle having been removed and the fuel gun repositioned. The hot wire probe plus probe support was secured to an adjustable mounting block which was fixed to a traversing mechanism, this mechanism enabled two dimensional traversing in a horizontal plane and was also bolted to the burner stand. The complete system was accurately aligned with the combustor axis of symmetry and a pair of scales set up to indicate the position of the probe. The probe was connected to a DISA 55D05 battery operated constant temperature Anemometer, whose frequency response was frequently checked using a square wave generator. As Fig.5.9 depicts, the DC level of the anemometer output signal was measured by a Fluke 8000A digital voltmeter after turbulence low frequency components had been suppressed by means of an RC filter (time constant 0.815 secs). This allowed stable readings of the anemometer mean bridge voltage to be easily obtained. A DISA RMS meter (55D35) was used to measure the anemometer output RMS voltage and a Solartron CD1400 oscilloscope employed to monitor anemometer response. The hot wire probe was calibrated in an air free jet system which is shown in Fig.5.10, the hot wire probe and a small pitot probe were closely positioned in the potential core region of this air jet. Pitot pressure was monitored on a 1.5" water manometer. Turbulence levels in this jet potential core were less than 2% and thus ideal for calibration purposes. Before each calibration, which was performed before every time the probe was used for actual measurement, the temper-

ature of the air issuing from the jet was measured using a Comark 3001 digital thermometer. The anemometer output characteristic is:

$$\bar{V}^2 = \bar{V}_o^2 + A\bar{U}^{0.45} \quad \ldots\ldots\ldots \quad (5.1)$$

Velocity profiles in the Coanda throat exit plane were measured using the hot wire anemometer setup, for various flowrates $\dot{Q}_j$, typical results for $\dot{Q}_j$ = 300 lit/min are presented in Fig.5.11, slit width S was 0.010". In order to calculate the exit skewness factor λ_o a polynomial was fitted to this velocity profile, this was:

$$\bar{U}_o(r) = 8.7 + 2.015 \times 10^5 r^2 - 1.763 \times 10^7 r^3 \text{ m/sec} \quad \ldots\ldots\ldots \quad (5.2)$$

where r = radial distance (inches) from Coanda central axis. The form of this velocity profile was the same for all $\dot{Q}_j$.

Velocity profiles in the Coanda throat inlet plane were similarly measured, after the combustor headplate had been removed to gain access and the combustor had been again rotated through 180°. A range of $\dot{Q}_j$ for S = 0.010" was again investigated, typical results for $\dot{Q}_j$ = 300 lit/min being presented in Fig.5.12. A simple polynomial was again used to fit the measured velocity profile, this was:

$$\bar{U}_i(r) = 6.5 + 20.83\, r^2 \text{ m/sec.} \quad \ldots\ldots\ldots \quad (5.3)$$

where r is as defined above.

Substituting the curves (5.3,2) into the general equation (4.74) yielded the respective results of Coanda inlet and exit skewness factor:

$$\left.\begin{aligned} \lambda_i &= 1.045 \\ \lambda_o &= 1.153 \end{aligned}\right\} \quad \ldots\ldots\ldots \quad (5.4)$$

These are approximately independent of $\dot{Q}_j$.

5.5 Investigation of the Combustor Flow Pattern.

The flow pattern in the blue flame combustor was investigated using the hot wire anemometry equipment. Probing within the chamber was limited by the exit orifice diameter so that mean velocities along the central axis and across the exit orifice diameter only were determined. Measurements were made for S = 0.010" and $\dot{Q}_j$ = 300, 400 and 500 lit/min., Fig.5.13 presents the results that were obtained, axial velocities being plotted as a function of dimensionless distance from the

Coanda exit plane (ℓ_4, ℓ_{ex} and b are defined in Fig.7.1). The highest axial mean velocity measured was 19 m/sec, it is important to note that these were again for cold flow throughout the combustor. Combustor exit mean velocity profiles were completely flat.

Estimates only of axial turbulence intensities were made using the anemometry system, although accurate measurements of this parameter cannot be made with a hot wire anemometer, the estimates obtained do succeed in giving a qualitative picture of how the parameter varies throughout the combustor. As equation (5.1) shows the hot wire anemometer output characteristic is highly nonlinear, one method of estimating turbulence intensity T from the anemometer RMS voltage is (103):

$$T = \frac{U_{RMS}}{\bar{U}} \cdot 100\% = V_{RMS} \frac{\bar{V}}{(\bar{V}^2 - \bar{V}_o^2)} \cdot 445\% \qquad \ldots\ldots\ldots (5.5)$$

This relation assumes:

$$U_{RMS} = V_{RMS} \frac{dU}{dV} \qquad \ldots\ldots\ldots (5.6)$$

Hinze (1) has shown that values of turbulence intensity measured by a hot wire anemometer are overestimated by a large amount for high turbulence intensities. For isotropic turbulence it was calculated that, to a first approximation, the error E was given by:

$$E = + \frac{19}{8} \frac{T^2}{100} \% \qquad \ldots\ldots\ldots (5.7)$$

Estimates of combustor axial turbulence intensity were made, using relations (5.6) and (5.7), for $\dot{Q}_j$ = 300,400,500 lit/min. Results obtained are given in Fig.5.14 the distance coordinate has again been non-dimensionalised.

The hot wire anemometer was further used to measure turbulence autocorrelation functions using a digital computer on-line analysis technique which is dealt with in Chapter 6.

5.6 Atomiser Fuel Mass Flow as a Function of Injection Pressure.

A relatively low throughput pressure jet atomiser (i.e. high atomising pressure) was used in all tests performed on the blue flame burner, this resulted in good atomisation of the fuel at injection pressures P_f up to 160 psig. The flow number F was nominally 0.05 and flowrate 0.6 gal/hr at P_f = 160 psig.

The atomiser mass flow as $f(P_f)$ characteristic for kerosine was determined as accurately as possible using a direct weight measurement technique. The fuel containing pressure vessel was placed on an 'Avery weighbridge' set of scales. Kerosine was allowed to discharge from the containing vessel through the complete fuel system and atomiser for a known time interval at fixed P_f. The decrease in pressure vessel weight was recorded and the mass flowrate $\dot{m}_{FUEL}$ computed, the procedure was repeated for other values of P_f. The mass flow calibration characteristic thus obtained is presented in Fig.5.15, the curve was fitted by a simple quadratic expression for use in the theoretical model:

$$\dot{m}_{FUEL} = 0.848\ P_f^{\frac{1}{2}} - 0.0274\ P_f - 1.710 \text{ . lb/hr} \quad \ldots\ldots\ldots \quad (5.8)$$

5.7 Atomiser Initial Size Distribution (ISD) Measurement.

As explained in 4.3 correlations exist for a pressure jet atomiser which predict the ISD characteristic of the spray produced for any value of P_f. Until recently no convenient experimental means existed for the actual measurement of the atomiser ISD , a new laser technique has been developed at Sheffield University (104) to provide a solution to this problem. This optical technique was used to investigate the ISD produced by the pressure jet atomiser which was used in the blue flame burner, over a complete range of P_f.

The operating principle is now briefly described but the complete theoretical analysis is given by Swithenbank et al (104). The amount of diffraction of incident light produced by a droplet or particle varies inversely with droplet (or particle) size, so that if a parallel monochromatic light beam is transmitted through a field of droplets, a divergence of the original beam is produced. If a lens is now used to focus the deflected light then it can be shown (104) that a circular energy intensity pattern is produced in the focal plane of this lens, furthermore this intensity pattern completely characterises the size distribution of the drops in the field through which the light beam passed. Fig.5.16(A) illustrates this diffraction process, the lens actually produces a two-dimensional Fourier Transform of the input and thus contains spatial frequency information independent of the droplet motion.

As Fig.5.16(A),(B) shows, a photodetector device (Recognition Systems Polar Coordinate type WRD-6400) was located at the focal plane of a 30 cm focal length lens to enable energy intensity patterns to be electrically transduced. Fig.5.16(B) represents the complete experimental arrangement that was employed for ISD measurement, signals from the 32 photodetector elements were amplified by a Recognition Systems Sampling Unit, which also displayed a digitised value for any selected element voltage. A 1 mW Ne/He laser provides a convenient monochromatic light source, optical components A,B & C ensured a parallel beam of suitable intensity was produced and a micro-traversing mechanism, on which the detector was mounted, enabled accurate alignment of the optics.

Actual measurement of the spray size distribution (cold conditions) was very rapid and simply involved the measurement of each photodetector element voltage for any particular fuel injection pressure. A background set of readings was first obtained without the spray, in order to account for any interference due to ambient particulate matter or light variations through the laser optical path. These two sets of data for any P_f were supplied as input to a PDP 8/E digital computer program which, based on the theoretical analysis given in (104), evaluated the required energy intensity profiles and then the weight fraction of drops present in each of 31 size ranges. The program (given in (104)) also calculated the Rosin Rammler distribution function which best fitted the measured data, as explained in 2.2(a) this function features two fit parameters. This BASIC program produced a "plot" of the measured data and the fitted Rosin Rammler function on the teletype input/output device. Fig.5.17 presents an example of such an ISD Data plot for P_f = 100 psig; the range of injection pressure investigated was P_f = 40 → 140 psig (20 psig increments). The program printout gives the above mentioned data for each of the 31 size classes, the corresponding $\bar{x}$ and n, plus a statistical error of fit term. In the normalised data plot "+" signifies a weight fraction data point and "*" is a point on the fitted curve; "θ" corresponds to a point where the two were coincident according to the teletype resolution. Note also that the maximum interval drop diameter appears at the top of the plot. The six sets of measured data were used to construct plots of

a) Rosin Rammler 'mean' drop size $\bar{x}$" microns as a function of P_f - Fig.5.18(A)

and b) Rosin Rammler distribution parameter n" also as $f(P_f)$ - Fig.5.18(B). Results presented in these two graphs are fully discussed in Chapter 7.

The point of measurement in the fuel spray, i.e. distance of the laser beam from the atomiser was 10 cm and corresponded to the fully developed spray region. ISD characteristics measured under these cold conditions are directly relevant to the combustion case by definition, the direct measurement of the size distribution of sprays evaporating under combustion conditions would be extremely useful. This is hampered though by the need for clean windows to sight into the combustor,Ref.(61), and the existence of flame light emission.

5.8 Gas Sampling Measurements.

As previously explained in Chapter 3 a primary aim of the experimental program was the measurement of the blue flame burner exit flow gas composition, with respect particularly to the pollutants CO and NO_x. This section then describes the design, construction and testing of the gas sampling system, the results obtained using the system are then presented.

5.8(a) Problems Associated with Gas Sampling.

A number of problems are raised when a gas sampling probe is introduced into a two phase flow. Apart from the obvious fouling of droplet trajectories, the probe distorts the gaseous stream lines at the point in the flow where the probe is located. This distortion of the streamlines causes a perturbation of the concentration gradients of all species in the flow, at present this situation cannot be alleviated by the adoption of optical measuring techniques since, as explained in (59) , these techniques are insufficiently developed. The use of a sampling probe was therefore unavoidable and one of the two types had to be selected. The first type consists of a small quartz tube, with external and internal diameters of a few millimetres, stretched and shaped until the tube entrance diameter is of the order 10 - 100 μ. Now, in order to obtain a representative sample, the composition of the sampled gases when introduced to the gas analysers must be identical with the composition of the combustor flow at the entrance to the probe. In turn this requires that chemical reactions in the sampled gases must be rapidly attenuated after they enter

the probe, the sample has to be "quenched". As explained in 2.2(d) chemical reaction rates are sensitive to the temperature and concentrations of the gases (consequently to the pressure also), so that the desired quenching of the gas sample can be achieved by either (i) a rapid reduction in sample pressure, or (ii) rapid conduction of heat from the sample to the probe walls to lower its temperature. In the narrow throat of the quartz probe the sampled gases are supersonically expanded to lower the pressure, rapid thermal exchange also occurs. An advantage of using such quartz "microprobes" is that, since the quartz is inert, solid surface chemical reaction is virtually eliminated. A considerable disadvantage of the microprobe is that the sampled mass flow is extremely small and can be computed (105) to be of the order of a few μ gm/sec, which is generally insufficient to continually supply gas analysers. Microprobes are thus normally restricted to small scale investigations.

For larger scale systems the larger water-cooled sampling probe is normally used, the internal diameter is invariably of the order of 1 mm and the external diameter of the order of say 6 mm. Expansion is not usually imparted to the sample, heat conduction being used to cool the sampled gases. The probe is invariably cooled with water although heated water under pressure or steam are sometimes used in an endeavour to prevent the condensation of water vapour present in the sample when wet analyses are needed. The thermal stresses which a metallic sampling probe experiences when immersed in a turbulent high temperature flowfield are considerable, this constitutes an additional complexity which has to be taken into account when designing a water cooled probe. Although sufficient sample mass flow can be supplied, the water cooled probe has a considerable drawback in that transition metals, which are normally employed for probe construction, can provide ideal environments for surface chemical reactions; all chemical reaction within the probe being extremely undesirable.

This surface reaction problem is most acute when sampling for NO_x species since it is known (106,107) that under reducing environment conditions the chemical reduction of nitrogen oxides by carbon monoxide, hydrogen and other reducing agents occurs in the presence of a metallic surface. The result is that NO_x concentrations

lower than the true values are measured by the analyser. In an effort to overcome this problem many investigators (106) have constructed their probes from stainless steel since this material does not display as high a tendency as pure transition metals (e.g. Cu, Ni and Fe) to promote surface reactions, stainless steel also being of good mechanical strength and oxidises only very slowly. A solution to the problem is to line the probe inner wall with a silica tube or coating, this is difficult for smaller probes however. There are two commonly used techniques for measuring NO and NO_x, these are Non Dispersive Infra Red (NDIR) Gas Analysis which relies on absorption of infra red radiation, and the now more commonly employed Chemiluminescent Analysis (CLA) which operates through determination of chemiluminiscent radiation from the reaction between NO and ozone. The second technique will be discussed in some detail shortly, it utilises a converter constructed of heated stainless steel tubing to convert NO_2 to NO in order to estimate NO_x (i.e. NO and NO_2). To investigate the possibility that one or more components of fuel-rich combustor exhaust gas may interfere with NO_x measurement when using a CLA , Siewert (107) carried out a series of interference tests. The analyser plus converter were exposed to each of the principal components of fuel rich exhaust gas for known amounts of time before standard concentrations of NO in N_2, plus NO_2 in N_2 were admitted to the analyser. Only hydrogen was found to exhibit interference but H_2 was discovered to have a considerable effect. Immediately following H_2 exposure zero NO (or NO_2) was detected, measured NO then increased gradually with time at a rate dependent on (i) exposure time to any concentration of H_2, and (ii) converter temperature. No such interference was obtained when the converter was bypassed so this component must have been the source of the interference. Siewert then conducted measurements of NO_x in undiluted fuel-rich exhaust from a spark ignition engine, in which H_2 but negligible NO_2 was expected. After purging with air the CLA-measured NO_x concentration initially agreed closely with both CLA NO and NDIR NO measurements. The NO_x reading then decreased with time to a minimum stabilised value as much as 95% less than the other NO readings; increasing deviation for (i) fuel richer exhaust gases, and ii) higher converter temperatures being recorded. Based on these tests Siewert postulated an interference mechanism which suggested the accumulation of H_2 on the metal surface and consequent

NO_x interaction. The result of flowing air through the converter before each test would be to ensure that the oxidised form of the metal, rather than the reduced form existed. Similar interference effects would be expected when actually sampling fuel rich combustion gases with a stainless steel probe, although no detailed study to investigate such effects in relation to prevailing temperatures exists.

Another problem encountered when sampling probes are used concerns the rate at which the sample is withdrawn from the probe. As mentioned above a distortion of the streamlines upstream of the probe is imposed, it is obvious that this distortion is a function of sampling rate. To minimise unwanted distortion the mean velocity of the gases at the probe entrance must clearly be equal to the mean velocity of the gases in this vicinity which would exist in the absence of the probe, this condition is referred to as ISOKINETIC SAMPLING. The effect of sampling velocity upon measured gas composition has been examined by Longelle & Verdier (105), who found a significant dependence.

5.8(b) Design of Sampling Probe.

In view of these complications a water cooled stainless steel probe was designed for the purpose of measuring the blue flame burner exit flow gas composition. The probe was designed to be mounted in an extra unit, since traverses into the actual combustion chamber were not required. This unit was composed simply of a 4" long flanged section of 4" ID pipe and compatible with the burner construction.

The diameter of the burner exit orifice, where the probe tip was to be located, was only 3.8 cm so that an important requirement of the probe design was that its crosssectional area should be as small as practicable. This unfortunately implied that the ID of the probe innermost tube should be correspondingly small, hence the use of a silica tube as an inert central lining had to be precluded. Fig.5.4 is an exploded view of the probe tip section, the probe consists of three concentric stainless steel hypodermic tubes which are attached to a stainless steel tip by means of silver soldering as shown. The probe overall OD was 4.8 mm and the inner capillary, through which the sample flowed, was 0.84 mm ID. Construction of the probe thus required much skill, due to its small dimensions and was certainly hampered by the fact that a 90° bend was required to facilitate mounting of the probe,

as shown in Fig.5.19. It was vital that the 3 tubes remained concentric so that the cooling water could flow easily along the narrow probe annuli. In order to ensure that the tip, which experiences considerable thermal and mechanical stress, was adequately cooled and the sample efficiently quenched the cooling water flowed through the innermost channel first before reaching the tip. No difficulties with any excessive sample condensation in the probe were encountered. A disadvantage of the innermost hypodermic low ID was that, under isokinetic sampling conditions, relatively low cooled sample flowrates to the gas analysers would be unavoidable, however sufficient flow was in fact obtained.

A detailed heat transfer analysis of the probe was not attempted as a design aid since such an analysis would be very complex mathematically - due to the large range of temperatures and hence thermal properties, which are encountered throughout the probe. Instead, an approximate heat transfer evaluation was made to estimate the necessary cooling water mass flowrate, and then relatively detailed calculations performed to assess the efficiency of the resultant probe design in quenching chemical reactions occurring in the sample flow through the probe. Results of these calculations, details of which appear in Appendix B, proved the vital quench capability of the design.

As Fig.5.19 shows, the overall length of the probe was about 26 cm. The diagram illustrates how the pressurised cooling water was supplied to the probe, a thermistor device (GT24) was employed to measure the temperature of the probe outlet cooling water in order to monitor probe heat transfer rates. Fig.5.23 presents the temperature-output voltage characteristic for this device. Flexible polythene tubing was used to transfer cooling water to and from the probe and brazing was used in the cooling water manifold construction. The probe inner sample capillary was expanded to $\frac{1}{8}$" OD stainless steel tubing in this manifold and connected to the $\frac{1}{8}$"OD Teflon sample line by means of a Swagelok $\frac{1}{8}$" stainless steel fitting. This fitting also housed a Chromel Alumel thermocouple, of approximately 0.7 mm bead diameter, this was used to estimate the probe sample exit flow temperature which was needed as input information for the probe quenching efficiency calculations. Brass locating fittings mounted the sampling probe to the actual sampling stage and enabled

reasonably simple probe removal. Plate 3 shows the gas sampling probe. As shown in Fig.5.19 a $\frac{1}{8}$" OD stainless steel pitot probe was similarly mounted into the sampling stage for the purpose of estimating the burner exit flow mean velocity, the pitot was connected directly to a 1.5" inclined water manometer. A bare 1.0 mm bead diameter Pt/Pt 13% Rh thermocouple, mounted in a mild steel tubular probe, was used to estimate the burner exit flow temperature. The probe was mounted by means of a clamp to the sampling stage unit and the thermocouple signal connected to a Fluke 8000A digital voltmeter as shown in Fig.5.20 , which also presents details of the Chromel Alumel thermocouple and thermistor signal measurement circuits. Cold junctions for the two thermocouples were not required, as will be explained further on. Translation of the burner exit flow thermocouple signal into mean gas temperature taking into account radiation heat losses is fully described in Appendix C.

5.8(c) The Sampling Probe Cooling System.

Pressurised cooling water was used to cool the probe, high pressure being required by virtue of the probe narrow annuli, Fig.5.4. Preliminary estimates showed that a cooling water mass flowrate of the order 0.25 kg/min would be needed to cool the probe and quench the sample. Hence a high pressure cooling water system was devised in which a finite quantity of water was discharged to the probe from a pressure vessel which was pressurised by means of nitrogen cylinders. The system is shown schematically in Fig.5.21, an empty gas cylinder was modified and used as a containing pressure vessel. Before pressurising with nitrogen the vessel was fitted with mains water as shown, a filter was also connected into the discharge line as a blockage preventing precaution to remove any particulate material, e.g. rust, from the water before it entered the sampling probe annuli. To inhibit rust formation in the pressure vessel air was excluded at all times by ensuring a small residual pressure of N_2 was always present. The rate of discharge of water through the complete probe cooling system as a function of probe injection pressure was determined by direct weight measurement, (5.6). this characteristic was approximately linear for injection pressures > 60 psig as shown in Fig.5.22. The pressure vessel internal volume was estimated ($0.024\ m^3$) using this result, the vessel emptying time characteristic was hence calculated, Fig.5.22. To ensure adequate probe cooling an injection pressure

of 100 psig i.e. 0.33 kg/min mass flow was used in all gas sampling runs. As Fig.5.22 indicates, the pressure vessel emptying time corresponding to this flow was 72 minutes, this then represented the maximum amount of sampling time during which the probe could be safely immersed in the flame.

5.8(d) Sampling Line and Gas Analysers.

As outlined in Chapter 3, the measurement of the CO and NO/NO_x pollutant species in the burner exit flow was the main aim of the gas sampling data acquisition. Before describing the analysers employed for this purpose, the sampling line used to transmit the quenched sample from the probe to the analysers will first be described. Fig.5.26 illustrates this sampling line, in order to eliminate the possibility of NO_x surface-cooled sample interactions the actual line was constructed completely of $\frac{1}{8}$" OD Teflon tubing and Swagelok $\frac{1}{8}$" stainless steel fittings used throughout to connect the various components in the line (106). As Fig.5.26 shows,the system was operated in either of two modes: i) Normal sampling, ii) Purging of the probe with air. The second mode of operation was selected at all times during which actual withdrawal of samples from the burner was not required and served two important purposes. Firstly it enabled the sampling line and probe to be maintained free of any solid/liquid deposits, and secondly it was used to directly check for any probe - NO_x interference reactions of the type described in 5.8(a). In the second mode of operation the water trap, filter and sample flow rotatmeter were bypassed, filtered air being pumped back through the probe as shown in Fig.5.26.

During the sampling mode the sample was passed through a water trap in order to condense out any water vapour present in the sample, the trap consisted of a glass coil immersed in a mixture of water/salt/ice, condensate draining into a small vessel as shown. The sample then flowed through a gauze/glass fibre (borosilicate) filter to remove any small particles, before reaching a Gapmeter (C6) 100-2000 cc/min rotameter which had an integral regulator that was used to meter the sample flow. The calibration curve for this rotameter is presented in Fig.5.24. The pump used to transport the sample was of the reciprocating diaphragm type (Charles Austen N391) and was driven by 3 phase power, the upstream side of the pump was under vacuum and hence a pressure gauge, 0-760 mm Hg Bourdon type, was used to monitor this

pressure. Three glass 3-Way taps were also employed in the system to enable either of the two operating modes to be set. The lengths of all interconnecting Teflon tubing were minimised so that the overall residence time of the sample in the system was correspondingly minimised, residence times were estimated to be typically 7 seconds. Due to:

i) low sample line residence times,

ii) inert materials used to construct the actual line,

iii) relatively low NO_x concentrations anticipated in the sample,

iv) available kinetic rate data (48),

the gaseous phase oxidation of NO to NO_2 via equation (2.61) in the sample line was assumed negligible (106), this was later confirmed experimentally. Leakages into the sample line were found to be negligible, this was performed by passing a standard NO containing gas through the probe and determining the composition of the resulting gas which reached the NO_x analyser.

The analyser selected for NO/NO_x measurement was of the continuous type and was the Thermo Electron model 10A modular type, see Plate 4 , and utilises the chemi-luminescent chemical reaction between NO and O_3:

$$NO + O_3 \rightleftharpoons NO_2 + O_2 + h\nu \quad (\lambda \simeq 0.6 - 3\mu) \quad \ldots\ldots\ldots \quad (5.9)$$

light emission occurs when electronically excited NO_2 molecules revert to their ground state. Fig.5.27 shows a schematic of the principal components which comprise this instrument plus the ancillary equipment necessary for its operation. To determine NO_x concentrations (i.e. $NO + NO_2$) the sample flow is diverted through an NO_2 to NO converter, of the type tested in Siewert's experiments (107). Instrument output is linear so that, in all cases, calibration is performed using a single standard gas (950 ppm); the ranges over which the analyser was operable were zero up to each of 2.5, 10, 25, 100, 250, 1000, 2500 and 10000 ppm.

Sample gas is withdrawn continually through the analyser by means of a bypass pump, a rotameter in the analyser indicates the bypass flowrate and a set of capillaries plus two pressure regulators maintained the correct flowrates of O_3 and sample to the reaction chamber, which was evacuated by a Welch 1399 Vacuum Pump.

Fig.5.27 shows how each of i) zero gas, ii) calibration gas or sample gas could be admitted to the analyser by means of a 3-way valve. Zero gas used was air external to the laboratory and filtered before reaching the instrument, laboratory air was not used due to the slight build up in ambient NO_x levels anticipated during burner operation. The instrument output response was monitored by means of a Chessell 301 miniature chart recorder which had three 10 mV input channels, chart scale width was 10 cm and the recorder response was extremely rapid.

The operating conditions under which the NO_x analyser was run were:

a) O_2 pressure:- 2 psi.

b) Reaction chamber vacuum:- 8-15 mm Hg.

c) Sample vacuum:- 5 ins. Hg.

d) Sample flow:- 0.5-2.0 scfh, typically 0.7 scfh of which ≈ 5% reached the reaction chamber, the remainder being bypassed.

Whenever the instrument was required for actual data acquisition it was turned on at least 24 hours beforehand to ensure that it had completely warmed up. The photo-multiplier dark current was then read (usually 0-0.5 ppm), before the instrument was zeroed and calibrated i.e. ready for use. Calibration gas used was 950 ppm NO in N_2.

Two Grubb Parsons SB2 Infra Red Gas Analysers (IRGA) were used for the purpose of continuously measuring CO and CO_2 concentrations in the sampled gases. As Fig.5.28(A) shows, they were connected in series, this posed no real disadvantage from a response time point of view since steady state readings only were required. A water manometer was connected as shown, sufficient flow to the analysers was assured if a pressure drop across them of 4" W.G., i.e. ≈ 500 cc/min was registered. Both IRGA's were connected to the remaining channels of the Chessell miniature chart recorder after the output potentiometers on each analyser were first substituted with lower range types, this enabled sensitive adjustment of the output signal in the range 0-10 mV. Fig.5.28(B) illustrates the principal components comprising the IRGA.

Nitrogen was employed as zero gas and a standard gas containing 7% CO_2, 3% CO used for calibration purposes. Both IRGA's were serviced before use and were

left permanently switched on to assure steady state operation. As Fig.5.28(A) shows, it was a simple matter to check the zero/calibration of each instrument before making any actual measurements.

As Fig.5.26 shows, provision was also made in the sampling line for the connection of another analyser, however this take-off point was normally used whenever batch samples were required to be accumulated in sample bottles for analysis by gas chromatograph. This method of analysis was used for checking IRGA operation and for the estimation of CH_4 levels, as the latter were found to be typically < 1% they were not in fact further investigated.

5.8(e) Isokinetic Sampling Procedure.

Due to the importance of sampling isokinetically which was stated in 5.8(a), an experimental procedure was devised that enabled the sample mass flowrate to be adjusted so that isokinetic sampling under any burner exit flow conditions could be obtained as accurately as possible. It is perhaps worth mentioning that various gas sampling probes have been designed which feature additional capillaries, these allow simultaneous measurement of static and dynamic pressures within the probe. The sample flowrate from the probe can then be adjusted until these pressures balance and the isokinetic sampling condition is achieved. Such probes suffer three drawbacks however, firstly construction difficulty is enhanced, secondly the overall probe cross-sectional area is inevitably increased and lastly the additional capillaries may be prone to blockage.

Four variables are required to be measured from the rig to provide input data for the procedure, they are:

i) thermocouple probe voltage output, MV millivolts.

ii) pitot probe manometer reading, h" W.G.

iii) rig ambient temperature, T_R ^{o}C (as measured using a Comark digital thermometer).

iv) sample line vacuum, ΔS mm Hg.

The thermocouple output MV was translated into the estimated mean gas temperature, after radiation heat losses had been corrected, using the technique described in Appendix C. Using this method together with the equation of state

a curve of burner exit flow density ρ_p as a function of the variable MV was constructed, assuming the gases to be composed predominantly of nitrogen. This curve is presented in Fig.5.25 and was fitted by the quadratic equation:

$$\rho_p = (0.497 - 0.0325\ MV + 0.00072\ MV^2)\ kg/m^3 \quad \ldots\ldots\ldots \quad (5.10)$$

$$8 \leq MV \leq 18 \text{ millivolts}$$

The burner exit flow mean velocity V was computed from:

$$V = \left(\frac{498.18\ h}{\rho_p}\right)^{\frac{1}{2}} \quad m/sec \quad \ldots\ldots\ldots \quad (5.11)$$

Now, mean isokinetic sample flowrate is given by:

$$\dot{m}_I = \pi \frac{d^2}{4} V\ \rho_p \quad kg/sec \quad \ldots\ldots\ldots \quad (5.12)$$

where, d = Probe sample capillary ID = 0.84×10^{-3} m.

Measurements of the probe sample exit flow temperature with the NiCr/NiAl thermocouple established that this temperature never exceeded 27° C (see next section 5.8(f)), hence after passing the cooled water trap, the sample temperature was assumed to be close to ambient.

Hence, sample volumetric flowrate at rotameter conditions is:

$$\dot{Q}_R = \pi \frac{d^2}{4} V \frac{\rho_P}{\rho_R} \cdot 60{,}000 \text{ lit/min} \quad \ldots\ldots\ldots \quad (5.13)$$

$$\rho_R = \frac{28}{22.4} \cdot \frac{273}{(273+T_R)} \frac{(730-\Delta S)}{760} \quad kg/m^3 \quad \ldots\ldots\ldots \quad (5.14)$$

The rotameter calibration was at N.T.P., Fig.5.30, so that it was necessary to apply a density correction before the rotameter could be used for measuring sample flowrate:

$$\dot{Q}_{NTP} = \dot{Q}_R \left(\frac{\rho_R}{\rho_{NTP}}\right)^{\frac{1}{2}} \quad \ldots\ldots\ldots \quad (5.15)$$

Now, the calibration curve Fig.5.24 was fitted by the linear relation:

$$SC = 5.16\ \dot{Q}_{NTP} + 0.46 \quad , (SC \leq 8) \quad \ldots\ldots\ldots \quad (5.16)$$

Combination of the above six equations then yields an expression for the rotameter scale reading SC which corresponds to isokinetic sampling for any rig experimental conditions:

$$SC \simeq 5\left[\frac{h\,\rho_p(273 + T_R)}{(730 - \Delta S)}\right]^{\frac{1}{2}} + 0.46 \quad \ldots\ldots\ldots \quad (5.17)$$

where ρ_p is given by (5.10).

A Hewlett Packard HP25 electronic calculator was programmed to compute SC, using (5.10) and (5.17), from the four rig variables. The sample line regulator could then be adjusted until this flowrate was indicated on the rotameter. ΔS was a function of regulator setting so that the program allowed updating of SC as the sample flowrate was varied. The advantage of using the portable calculator was that the isokinetic sample flowrate for any experimental conditions could be rapidly and easily set (essential due to finite sampling run times) whilst working on the rig.

5.8(f) Gas Sampling Runs.

With the blue flame burner fired on kerosine a series of data acquisition runs was made to measure exit flow velocities, temperatures and $CO/CO_2/NO_x$ species concentrations for a range of operating conditions. Such data was acquired after burner steady state exit flow temperatures had been reached ($\simeq$ 15 minutes), at which point the cooled sampling probe was mounted into the sampling stage. The probe was purged as described in 5.8(d) whenever not actually sampling; a single probe failure, as manifested by a water leak from the tip, was experienced after $\simeq$ 10 hours sampling time. This was remedied by resoldering the tip. Due to the limited sample flow available analysis for either CO/CO_2 or NO_x was made during each run, throughout which frequent zero and calibration checks were made. The maximum probe cooling water exit temperature observed was $\simeq 43^{\circ}$ C.

The maximum sample temperature at the probe exit measured throughout the sampling runs was 27° C, this value was used in the quench efficiency calculations, Appendix C.

Initial test runs proved that, under all conditions, the NO_2 content of the sampled gases never exceeded 5% of the measured NO_x. The NO_x Analyser (CLA) was therefore used only in the NO mode, so that use of the CLA converter and hence the associated interference errors for this device (5.8(a)), were avoided.

A series of tests under various conditions was carried out to determine whether or not the actual probe could introduce similar interference errors, the procedure used was:

1. Set the isokinetic sampling rate, 5.8(e), and measure the corresponding NO concentration with the CLA for the probe located in the hot exit flow.
2. Turn off sample pump; change from sampling to purging mode and switch pump back on. (Air pumped back through the probe and hence no surface (reduction) interference reactions).
3. Turn off sample pump; quickly change from purging to sampling mode and turn the pump on again.
4. Examine the time dependency of the CLA-measured NO response using the chart recorder. Compare steady state value with 1.

Fig.5.29 shows typical transient responses observed for CLA-detected NO using the chart recorder, for both stoichiometric and fuel rich overall burner operation, where the estimated overall equivalence ratio for the burner ϕ_{ov} is defined as:

$$\text{Fuel flow rate} = \dot{m}_{FUEL} = -0.0129 + 0.00641\, P_f^{\frac{1}{2}} - 0.000207\, P_f \text{ kg/min} \quad \ldots (5.18)$$

$$\text{Air flow rate} = \dot{m}_{AIR} = \dot{Q}_j\, \rho_j \times 10^{-3} \text{ kg/min} \quad \ldots (5.19)$$

Applying a density correction to $\dot{Q}_j$ to allow for the rotameter calibration (NTP):

$$\dot{m}_{AIR} = \dot{Q}_j\, \rho_j \left(\frac{1.227}{\rho_j}\right)^{\frac{1}{2}} \times 10^{-3}$$

$$= 7.554 \times 10^{-4}\, \dot{Q}_j \left(\frac{730 + 25.4\, P_{cc}}{273 + T_{ROT}}\right)^{\frac{1}{2}} \text{ kg/min} \quad \ldots (5.20)$$

where, P_{cc} = blue flame burner air manifold pressure, "Hg.

T_{ROT} = rotameter air temperature, ^{o}C.

Hence, ϕ_{ov} is given by:

$$\phi_{ov} \simeq \frac{\left(\frac{\dot{m}_{FUEL}}{\dot{m}_{AIR}}\right)}{\left(\frac{\dot{m}_{FUEL}}{\dot{m}_{AIR}}\right)_{stoich}} = \frac{\dot{m}_{FUEL}}{0.068\, \dot{m}_{AIR}} \quad \ldots (5.21)$$

when the burner is fuelled with kerosine.

Referring back to Fig.5.29 it is apparent that steady state levels are attained after ≈ 20 sec. although kinks in the curves are observed before the same

steady state levels are regained. These kinks are due to the pressure pulse transmitted by the pump when it is turned on. It is important to note that only a decay of about 5% in steady state response is apparent for rich operation only, hence it was concluded that possible interference reactions within the probe would have minimal effect on the accuracy of NO gas sampling measurements. Similar tests were conducted for CO/CO_2 measurement, for which zero decay in steady state level was observed.

Fig.5.31 shows the CO_2 measured in the burner exit flow as a function of the indicated air rotameter reading $\dot{Q}_j$ (i.e. density correction not applied, small) and for a range of P_f. Fig.5.32 presents the similar characteristic for CO pollutant emissions, it should be noted that all gas sampling data was obtained under isokinetic sampling conditions and is expressed on a dry basis.

In the next series of runs the BFB NO emission characteristic was measured, soon after commencing this series the burner became noticeably noisier, with exit flow mean temperatures somewhat higher than usual. On dismantling the burner the recycle path was found to be partially blocked with flaked/oxidised mild steel which had lifted away from the combustion chamber wall. Removal of this material caused a resumption of normal BFB operation. NO emissions and exit temperatures were determined for each of these 2 "modes" of operation, Figs. 5.33, 34, 35 present this data for 3 values of P_f and for the former mode of operation. Figs. 5.36, 37, 38 give the same characteristics for exactly the same conditions but for the latter, i.e., normal, mode of operation. The former set of curves then, correspond to reduced levels of internal recirculation, accordingly higher values of NO and exit temperature were observed than for normal burner operation. Note that selected values of ϕ_{ov} are additionally given on each plot (non linear scale) and that in all cases NO decreases as $\dot{Q}_j$ is reduced from stoichiometric proportions, until a minimum is attained, after this point it increases again as the burner operation changes from the Blue- to the Yellow-Flame mode.

Fig.5.30 shows the effect of the probe sampling rate on the measured gas concentration for each of the species CO, CO_2 and NO. The curves were obtained for the former mode of BFB operation (as described above), as were the transient response curves given in Fig.5.29.

The BFB air manifold pressure P_{cc} as $f(\dot{Q}_j)$ is depicted in Fig.5.39, it is only a weak function of P_f. Another burner operating characteristic, the exit flow mean velocity as $f(\dot{Q}_j)$ is given in Fig.5.40, this is also only weakly dependent on P_f.

5.8(g) Additional measurements.

CO, CO_2, NO profiles in the BFB exit flow orifice were found to be nearly flat with the maximum in each occurring on or close to the burner central axis.

Since a cooling of the recirculated combustion products is to be expected during flow around the Coanda unit it was decided to estimate the mean temperature of these gases just prior to entry of the inlet plane of this unit, i.e. after heat exchange. A Pt/Pt 13% Rh thermocouple(bead diameter 0.4 mm) was thus mounted through the burner headplate after being conventionally coated with silicon to minimise catalytic effects. Radiation heat losses experienced by this thermocouple were assumed to be low. Table V presents the results that were obtained, this temperature is seen to be 1100 $\pm$ 70 K.

Finally, Plate 5 shows the condition of the burner combustion chamber and Coanda unit after completion of all the above tests. Note the "scaling" exhibited by these mild steel components, particularly (i) combustion chamber - immediately downstream of Coanda (i.e. main flame zone), (ii) Coanda unit - rear face. Note also the absence of such effects in the cooler recirculation and exit flow regions.

TABLE V. MEASURED MEAN GAS TEMPERATURES; BFB RECIRCULATION PATH

Indicated $\dot{Q}_j$(lit/min)	550	500	450	400	380	350	320	300	280	250
A-Temperature(K); P_f=160 psig	1033	1033	1041	1114	1146	1138	1090	1066	-	1041
B-Temperature(K); P_f= 120 psig	1024	1024	1033	1049	-	1122	1138	1114	-	1057
C-Temperature(K); P_f=80 psig	1033	1033	1041	1049	-	1016	1066	1114	1114	1074

CHAPTER 6.

ON-LINE AUTOCORRELATION MEASUREMENTS

6.1 Introduction.

The phenomenon of turbulence and its influence on physical mixing processes in heterogeneous combustion has been introduced previously, 2.2(c) and 3.5, where it was shown that energy spectra, intensities and characteristic scales are the most important turbulence parameters with respect to mixing. The various eddy size ranges comprising the energy spectrum were also identified in this section, rates of turbulent mixing are governed by the energy containing eddies although the actual process is carried out by the dissipation eddies. Because a) relatively little is known about the behaviour of turbulence eddies under hot or isothermal conditions, b) turbulent mixing processes are fundamental to all types of combustion, it was decided to measure typical turbulence scales encountered in the blue flame burner internal flow. Use was made of the hot wire anemometry setup that was employed for mean velocity measurements described in 5.4, this unfortunately ruled out investigation of the hot flow. This Chapter then, describes an extremely interesting technique that was developed for the estimation of characteristic turbulence scales by the on-line analysis of hot wire anemometer signals, using a digital computer.

It is possible to make reasonable estimates for characteristic turbulence scales from turbulence correlation functions, these are of two types.

6.2 Cross Correlation Function.

This is defined mathematically:

$$R_{xy}(\tau) = \lim_{T\to\infty} \frac{1}{T} \int_0^T x(t)y(t-\tau)dt \quad \ldots\ldots\ldots \quad (6.1)$$

for the two signals x(t) and y(t) obtained from two hot wire probes placed close together in the turbulent flow, the function relates the similarity between one of the waveforms and a time shifted version of the other waveform. It is possible to

derive characteristic eddy length scales from the form of curve (6.1) but the method has the serious drawback that spurious results can be obtained due to the eddy shedding of the forward probe. In addition, the limited area available at the burner exit for the insertion of probes, ruled out the accurate positioning of more than one probe within the combustor flowfield.

6.3 Auto Correlation Function.

This function is defined:

$$R_{xx}(\tau) = \lim_{T\to\infty} \frac{1}{T} \int_{o}^{T} x(t)x(t-\tau)\, dt \quad \ldots\ldots\ldots \quad (6.2)$$

The autocorrelation function relates the similarity between a waveform and a time-shifted version of the same waveform. It is again possible to derive characteristic length scales from the curve, this approach has the considerable advantage that a single probe is required to measure this curve. When a particular eddy is distant from the probe $|R_{xx}(\tau)|$ is zero and when the eddy is central about the probe $|R_{xx}(\tau)|$ has the value unity; hence the time taken for the eddy to sweep past the probe can be deduced and consequently the eddy size estimated.

The autocorrelation function is convenient to work with also since:

$$R_{xx}(\tau) = R_{xx}(-\tau)$$

As Fig.6.1(ii) depicts the curve maximum occurs at $\tau = 0$, the diagram shows also that for a typical autocorrelation function there is a zero crossing before the curve gradually settles back to zero. The autocorrelation shown in Fig.6.1(ii) is of the normalised type $\rho_{xx}(\tau)$, where:

$$\rho_{xx}(\tau) = R_{xx}(\tau)/R_{xx}(0) \quad \text{and} \quad -1 \leq \rho_{xx}(\tau) \leq +1 \quad \ldots\ldots\ldots \quad (6.3)$$

As will be seen shortly, it is possible to transform (6.2) to the frequency domain by means of the Wiener-Khintchine relation to obtain the corresponding Power Spectrum, which can give useful information concerning the dominant turbulence frequencies.

Turning to characteristic autocorrelation-derived length scales, the macro timescale τ_{ma} is defined as the integral of the normalised autocorrelation function:

$$\tau_{ma} = \int_{o}^{\infty} \rho_{xx}(\tau)d\tau \quad \ldots\ldots\ldots \quad (6.4)$$

It is then, simply the area under the curve. Now for a turbulence of relatively low intensity it is possible to invoke Taylor's Hypothesis to obtain the corresponding length scale λ_{ma}. This hypothesis states that time variations in the flow velocity observed at a fixed point would be approximately those due to the convection of an unchanging spatial pattern past the point with the mean flow velocity $\bar{U}$. Hence,

$$\lambda_{ma} = \tau_{ma} \bar{U} = \bar{U} \int_0^\infty \rho_{xx}(\tau) d\tau \quad \ldots\ldots\ldots \quad (6.5)$$

This macroscale is also known as the integral scale, it tends to select the average size of the largest eddies in the turbulence spectrum. The micro time and length turbulence length scales are defined mathematically:

$$\tau_{mi}^2 = - \frac{1}{\rho_{xx}^{(2)}(0)} \quad \ldots\ldots\ldots \quad (6.6)$$

and using Taylor's Hypothesis again,

$$\lambda_{mi} = \tau_{mi} \bar{U} \quad , \quad \therefore \quad \lambda_{mi}^2 = - \bar{U}^2 \frac{1}{\rho_{xx}^{(2)}(0)} \quad \ldots\ldots\ldots \quad (6.7)$$

The microscale is characterised by the correlation function near the origin since the shape of the curve in this region is attributable to the smallest eddies of corresponding high frequency present in the turbulence. For small values of τ the autocorrelation curve may be approximated by a parabola, Fig.6.2, this is known as the osculation parabola. The micro length scale λ_{mi} is considered to be a measure of the smallest eddies, to measure this to any real accuracy naturally requires that the length of the hot wire probe be of the same order as the smallest eddies present. It is well known that the correlation function may be expressed in the form of a Taylor Series:

$$\rho(\tau) = 1 + \frac{1}{2!} \tau^2 \left[\frac{\partial^2 \rho}{\partial \tau^2}\right]_{\tau=0} + \frac{1}{4!} \tau^4 \left[\frac{\partial^4 \rho}{\partial \tau^4}\right]_{\tau=0} + \ldots \quad \ldots\ldots \quad (6.8)$$

Taking only the first 2 terms of this series, we can deduce an expression for the osculation parabola, using (6.6):

$$\rho(\tau) = 1 - \frac{1}{2} \frac{\tau^2}{\tau_{mi}^2} \quad \ldots\ldots\ldots \quad (6.9)$$

and (6.8) can be conveniently reexpressed:

$$\rho(\tau) = 1 - \frac{1}{2} \frac{\tau^2}{\tau_{mi}^2} + \frac{1}{24} \rho^{(4)}(0) \tau^4 + \ldots\ldots \quad \ldots\ldots\ldots \quad (6.10)$$

6.4 Correction of Measured Autocorrelation Length Scales.

Any correlation measuring system has a finite time-resolution power, this causes a smoothing of the correlation function which is naturally undesirable, the time-resolution power is characterised by amplitude and phase attenuation at high frequencies. It can be shown (113) that the time resolution error is usually negligible for a properly adjusted hot wire anemometer, so that the time resolution error (i.e. finite frequency response) of the correlation measuring system need only be evaluated. Before describing the correlation measuring system used a method for correcting measured autocorrelation length scales is presented, the method is due to Andersen (114). Measured autocorrelations and associated length scales are bracketed as < >. Fig.6.3 illustrates the general setup in which a hot wire anemometer is used to transduce the turbulent velocity fluctuations and X(f) is the frequency response function for the Total Measurement System. X(f) has separate phase and amplitude components.

Now it may be shown that (1) the power spectrum of the output signals $\langle G_{xx}(f) \rangle$ is related to the power spectrum of the input signals $G_{xx}(f)$ by:

$$\langle G_{xx}(f) \rangle = X(f)^* X(f) . G_{xx}(f) \quad \ldots\ldots\ldots \quad (6.11)$$

where, * denotes a complex conjugation.

The Wiener-Khintchine relation is:

$$F\left[R(\tau)\right] = \int_{-\infty}^{\infty} R(\tau) . e^{-i\omega\tau} \, d\tau = \tfrac{1}{2} G(f) \quad \ldots\ldots\ldots \quad (6.12)$$

where, $F\left[\ \right]$ denotes a Fourier Transform; $\omega = 2\pi f$

Hence, (6.11) may be rewritten:

$$F\left[\langle R_{xx}(\tau) \rangle\right] = X(f)^* X(f) . F\left[R_{xx}(\tau)\right] \quad \ldots\ldots\ldots \quad (6.13)$$

or, alternatively, in the more useful form:

$$R_{XX}(\tau) = \int_{-\infty}^{\infty} \langle R_{xx}(\tau-t)\rangle \, \alpha_{XX}(t) = \hat{K}_{XX} \langle R_{xx}(\tau)\rangle \quad \ldots\ldots\ldots \quad (6.14)$$

after transforming to the time domain, where,

$\alpha_{XX}(t) = F^{-1}\left[\frac{1}{X^*X}\right]$ = the Weighting Function describing correlation correction

$\hat{K}_{XX}$ = the Operator for correction of measured autocorrelations.

The problem then is to derive an expression for $\hat{K}_{XX}$ to enable measured autocorrelation functions to be corrected for the finite frequency response property of the total measuring system. As a first approximation this property is represented by the characteristics of a low pass filter, i.e.:

$$X = \frac{b_x}{b_x + p} \quad \ldots\ldots\ldots \quad (6.15)$$

where, $p = i\omega$

$f_x = b_x/2\pi$ = filter cut off frequency.

Therefore:

$$\alpha_{XX} = F^{-1}\left[\frac{b_x}{(b_x-p)} \cdot \frac{b_x}{(b_x+p)}\right]^{-1} = F^{-1}\left[1 - \frac{p^2}{b_x^2}\right]$$

$$= \delta(t) - \frac{1}{b_x^2}\,\delta^{(2)}(t) \quad \ldots\ldots\ldots \quad (6.16)$$

Since, (114):

$F^{-1}(p^n) = \delta^{(n)}(t)$; δ = delta function

(n) = n^{th} derivative

So that (6.16) into (6.14) becomes:

$$\int_{-\infty}^{\infty} \langle R_{xx}(\tau-t)\rangle \, \alpha_{XX}(t)\,dt$$

$$= (-1)^0 \langle R_{xx}(\tau)\rangle - \frac{1}{b_x^2}(-1)^2 \langle R_{xx}^{(2)}(\tau)\rangle$$

$$= \left(1 - \frac{1}{b_x^2}\frac{\partial^2}{\partial\tau^2}\right) \langle R_{xx}(\tau)\rangle \qquad \ldots\ldots\ldots \qquad (6.17)$$

Since, (114):

$$\int_{-\infty}^{\infty} \delta^{(n)}(t)\, R(\tau - t)\, dt = (-1)^n R^{(n)}(\tau)$$

Hence, the required correction expression for this case is:

$$\hat{K}_{XX} = \left(1 - \frac{1}{b_x^2}\frac{\partial^2}{\partial\tau^2}\right) \qquad \ldots\ldots\ldots \qquad (6.18)$$

An expression for the undistorted macroscale λ_{ma} in terms of $\langle\lambda_{ma}\rangle$, the measured macroscale, may now be deduced. From (6.5):

$$\frac{\langle\lambda_{ma}\rangle}{\lambda_{ma}} = \frac{\bar{U}\int_{-\infty}^{\infty}\langle\rho_{xx}\rangle\, d\tau}{\bar{U}\int_{-\infty}^{\infty}\rho_{xx}\, d\tau} = \frac{R_{xx}(0)}{\langle R_{xx}(0)\rangle}$$

this is because X*X = 1 at f = 0.

Hence, using (6.3),(6.14) and (6.18):

$$\frac{\langle\lambda_{ma}\rangle}{\lambda_{ma}} = \left(1 - \frac{1}{b_x^2}\frac{\partial^2}{\partial\tau^2}\right)\langle\rho_{xx}(\tau)\rangle\Big|_{\tau=0}$$

Inserting (6.10) into this equation gives:

$$\frac{\langle\lambda_{ma}\rangle - \lambda_{ma}}{\lambda_{ma}} = \frac{\langle\tau_{ma}\rangle - \tau_{ma}}{\tau_{ma}} = \beta' = \frac{1}{b_x^2\langle\tau_{mi}\rangle^2} \qquad \ldots\ldots\ldots \qquad (6.19)$$

An expression for the undistorted microscale λ_{mi} in terms of $\langle\lambda_{mi}\rangle$, the measured microscale, may now be similarly obtained. Using (6.10):

$$\langle\rho^{(2)}(\tau)\rangle = -\frac{1}{\langle\tau_{mi}\rangle^2} + \frac{1}{2}\langle\rho^{(4)}(0)\rangle\,\tau^2$$

Since $\hat{K}_{XX}$ is linear:

$$R^{(2)}_{xx}(\tau) = \hat{K}_{XX}\langle R^{(2)}_{xx}(\tau)\rangle$$

$$\therefore \quad \frac{R_{xx}^{(2)}(\tau)}{\langle R_{xx}(0)\rangle} = \hat{K}_{XX}\langle\rho_{xx}^{(2)}(\tau)\rangle = \left(1 - \frac{1}{b_x^2}\frac{\partial^2}{\partial\tau^2}\right)\left(-\frac{1}{\langle\tau_{mi}\rangle^2} + \frac{1}{2}\langle\rho^{(4)}(0)\rangle\tau^2\right) \quad \ldots\ldots (6.20)$$

Substituting $\tau = 0$ into (6.20) and using the previous result (6.19):

$$\rho_{xx}^{(2)}(0) = \left(-\frac{1}{\langle\tau_{mi}\rangle^2} - \frac{1}{b_x^2}\langle\rho^{(4)}(0)\rangle\right)\left(\frac{b_x^2\langle\tau_{mi}\rangle^2}{1 + b_x^2\langle\tau_{mi}\rangle^2}\right)$$

So that, using (6.6):

$$\frac{\langle\tau_{mi}\rangle^2}{\tau_{mi}^2} = \frac{1 + (b_x/\langle\tau_{mi}\rangle)^{-2}\langle\rho^{(4)}(0)\rangle}{1 + \beta'} \quad \ldots\ldots\ldots \quad (6.21)$$

Equations (6.19) and (6.21) enable approximate corrections to the measured macro and micro scales respectively to be made using a simple frequency response analysis. This treatment could be made more detailed if X(f) for any actual measuring system is accurately known.

6.5 Autocorrelation Measurement Facility.

A PDP 8/E digital computer was used for the on-line acquisition of autocorrelation data, a DISA 55D05 hot wire anemometer being employed to transduce isothermal turbulent velocity fluctuations. The complete hot wire anemometry setup has been previously described in (5.4,5.5), see Fig.5.9,5.10. After appropriate filtering, the hot wire anemometer signal (from point A of Fig.5.9. Fig.6.1(i) shows a typical hot wire anemometer output signal at any instant in time, the DC Level having been removed, note the range of frequencies present.) was fed into a LAB 8/E (Dec Standard Equipment) interface system, before actually entering the computer which was programmed to control i) data acquisition, ii) data storage and iii) data processing to derive the required autocorrelation function.

Fig.6.4 schematically shows the complete hardware arrangement which was used, the function of the filter network F will be discussed shortly. As this diagram shows, magnetic disc and tape deck peripheries were available for intermediate and final data storage, the computer was interactively controlled by a teletype device.

Hot wire anemometer signals were digitised by an A→D converter before being processed by the PDP8/E, a multiplexing unit was needed for the electronic scanning of information input channels - although only one channel was required for auto-correlation measurement. An electronic clock unit provided input to the computer since time-dependent calculations had to be performed. On the output side a Visual Display Unit and an XY Plotter were connected via a D→A converter. The VDU enabled instantaneous display of either the input anemometer signal or the computed autocorrelation function as desired, throughout the course of data acquisition. From equation (6.2) it can be appreciated that a considerable amount of time is required to accurately compute an autocorrelation, hence the value of the VDU for monitoring purposes. The XY Plotter was used for making hard copies of any particular curve displayed on the VDU, the XY plotter was synchronised to the VDU device.

Now the sampling of continuous information is in fact a critical operation which is subject to important restrictions. The most important limitation to continuous sampling of information was first formulated by Shannon, whose theorem states that the maximum frequency of a sampled signal must not be greater than one half the frequency corresponding to the maximum sampling rate of the system. Frequencies greater than this maximum value are incorrectly interpreted as lower ones, unless they are removed noise is introduced into the sampled signal. As will be discussed below the maximum sampling rate of the autocorrelation measurement facility was 0.1 millisec so that the maximum frequency which could be sampled was 5000 Hz, hence the use of the filter network F which is shown in more detail in Fig.6.5. Since only the fluctuating component of the anemometer signal was required the DC level was removed by means of the high pass section of the filter, time constant R'C' = 0.1 sec. Frequencies greater than the maximum permissable were suppressed by means of the differential amplifier, whose bandwidth was set at 6 - 6000 Hz. The differential amplifier was thus effectively used as a low pass filter which would have dropped the signal down to 3 dB at 10,000 Hz; the rate of signal dropoff was boosted to ensure that it was 10 dB down at this frequency, a

low pass filter section of time constant RC = 0.2 millisec was thus used. Now the range of signal voltage which could be fed to the A→D converter was $\pm$ 1 volt, the input potentiometer located on the interface was therefore adjusted to ensure that the filtered signal was within this range. It should be appreciated that the net measuring system exhibited approximately the characteristics of a lowpass filter of cut off frequency f_x = 5000 Hz. The technique described in 6.4 was used to correct measured autocorrelations for the associated time resolution error.

Turning now to the software side of the PDP 8/E on-line technique, a standard (Dec) program CORD3 was employed for the acquisition of autocorrelation data. CORD3 completely handled the input of information to the system, data storage and evaluation of the normalised autocorrelation function, control of CORD3 was effected by means of high level commands transmitted from the teletype. The maximum sampling rate of the hardware plus software combination was 0.1 millisec. Processing of the acquired data will be described in 6.7.

6.6 Experimental Procedure.

The turbulence autocorrelation function was measured at various points along the combustor central axis. At each point of measurement the location of the hot wire probe was accurately set by means of its traversing mechanism, after the probe had first been calibrated so that $\bar{U}$ at each point could be determined. All data was obtained at air input flowrates of 300 lit/min. Since the initial section of the autocorrelation curve i.e. before the zero crossing, is of most importance, the range of displaced time τ over which each curve was acquired was 0 → 10 millisec. At each measurement point the correlation function was "built up" for an integration time of at least 30 mins, combustor conditions being frequently checked throughout this period, $\dot{Q}_j$ and anemometer bridge voltage were periodically recorded. The acquired autocorrelation function was then stored as a data file on a magnetic tape for subsequent processing.

6.7 Processing of Autocorrelation Data and Results Obtained.

The data file for each autocorrelation curve was plotted out accurately using the XY plotter and A3 sized paper, these plots then being reduced to A4 size.

A standard (Dec) program DAQUAN for data processing was employed for controlling the XY plotter, the plot routine incorporated in this program was extremely sophisticated and had provision for:

a) Controlling the VDU monitor (on which the particular curve was first displayed).

b) Synchronizing the XY Plotter.

c) Calibrating the Plotter.

d) Plotting a graticule plus scales on the paper as well as the curve.

e) Overall control of the plotting routine from the teletype.

f) Providing a linear interpolation between each point.

Before the actual autocorrelation data file could be loaded into DAQUAN a series of conversions was necessary to ensure that the data had the correct format and was in the range, $0 \leq$ (data value) ≤ 1000. A BASIC program was written to handle this conversion and also compute measured correlation timescales, the program then corrected these values for the time resolution error as detailed in (6.4). Appendix D describes this program in some detail. Multiplication of these timescales by the prevailing mean velocity $\bar{U}$ then yielded the required estimates of micro and macro length scales for that measurement point.

Using the above measurement and processing techniques data was acquired for a range of points along the combustor central axis, Fig.6.7 is an example of a measured autocorrelation for $\ell/(\ell_4 + \ell_{ex}) = 0$. In each case isothermal flow, characterised by $\dot{Q}_j$ = 300 lit/min , was prevalent. Fig.6.6 then shows the profiles of λ_{ma} and λ_{mi} that were derived, these results are discussed in Chapter 8.

CHAPTER 7.

THEORETICAL MODEL AND PREDICTIONS

7.1 Foreword.

This section presents details of the mathematical model which was derived for the blue flame burner and utilised the general stirred reactor and evaporation theory given in Chapter 4. A great deal of model input information was obtained experimentally, as described in Chapter 5, this data is hence discussed in this Chapter rather than in the succeeding one. Model predictions are then presented.

7.2 The Blue Flame Burner Stirred Reactor Network.

In 3.2 the BFB "expected" flow pattern was described in order to explain the burner operating principle, confirmation of this flow pattern was provided by the isothermal hot wire anemometer measurements of $\bar{U}$ and T%, 5.5. Examination of Fig.5.12 shows the position of the high velocity attached layer, this profile decays to that shown in Fig. 5.11 at the Coanda exit plane due to mixing across the attached layer. Notice that the centre line velocity is increasing as would be expected. As Fig. 5.13 shows this axial mean velocity continues to increase until $\ell \approx 0.15\ (\ell_4 + \ell_{ex})$, after this point $\bar{U}$ decays until a constant value is reached at $\ell \approx 0.55\ (\ell_4 + \ell_{ex})$. Now the Coanda exit flow is a type of enclosed jet flow, as illustrated in Fig.7.1, with the point of impingement on the combustor wall Z occurring at distance $\ell_3 = 0.55\ (\ell_4 + \ell_{ex})$ from the Coanda exit plane. Hence the boundary of this enclosed jet, prior to Z, is given approximately by the dashed line in Fig.7.1, $\bar{U}$ thus decreases in this region as the flow effective cross sectional area increases. Recirculation of combustion products from the flame zone takes place across this boundary. Fig.5.14 shows that the axial turbulence intensity varies as the reciprocal of $\bar{U}$, again it should be emphasised that Fig.5.14 provides only the trend in, and not accurate magnitude of, axial T%. Regions of accelerating flow are characterised by decreasing T% and vice versa. T% decays through the dissipation of turbulence energy although, as Fig.5.14 shows, not to very low levels as required for perfect mixing. Note that $\bar{U}$ decreases slightly just before $\ell = 0.83\ (\ell_4 + \ell_{ex})$,

this is due to the fact that a small amount of flow recirculates at this point as shown in Fig.7.1. Beyond this point $\bar{U}$ increases to a new constant value at $\ell = 0.9\ (\ell_4 + \ell_{ex})$ due to a contraction of the flow by the exit orifice.

From the above flow pattern considerations it is possible to deduce a stirred reactor network to model the BFB combusting flow at steady state, assuming the hot flow pattern to be essentially the same as the isothermal flow; this network is given in Fig.7.2.

Since the mean gaseous residence time in the Coanda unit throat is so small (volume ≈ 30 cm^3) it follows that a stirred reactor (stable) could not be used to represent this region, hence the throat is assumed to act as an isothermal mixer of atomising spray, feed air and recirculated gases. The mean gaseous residence time in this volume is assumed to be equal to the spray atomisation time. WSR_1 is used to approximate the main flame zone, its volume is assumed equal to the truncated cone bounded by the dashed lines in Fig.7.1, i.e. 240 cm^3. Equation (2.22) and Figs. 5.39,40 were used to estimate the mixing parameter τ_{SD} for this reactor, its value is thus 300. The secondary flame zone is represented by another well stirred reactor WSR_2, rather than a PFR due to two main considerations. Firstly the level of CO_2 in the BFB exit flow, Fig.5.31, is not compatible with complete burnout, and secondly the relatively high levels of $\bar{U}$ and T% in the exit flow suggest insufficient dissipation of turbulence energy. The volume WSR_2 is the combustion chamber volume downstream of the point Z i.e. 280 cm^3, τ_{SD} for this reactor was therefore set to a low value - it was estimated as being of the order of 7. Plate 5, which is discussed in 5.8(g), also confirms the position of the main flame and cooler zones. Both stirred reactors in Fig.7.2 are assumed to operate adiabatically as a first approximation.

7.2(a) Blue Flame Burner Recirculation Level.

Measurements of the BFB internal recirculation characteristic under isothermal flow conditions were described in 5.4. Fig.5.8 portrays ψ as $f(\dot{Q}_j)$ for 3 values of slit width S. Now if the measured estimates for λ_j and λ_o given in this section are inserted into (4.79) for S = 0.010 inches, i.e. $A_o/A_j = 23$, then this theoretical equation may be directly compared with the appropriate curve in Fig.5.8. Hence it is

estimated that the entrainment efficiency factor η relating the theoretical value of ψ to the typical measured value, $\simeq$ 0.39 for $\dot{Q}_j > \simeq$ 250 lit/min. The justification for permitting this term in (4.78,79) is provided by the fact that the simple momentum exchange analysis given in 4.5 is almost independent of the "mixing length" between the Coanda inlet and exit planes, since the influence of the skewness factors on ψ is comparatively weak, Fig.4.11. All hot tests made on the BFB were conducted for the above value of S, also, it was necessary to assume that this value of η prevailed under combustion conditions. The term ρ_i in (4.78) corresponds to the recycle gas composition and is evaluated at the measured recycle gas mean temperature given in Table V. The air feed density ρ_j is evaluated at temperature T_{AIR}, which is the estimated air temperature as it passes through the Coanda slit. Hence R_{int} is now directly available via (4.80).

7.3 Spray Evaporation Data.

The molecular formula for the kerosine fuel used in all tests except 5.3 is assumed to be $C_{12}H_{24}$, this is reasonable as its ultimate chemical composition is 86.3% C, 13.6% H_2 and 0.1% S. Other properties of the fuel are density 790 kg/m^3, B.Pt.$\simeq$ 493 K and LHV 300 kJ/kg.

In order to estimate fuel evaporation rates in WSR_1 and WSR_2 the general theory given in 4.4 is used, where $\Delta t = 10^{-4}$ sec. Equation (5.8) is used for calculating $\dot{m}_{FUEL}$ and (4.48→52,55) employed for calculating the fuel spray ISD. Note that these correlations have been adjusted so that they in fact predict the experimentally measured data given in 5.7, also, $\bar{x}'' < \bar{x}$.

The evaporation calculations given in 4.4 are essentially for 1-dimensional flow by necessity. Also, although $V_{Rel}(t)$ exists between the two phases, it is convenient to assume equal phase residence times in all reactors to avoid excessive analytical complexity. Droplet-droplet interference effects within the spray are neglected.

Employing this evaporation model for the BFB Figs. 7.3→5 were predicted, they show FU as a f (time, i.e. distance from the atomiser). the sensitivity of FU(t) to T, $\dot{Q}_j$ and P_f is reflected in Figs. 7.3, 4, 5 respectively.

7.4 General WSR Input Data.

The identity and order of the gaseous species used in the WSR system of equations is as follows:

$(H,N,O,OH,H_2O,Kero,CO,NO,N_2O,CO_2,H_2,O_2,N_2)_{mixed}$; $(O_2,N_2,Kero)_{unmixed}$

hence the values of the integers :- N=9, MT=13, NT=16. The four element conservation balances which are used for calculating γ_i for the last four mixed species are:

$$(\text{Carbon}) = 12\,\text{Kero} + CO + CO_2 \quad \ldots\ldots\ldots \quad (7.1)$$

$$(\text{Hydrogen}) = \tfrac{1}{2}H + \tfrac{1}{2}OH + H_2O + 12\,\text{Kero} + H_2 \quad \ldots\ldots\ldots \quad (7.2)$$

$$(\text{Oxygen}) = \tfrac{1}{2}O + \tfrac{1}{2}OH + \tfrac{1}{2}H_2O + \tfrac{1}{2}CO + \tfrac{1}{2}NO + \tfrac{1}{2}N_2O + CO_2 + O_2 \ldots\ldots \quad (7.3)$$

$$(\text{Nitrogen}) = \tfrac{1}{2}N + \tfrac{1}{2}NO + N_2O + N_2 \quad \ldots\ldots\ldots \quad (7.4)$$

The chemical reaction mechanism and associated kinetic data used to describe kerosine combustion in the BFB model is given in Table VI.

TABLE VI. BFB MODEL REACTION MECHANISM

	Reaction	A_j	E_j (cal/mole)	n_j
1	KERO + 6O2 = 12H2 + 12CO	.552000E+09	.124000E+05	.100000E+01
2	CO + OH = CO2 + H	.560000E+12	.544000E+03	0.
3	H + O2 = OH + O	.220000E+15	.845000E+04	0.
4	O + H2 = OH + H	.180000E+11	.448000E+04	.100000E+01
5	H + O = OH + M	.530000E+16	-.278000E+04	0.
6	H + OH = H2O + M	.140000E+24	0.	-.200000E+01
7	H + H = H2 + M	.300000E+16	0.	0.
8	O + O = O2 + M	.470000E+16	0.	-.280000E+00
9	N + O2 = NO + O	.640000E+10	.315000E+04	.100000E+01
10	N2 + O = NO + N	.760000E+14	.380000E+05	0.
11	N + OH = NO + H	.320000E+14	0.	0.
12	N2 + O = N2O + M	.162200E+12	.160100E+04	0.
13	N2O + O = NO + NO	.458100E+14	.121300E+05	0.
14	N2O + O = N2 + O2	.381100E+14	.121300E+05	0.
15	N2O + H = N2 + OH	.295100E+14	.542000E+04	0.
16	OH + H2 = H + H2O	.219000E+14	.259180E+04	0.
17	OH + OH = O + H2O	.575000E+13	.393000E+03	0.

Note that the first reaction is the quasiglobal reaction (2.27) with n = 12 and m = 24, the reverse rate for this step is zero. The remaining 16 reactions were previously introduced in 2.2(d), the kinetic data for these reactions was taken from Baulch et al (48). It is apparent from Table VI that NR = 17. The coefficients in the thermodata polynomials (4.43) were obtained from McBride et al (110) for all species except gaseous kerosine, the technique devised for obtaining the coefficients for this important species is given in Appendix A.

The equations used to compute equilibrium composition for any specified T are given in Appendix E, in order to additionally calculate T_{eq}, the equilibrium (adiabatic) flame temperature, it is necessary to iteratively solve a heat balance involving product species heat contents and heats of formation. Hence this "full" equilibrium calculation is very time consuming, Fig.7.6 shows the results of such a calculation using a modified computer program written by Burdett (116). T_1 is the reactor feed temperature and the equivalence ratio ϕ_{WSR} is defined:

$$\phi_{WSR} = \frac{\text{Fuel/oxygen}}{(\text{Fuel/oxygen})_{\text{stoich.}}} = \frac{18(\text{Carbon})}{12(\text{Oxygen})} = \frac{3\,[(7.1)\ \text{RHS}]}{2\,[(7.3)\ \text{RHS}]} \quad \ldots\ldots \quad (7.5)$$

ϕ_{WSR} is conveniently defined in this way since a reactor feed stream may contain any species which appears in(7.1,3) as reactants. It was found that the temperature $(T_{eq} - 200)$ provided a good initial guess for commencing the WSR solution procedure shown in Fig.4.2. In order to avoid the time consuming computation of $(T_{eq} - 200)$ in the model, each of the curves in Fig.7.6 were fitted by three straight lines, linear interpolation being used for any T_1 between these curves. The above relation for ϕ_{WSR} allowed this guess to be applicable to all reactors in a network.

7.5 Computer predictions.

The computer program GRASP was developed for general heterogeneous combustor simulation studies in accordance with the requirements in 2.5. It is intended that a wide variety of stirred reactor networks may be investigated using this basic program. GRASP is presented and fully described in Appendix F.

7.5(a) Effect of τ_{SD} on WSR temperature.

As mentioned in F(a)parametric evaluations are efficiently carried out using Subroutine DALTER of GRASP, this facility was used to determine the effect of τ_{SD} on WSR performance with respect to T_2. Fig.7.7 shows the results obtained for a single WSR fed with air and completely vapourised kerosine, $\phi_{WSR} = 0.7$; the results are given for three levels of recirculation.

7.5(b) General WSR observations.

It was found that WSR solution oscillation occurred for the full scheme given in Fig.4.2, this was overcome by evaluating the intermediate concentrations γ_i^* for the first 10 temperature iterations only. Values for T_2 and τ_s at this point

are very close to the final values. This type of oscillation was also encountered in the T_2 variable during the solution of recycle loops under certain conditions, however if the WSR feed temperature T_1 was fixed after 15 loops of calculation then oscillations in T_2 were reduced to 8→20 K, i.e. negligible.

Introducing recirculation of combustion products to a single liquid fuelled WSR lowers the reactor temperature, for a WSR fed with vapourised fuel the opposite effect is apparent. This phenomenon is due to the reduced reactor τ_s and hence FE which results, Figs. 4.9, 7.3→5.

Another important WSR observation was the failure of the solution scheme to converge under fuel rich conditions, the method worked very efficiently under fuel lean and stoichiometric conditions, however. The fuel rich convergence problem is discussed in the next chapter.

7.5(c) BFB Model results - sensitivity to WSR$_2$ τ_{SD}

In 7.2 it was explained that the value of τ_{SD} for the 2nd reactor in the BFB network given in Fig.7.2 had to be estimated, hence the influence of this variable on NO and CO emissions for the BFB model was investigated, results are presented in Table VII. In all the model predictions the indicated rather than the calibration corrected values of $\dot{Q}_j$ are used so that direct comparison between model and measured pollutant emissions can be made. In the experimental gas sampling system, Fig.5.26, any water in the sample will condense out in the probe, sampling line and water trap, it is assumed that 90% of the water vapour condensed out in the system so that the model predictions, i.e. exit flow composition was corrected accordingly.

TABLE VII. FULL MODEL: Effect of WSR_2 — τ_{SD} on pollutant emissions.

Network as shown in Fig.7.2.

BFB conditions: P_f = 120 psig, Indicated $\dot{Q}_j$ = 500 lit/min, P_{cc} = 8" Hg,

T_{AIR} = 353 K, T_{ROT} = 288 K, recirculated flow temperature = 1025 K.

ϕ_{ov} = 0.704

Model predictions:

WSR_1 —

ϕ_{WSR} = 0.62 T_2 = 1454.5 K NO = 1.57 ppm CO = 0.45% CO_2 = 7.36%

$Kero_{(mixed)}$ = 5.29 ppm $O_{2(mixed)}$ = 8.45%

WSR_2 —			EXIT FLOW COMPOSITION (90% H_2O removed)				
τ_{SD}	ϕ_{WSR}	T_2 (K)	NO (ppm)	CO (%)	CO_2 (%)	O_2(mixed) (%)	Kero(mixed) (%)
300	0.70	1724.8	4.94	0.38	9.79	6.56	0.036
50	0.70	1721.4	4.87	0.37	9.77	6.60	0.035
10	0.69	1706.6	4.61	0.35	9.67	6.76	0.032
7	0.69	1699.4	4.48	0.33	9.63	6.84	0.031

MEASURED EXIT FLOW COMPOSITION (Figs. 5.31 → 38):

T = 1590 K NO = 5.3 ppm CO = 0.1% CO_2 = 4.5%

The Table shows the effect then of unmixedness in WSR_2 on BFB emissions of NO, CO and mixed O_2, Kero reactants.

7.5(d) BFB Model results as a function of $\dot{Q}_j$ and T_{AIR}.

Table VIII presents model predictions for a range of air flow rates and estimated feed air flow entry temperature T_{AIR}. Corresponding measured emissions of NO, CO and CO_2 plus exit flow temperature are again included. Compared with the predicted values of CO_2 the measured values for this species are rather low, this observation is discussed in 8.1(b), CO_2 is therefore excluded from the remaining predictions.

7.5(e) BFB Model results as a function of P_f.

Table IX presents model predictions for a range of P_f and constant air flowrate.

TABLE VIII. FULL MODEL: Effect of A) air flowrate, and B) air feed temperature, on pollutant emissions.

Network as shown in Fig.7.2. WSR_2, τ_{SD} = 7.

P_f = 120 psig, T_{ROT} = 288 K.

Model predictions and corresponding measured values (Figs. 5.31 → 38):

	BFB CONDITIONS				WSR_1					WSR_2		EXIT FLOW (90% H_2O removed)			MEASURED EXIT FLOW COMPOSITION			
	T_{AIR} (K)	$\dot{Q}_j$ (ℓ/min)	P_{cc} ("Hg)	ϕ_{ov}	ϕ_{WSR}	T_2 (K)	NO (ppm)	CO (%)	CO_2 (%)	ϕ_{WSR}	T_2 (K)	NO (ppm)	CO (%)	CO_2 (%)	T (K)	NO (ppm)	CO (%)	CO_2 (%)
A	353	620	15.4	0.518	0.43	1216.6	0.56	0.45	5.04	0.50	1462.7	1.96	0.20	7.02	1480	1.2	-	-
	353	500	8	0.704	0.62	1454.5	1.57	0.45	7.36	0.69	1699.4	4.48	0.33	9.63	1590	5.3	0.1	4.5
	353	430	7.3	0.827	0.72	1601.7	2.30	0.65	8.76	0.81	1840.1	8.39	0.54	11.26	1675	14.4	0.4	5.9
	353	370	5.2	0.990	0.89	1767.1	5.08	1.2	10.09	0.97	2007.8	20.23	1.35	12.85	1765	28	1.55	6.1
B	353	500	8	0.704	0.62	1454.5	1.57	0.45	7.36	0.69	1699.4	4.48	0.33	9.63	1590	5.3	0.1	4.5
	453	500	8	0.704	0.62	1482.3	1.85	0.46	7.28	0.69	1736.1	5.61	0.36	9.58	1590	5.3	0.1	4.5
	553	500	8	0.704	0.62	1525.3	2.22	0.47	7.27	0.69	1776.9	7.23	0.39	9.55	1590	5.3	0.1	4.5
	653	500	8	0.704	0.62	1563.0	2.62	0.50	7.32	0.69	1805.9	8.79	0.40	9.55	1590	5.3	0.1	4.5

TABLE IX. FULL MODEL: Effect of P_f on pollutant emissions

Network as shown in Fig.7.2. WSR_2 τ_{SD} = 7.

BFB conditions: $\dot{Q}_j$ = 430 lit/min, P_{cc} = 7.3" Hg, T_{ROT} = 288 K.

Model predictions and corresponding measured values (Figs. 5.31 → 38):

			WSR_1				WSR_2		EXIT FLOW (90%H_2O removed)		MEASURED EXIT FLOW COMPOSITION		
P_f (psig)	T_{AIR} (K)	ϕ_{ov}	ϕ_{WSR}	T_2 (K)	NO (ppm)	CO (%)	ϕ_{WSR}	T_2 (K)	NO (ppm)	CO (%)	T (K)	NO (ppm)	CO (%)
80	353	0.710	0.59	1433.2	1.78	0.38	0.69	1723.6	5.76	0.35	1570	5.2	-
100	353	0.776	0.68	1533.8	2.08	0.51	0.76	1791.2	7.03	0.44	-	-	0.15
120	453	0.827	0.74	1643.4	2.96	0.69	0.81	1876.7	11.35	0.57	1675	14.4	0.4
140	553	0.865	0.79	1710.7	4.26	0.83	0.85	1954.8	19.70	0.76	-	-	0.7
160	653	0.893	0.83	1779.5	6.71	1.04	0.88	2009.0	29.07	0.90	1830	35	1.2

7.5(f) BFB simplified model results.

As an experiment some predictions were made for the BFB network with no WSR_2 i.e. a single WSR_1 reactor of volume equivalent to the 2 other reactors, the results appear in Table X.

TABLE X. PARTIAL MODEL: Single WSR_1, effect of air flowrate on pollutant emissions.

Network as shown in Fig.7.2 but no WSR_2. Volume WSR_1 = 520 cm^3.

τ_{SD} = 300 as before.

P_f = 120 psig, T_{AIR} = 353 K, T_{ROT} = 288 K.

BFB CONDITIONS			WSR_1		EXIT FLOW (90% H_2O removed)		MEASURED EXIT FLOW COMPOSITION		
$\dot{Q}_j$ (ℓ/min)	P_{cc} ("Hg)	ϕ_{ov}	ϕ_{WSR}	T (K)	NO (ppm)	CO (%)	T (K)	NO (ppm)	CO (%)
620	15.4	0.518	0.45	1319.7	1.75	0.28	1480	1.2	-
500	8	0.704	0.66	1540.7	3.62	0.40	1590	5.3	0.1
430	7.3	0.827	0.78	1685.4	5.64	0.66	1675	14.4	0.4
370	5.2	0.990	0.94	1839.7	13.47	1.39	1765	28	1.55

CHAPTER 8.

DISCUSSION

8.1(a) Experimental measurements - Model input data.

Determination of the BFB recirculation characteristic R_{int} $(\dot{Q}_j, S)$ using the baffle technique for isothermal conditions was described in 5.4, in order to use the simple recirculation theory given in 4.5 it was necessary to estimate the efficiency factor η, for combustive conditions. This has been covered in 7.2(a). On the basis of the measurements given in 5.5, plus the discussion contained in 3.2 and 7.2, the BFB flow pattern was determined sufficiently accurately to enable deduction of the model stirred reactor network shown in Fig.7.2. The fuel spray ISD correlations given in 4.3 were adjusted so that they predicted the experimentally measured values, 5.7, this has been explained in 7.3. Fig.5.18 shows the difference in $\bar{x}$ and n between the uncorrected correlations and the measurements; the large difference in $\bar{x}$ is due to the fact that the flow number for the atomiser was only 0.05 gal/hr(psi)$^{\frac{1}{2}}$ whilst Bowen & Joyce's correlations were derived for the range $0.5 \leq F \leq 4.0$ gal/hr(psi)$^{\frac{1}{2}}$.

8.1(b) Experimental measurements - BFB characteristics.

General burner operating characteristics were described in 5.2 and the FRONTISPIECE shows the flame colour for three fuel/air ratios, also, Figs. 5.36 → 38 depict the practical blue flame operating limits. In order to achieve such wide limits however, feed air pressure drops are high, Fig.5.39; it may be possible to reduce these through the use of larger Coanda slit widths if overall performance is not impaired.

The technique and program given in Appendix B for assessing the quench efficiency of a water cooled sampling probe was found to be particularly useful and is recommended as an aid to the design of such probes. Using the techniques given in 5.8 the BFB CO and NO pollutant emissions were measured over a range of operating conditions, Figs. 5.32 → 38. NO and temperature levels were observed to decrease when a blockage discovered in the recirculation path was removed, it is extremely interesting to note that a similar decrease in both variables with increased R_{int} was

detected whilst using the mathematical model, 7.5(b). Emissions of NO from the BFB are thus very low, (maximum of 40 ppm) especially under substantially fuel rich or fuel lean conditions although CO emissions are quite high, Fig.5.32, and peak at around 7%. There is good reason then to suppose that the 2 stage combustor configuration described in 3.3 would be effective in suppressing NO and CO emissions. This is because NO formed in theBFB can be maintained at very low levels under fuel rich conditions (e.g. 8 ppm), it should also be possible to design the 2nd stage so that all the BFB-generated CO is oxidised to CO_2, excessive temperature rise in this stage should naturally be avoided. The secondary maxima in the NO curves occur when the blue flame fuel rich limits have been exceeded and the droplet diffusion mode of combustion prevails, 2.2(b).

As mentioned in 7.5(d) the measured CO_2 levels,(Fig.5.31), are intuitively very low so that their accuracy is extremely doubtful. The model predictions for CO_2 given in Tables VII and VIII emphasise this point, the predictions for this species seem very reasonable. The reason for the erroneous CO_2 measurements would appear to be an invalid calibration chart, the validity of the IRGA chart at CO_2 concentrations > 7% was regrettably not checked since no such standard gases were available. The calibration chart for the CO IRGA however was completely verified and complete confidence is placed in the data given in Fig.5.32. Accurate CO_2 measurements are fortunately not of prime importance to this project.

8.2 The autocorrelation results.

As outlined in 2.5(a), the derivation of the most suitable reactor network for a particular combustor is one of the characteristic problems encountered in stirred reactor modelling. Apart from the mean flow pattern, knowledge of two other properties of the flow would be useful in the evaluation of combustor mixing patterns, these are the turbulence structure and the spatial turbulence dissipation rates. Clearly a continuum model (2.5(b)) would appear capable of the prediction of these, the alternative approach is to try and deduce this information experimentally. The on-line technique for measuring auto correlation functions described in Chapter 6 then is a step in the direction of the implementation

of the latter approach since the eddy length scale information provides a useful insight into the turbulence structure. Fig.6.6 shows the axial profile of the corrected λ_{mi} and λ_{ma}, it is worthwhile noting that the effect of the correction was surprisingly small and typically < 1%. The action of removing high frequencies from the turbulence would be expected to substantially affect λ_{mi} but this did not prove to be the case. This may be partially due to the fact that the expression for $X(f)$ takes account of frequencies present in the measured signal but is independent of the actual bandwidth of frequencies present in the turbulence. The measured λ_{mi} would be expected to be relatively constant since the finite length of the hot wire limits the size of the smallest discernable eddies; it should also be said that the microscale is expected to be larger than the size of the smallest dissipating eddies, Bradshaw (124). It would thus appear desirable to replace the Hot Wire Anemometer with a Laser Doppler type to eliminate this difficulty, exactly the same technique could be applied to this transducer.

Now λ_{ma} is normally considered to be representative of the energy containing eddies which are responsible for gaseous phase mixing, the measured λ_{ma} grows linearly with distance downstream from the Coanda. This type of dependence is very reasonable and has been found for other types of flow by other workers, Coates (125). On a practical note it has been demonstrated, (38), that whereas λ_{ma} is approximately independent of temperature, λ_{mi} is roughly $\propto (\text{temperature})^2$. Use of the Laser Doppler technique however, would circumvent the need for such corrections.

8.3 The BFB mathematical model.

The solution oscillations described in 7.5(b) are a result of incorporating so many temperature dependent variables (physical properties) into the model, 4.2, 4.5; not all of these are actually in the Newton Raphson scheme, Fig.4.2. The inclusion of a relaxation scheme in Subroutine TEST for recycle loop calculations would appear worthwhile, since undesirable step changes in the recycle flow composition and temperature could then be damped.

Turning to the WSR fuel rich convergence problem, the PSR Newton Raphson scheme which forms a large part of the model (equations (4.29→40)) is due to Osgerby (115), who claims it to be efficient over a wide range of pressures, stay times and stoichiometry. However, testing Osgerby's PSR program (115) revealed that convergence could not be attained under fuel rich conditions except at a single point when the scheme for adjusting the correction terms had been modified. Without this alteration, and at all other points tested, over- or (more usually) under-correction resulted. Clearly the correction procedure requires optimisation and this is a numerical mathematics problem. This unfortunately precludes the use of the BFB model for fuel rich ($\phi_{ov} > 1$) conditions only at present.

8.4 Model predictions discussion.

Predicted spray evaporation characteristics for the BFB are given in Figs. 7.3→7.5, the stepped effect is due to the disappearance of complete intervals at appropriate elapsed times. The first set of curves show that PU(t) is strongly dependent on T via the physical properties, the next set shows PU(t) is only weakly dependent on $\dot{Q}_j$ and hence V_{Rel}. As expected PU(t) is strongly dependent on P_f, Fig.7.5, this naturally reflects the influence of drop sizes and the ISD. In all cases at least 80% evaporation is obtained after 3 mSec.

Fig.7.7 conveniently isolates the effect of mixing on the temperature of a homogeneously-fed WSR for three recirculation levels, in each case blowout occurs at $4 \leq \tau_{SD} \leq 5$. Note also the dependence of a) reactants burnout and b) pollutants emissions on WSR_2 unmixedness which is reflected in Table VII, $\tau_{SD} = 7$ being normally selected.

The influence of each of the model primary variables on predictions may be discerned from Tables VII → X; the temptation of optimising the values of these (and other) parameters to force agreement between predictions and specific measured values has been resisted. It is very encouraging that both the correct trends in, and orders of magnitude of, BFB exit flow pollutant concentrations and temperature are predicted, e.g. Table VIII. Using the relatively simple reaction mechanism for kerosine combustion shown in Table VI the predicted NO and CO

emissions are quite close to, although usually a little lower than, the measured values for fuel lean and stoichiometric conditions.

Section A) of Table VIII presents predictions as a function of air flowrate for constant fuel feedrate and estimated air inlet temperature, agreement with the measurements is very reasonable. Section B) of this table reveals that predictions are moderately sensitive to T_{AIR}, for $\phi_{ov} = 0.704$ then a 100K increase in its value results in roughly a 36K increase in exit temperature, note also the effect on NO and CO. Clearly T_{AIR} is not a constant for BFB operation over a range of conditions but is strongly related to prevalent flame temperature. Table IX shows the predictions for constant $\dot{Q}_j$ and a range of P_f, the estimated T_{AIR} is allowed to increase with ϕ_{ov} in this set of predictions.

It can be seen from Tables VIII, IX that at operating points corresponding to $\phi_{ov} < \simeq 0.87$ the predicted CO exceeds the measured value, the reverse is true for $\phi_{ov} > \simeq 0.87$. However, the magnitude of the difference is always less than 0.3% (actual concentration, not percent error).

In most cases the measured exit temperature is less than the model value, this suggests two things. Firstly the latter temperatures may be slightly high since both reactors are assumed to operate adiabatically, if heat loss data were available then non zero values of $\dot{H}_L$ could be utilised. Combustor heat loss has been partially allowed for in that measured temperatures of the cooled recycle flow have been deliberately employed. Secondly, the exit temperature measurement technique used, 5.8(e), is undeniably approximate; even though thermocouple radiation heat losses have been corrected using Appendix C it should be remembered that forced convection and/or turbulent heating effects, plus conduction losses, have been ignored. Hence the measured temperatures are expected to be on the low side.

In spite of the above the predicted NO is invariably less than the measured values, this may indicate that some significant NO formation steps are missing from the reaction mechanism, e.g. of the type (2.53→55). CO predictions are reasonable in spite of the fact that a single destruction reaction only is used.

For an example of other species predictions refer to the GRASP program sample output given in F(e) which usefully gives the composition of all network streams. Prediction of R_{int} are governed largely by the measured recycle flow temperature and are typically 35%. Almost complete fuel vapourisation is predicted and in WSR_2, $\phi_{WSR} \approx \phi_{ov}$.

Although predicted and measured exit temperatures agree well for the single WSR_1 partial model, Table X, this is only superficial since incomplete fuel evaporation is apparent. Agreement for CO and NO is not so good as for the full model.

Parametric evaluations were found to be particularly easy to carry out using GRASP. An important conclusion of this discussion is that experimental measurements made for comparison with mathematical models should be of the highest possible accuracy.

CHAPTER 9.

CONCLUSIONS AND SUGGESTIONS FOR FUTURE WORK

9.1 Conclusions.

1) Pollution suppression techniques applicable to heterogeneous combustors have been discussed, it was concluded that the approach of combustor redesign constitutes the most satisfactory solution. The present need for a general mathematical model capable of predicting realistic pollution emissions was identified and the potential of stirred reactor modelling demonstrated.

2) The emission performance of a laboratory scale Blue Flame Burner (BFB) which was fuelled with kerosine was experimentally determined, blue flame (soot free) combustion was obtained for overall equivalence ratios of ϕ_{ov} of at least 0.5 → 2.0. This performance was obtained at the expense of high inlet air pressures which were typically 2 → 4" Hg for fuel rich conditions but it may be possible to reduce these by increasing the Coanda ejector slit width. A low throughput pressure jet atomiser (0.05 gal/hr(psig)$^{\frac{1}{2}}$) was used to ensure the production of fine sprays, for which the Rosin Rammler "mean" drop size was measured as 40→70 μ using a laser diffraction technique. The maximum detected NO for the BFB exit flow was 40 ppm although concentrations as low as 8 ppm, under fuel rich conditions, are practicable. CO emissions peaked at around 7% although incorporation of the BFB into the 2 stage configuration would eliminate this and probably all major pollutant species.

3) A completely general analysis for a heterogeneous WSR operating at steady state has been derived in which the processes of evaporation, turbulent mixing and finite rate chemical kinetics are included. The analysis was used to construct a model for the BFB which additionally features: i) atomisation to the experimentally measured ISD, ii) 17 step quasiglobal reaction mechanism, iii) a simple internal recirculation sub-model, iv) measured temperatures of the cooled recycle flow and v) a stirred reactor network employing 2 adiabatic WSR's.

4) The modular computer program GRASP was developed to enable the solution of a wide variety of heterogeneous stirred reactor networks and was used for the BFB model calculations.

5) Compared to the measured values the correct trends in, and orders of magnitude of, BFB exit flow NO, CO and temperature T are predicted using the mathematical model. Convergence of the model solution scheme could be obtained for fuel lean and stoichiometric conditions only, 9.2.

The amount by which the predicted T exceeded the measured T increased from typically-1% at $\phi_{ov} = 0.52$, to+12% at $\phi_{ov} = 0.99$. However, measured T is expected to be on the low side since a simple bare thermocouple plus approximate radiation heat loss correction were employed; predicted T is likely to be a little high in view of the adiabatic WSR assumption. The difference between measured and predicted NO was as much as 42%, the magnitude of the corresponding difference for CO emissions was always <3% (actual concentration, not % error).

6) Experience gained through the use of GRASP confirmed its suitability to i) general model parametric evaluations and ii) use by a relatively inexperienced design engineer.

7) Modification to the reaction mechanism, e.g. addition of SO_x formation reactions, are particularly easy to implement using GRASP.

8) A convenient on-line digital computer technique for measuring turbulence autocorrelation functions and length scales has been presented, a means of correcting such measurements for time resolution error has also been developed. The effect of the correction depends on the assumed system frequency response function.

9.2 Suggestions for future work.

1) In order to extend the applicability of the model to fuel rich conditions the correction procedure of the basic PSR Newton Raphson solution scheme, which is due to Osgerby (115), requires numerical optimisation in order to avoid the hitherto experienced over- or under-correction which is often a characteristic of Newton Raphson techniques.

2) The testing of GRASP for other stirred reactor networks, especially those featuring PFR's and different reaction mechanisms, is naturally required. Comparison between predicted and measured pollutant emissions should be retained as a prime objective.

3) Experimental measurements to ascertain actual BFB heat loss rates could be usefully carried out, this would enable similar heat loss terms to be incorporated into the WSR analysis, hence more accurate temperature predictions could be made.

4) The evaluation of BFB emission performance for fuels other than kerosine, and which contain significant amounts of sulphur should clearly be made in order to examine SO_x suppression.

5) A logical extension of this project is the experimental testing and modelling of the 2 stage combustor design. It would then be possible to determine more precisely the extent to which the suppression of all major pollutant species is possible with this type of configuration.

6) Finally it is recommended that further computer on-line techniques (involving possibly Laser Doppler anemometry or Photon Correlation) be developed for the elucidation of turbulent combusting flow structures, and the measurement of spatial turbulence dissipation rates, to aid the construction of stirred reactor networks.

APPENDIX A.

Estimation of Kerosine Thermodynamic Data.

The WSR submodel requires thermodynamic data for all gaseous phase species as an input. Chapter 4 describes how a 7th order polynomial for each species is used to describe the thermodynamic functions of heat capacity, enthalpy and free energy. Two sets of the polynomial coefficients a_{1-7} per species are necessary since the two temperature ranges:

$$300 \leqslant T < 1000 \text{ K}$$
$$1000 \leqslant T \leqslant 5000 \text{ K}$$

are employed, i.e. 14 coefficients/species. As explained in Chapter 7 no such coefficients were available for gaseous kerosine, this species appearing in the quasiglobal chemical reaction. This appendix describes the methods that were used to estimate the set of polynomial coefficients for gaseous kerosine.

Due to the marked lack of such thermodynamic data for kerosine i.e. the hydrocarbon $\simeq C_{12}H_{24}$ it was necessary to approximate the species properties by considering them to be equal to the arithmetic mean of those corresponding to Undecane $C_{11}H_{24}$ and Dodecane $C_{12}H_{26}$. This seems reasonable when one considers that i) the thermal properties for such high hydrocarbons are very comparable ii) kerosine tends to behave very much as a pure hydrocarbon. Since reaction (2.27) is considered irreversible free energy data for the reaction is not needed, hence values for a_{1-6} only are required for kerosine:

$$C_p^{\circ}/R = a_1 + a_2 T + a_3 T^2 + a_4 T^3 + a_5 T^4 \quad (C_p^{\circ} \text{Cal/mole K}) \quad \ldots\ldots \quad (A1)$$

$$H_T^{\circ}/RT = a_1 + \frac{a_2}{2} T + \frac{a_3}{3} T^2 + \frac{a_4}{4} T^3 + \frac{a_5}{5} T^4 + \frac{a_6}{T} \quad (H_T^{\circ} \text{ cal/mole}) \quad \ldots. \quad (A2)$$

These 6 coefficients could be determined in each temperature range if values of H_T° at 6 different temperatures in each range were known, the solution of 6 simultaneous equations then being required. The exact methods used to calculate a_{1-6} in each temperature range are now given.

A(a) $300 \leq T < 1000$ K Range.

Values of (H_T^o/RT) were first computed at T = 300, 500, 600, 700, 900 and 1000 K for Undecane and Dodecane from the Enthalpy Function $(H_T^o - H_o^o)$ for these 2 species at these 6 temperatures from (108); H_o^o for either paraffin was calculated from:

$$(\Delta H_f^o)_o = (H_o^o)_{CnHm} - n(H_o^o)_{C(graphite)} - \frac{m}{2}(H_o^o)_{H_2(g)} \quad \ldots\ldots\ldots \quad (A3)$$

where, ΔH_f^o = Heat of formation of the hydrocarbon (ideal gas state) from carbon (solid state) and hydrogen (ideal gas state) at 298.16^o K, cal/mole.

$(\Delta H_f^o)_T$ = as above but at absolute temperature T(K)

Hence substituting these 6 values of H_T^o and T into (A2) gives 6 linear simultaneous equations in the 6 unknowns a_{1-6}, a FORTRAN IV computer program was written to solve these equations, the program is discussed in A(c) and presented in A(d).

A(b) $1000 \leq T \leq 2000$ K Range.

Insufficient high temperature data for hydrocarbons placed an upper temperature limit of 2000 K on the range of the second polynomial. Values of H_T^o were obtained at T = 1000, 1200, 1400, 1600, 1800, 2000 K; for the first 3 temperatures data for H_T^o was again calculated using the above procedure. For the latter 3 temperatures the following equation was employed:

$$(\Delta H_f^o)_T = (H_T^o)_{CnHm} - n(H_T^o)_{C(graphite)} - \frac{m}{2}(H_T^o)_{H_2(g)} \quad \ldots\ldots\ldots \quad (A4)$$

Values of $(\Delta H_f^o)_T$ were computed using the technique developed by Souders et al (109) which is based on the premise that thermodynamic functions within a molecule are additive, so that the values for the whole molecule can be built up from an assignment of definite contributions to the various molecular constituent groups. The technique (maximum error < 3%) plus necessary data is fully described in this reference, values of H_T^o for carbon and hydrogen were taken from (110). The coefficients a_{1-6} for this temperature range were calculated in exactly the same manner as A(a).

A(c) Thermodata Program Description.

Program MASTER BB3DATA was developed on the Sheffield University ICL 1907 computer for the evaluation of the coefficients a_{1-6} for kerosine in each of the two temperature ranges using the above techniques. The program can also be used for the fitting of polynomials to other species for the derivation of corresponding coefficients.

After reading in all the necessary thermo data the L.H.S's B of equation (A2) are first calculated, a (6x6) matrix A of the corresponding temperature coefficients is then computed:

$$A.X = B \quad \ldots\ldots\ldots \quad (A5)$$

where, $X = a_{1-6}$

A standard subroutine F4ACSL was called to solve the simultaneous equations for X, the routine uses a Crout method; before this routine could be used a matrix transformation operation had to be performed, see A(d). This was necessary due to the non linearity of the columns in the matrix A. Having evaluated X, i.e. a_{1-6}, C_p° and H_T° were computed throughout each temperature range, the results of which appear in the program output which follows the program listing below in A(d).

A(d) Thermo Data Program Listing and Output.

Program MASTER BB3DATA is now presented together with sample output for the first temperature range only, FORTRAN IV was employed.

```
      MASTER BB3DATA
C     THERMO DATA -KEROSINE-,AVERAGE OF UNDECANE/DODECANE
C     H=ENTHALPY  CAL/MOLE
C     CP=HEAT CAPACITY  CAL/DEG.MOLE
      DIMENSION AA(36),BB(6),REINT(30),F(6),HU(6),HD(6),ENN(5),CPN(5)
      DIMENSION B(6),T(6),X(6),A(36),EN(41),CP(41),T1(41)
      DIMENSION V1(3),V2(3),R1(3),R2(3),HC(3),HH(3)
      R=1.98726
      DO 100 L=1,2
C     SET UP L.H.S.'S
      READ(2,1) (T(I),I=1,6)
      IF(L-1) 25,27,25
   27 READ(2,1) (HU(I),I=1,6)
      READ(2,1) (HD(I),I=1,6)
      IM=6
      GO TO 51
```

```
   25 READ(2,1)(HU(I),I=1,3),(HD(I),I=1,3)
      READ(2,1)(V1(KK),KK=1,3),(V2(KK),KK=1,3)
      READ(2,1)(R1(KK),KK=1,3),(R2(KK),KK=1,3)
      READ(2,1)(HC(KK),KK=1,3),(HH(KK),KK=1,3)
      DO 28 KK=1,3
      TD=4.0*R*(T(KK+3)-298.16)/1000.0
      HU(KK+3)=(2.0*V1(KK))+(9.0*V2(KK))+(2.0*R1(KK))+(8.0*R2(KK))
     1+TD-64.6
      HU(KK+3)=(1000.0*HU(KK+3))+(11.0*HC(KK))+(12.0*HH(KK))
      HD(KK+3)=(2.0*V1(KK))+(10.0*V2(KK))+(2.0*R1(KK))+(9.0*R2(KK))
     1+TD-69.52
      HD(KK+3)=(1000.0*HD(KK+3))+(12.0*HC(KK))+(13.0*HH(KK))
      B(KK+3)=(HU(KK+3)+HD(KK+3))/(2.0*R*T(KK+3))
   28 CONTINUE
      IM=3
   31 DO 33 I=1,IM
      B(I)=HU(I)+HD(I)-76178.8-82095.8
      B(I)=B(I)/(T(I)*2.0*R)
   33 CONTINUE
C     SET UP TEMP. COEFFS. MATRIX
      DO 10 J=1,6
      A(J)=1.0
      DO 20 K=2,5
      A((K-1)*6+J)=(T(J)**(K-1))/K
   20 CONTINUE
      A(30+J)=1.0/T(J)
   10 CONTINUE
C     MATRIX TRANSFORMATION
      DO 15 J=1,6
      E(J)=A(6+6*(J-1))
   15 CONTINUE
      DO 30 J=1,5
      DO 30 K=1,6
      A(J+6*(K-1))=A(J+6*(K-1))/A(6+6*(K-1))
   30 CONTINUE
      DO 40 K=1,6
      A(6+6*(K-1))=1.0
   40 CONTINUE
      WRITE(3,7)
      DO 45 J=1,6
      WRITE(3,8)(A(J+6*(K-1)),K=1,6)
   45 CONTINUE
C     SOLVE MATRIX
      N=6
      NA=36
      NB=6
      IN=1
      CALL F44CSL(A,B,N,NA,NB,IN,X,D,ID,IT,AA,BB,REINT)
      IF(L-1) 60,70,60
   70 WRITE(3,3)
      MT=15
      Y=500.0
      Z=50.0
      GO TO 80
   60 WRITE(3,4)
      MT=41
      Y=1000.0
      Z=100.0
C     TRANSFORM POLYNOMIAL COEFFS.
   80 DO 50 II=1,6
      X(II)=X(II)/E(II)
   50 CONTINUE
```

```
      WRITE(3,5)II,(X(I),I=1,6)
      WRITE(3,6)
C     COMPUTE THERMO DATA
      DO 100 M=1,MT
      T1(M)=Y+(Z*FLOAT(M-1))
      SUM=0.0
      DO 105 M1=2,5
      ENN(M1)=(X(M1)/M1)*(T1(M)**(M1-1))
      SUM=SUM+ENN(M1)
  105 CONTINUE
      EN(M)=X(1)+SUM+(X(6)/T1(M))
      SUM=0.0
      DO 110 M2=2,5
      CPN(M2)=X(M2)*(T1(M)**(M2-1))
      SUM=SUM+CPN(M2)
  110 CONTINUE
      CP(M)=X(1)+SUM
      WRITE(3,9) T1(M),CP(M),EN(M)
  100 CONTINUE
    1 FORMAT(6E0.0)
    3 FORMAT(1H1,51X,42HAPPROXIMATED BBS COEFFICIENTS: T=300-1000K)
    4 FORMAT(1H1,51X,43HAPPROXIMATED BBS COEFFICIENTS: T=1000-5000K)
    5 FORMAT(1H ,17HNO OF ITERATIONS=,I4,/,6E17.8,//)
    6 FORMAT(1H ,10X,6HTEMP K,13X,4HCP/R,15X,4HH/RT)
    7 FORMAT(1H ,////,39X,29H(R.H.S.'S) TRANSFORMED MATRIX)
    8 FORMAT(1H ,5E17.8)
    9 FORMAT(1H ,9X,F7.2,9X,E11.5,9X,E11.5)
      STOP
      END
```

(R.M.S.'S) TRANSFORMED MATRIX

0.10000000E 01	0.30000000E 00	0.90000000E-01	0.27000000E-01	0.81000000E-02	0.33333333E 01
0.10000000E 01	0.50000000E 00	0.25000000E 00	0.12500000E 00	0.62500000E-01	0.20000000E 01
0.10000000E 01	0.60000000E 00	0.36000000E 00	0.21600000E 00	0.12960000E 00	0.16666667E 01
0.10000000E 01	0.70000000E 00	0.49000000E 00	0.34300000E 00	0.24010000E 00	0.14285714E 01
0.10000000E 01	0.90000000E 00	0.81000000E 00	0.72900000E 00	0.65610000E 00	0.11111111E 01
0.10000000E 01	0.10000000E 01	0.10000000E 01	0.10000000E 01	0.10000000E 01	0.10000000E 01

APPROXIMATED BBS COEFFICIENTS: T=300-1000K

NO OF ITERATIONS= 5

-0.26016853E 01	0.14754419E 00	-0.12031326E-03	0.75750574E-07	-0.26563020E-10	-0.38534585E 05

TEMP K	CP/R	H/RT
300.00	0.52478E 02	-.11227E 05
350.00	0.36967E 02	-.91266E 02
400.00	0.41153E 02	-.74973E 02
450.00	0.45065E 02	-.61850E 02
500.00	0.48724E 02	-.50974E 02
550.00	0.52151E 02	-.41753E 02
600.00	0.55359E 02	-.33792E 02
650.00	0.58360E 02	-.26818E 02
700.00	0.61161E 02	-.20652E 02
750.00	0.63764E 02	-.15092E 02
800.00	0.66169E 02	-.10087E 02
850.00	0.68371E 02	-.55355E 01
900.00	0.70360E 02	-.13734E 01
950.00	0.72125E 02	0.24495E 01
1000.00	0.73647E 02	0.59724E 01

A(e) Discussion.

The actual computed values of the required coefficients appear in the program output, A(e), whilst Fig.A.1 presents graphical comparisons between the available thermo data and the fitted polynomials. The fits obtained for each temperature range are excellent although, for the second temperature range, the function C_p^o/R diverges rapidly as would be expected after T > 2100 K, ie outside the range of fit. However, actual model temperatures encountered were <2000 K.

APPENDIX B

Gas Sampling Probe - Quenching Calculations.

This Appendix presents details of the calculations that were made to determine the efficiency of the gas sampling probe in quenching chemical reactions occurring in the sample. The method uses a simple heat transfer analysis plus chemical reaction rate data to determine the practical reductions in chemical reaction possible in a water cooled probe which imparts no expansion to the sample.

The decrease in temperature of the sample after it enters the probe is assumed to be exponential:

$$T - T_w = (T_p - T_w) \exp(-x/L) \quad \ldots\ldots\ldots \quad (B1)$$

where, T = sample temperature at any distance x from the probe entrance.

T_p = initial sample temperature, i.e. at probe entrance.

T_w = probe mean wall temperature.

L = order of magnitude of flow distance required for the equalisation of T with T_w.

Now L is given approximately by (105):

$$L = C_p \dot{m}_I / \lambda_p Nu\, \pi \quad \ldots\ldots\ldots \quad (B2)$$

where, $Nu \simeq 4$ for a cylindrical pipe.

C_p = sample mean specific heat, cal/gm K.

λ_p = sample mean thermal conductivity, cal/cms K

ρ_p = sample mean density, gm/cm^3.

Hence, the time to flow over this distance τ_f is:

$$\tau_f = L/V = \frac{C_p}{\lambda\, Nu} \cdot \rho_p \cdot \frac{d_p^2}{4} \quad \ldots\ldots\ldots \quad (B3)$$

Now chemical production/destruction reaction rates are extremely sensitive to temperature, equation (2.24), so that even a moderate drop in T produces a considerable reduction in reaction rate. It is now assumed that a decrease in reaction rate by a factor of 100 is sufficient to quench a sample so that composition changes

within the sampling system are negligible. Estimates of the probe flow distance and corresponding quench time to obtain this order of magnitude are now derived for a general chemical reaction in which:

$$\omega(T) \propto T^{\delta} \cdot \exp(-E/RT) \quad \ldots\ldots\ldots \quad (B4)$$

where, $\omega(T)$ = general chemical reaction rate, mole/cm^3 sec.

δ = temperature exponent.

E = activation energy, cal/mole.

Hence: $\omega(T_p) \propto T_p^{\delta} \exp(-E/RT_p)$

$$\omega(T_p-\Delta T) \propto (T_p-\Delta T)^{\delta} \exp(-E/R(T_p-\Delta T))$$

where, ΔT = actual temperature drop experienced by the sample.

So that the corresponding reaction rate ratio is:

$$\frac{\omega(T_p-\Delta T)}{\omega(T_p)} = \left(1 - \frac{\Delta T}{T_p}\right)^{\delta} \exp\left(\frac{-E\ \Delta T}{RT_p(T_p-\Delta T)}\right) \quad \ldots\ldots\ldots\ldots \quad (B5)$$

Rearranging:

$$\delta \ln\left(1 - \frac{\Delta T}{T_p}\right) + \ln\left(\frac{\omega(T_p)}{\omega(T_p-\Delta T)}\right) = \frac{E}{RT_p} \cdot \frac{\Delta T}{(T_p-\Delta T)} \quad \ldots\ldots\ldots \quad (B5)$$

For $\delta = 0$:

$$\ln\left(\frac{\omega(T_p)}{\omega(T_p-\Delta T)}\right) = \frac{E}{RT_p} \cdot \frac{\Delta T}{(T_p-\Delta T)} \quad \ldots\ldots\ldots\ldots \quad (B6)$$

For $E = 0$:

$$\frac{\omega(T_p)}{\omega(T_p-\Delta T)} = \left(1 - \frac{\Delta T}{T_p}\right)^{-\delta} \quad \ldots\ldots\ldots \quad (B7)$$

For $\delta = E = 0$:

$$\omega(T_p-\Delta T) = \omega(T_p) \quad \ldots\ldots\ldots \quad (B8)$$

Hence for any given E, R, T_p and δ it is possible to calculate the actual ΔT required to achieve $\frac{\omega(T_p)}{\omega(T_p-\Delta T)} = 100$, clearly a minimum reaction activation energy exists for which this is possible however. Having found ΔT then, x/L can be obtained from (B1) and the reaction quench time τ_q estimated (order of magnitude):

$$\tau_q \simeq \frac{x}{V} = \frac{x}{L} \cdot \frac{L}{V} = \frac{x}{L} \cdot \frac{C_p\, d_p^{\,2}\, \rho_p}{4\, \lambda_p\, Nu} \quad \ldots\ldots\ldots \quad (B9)$$

It should be noted however, that although (B6,7,8) are solved trivially, equation (B5) has to be solved iteratively.

A FORTRAN IV computer program was developed on the Departmental PDP 8/E digital computer for the purposes of testing whether or not the gas sampling probe designed, could quench any general chemical reaction. The temperature estimates used were:

$$T_p\Big|_{max.} \simeq 2000\ K\ ; \qquad T_w \simeq 300\ K, \text{ see } 5.8(f).$$

B(a) Probe Quenching Program and Output.

The listing of this program , together with the corresponding output is given below. The output presents quenching efficiency details for each of the 17 chemical reactions used in the WSR model.

```
C       GAS SAMPLING PROBE(H2O-COOLED S.S.)   PROGRAM
C       ASSESSMENT OF QUENCHING OF UP TO 30 REACTIONS
        DIMENSION TEX(30),EX(30),DT(30),XL(30),TAU(30)
        DIMENSION RR(30),E1(30),E2(30),JK(30)
C       TEX=REACTION RATE CONSTANT TEMPERATURE EXPONENT
C       EX =REACTION RATE CONSTANT ACTIVATION  ENERGY/R
C       R  =GAS CONSTANT  (CAL/MOLE.K)
99      WRITE(4,1)
1       FORMAT(//  "  NUMBER OF REACTIONS ?")
        READ(4,2)NR
2       FORMAT(I5)
        READ(4,3) (TEX(IR),EX(IR),IR=1,NR)
3       FORMAT(F5.2,F8.1)
        RP=0.419E-01
        PI=3.1416
C       EXPONENTIAL PROBE TEMP. DIST.N
        TI=2000.0
        TC=300.0
        DTM=TI-TC
        NU=4
        CP=0.25
        BK=1.7E-04
        RO=(28.0/22.4)*(273.0/TI)*(1.0E-03)
        TAU1=1000.0*(CP*RO*(RP**2.0))/(BK*NU)
        WRITE(4,5)TAU1
5       FORMAT(  //  " APPROXIMATE SAMPLE COOLING TIME = ",F7.3,
     1  "MILLISEC",//)
C       REACTION RATE RATIO =100 FOR QUENCHED REACTION IR
        JKJ=0
        DO 50 IR=1,NR
        IF(TEX(IR)) 40,30,40
30      EXM=4.6052*(TI-DTM)*TI/DTM
        IF(EX(IR)-EXM) 32,34,34
34      DT(IR)=TI/(1.0+(EX(IR)/(TI*4.6052)))
        JK(IR)=1
        GO TO 47
32      RR(IR)=EXP(EX(IR)*DTM/(TI*(TI-DTM)))
        JKJ=1
        JK(IR)=2
        GO TO 50
40      TD=TI*(TI-DTM)/DTM
        EXM=TD*(4.6052+(TEX(IR)*ALOG(1.0-(DTM/TI))))
```

```
      IF(EX(IR)-EXM) 42,44,44
44    DT(IR)=20.0
60    E1(IR)=EX(IR)*DT(IR)/(TI*(TI-DT(IR)))
      E2(IR)=4.6052+(TEX(IR)*(ALOG(1.0-(DT(IR)/TI))))
      IF(ABS(E1(IR)-E2(IR))-0.01) 47,47,43
43    DT(IR)=DT(IR)+1.00
      IF(DT(IR).GT.DTM) GO TO 90
      GO TO 60
42    RR(IR)=EXP(EX(IR)/TD)/((1.0-(DTM/TI))**TEX(IR))
      JKJ=1
      JK(IR)=2
      GO TO 50
47    XL(IR)=ALOG(DTM/(TI-DT(IR)-TC))
      TAU(IR)=TAU1*XL(IR)
      JK(IR)=1
50    CONTINUE
      WRITE(4,6)
      WRITE(4,7)
      DO 70 IR=1,NR
      IF(JK(IR).NE.1)GO TO 70
      WRITE(4,72)IR,DT(IR),XL(IR),TAU(IR)
70    CONTINUE
      IF(JKJ.EQ.0)GO TO 90
      WRITE(4,8)
      WRITE(4,9)
      DO 80 IR=1,NR
      IF(JK(IR).NE.2)GO TO 80
      WRITE(4,82)IR,RR(IR)
80    CONTINUE
90    CONTINUE
6     FORMAT("                    ***COMPLETELY QUENCHED REACTIONS***
     1 ",/)
7     FORMAT(  " REACTION NUMBER    DELTA T     X/L
     1 QUENCH TIME(MILLISEC)")
72    FORMAT(1H,6X,I2,10X,F6.1,4X,F5.3,17X,F6.4)
8     FORMAT(//"                    ***PARTIALLY QUENCHED REACTIONS***
     1 ",/)
9     FORMAT(  " REACTION NUMBER          DEGREE OF QUENCHING %")
82    FORMAT(1H,6X,I2,26X,F6.2)
      GO TO 99
      END
```

```
 NUMBER OF REACTIONS ?
 17
  1.00 12400.0
  0.00   544.0
  0.00  8450.0
  1.00  4480.0
  0.00 -2780.0
 -2.00     0.0
  0.00     0.0
 -0.28     0.0
  1.00  3150.0
  0.00 38000.0
  0.00     0.0
  0.00  1601.0
  0.00 12130.0
  0.00 12130.0
  0.00  5421.0
  0.00  2591.8
  0.00   393.0
```

APPROXIMATE SAMPLE COOLING TIME = Ø.11ØMILLISEC

COMPLETELY QUENCHED REACTIONS

REACTION NUMBER	DELTA T	X/L	QUENCH TIME(MILLISEC)
1	795.Ø	Ø.63Ø	Ø.Ø694
3	1Ø43.1	Ø.951	Ø.1Ø47
4	1237.Ø	1.3Ø1	Ø.1432
9	1372.3	1.645	Ø.1812
10	390.2	Ø.261	Ø.Ø287
13	863.2	Ø.7Ø9	Ø.Ø781
14	863.2	Ø.7Ø9	Ø.Ø781
15	1259.1	1.35Ø	Ø.1486
16	1560.8	2.5Ø2	Ø.2756

PARTIALLY QUENCHED REACTIONS

REACTION NUMBER	DEGREE OF QUENCHING %
2	4.67
5	Ø.ØØ
6	Ø.Ø2
7	1.ØØ
8	Ø.59
11	1.ØØ
12	93.33
17.	3.Ø4

B(b) Probe Quenching Efficiency.

The reaction numbers in the output given in B(a) correspond exactly to those in the reaction kinetics section of the WSR submodel. Virtually all of the reactions are predicted to be quenched, reactions 2 and 17 being the only notable exceptions. The other partially quenched reactions in fact are special cases of zero or negative activation energy and as such would not be expected to be "quenched". The results of these calculations then, appear to verify the quench efficiency of the gas sampling probe design; the method used is relatively simple and constitutes a useful water-cooled probe design aid.

APPENDIX C.

Calculation of Ambient Flame Gas Temperature from Thermocouple Bead Temperature

As explained in 5.8 a Pt/Pt.13% Rh thermocouple was used for the purposes of estimating mean values of burner exit flow temperature T_f (^oC). Due to heat transfer considerations the thermocouple bead temperature T_b does not equal this value, a heat balance in fact is necessary to relate the two. This Appendix outlines the method by which T_f was calculated from T_b.

Fig.5.19 shows a sketch of the thermocouple, whose bead was approximately spherical and of 1 mm diameter. For any output signal MV the bead temperature was determined through the use of standard conversion tables, since no cold junction was used, room temperature was added on to this value.

Thermocouple bead steady state heat balance:

$$\begin{pmatrix}\text{Rate of heat transferred}\\ \text{to bead by convection}\\ \text{from gases}\end{pmatrix} = \begin{pmatrix}\text{Rate of heat transferred}\\ \text{from bead by radiation}\\ \text{to the combustor walls}\end{pmatrix} + \begin{pmatrix}\text{Rate of heat transferred}\\ \text{from bead by conduction}\\ \text{along the leads}\end{pmatrix}$$

$$\dot{q}_1 \qquad\qquad \dot{q}_2 \qquad\qquad \dot{q}_3$$

$$\therefore\ h A_b (T_f - T_b) = \sigma A_b(\varepsilon T_b^4 - \alpha T_\omega^4) + \dot{q}_3 \quad \ldots\ldots \quad (C1)$$

where, T_ω = mean combustor wall temperature, K.

h = heat transfer coefficient, $\frac{W}{m^2 K}$

ε = bead emissivity

σ = Stefan Boltzmann constant, $5.67 \times 10^{-8}\ \frac{W}{m^2 K^4}$

α = absorptivity of walls

D_b = bead diameter, m.

Forced convection and turbulence effects constitute additional complexities but were neglected since first order approximations only are required; it is further assumed:

i) $\dot{q}_2 \gg \dot{q}_3$, in practice $\dot{q}_3$ can be minimised by the use of small diameter leads.

ii) $T_b^4 \gg T_\omega^4$, T_ω is difficult to measure without resorting to the implantation of further thermocouples.

For heat transfer to a cylindrical object

$$Nu = \frac{h D_b}{\lambda} \simeq 2.0 \quad \ldots\ldots\ldots \quad (B2)$$

Now λ and ε are not constants but functions of temperature, in the interests of mathematical simplicity both these thermal properties were expressed as linear relations.

$$\lambda \simeq \lambda_{air} = 6.13 \times 10^{-5} T_f + 3.01 \times 10^{-2} \cdot \frac{W}{mK} \quad \ldots\ldots\ldots \quad (B3)$$

For $500 \leq T_f \leq 1800^o$ C, using data available from (111).

$$\varepsilon \simeq \varepsilon_{\substack{platinum \\ wire}} = 9.63 \times 10^{-5} T_b + 0.05 \quad \ldots\ldots\ldots \quad (B4)$$

For $500 \leq T_b \leq 1700$ K, using data from (112)

Substituting (B2,3,4) into(B1) and rearranging gives:

$$\frac{2(T_f - T_b)}{D_b} (6.13 \times 10^{-5} T_f + 3.01 \times 10^{-2}) = \sigma (9.63 \times 10^{-5} T_b + 0.05) T_b^4 \quad (B5)$$

For specified D_b and T_b then, equation (B5) is quadratic in T_f, the desired gas temperature. A FORTRAN IV program was written for use on the Departmental PDP 8/E digital computer, in addition to evaluating T_f for any given T_b the program estimates the density of nitrogen at corresponding T_f for use in the isokinetic gas sampling procedure, 5.8(e).

C(a) Gas Temperature Estimation Program and Output.

The program listing, plus output for three different thermocouple bead temperatures is given below.

```
C
C
C
C
C
C
C
C
C
C
C
```

```
10      DIMENSION(4,4)
        READ(4,2)TB1
        TB=TB1+D1
        DB=1.44E-03
        SBC=5.67E-08
        EB=(0.10*TB/1132.22)+0.05
        RADH1=((TB+273.15)**4.0)*SBC*EB
        A=1.4645E-07
        B=0.725E-04
        F=B-(A*TB)
        C=(D*TB)+(DB*RADH1/837.4)
        TF=((-F)+SQRT((F**2)+(4.0*A*C)))/(2.0*A)
        RO=(28.0/22.4)*(273.0/760.0)*(273.0/(273.0+TF))
        WRITE(4,3)TF,RO
2       FORMAT(F8.3)
3       FORMAT(1H,"FLAME TEMP =",F8.3,"DEG C",5X,"RO=",F8.3,"KG/M3",//)
4       FORMAT(1H,"THERMOCOUPLE TEMP ?")
5       FORMAT(1H,"THERMOCOUPLE RADIATION HEAT LOSS CORRN. PROGRAM")
        GO TO 10
        END
```

```
#0

.R F4
*DP5/SS

THERMOCOUPLE RADIATION HEAT LOSS CORRN. PROGRAM
THERMOCOUPLE TEMP ?
1000.0
FLAME TEMP =1136.589DEG C       RO=   0.233KG/M3


THERMOCOUPLE TEMP ?
1200.0
FLAME TEMP =1422.438DEG C       RO=   0.193KG/M3


THERMOCOUPLE TEMP ?
1400.0
FLAME TEMP =1742.532DEG C       RO=   0.163KG/M3
```

C(b) Discussion of Method.

Catalytic bead heating from surface reactions and possible droplet interferement effects have also been excluded from this method as these are very difficult to incorporate. Fig.C.1 shows T_f as $f(T_b)$ for the thermocouple used in the experimental measurements, due to the fourth power effect the difference between the two variables clearly becomes more important at higher temperatures.

APPENDIX D.

Autocorrelation Data Processing Program.

D(a) Program Description.

A BASIC Program ACPROC.BA was written for the purpose of converting the range of autocorrelation data before the plot routine could be used. The program also evaluated the measured time scales by means of equations presented in Chapter 6 and corrected these for the net time resolution error of the autocorrelation measuring system, using equations presented in (6.4).

A standard program (Dec)COND14 was first of all employed to convert each data file from CORD3 format, to BASIC format. The next step in the processing routine, which is illustrated in the printout given in D(c), involved the running of program ACPROC.BA. A listing of the actual program appears in D(b). The program takes as input a data file which is the result of this format conversion and generates an output file in which the value V of each point lies in the range: $0 \leqslant V \leqslant 1000$. Negative values of V being converted to the range: $0 \leqslant V \leqslant 200$ and positive values: $200 \leqslant V \leqslant 1000$. ACPROC.BA was written so that, for curves in which the zero crossing did not occur in the 100 points (i.e. 10 millisec)of displaced time τ, it was possible to extend the curve by typing in extrapolated values until the zero crossing was obtained. This naturally affected the macroscale since underestimation of the area under the curve would have resulted without this modification, area under the curve after the zero crossing was neglected since this oscillates about the displacement axis and is very small. Area under the curve was estimated, and hence $<\tau_{ma}>$, using Simpson's Rule. A least squares curve fit is then performed for the normalised autocorrelation curve to derive the constants $<\tau_{mi}>$ and $<\rho^{(4)}(0)>$ for the osculation parabola. Finally equations (6.19) and (6.21) are applied, in order to correct these measured time scales for the time resolution error of the measuring system. All pertinent data is printed out.

Having run this program, COND14 was then run a second time in order to convert the output file format from that of BASIC, to that of DAQUAN. The program DAQUAN could then be called and the converted data file loaded for display and plotting.

D(b) Data Processing Program ACPROC.BA

```
ACPROC  BA     3.0      05-NOV-75

1 REM -- PROGRAM FOR PROCESSING AUTOCORRELATION DATA
2 REM -- 1 CONVERSION OF DATA TO DAQUAN INPUT
3 DIM Y(200),Z(100),X(10),R(10)
4 PRINT "NO. OF EXTRA POINTS M ?"
5 INPUT M
6 IF M=0 GO TO 20
7 PRINT "SPECIFY EXTRA POINTS"
8 FOR I=1 TO M
9 INPUT Z(I)
10 NEXT I
20 FILEN#1:"PSAC1.TM"
60 FILEVN#2:"PSAC1.TP"
70 INPUT#1:A,B,C,D,E,F
72 PRINT#2:A,B,C,D,E,F,1000
75 INPUT#1:G
80 FOR I=1 TO 99
90 INPUT#1:T
100 T1=200+800*T/G
102 J=I+1
104 Y(J)=T/G
110 PRINT#2:T1
120 NEXT I
121 FOR I=1 TO M
122 T2=200+800*Z(I)
123 J=I+100
124 Y(J)=Z(I)
125 PRINT#2:T2
126 NEXT I
130 CLOSE#2
140 PRINT
150 PRINT
160 PRINT "CONVERSION COMPLETE"
170 PRINT
175 PRINT
180 Y(1)=1.0
185 P=0.0001
190 REM -- 2 INTEGRATION BY SIMPSON'S RULE
200 REM --    P=T INCREMENT
210 S=0.0
214 IF INT(J/2)<(J/2) GO TO 218
216 J=J-1
218 K1=(J-3)/2
220 FOR N=1 TO K1
230 L=2*N
240 K=L+1
250 S=S+(4.0*P*Y(L)/3.0)
260 S=S+(2.0*P*Y(K)/3.0)
270 NEXT N
280 S=S+(4.0*P*Y(J-1)/3.0)
290 S=S+((Y(1)+Y(J))*P/3.0)
```

```
300 PRINT "ESTIMATE OF INTEGRAL=";S
310 PRINT
320 PRINT
330 REM -- 3 LEAST SQUARES FIT OF NORMALISED AUTOCORRELATION
340 REM --    FUNCTION AROUND PEAK
350 FOR I=1 TO 8
360 R(I)=0.0
370 NEXT I
380 FOR I=1 TO 10
390 X(I)=((I-1)*P)**2
400 R(1)=R(1)+1.0
410 R(2)=R(2)+X(I)
420 R(3)=R(3)+X(I)*X(I)
430 R(4)=R(4)+X(I)**3
440 R(5)=R(5)+X(I)**4
450 R(6)=R(6)+Y(I)
460 R(7)=R(7)+Y(I)*X(I)
470 R(8)=R(8)+Y(I)*X(I)*X(I)
480 NEXT I
490 A1=R(3)*R(5)-R(4)*R(4)
500 B1=R(3)*R(4)-R(2)*R(5)
510 C1=R(2)*R(4)-R(3)*R(3)
520 D1=R(1)*R(5)-R(3)*R(3)
530 E1=R(2)*R(3)-R(1)*R(4)
540 F1=R(1)*R(3)-R(2)*R(2)
550 Z=A1*R(1)+B1*R(2)+C1*R(3)
560 U=(A1*R(6)+B1*R(7)+C1*R(8))/Z
570 V=(B1*R(6)+D1*R(7)+E1*R(8))/Z
580 W=(C1*R(6)+E1*R(7)+F1*R(8))/Z
590 PRINT "RO=A+B*T**2+C*T**4"
600 PRINT " A=";U
610 PRINT " B=";V
620 PRINT " C=";W
630 PRINT
640 PRINT
645 REM -- 4 CORRECTION OF MEASURED MICRO&MACRO TIME SCALES
647 REM --    FOR SYSTEM FREQUENCY RESPONSE
650 B2=9.87E+008
660 W=W*24.0
670 Q=-1.0/(2.0*V)
680 B3=1.0/(B2*Q)
690 A2=((W*Q/B2)+1.0)/(B3+1.0)
700 Q1=SQR(Q/A2)*1000
710 Q=SQR(Q)*1000
715 S=S*1000
720 S1=S/(1.0+B3)
730 PRINT " <TMA>=";S;"MSEC"
740 PRINT "  TMA =";S1;"MSEC"
742 PRINT
744 PRINT
750 PRINT " <TMI>=";Q;"MSEC"
760 PRINT "  TMI =";Q1;"MSEC"
900 END
```

D(c) Data Processing Routine.

The teletype listing given below shows the complete processing routine used.

```
 R COND14

*PSAC1.TM<PSAC1.DA
*F4<CO

*↑C

.R BASIC
NEW OR OLD--OLD DTA0:ACPROC.BA

READY
RUNNH
NO. OF EXTRA POINTS M ?
?0


CONVERSION COMPLETE


ESTIMATE OF INTEGRAL= 0.00249433


RO=A+B*T**2+C*T**4
 A= 0.988218
 B=-513720
 C= .263815E+012


 <TMA>= 2.49434 MSEC
  TMA = 2.49174 MSEC

 <TMI>= 0.986555 MSEC
  TMI = 0.984001 MSEC

READY
BYE

.R COND14

*PSAC1.D0<PSAC1.TP
*DA<F4

*↑C

.R DAQUAN


DAQUAN 05-8 !
TITLE: DISPLAY AND PLOT AUTOCORRELATION CURVE : POINTI

OK, HIT ME!

MA:*PSAC1.D0


NO. POINTS= 100
PTS. TO SKIP=6
PL:
LINE PLOT?Y
XYOM

PLOTTER OFF?Y
```

APPENDIX E.

Calculation of Equilibrium Composition.

The concept of chemical equilibrium was introduced in 2.2(d), this appendix then describes the method used for calculating flame equilibrium composition which, as mentioned in 4.2(a), is employed as an initial guess for WSR solution.

The following dissociation equilibria are used:

$$CO_2 \rightleftharpoons CO + \tfrac{1}{2} O_2 \qquad K_1 = \frac{P_{CO}\, P_{O_2}^{\frac{1}{2}}}{P_{CO_2}} \qquad \text{.....} \qquad \text{(E1)}$$

$$H_2O \rightleftharpoons H_2 + \tfrac{1}{2} O_2 \qquad K_2 = \frac{P_{H_2}\, P_{O_2}^{\frac{1}{2}}}{P_{H_2O}} \qquad \text{.....} \qquad \text{(E2)}$$

$$H_2O \rightleftharpoons \tfrac{1}{2} H_2 + OH \qquad K_3 = \frac{P_{OH}\, P_{H_2}^{\frac{1}{2}}}{P_{H_2O}} \qquad \text{.....} \qquad \text{(E3)}$$

$$\tfrac{1}{2} H_2 \rightleftharpoons H \qquad K_4 = \frac{P_H}{P_{H_2}^{\frac{1}{2}}} \qquad \text{.....} \qquad \text{(E4)}$$

$$\tfrac{1}{2} O_2 \rightleftharpoons O \qquad K_5 = \frac{P_O}{P_{O_2}^{\frac{1}{2}}} \qquad \text{.....} \qquad \text{(E5)}$$

$$\tfrac{1}{2} N_2 + \tfrac{1}{2} O_2 \rightleftharpoons NO \qquad K_6 = \frac{P_{NO}}{(P_{N_2} \cdot P_{O_2})^{\frac{1}{2}}} \qquad \text{.....} \qquad \text{(E6)}$$

$$\tfrac{1}{2} N_2 \rightleftharpoons N \qquad K_7 = \frac{P_N}{P_{N_2}^{\frac{1}{2}}} \qquad \text{.....} \qquad \text{(E7)}$$

Now :

$$n_C = P_{CO} + P_{CO_2} \qquad \text{.....} \qquad \text{(E8)}$$

$$n_H = 2\, P_{H_2O} + P_{OH} + 2\, P_{H_2} \qquad \text{.....} \qquad \text{(E9)}$$

$$n_O = 2\, P_{CO_2} + P_{CO} + P_{H_2O} + 2\, P_{O_2} + P_{OH} + P_O + P_{NO} \qquad \text{.....} \qquad \text{(E10)}$$

$$n_N = P_N + P_{NO} + 2\, P_{N_2} \qquad \text{.....} \qquad \text{(E11)}$$

The total pressure is considered to be 1 atmosphere so that:

$$P = \sum p_i = 1.0 \qquad \text{.....} \qquad \text{(E12)}$$

Now, the ratios n_O/n_H, n_C/n_H and n_N/n_H must clearly be the same for the feed composition and the equilibrium composition so that the values of these ratios for any particular feed, together with equations (E1-12), form a closed system at any temperature T. At any known T the equations can be solved by a modified iterative triangulation process (116), provided that K_{1-7} which are functions of temperature, are also known. K_{1-6} as f(T) were obtained from Reference (14) whilst K_7 as f(T) was taken from Reference (117). When the equilibrium flame temperature (adiabatic) is also required a heat balance, involving species heats of formation and heat contents (14), must be additionally satisfied, so that further iteration is needed. Using the basic method (116) a FORTRAN IV computer program was developed to enable the calculation of flame equilibrium composition for a feed of variable temperature and general composition, in terms of the chemical species used in the WSR model described in Chapter 7, the program was capable of operating in the two modes:

a) specified flame temperature,

b) unknown equilibrium flame temperature (adiabatic).

A simplified version of the program, SUBROUTINE EQUILB, is described in Chapter 7 and presented in Appendix F; the program operates in the former mode.

APPENDIX F.

PROGRAM GRASP

F(a) Program description.

The FORTRAN IV computer program GRASP (General Reactor Analysis and Simulation Program) was written to enable stirred reactor combustion calculations to be carried out for a wide range of reactor networks and options. GRASP was used to derive the BFB model predictions which are presented in 7.5; a listing of GRASP appears in F(f). The program was run on the Manchester University CDC 7600 regional computer due to the large storage and computation rate facilities. GRASP requires approximately 36K storage.

GRASP is organised into a PROGRAM control segment plus a set of SUBROUTINES. Table XI lists these routines and identifies the function type and contributing authors of each, it may be seen that certain SUBROUTINEs have the status of a Module. A Module is considered to be a unit in which specified chemical and/or physical processes occur, the function of a Module then is the evaluation of the composition/T/P of its output stream(s) - for defined input stream(s). TEST and LOOP1 have a different status as will be appreciated shortly. For each Module a 30 element UNIT list is defined which contains pertinent data. GRASP is dimensioned so that up to 10 Modules may be used in any reactor network. Modules are numbered left→right in any network, e.g. Fig.F.1 which is the GRASP equivalent of the BFB model Fig.7.2.

All Modules are interconnected by streams of distinct composition/T/P which are represented by a 25 element FLOW list, up to 20 streams may be used in a network at present. All elements of UNIT and FLOW, plus the various program control variables, are defined in GRASP.

a) PROGRAM Segment.

This constitutes the "Executive" or control section of GRASP, it controls data loading, the calling of each Module in sequence and selection of the required printout routines. If more than one run is required then DALTER is called for the modification of program input information.

b) SUBROUTINE MODULE

This routine is called by the PROGRAM segment each time a new Module is to be entered, the type number of each Module is given in this routine.

c) SUBROUTINE DLOAD

DLOAD reads all the reactor network parameters including UNIT and FLOW plus various network options. If required a printout of the loaded UNIT and independent FLOW data is made.

d) SUBROUTINE DALTER

DALTER loads the modified input data if NRUNS >1. For each run a maximum of 20 changes to each of the UNIT and FLOW arrays may be implemented.

e) SUBROUTINE WRITE1

WRITE1 outputs the final flow analysis after all recycle loops and individual Modules have been solved. In addition a separate set of information regarding the state of all WSR and PFR network modules is printed. Output Channel 3 is principally used by GRASP for data printout.

f) SUBROUTINE WRITE2

WRITE2 outputs the values of the UNIT and independent FLOW arrays whenever called, i.e. performs a useful intermediate check of this network data.

g) SUBROUTINE WRITE3

WRITE3 was written specifically for the BFB reactor model; it prints out air and fuel feed flows and initial mean velocities, also the fuel spray ISD, ϕ_{ov} and R_{int}.

h) SUBROUTINE WSR

This routine is the control and initialisation section of the most important Module in GRASP, it is called for the solution of a single WSR or a chain if in a PFR; WSR employs 8 service routines. The order of species used must be the same in all the various calculations, data input and FLOW list, the order is (with reference to the BFB model):

	GASEOUS PHASE (Mixed)													(Unmixed)			LIQUID PHASE
MODULE WSR	1	2	3	4	5	6	7	8	9	10	11	12	13	14	15	16	17
FLOW List	9	10	11	12	13	14	15	16	17	18	19	20	21	22	23	24	25
BFB MODEL	H	N	O	OH	H_2O	Kero	CO	NO	N_2O	CO_2	H_2	O_2	N_2	O_2	N_2	Kero	Kero
	← Independent species →									← Dependent species →							(Fuel)

WSR may be operated in either the constant temperature or constant enthalpy mode, the latter being usually used. Note that P and $\dot{m}_1/V$ must be specified.

The main functions of WSR are i) reading of input data, ii) initialisation before COMP is called and iii) the setting up of the output FLOW and UNIT lists. For any WSR which is either not in a recycle loop or for the 1st pass through one which is located in such a loop, it is necessary to guess T and ρ_G in order to estimate τ_s. EVAP is then called to compute γ_i^*, BB1 is then called before calculating ϕ_{WSR} and finally entering EQUILB for a modified equilibrium initial guess. For the 2nd and subsequent passes through a WSR (in recycle) the initial guesses for γ_i^*, T, ρ_G and τ_s are set to the previous converged values for that Module.

i) SUBROUTINE PFR

PFR calls WSR 10 times (4.2(b)), if in a recycle loop and LOOP > 1 the first subvolume initial guesses for T, ρ_G and τ_s are set to the previous values for that Module subvolume - an equilibrium guess at that T is then used to derive initial values for ν_i. A set of LOGICAL variables control EVAP and WSR when solving a PFR.

j) SUBROUTINE MIXER

MIXER enables streams to be adiabatically mixed/split at any point in a network, thus general mass and heat balances are performed on the gaseous phase, BB3 supplies the species specific heat terms. A separate mass balance is performed on the liquid phase, negligible sensible heat for this phase and $V_{Rel} = 0$ being assumed. For more than one output stream it is necessary to supply the appropriate split fractions using the MIXER UNIT list. MIXER was also used to set the temperature of the recycle flow, 7.2.

k) SUBROUTINE COAN

COAN was written for the BFB model, it describes the operation of the Coanda internal recirculation unit for this combustor. From values of T_{AIR}, T_{ROT}, $\dot{Q}_j$ and P_{cc} the calibration-corrected air mass flowrate is calculated. COAN is also called by EVAP when $V_G(0)$ is needed, equations (4.78,81) being employed. (4.80) is then applied for evaluating R_{int} and hence the split fractions for Module No.6. COAN also feeds 2 network control parameters into EVAP.

ℓ) SUBROUTINE PJET

PJET is a general routine for pressure jet atomiser calculations although it contains the BFB device mass flow calibration. From the single variable P_f PJET returns $\dot{m}_{FUEL}$ (eqn. (5.8)), $V_s(0)$ (eqns. (4.56,57)) and the spray ISD(eqns. (4.48→52,55)) for use in EVAP.

m) SUBROUTINE TEMPRES

TEMPRES enables T or P (or both) for any network flow to be set to desired values.

n) SUBROUTINE TEST

TEST is a standard routine developed by Burgess et al (123) for the iterative solution of recycle loops, to a specified accuracy. A convergence promoter may be used to increase the rate of convergence.

o) SUBROUTINE LOOP1

LOOP1 is the 1st Module to be entered after a recycle loop has been solved, NCYCLE and LOOP are reset according to whether or not further recycle is required.

p) SUBROUTINE COMP

COMP solves (4.29→40) by means of a Newton Raphson iteration scheme, BB4 being called for the partial derivatives required to evaluate a composition change, CHOLES reduces the interation matrix thus generated. A scheme for reducing the correction terms to prevent over-correction is used, when the species eqn. (4.29) and energy balance (4.30) are satisfied control is returned to WSR. EVAP is called for the first 10 temperature iterations to obtain γ_i^* for good estimates of T and τ_s, in this way oscillatory iteration was avoided. BB1 is called each time γ_i^* are modified and BB3 each time T changes.

q) SUBROUTINE BB1

BB1 evaluates the coefficients of the element conservation equations used for the WSR dependent species. The first time through BB1 the independent species conservation coefficients are read.

r) SUBROUTINE BB3

BB3 computes species enthalpy, specific heat and free energy values, it may be called from MIXER, WSR or COMP. The 1st time through BB3 a set of 14 coefficients for each physical species are read in, these coefficients correspond to those in (4.41→43). This data for Kero and N_2 is also available to EVAP for use in (4.59,60).

s) SUBROUTINE BB4

BB4 contains the chemical kinetics of the system being investigated, the 1st time through kinetic data including participating species, rate constants, 3rd body efficiencies and reverse rate options for each reaction are read. If it is specified that IK = 1 then the 1st chemical reaction is selected as the quasi-global finite rate pyrolysis step (2.27). BB4 produces a printout of the above data, e.g. Table VI for the BFB model. The partial derivatives required in COMP are then computed.

t) SUBROUTINE EVAP

EVAP evaluates γ_i^* for specified T and τ_s for any network WSR. Since this involves time dependent quantities a number of control parameters are required for incorporation into both the WSR and recycle loop iterative solution schemes, these parameters are defined in GRASP. An option is provided for region A or B thermal properties in (4.59). EVAP was written as a completely general evaporation/mixing routine, it requires additional inputs of spray ISD, $V_s(0)$ and $V_G(0)$.

u) SUBROUTINE EQUILB

EQUILB generates an equilibrium initial guess for WSR composition when T_1 and ϕ_{WSR} are specified. As explained in 7.4, $(T_{eq}-200)$ is curve fitted, an alternative value of T may be supplied if IEQ ≠ 1 is selected. The equations given in Appendix E are then used to compute the equilibrium γ_i^*.

v) SUBROUTINE CHOLES

CHOLES is a standard service subroutine which reduces the iteration matrix generated in COMP by means of the Choleski factorisation method.

w) SUBROUTINE RATES

RATES evaluates the values of the rate constants and their derivatives required in BB4. Equations (4.36→39) are employed for this purpose and K_j are calculated using free energies derived from BB3.

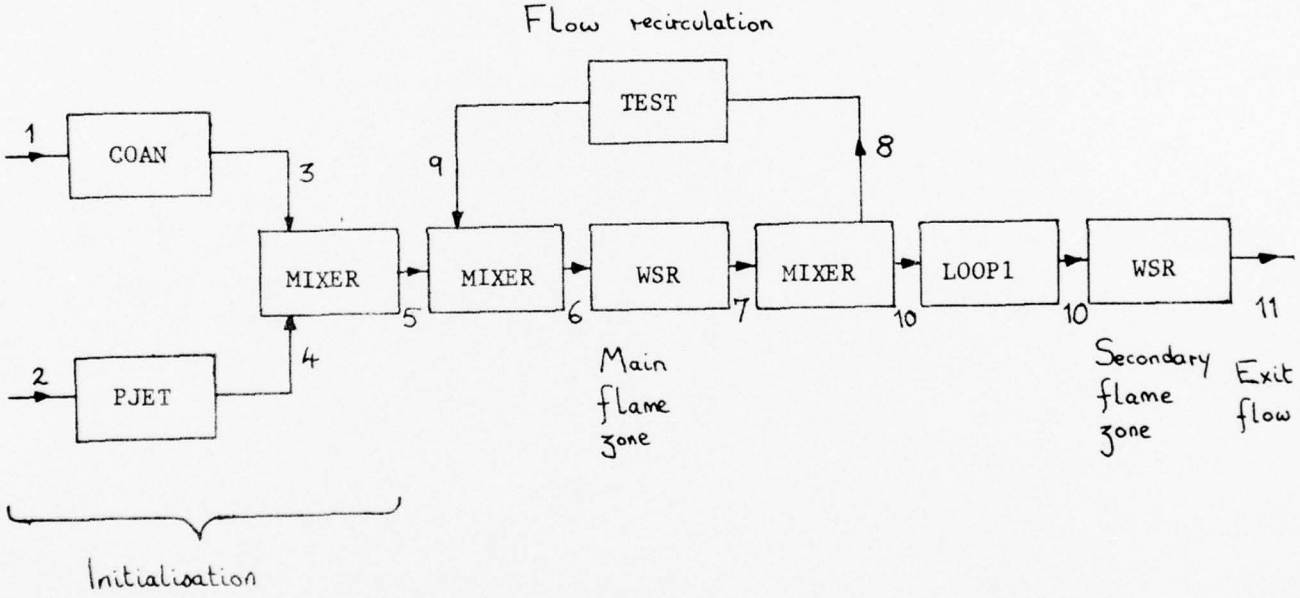

GRASP modular equivalent of FIG 7.2

FIG.F.1 GRASP MODULE NETWORK FOR THE BFB MATHEMATICAL MODEL.

TABLE XI. Program GRASP, Breakdown of Routines.

Subroutine	Function type	Contributing authors
PROGRAM SEGMENT	1	B,F
MODULE	2	B
DLOAD	3	B
DALTER	3	B
WRITE1	4	B,F,P
WRITE2	4	B
WRITE3	4	P
WSR	5	P,F,O
PFR	5	F,P
MIXER	5	F,P
COAN	5	P
PJET	5	P
TEMPRES	5	B
TEST	5	B
LOOP1	5	P
COMP	6	O,P
BB1	6	O
BB3	6	O,P
BB4	6	O,P,F
EVAP	6	P
EQUILB	6	P
CHOLES	6	O
RATES	6	O

B = Burgess, Robson & Wells - joint authors of chemical engineering flowsheet program PRIMER: Ref.(123).

O = Osgerby - author of a PSR program: Ref.(115)

F = Felton - coauthor of program GRASP, version for PSR type calculations.

P = Prior - main author of WSR version of GRASP.

1 = Main control segment.

2 = Module selection segment.

3 = Data input or modification.

4 = Data printout.

5 = Module.

6 = WSR Module service routine.

F(b) Program data input.

Two data input files are required by GRASP, the 1st is read by DLOAD (also DALTER if NRUNS > 1), data is specified in NAMELIST format, F(c). The 2nd input file contains information required by BB3, BB1 and BB4, standard format is used, F(d). Species names and molecular weights are contained in a WSR DATA statement.

F(c) BFB Model; typical module network data file.

```
$EXECL
NRUNS=1,
TITLE=18*0,
LIST=1,2,3,4,5,6,7,8,9,0,
IDCP=1,2,3,4,5,6,7,8,9,10,11,12,13,14,15,16,
KPRINT=3*1,0,
$
$UNITL
UNIT1=1,9,3*1,3,8*0,430,7.3,288,11*0,6,0,
UNIT2=2,10,2*1,2,4,8*0,120,15*0,
UNIT3=3,3,2,1,3,4,5,7*0,1,14*0,1,
UNIT4=4,3,2,1,3,9,6,7*0,1,14*0,1,
UNIT5=5,1,2*1,6,7,9*0,300,13*0,240,
UNIT6=6,3,1,2,7,8,10,7*0,14*0,1035,1,
UNIT7=7,8,2*1,8,9,8*0,30.0.02,12,3,12*0,
UNIT8=8,5,1,1,10,10,8*0,15*0,
UNIT9=9,3*1,10,11,9*0,7,13*0,280,
$
$FLOWL
FLOW1=1,4*0,353,0.96,1,17*0,
FLOW2=2,4*0,300,0.96,1,17*0,
FLOW9=9,4*0,300,0.96,18*0,
$
```

F(d) BFB Model; thermodynamic, conservation and reaction mechanism data.

```
  9     2    17
 .25000000E+01   .00000000E+00   .00000000E+00   .00000000E+00   .00000000E+00
 .25470497E+05  -.46001096E+00   .25000000E+01   .00000000E+00   .00000000E+00
 .00000000E+00   .00000000E+00   .25470497E+05  -.46001096E+00
 .25147937E+01  -.11243791E-03   .29647506E-06  -.32464049E-09   .12595465E-12
 .56127767E+05   .41193032F+01   .24422261E+01   .12276187E-03  -.84992719E-07
 .21400830E-10  -.12511058E-14   .56148821E+05   .44925708E+01
 .30218894E+01  -.21737249E-02   .37542203E-05  -.29947200E-08   .90777547E-12
 .29137190E+05   .26460076E+01   .25372567E+01  -.18422190E-04  -.88017921E-08
 .59643621E-11  -.55743608E-15   .29230007E+05   .49467942E+01
 .38234708E+01  -.11187229E-02   .12466819E-05  -.21035896E-09  -.52546551E-13
 .35852787E+04   .58253029E+00   .28895544E+01   .99835061E-03  -.21879904E-06
 .19802785E-10  -.38452940E-15   .38811792E+04   .55597016E+01
 .41565016E+01  -.17244334E-02   .56982316E-05  -.45930440E-08   .14233654E-11
-.30288770E+05  -.68616246E+00   .26707532E+01   .30317115E-02  -.85351572E-06
 .11790853E-09  -.61973568E-14  -.29888994E+05   .68838391E+01
-.28016853E+01   .14759419E+00  -.12031326E-03   .75750374E-07  -.26583020E-10
-.38539585E+05   .10000000E+01   .22826085E+03  -.49113240E+00   .54592029E-03
-.24909955E-06   .40924460E-10  -.10460569E+06   .10000000E+01
```

```
 .37871332E+01 -.21709526E-02  .50757337E-05 -.34737726E-08  .77216841E-12
-.14363508E+05  .26335459E+01  .29511519E+01  .15525569E-02 -.61911411E-06
 .11350336E-09 -.77882732E-14 -.14231827E+05  .65314450E+01
 .41469476E+01 -.41197237E-02  .96922467E-05 -.78633639E-08  .22309512E-11
 .97447894E+04  .25694290E+01  .31529360E+01  .14059955E-02 -.57078462E-06
 .10628209E-09 -.73720783E-14  .98522048E+04  .69446465E+01
 .23821171E+01  .10350556E-01 -.11167634E-04  .69583165E-08 -.18780192E-11
 .87229964E+04  .10227044E+02  .46265479E+01  .30216807E-02 -.12156014E-05
 .22855952E-09 -.15849701E-13  .81356645E+04 -.11463655E+01
 .21701000E+01  .10378115E-01 -.10733938E-04  .63459175E-08 -.16280701E-11
-.48352602E+05  .10664388E+02  .44129266E+01  .31922896E-02 -.12978230E-05
 .24147446E-09 -.16742986E-13 -.48944043E+05 -.72875769E+00
 .28460849E+01  .41932116E-02 -.96119332E-05  .95122662E-08 -.33093421E-11
-.96725372E+03 -.14117850E+01  .30436897E+01  .61187110E-03 -.73993551E-08
-.20331900E-10  .24593790E-14 -.85491000E+03 -.16481339E+01
 .37189946E+01 -.25167290E-02  .85837353E-05 -.82998720E-08  .27082180E-11
-.10576700E+04  .39081704E+01  .35976129E+01  .78145603E-03 -.22386670E-06
 .42490160E-10 -.33460200E-14 -.11927910E+04  .37492669E+01
 .36916148E+01 -.13332552E-02  .26503100E-05 -.97688341E-09 -.99772234E-13
-.10628336E+04  .22874980E+01  .28545761E+01  .15976316E-02 -.62566254E-06
 .11315849E-09 -.76897070E-14 -.89017445E+03  .63902879E+01
 .37189946E+01 -.25167290E-02  .85837353E-05 -.82998720E-08  .27082180E-11
-.10576700E+04  .39081704E+01  .35976129E+01  .78145603E-03 -.22386670E-06
 .42490160E-10 -.33460200E-14 -.11927910E+04  .37492669E+01
 .36916148E+01 -.13332552E-02  .26503100E-05 -.97688341E-09 -.99772234E-13
-.10628336E+04  .22874980E+01  .28545761E+01  .15976316E-02 -.62566254E-06
 .11315849E-09 -.76897070E-14 -.89017445E+03  .63902879E+01
-.28016853E+01  .14759419E+00 -.12031326E-03  .75750374E-07 -.26583020E-10
-.38539585E+05  .10000000E+01  .22826085E+03 -.49113240E+00  .54592029E-03
-.24909955E-06  .40924460E-10 -.10460569E+06  .10000000E+01
   3     5     8     4
 6 .1200E+02  7 .1000E+01 10 .1000E+01
 1 .5000E+00  4 .5000E+00  5 .1000E+01  6 .1200E+02 11 .1000E+01
 3 .5000E+00  4 .5000E+00  5 .5000E+00  7 .5000E+00  8 .5000E+00
 9 .5000E+00 10 .1000E+01 12 .1000E+01
 2 .5000E+00  8 .5000E+00  9 .1000E+01 13 .1000E+01
   1
   2     2     6    12    11     7 .552000E+09 .124000E+05 .100000E+01  0  0  0
   2     2     7     4    10     1 .560000E+12 .544000E+03 .000000E+00  0  0  1
   2     2     1    12     4     3 .220000E+15 .845000E+04 .000000E+00  0  0  1
   2     2     3    11     4     1 .180000E+11 .448000E+04 .100000E+01  0  0  1
   2     1     1     3     4    14 .530000E+16-.278000E+04 .000000E+00  0  0  1
   2     1     1     4     5    14 .140000E+24 .000000E+00-.200000E+01  0  0  1
   2     1     1     1    11    14 .300000E+16 .000000E+00 .000000E+00  0  0  1
   2     1     3     3    12    14 .470000E+16 .000000E+00-.280000E+00  0  0  1
   2     2     2    12     8     3 .640000E+10 .315000E+04 .100000E+01  0  0  1
   2     2    13     3     8     2 .760000E+14 .380000E+05 .000000E+00  0  0  1
   2     2     2     4     8     1 .320000E+14 .000000E+00 .000000E+00  0  0  1
   2     1    13     3     9    14 .162200E+12 .160100E+04 .000000E+00  0  0  1
   2     2     9     3     8     8 .458100E+14 .121300E+05 .000000E+00  0  0  1
   2     2     9     3    13    12 .381100E+14 .121300E+05 .000000E+00  0  0  1
   2     2     9     1    13     4 .295100E+14 .542000E+04 .000000E+00  0  0  1
   2     2     4    11     1     5 .219000E+14 .259180E+04 .000000E+00  0  0  1
   2     2     4     4     3     5 .575000E+13 .393000E+03 .000000E+00  0  0  1
```

F(e) BFB Model; GRASP Sample Output.

```
ESTIMATED AIR INLET TEMPERATURE       =  353,000K
AIR MANIFOLD PRESSURE                 =    7,300IN,HG
AIR FEED FLOWRATE                     =  391,787LIT/MIN
COANDA INLET PLANE,MEAN GAS VELOCITY  =   22,872M/SEC


FUEL INJECTION PRESSURE               =  120,000PSIG
ATOMISER FUEL MASS FLOWRATE           =     ,540GM/SEC
SPRAY INITIAL MEAN VELOCITY           =    9,989M/SEC
SPRAY INITIAL SIZE DISTRIBUTION :
      ROS,RAM, EXPONENT               =    2,542
      ROS,RAM,    MEAN                =  49,769MICRON


ESTIMATED BURNER OVERALL EQUIVALENCE  =     ,827
DEGREE OF INTERNAL RECIRCULATION      =  35,439%



          *****FINAL FLOW ANALYSIS*****


     STREAM NUMBER    1

SPECIES    FLOW RATE      TEMPERATURE  353,0,K   PRESSURE  ,96 ATM,   TOTAL FLOWRATE 1,0000E+00 MOLE/SEC

  H         0,
  N         0,
  O         0,
  OH        0,
  H2O       0,
  KERO      0,
  CO        0,
  NO        0,
  N2O       0,
  CO2       0,
  H2        0,
  O2        0,
  N2        0,
  O2        0,
  N2        0,
  KERO      0,
  LIQF      0,

     STREAM NUMBER    2

SPECIES    FLOW RATE      TEMPERATURE  300,0,K   PRESSURE  ,96 ATM,   TOTAL FLOWRATE 1,0000E+00 MOLE/SEC

  H         0,
  N         0,
  O         0,
  OH        0,
  H2O       0,
  KERO      0,
  CO        0,
  NO        0,
  N2O       0,
  CO2       0,
  H2        0,
  O2        0,
  N2        0,
  O2        0,
  N2        0,
  KERO      0,
  LIQF      0,

     STREAM NUMBER    3

SPECIES    FLOW RATE      TEMPERATURE  353,0,K   PRESSURE  ,96 ATM,   TOTAL FLOWRATE 3,3280E-01 MOLE/SEC

  H         0,
  N         0,
  O         0,
  OH        0,
  H2O       0,
  KERO      0,
  CO        0,
  NO        0,
  N2O       0,
  CO2       0,
  H2        0,
  O2        0,
  N2        0,
  O2        6,9888E-02
  N2        2,6291E-01
  KERO      0,
  LIQF      0,
```

STREAM NUMBER 4

SPECIES	FLOW RATE	TEMPERATURE 300.0,K	PRESSURE .96 ATM.	TOTAL FLOWRATE 0. MOLE/SEC
H	0.			
N	0.			
O	0.			
OH	0.			
H2O	0.			
KERO	0.			
CO	0.			
NO	0.			
N2O	0.			
CO2	0.			
H2	0.			
O2	0.			
N2	0.			
O2	0.			
N2	0.			
KERO	0.			
LIQF	5.4031E-01			

STREAM NUMBER 5

SPECIES	FLOW RATE	TEMPERATURE 353.0,K	PRESSURE .96 ATM.	TOTAL FLOWRATE 3.3280E-01 MOLE/SEC
H	0.			
N	0.			
O	0.			
OH	0.			
H2O	0.			
KERO	0.			
CO	0.			
NO	0.			
N2O	0.			
CO2	0.			
H2	0.			
O2	0.			
N2	0.			
O2	6.9888E-02			
N2	2.6291E-01			
KERO	0.			
LIQF	5.4031E-01			

STREAM NUMBER 6

SPECIES	FLOW RATE	TEMPERATURE 633.3,K	PRESSURE .96 ATM.	TOTAL FLOWRATE 5.2576E-01 MOLE/SEC
H	2.5868E-04			
N	6.5297E-12			
O	4.2669E-04			
OH	6.0312E-04			
H2O	1.7343E-02			
KERO	5.5243E-07			
CO	1.2500E-03			
NO	4.5094E-07			
N2O	9.4951E-08			
CO2	1.6852E-02			
H2	3.2792E-06			
O2	1.1591E-02			
N2	1.4391E-01			
O2	6.9970E-02			
N2	2.6322E-01			
KERO	3.2553E-06			
LIQF	5.8218E-01			

STREAM NUMBER 7

SPECIES	FLOW RATE	TEMPERATURE 1601.4,K	PRESSURE .96 ATM.	TOTAL FLOWRATE 5.4477E-01 MOLE/SEC
H	7.3196E-04			
N	1.8566E-11			
O	1.2033E-03			
OH	1.7046E-03			
H2O	4.9043E-02			
KERO	1.5683E-06			
CO	3.5419E-03			
NO	1.2614E-06			
N2O	2.6688E-07			
CO2	4.7648E-02			
H2	9.2946E-04			
O2	3.2597E-02			
N2	4.0626E-01			
O2	2.3246E-04			
N2	8.7449E-04			
KERO	9.1946E-06			
LIQF	1.1695E-01			

STREAM NUMBER 8

SPECIES	FLOW RATE	TEMPERATURE 1035.0,K	PRESSURE .96 ATM,	TOTAL FLOWRATE 1.9306E-01 MOLE/SEC
H	2.5940E-06			
N	6.5797E-12			
O	4.2643E-06			
OH	6.0411E-06			
H2O	1.7380E-02			
KERO	3.5578E-07			
CO	1.2552E-03			
NO	4.4703E-07			
N2O	9.4581E-08			
CO2	1.6886E-02			
H2	3.2940E-06			
O2	1.1552E-02			
N2	1.4397E-01			
O2	8.2382E-05			
N2	3.0991E-04			
KERO	3.2585E-06			
LIQF	4.1445E-02			

STREAM NUMBER 9

SPECIES	FLOW RATE	TEMPERATURE 1035.0,K	PRESSURE .96 ATM,	TOTAL FLOWRATE 1.9296E-01 MOLE/SEC
H	2.5868E-06			
N	6.5297E-12			
O	4.2669E-06			
OH	6.0312E-06			
H2O	1.7363E-02			
KERO	3.5243E-07			
CO	1.2500E-03			
NO	4.5094E-07			
N2O	9.4951E-08			
CO2	1.6852E-02			
H2	3.2792E-06			
O2	1.1591E-02			
N2	1.4391E-01			
O2	8.2382E-05			
N2	3.0991E-04			
KERO	3.2533E-06			
LIQF	4.1867E-02			

STREAM NUMBER 10

SPECIES	FLOW RATE	TEMPERATURE 1601.6,K	PRESSURE .96 ATM,	TOTAL FLOWRATE 3.5171E-01 MOLE/SEC
H	4.7256E-06			
N	1.1986E-11			
O	7.7683E-06			
OH	1.1005E-03			
H2O	3.1662E-02			
KERO	1.0125E-06			
CO	2.2866E-03			
NO	8.1436E-07			
N2O	1.7230E-07			
CO2	3.0762E-02			
H2	6.0007E-06			
O2	2.1043E-02			
N2	2.6228E-01			
O2	1.5008E-04			
N2	5.6458E-04			
KERO	5.9361E-06			
LIQF	7.5500E-02			

STREAM NUMBER 11

SPECIES	FLOW RATE	TEMPERATURE 1841.2,K	PRESSURE .96 ATM,	TOTAL FLOWRATE 3.5333E-01 MOLE/SEC
H	1.7141E-04			
N	1.1796E-10			
O	3.4986E-04			
OH	1.1317E-03			
H2O	3.6713E-02			
KERO	6.2737E-09			
CO	1.7384E-03			
NO	2.7184E-06			
N2O	1.3217E-07			
CO2	3.6048E-02			
H2	4.2173E-04			
O2	1.3836E-02			
N2	2.6277E-01			
O2	1.8760E-03			
N2	7.0572E-03			
KERO	5.6257E-05			
LIQF	7.5500E-04			

F(£) GRASP listing.

*****FINAL REACTOR ANALYSIS*****

MODULE NO, 5 REACTOR TYPE 1 INPUT FLOW 6 OUTPUT FLOW 7
RESIDENCE TIME .3219E-02 SEC MDOTV .2191E-02 MOLE/SEC,CC REACTOR TEMPERATURE 1601.4,K

HOMOGENEOUS FEED EQUIVALENCE RATIO .76E+00
UNMIXEDNESS FACTOR TAU SD 300.00

GASEOUS PHASE	MIXED SPECIES	CONCENTRATION (MOLE/GM)	UNMIXED SPECIES	CONCENTRATION (MOLE/GM)
	H =	4.6974E-03	O2 =	1.4918E-05
	N =	1.1915E-12	N2 =	5.6121E-05
	O =	7.7220E-05	KERO=	5.9007E-07
	OH =	1.0940E-04		
	H2O =	3.1474E-03		
	KERO=	1.0065E-07		
	CO =	2.2730E-04		
	NO =	8.0951E-08		
	N2O =	1.7127E-08		
	CO2 =	3.0579E-03		
	H2 =	5.9649E-05		
	O2 =	2.0919E-03		
	N2 =	2.6072E-02		

LIQUID PHASE	EXIT MASS FLOWRATE (GM/SEC)	MEAN EVAPORATION RATE (GM/SEC)
	LIQF=1.1695E-01	4.6524E-01

KOUNT= 22

MODULE NO, 9 REACTOR TYPE 1 INPUT FLOW 10 OUTPUT FLOW 11
RESIDENCE TIME .5036E-02 SEC MDOTV .1256E-02 MOLE/SEC,CC REACTOR TEMPERATURE 1841.2,K

HOMOGENEOUS FEED EQUIVALENCE RATIO .81E+00
UNMIXEDNESS FACTOR TAU SD 7.00

GASEOUS PHASE	MIXED SPECIES	CONCENTRATION (MOLE/GM)	UNMIXED SPECIES	CONCENTRATION (MOLE/GM)
	H =	1.6914E-05	O2 =	1.8511E-06
	N =	1.1640E-11	N2 =	6.9638E-06
	O =	3.4523E-05	KERO=	5.5512E-06
	OH =	1.1167E-04		
	H2O =	3.6227E-03		
	KERO=	6.1907E-10		
	CO =	1.7154E-04		
	NO =	2.6824E-07		
	N2O =	1.3042E-08		
	CO2 =	3.5571E-03		
	H2 =	4.1615E-05		
	O2 =	1.3652E-03		
	N2 =	2.5930E-02		

LIQUID PHASE	EXIT MASS FLOWRATE (GM/SEC)	MEAN EVAPORATION RATE (GM/SEC)
	LIQF=7.5500E-04	7.4745E-02

KOUNT= 61

```
      PROGRAM GRASP(DATA1A,TAPE2=DATA1A,DATA2A,TAPE29=DATA2A,
     *OUTPUT,TAPE3=OUTPUT,OUTPT2,TAPE21=OUTPT2,DEBUG=OUTPUT)
C
C          GGGGGG     RRRRRR     AAAAAA     SSSSS      PPPPPP
C        GG     GG   RR     RR   AA     AA  SS    S    PP     PP
C        GG          RR     RR   AA     AA  SS         PP     PP
C        GG          RR     RR   AA     AA   SS        PP     PP
C        GG          RRRRRRR    AAAAAAAA     SS       PPPPPPP
C        GG          RR  RR     AA     AA        SS    PP
C        GG    GGG   RR   RR    AA     AA         SS   PP
C        GG     GG   RR    RR   AA     AA  S      SS   PP
C         GGGGGGG   RR     RR  AA     AA   SSSSSS    PP
C
C     THIS SIMULATOR WAS DEVELOPED BY D.S.PRIOR FOR WSR
C     CALCULATIONS ; IT IS A MODIFICATION OF 'PRIMER' WHICH
C     WAS DEVELOPED BY BURGESS ROBSON & WELLS FROM 'GEMCS'
C
      LOGICAL FLAG
      COMMON/FLAGS/FLAG
      COMMON/UNITS/UNIT(30,10)
      COMMON/FLOWS/FLOW(25,20)
      COMMON/PARAMS/LIST(10),JJ,LOOP,NIN,NOUT,NCALC,NFLOW,NCOMP,NU,
     1KPRINT(4),MLOOP,NF(10),IOCP(16),NL,INFLOW(20),NRUNS,NCYCLE,KK
      DATA KK/0/
      MRUN=1
      FLAG=.FALSE.
   20 IF(MRUN-1)30,30,40
C     NOW LOAD DATA
   30 CALL DLOAD
      GO TO 50
   40 CALL DALTER
C     INITIALISE MODULE COUNTER
   50 WRITE(3,101)MRUN
      NL=1
   80 WRITE(3,103)LOOP
C     SET UNIT PARAMETERS FOR CURRENT MODULE
   90 NU=LIST(NL)
      NIN=UNIT(3,NU)+0.001
      NOUT=UNIT(4,NU)+0.001
      NTYPE=ABS(UNIT(2,NU))+0.001
      DO 100 K=1,10
  100 NF(K)=UNIT(4+K,NU)
C     NOW CALL MODULE
      CALL MODULE(NTYPE)
C     RESET MODULE COUNTER
  110 NL=NL+1
      IF(FLAG)GO TO 200
      IF(NL-NCALC)90,90,120
  120 IF(LOOP-999)90,190,190
C     OUTPUT FINAL STREAM ANALYSIS
  190 IF(KPRINT(3).EQ.1)CALL WRITE3
      IF(KPRINT(1).EQ.1)CALL WRITE1
  200 CONTINUE
      MRUN=MRUN+1
      WRITE(3,106)
      IF(NRUNS-MRUN)999,20,20
  101 FORMAT(1H0,10X,' RUN ',1X,I5)
  103 FORMAT(1H0,' LOOP',I5)
  106 FORMAT(1H0,' END OF RUN')
  999 CONTINUE
      STOP
      END

      SUBROUTINE DLOAD
C
C     LOADS DATA
C
C
C     THE FOLLOWING ARRAYS ARE USED IN THIS PROGRAM
C
C     UNIT ARRAY   UNIT(N,I)  I IS THE MODULE NUMBER
C     N=1 MODULE NUMBER
C     N=2 MODULE TYPE
C     N=3 NUMBER OF INPUT STREAMS TO MODULE NIN
C     N=4 NUMBER OF OUTPUT STREAMS TO MODULE NOUT
C     N=5-14 INPUT AND OUTPUT STREAM NUMBERS
C     N=15-30 EQUIPMENT PARAMETERS FOR A SPECIFIC MODULE
C
C     FLOW ARRAY   FLOW(J,I)  I IS THE STREAM NUMBER
C     J=1 STREAM NUMBER
C     J=2-5 STREAM NAME
C     J=6 TEMPERATURE
C     J=7 PRESSURE
C     J=8  TOTAL FLOWRATE = GASEOUS PHASE (GM.MOLE/SEC)
C     J=9  FLOW OF COMPONENT 1  GASEOUS,MIXED
C     J=10 FLOW OF COMPONENT 2  GASEOUS,MIXED
C     ETC
C     J=21 FLOW OF COMPONENT 13 GASEOUS,MIXED
C     J=22 FLOW OF COMPONENT 14 GASEOUS,UNMIXED
C     J=23 ETC
C     J=24 FLOW OF COMPONENT 15 GASEOUS,UNMIXED
C     J=25 FLOW OF COMPONENT 16 LIQUID PHASE (GM/SEC)
C
C     EXCLUDING EXTRA SUBROUTINES THE FOLLOWING VARIABLE NAMES ARE USED
C
C     AVMOL     AVERAGE MOLECULAR WEIGHT
C     CPMASS    MASS FLOWRATE OF COMPONENT
C     INFLOW    NUMBER OF INITIAL STREAMS
C     LOOP      ITERATION COUNTER FOR CYCLIC SYSTEMS
C     MRUN      RUN NUMBER
C     NF        STREAM NUMBER ASSOCIATED WITH CURRENT MODULE
C     NIF       INITIAL STREAM NUMBER
C     NIN       NUMBER OF INPUT STREAMS TO CURRENT MODULE
C     NL        RUNNING TOTAL OF MODULES EXECUTED
C     NOUT      NUMBER OF OUTPUT STREAMS FROM CURRENT MODULE
C     NRUNS     TOTAL NUMBER OF RUNS REQUIRED
C     NTYPE     CURRENT MODULE UNIT TYPE
C     NU        CURRENT MODULE NUMBER
C     TMASS     MASS FLOWRATE OF STREAM
C
C     SEE ALSO DALTER
C
C     SET DUMMY ARRAYS TO FACILITATE NAMELIST INPUT
C     AS DIMENSIONED FLOW PERMITS 100 STREAMS
C     AS DIMENSIONED UNIT PERMITS 50 MODULES
C
      INTEGER TITLE(18)
```

```
      DIMENSION UNIT(30,10),FLOW(25,20)
      COMMON/UNITS/UNIT1(30),UNIT2(30),UNIT3(30),UNIT4(30),UNIT5(30),
     1UNIT6(30),UNIT7(30),UNIT8(30),UNIT9(30),UNIT10(30)
      COMMON/FLOWS/FLOW1(25),FLOW2(25),FLOW3(25),FLOW4(25),FLOW5(25),
     1FLOW6(25),FLOW7(25),FLOW8(25),FLOW9(25),FLOW10(25),FLOW11(25),
     2FLOW12(25),FLOW13(25),FLOW14(25),FLOW15(25),FLOW16(25),FLOW17(25),
     3FLOW18(25),FLOW19(25),FLOW20(25)
      COMMON/PARAMS/LIST(10),JJ,LOOP,NIN,NOUT,NCALC,NFLOW,NCOMP,NU,
     1KPRINT(4),MLOOP,NF(10),IDCP(16),NL,INFLOW(20),NRUNS,NCYCLE
      EQUIVALENCE (UNIT,UNIT1),(FLOW,FLOW1)
      NAMELIST/EXECL/NRUNS,TITLE,LIST,IDCP,KPRINT
      NAMELIST/UNITL/UNIT1,UNIT2,UNIT3,UNIT4,UNIT5,UNIT6,UNIT7,UNIT8,
     1UNIT9,UNIT10
      NAMELIST/FLOWL/FLOW1,FLOW2,FLOW3,FLOW4,FLOW5,FLOW6,FLOW7,FLOW8,
     1FLOW9,FLOW10,FLOW11,FLOW12,FLOW13,FLOW14,FLOW15,FLOW16,FLOW17,
     2FLOW18,FLOW19,FLOW20
C     INITIALISE ARRAYS UNIT AND FLOW
      DO 10 I=1,10
      DO 10 J=1,30
   10 UNIT(J,I)=0.0
      DO 20 I=1,20
      INFLOW(I)=0.0
      DO 20 J=1,25
   20 FLOW(J,I)=0.0
C
C     READ MAIN PARAMETERS OF THE REACTOR NETWORK
C
      READ(2,EXECL)
      WRITE(3,1000)TITLE
 1000 FORMAT(1H1,18A4)
C
C     IS RECYCLE REQUIRED?
C
      READ(2,UNITL)
      NCALC=0
      DO 40 I=1,10
      IF(LIST(I).EQ.0)GO TO 45
      NCALC=NCALC+1
   40 CONTINUE
   45 NCYCLE=0
      DO 70 J=1,NCALC
      I=LIST(J)
      IF(IFIX(UNIT(2,I)).EQ.8)NCYCLE=1
   70 CONTINUE
      IF(NCYCLE)50,50,60
C
C     INITIALISE LOOP COUNTER
C
   50 LOOP=0.99
      MLOOP=0
      GO TO 80
   60 LOOP=1
      MLOOP=1
   80 NCOMP=0
      DO 90 I=1,16
      IF(IDCP(I).EQ.0)GOTO 95
      NCOMP=NCOMP+1
   90 CONTINUE
   95 JJ=NCOMP+8
      READ(2,FLOWL)
      DO 200 L=1,NCALC
      I=LIST(L)
      DO 140 J=5,14
      IF(UNIT(J,I).EQ.0.)GOTO 200
      K=UNIT(J,I)+.001
      INFLOW(K)=K
  100 CONTINUE
  200 CONTINUE
      NFLOW=0
      DO 105 I=1,20
      IF(INFLOW(I).NE.0)NFLOW=I
  105 CONTINUE
      DO 300 I=1,NFLOW
      FLOW(1,I)=INFLOW(I)
  300 CONTINUE
      IF(KPRINT(2).EQ.1)CALL WRITE2
      RETURN
      END

      SUBROUTINE DALTER
C
C     LOADS MODIFIED DATA
C     MODIFICATIONS  TO
C          STREAMS AND MODULES IF MOD=0
C          STREAMS ONLY IF MOD=1
C          MODULES ONLY IF MOD=2
C     20 FLOW AND 20 UNIT MODIFICICATIONS ARE ALLOWED
C     IUNIT=NUMBERS OF MODIFIED MODULES
C     JUNIT=MODULE ELEMENTS TO BE MODIFIED
C     VUNIT=MODIFIED VALUE MODULE ELEMENT
C     IFLOW=NUMBERS OF MODIFIED FLOWS
C     JFLOW=FLOW ELEMENTS TO BE MODIFIED
C     VFLOW=MODIFIED VALUES OF STREAM ELEMENTS
C
      DIMENSION IFLOW(20),JFLOW(20),VFLOW(20),IUNIT(20),JUNIT(20),VUNIT(
     120)
      COMMON/UNITS/UNIT(30,10)
      COMMON/FLOWS/FLOW(25,20)
      COMMON/PARAMS/LIST(10),JJ,LOOP,NIN,NOUT,NCALC,NFLOW,NCOMP,NU,
     1KPRINT(4),MLOOP,NF(10),IDCP(16),NL,INFLOW(20),NRUNS,NCYCLE
      COMMON/RGAS/RG,RR,IK,AA(20,20),CC(20),JENT,T0,W0
      NAMELIST/CLIST/MOD,NMUNIT,NMFLOW
      NAMELIST/MFLOWL/IFLOW,JFLOW,VFLOW
      NAMELIST/MUNITL/IUNIT,JUNIT,VUNIT
C
C     INITIALISE MODIFIED DATA ARRAYS FOR UNITS AND FLOWS
C
      DO 10 K=1,20
      IFLOW(K)=0
      IFLOW(K)=0
      JFLOW(K)=0
      VFLOW(K)=0
      IUNIT(K)=0
      JUNIT(K)=0
      VUNIT(K)=0
   10 CONTINUE
      IF(MLOOP)40,40,20
   20 LOOP=1
   40 READ(2,CLIST)
      IF(MOD.EQ.1)GO TO 60
C
C     UNIT MODIFICATIONS
C
      READ(2,MUNITL)
```

```
      WRITE(3,105)NMUNIT
      DO 700 I=1,NMUNIT
      UNIT(IUNIT(I),IUNIT(I))=VUNIT(I)
      WRITE(3,106)IUNIT(I),JUNIT(I),VUNIT(I)
      IF(IUNIT(I+1).EQ.IUNIT(I))GO TO 700
      WRITE(3,107)IUNIT(I)
      WRITE(3,104)(UNIT(J,IUNIT(I)),J=1,30)
  700 CONTINUE
      IF(MOD.EQ.2)GO TO 70
C
C     FLOW MODIFICATIONS
C
   60 READ(2,NFLOWL)
      WRITE(3,101)NMFLOW
      DO 800 I=1,NMFLOW
      FLOW(JFLOW(I),IFLOW(I))=VFLOW(I)
      WRITE(3,102)IFLOW(I),JFLOW(I),VFLOW(I)
      IF(IFLOW(I+1).EQ.IFLOW(I))GO TO 500
      WRITE(3,103)IFLOW(I)
      WRITE(3,109)(FLOW(J,IFLOW(I)),J=1,JJ)
  500 CONTINUE
  101 FORMAT(1H0NUMBER OF FLOW MODIFICATIONS IS ',I5)
  102 FORMAT(1H0STREAM NUMBER ',I5,' HAS ELEMENT NUMBER ',I5,' MODIFIED=-
     1NEW VALUE IS ',F12.4)
  103 FORMAT(1HNEW DATA BLOCK FOR STREAM NUMBER ',I5,' IS')
  104 FORMAT(5F12.4)
  105 FORMAT(1H0,' NUMBER OF UNIT MODIFICATIONS IS ',I5)
  106 FORMAT(1H0,' UNIT NUMBER',I5,' HAS ELEMENT NUMBER ',I5,' MODIFIED=
     1-NEW VALUE IS ',F12.4)
  107 FORMAT(1H0,' NEW DATA BLOCK FOR UNIT NUMBER ',I5,' IS')
  108 FORMAT(1H0,' ERROR-----EITHER NO. OF FLOW OR UNIT MODIFICATIONS EX
     1CEEDS MAXIMUM ALLOWED')
  109 FORMAT(1H0,T8,'FLOW',F6.0,5X,4A4,//,T2,'TEMPERATURE',T15,F6.2,/,T2
     1,'PRESSURE',T15,F6.2,/,T2,'TOTAL FLOW',T15,F10.4,/,T2,'COMP. FLOWS
     2',12(/,F10.4))
   70 IF(MLOOP.EQ.1)NCYCLE=1
      JENT=0
      RETURN
      END

      SUBROUTINE TEST
C
C     CONVERGENCE TEST ROUTINE WITH WEGSTEIN CONVERGENCE PROMOTER
C
C     UNIT J=1-14 STANDARD
C          J=15 MAXIMUM NUMBER OF LOOPS
C          J=16 FRACTIONAL TOLERENCE
C          J=17 LOOP WHEN WEGSTEIN 1ST USED OR ZERO IF WEGSTEIN NOT USED
C          J=18 NO OF MODULES IN LOOP CONTROLLED BY TEST
C          J=19-18+NCOMP STORE LATEST COMPONENT FLOW VALUES
C
      DIMENSION SAVE(28)
      COMMON/UNITS/UNIT(30,10)
      COMMON/FLOWS/FLOW(25,20)
      COMMON/PARAMS/LIST(10),JJ,LOOP,NIN,NOUT,NCALC,NFLOW,NCOMP,NU,
     1KPRINT(4),MLOOP,NF(10),IDCP(16),NL,INFLOW(20),NRUNS
      DATA SAVE/28*0/
      JTEST=0
      JJ1=JJ+1
      IF(LOOP-999)1,13,13
    1 WRITE(21,9)LOOP
C
C     ROUTINE BY-PASSED WHEN LOOP=1
C
      IF(LOOP.EQ.1)GO TO 7
      DO 3 J=6,JJ
C
C     COMPARE FLOW WITH PREVIOUS VALUE
C
      IF(FLOW(J,NF(1)))41,42,41
   41 DIFF=ABS((FLOW(J,NF(1))-FLOW(J,NF(2)))/FLOW(J,NF(1)))
      GO TO 43
   42 DIFF=ABS(FLOW(J,NF(1))-FLOW(J,NF(2)))
   43 WRITE(21,10)J,DIFF
C
C     TEST FOR CONVERGENCE
C
      IF(DIFF-UNIT(16,NU))3,3,2
    2 JTEST=1
    3 CONTINUE
      IF(JTEST)4,4,5
    4 WRITE(3,11)
      LOOP=999
      GO TO 13
    5 WRITE(21,12)
      ML=UNIT(15,NU)+.001
C
C     HAS MAXIMUM LOOP BEEN REACHED
C
      IF(LOOP-ML)7,6,6
    6 LOOP=999
      GO TO 13
   13 RETURN
    7 LW=UNIT(17,NU)+0.001
C
C     IS WEGSTEIN TO BE USED?
C
      IF(LW.EQ.0.)GOTO 15
      IF(LOOP-LW)15,14,14
   14 WRITE(21,16)
C
C     RETAIN PREVIOUS FLOW VALUES
C
   15 DO 17 J=9,JJ
      JK=J-8
      KK=NCOMP+JK
      WN=FLOW(J,NF(1))
      WO=SAVE(JK)
      WC1=FLOW(J,NF(2))
      WC2=SAVE(KK)
      IF(LW.EQ.0.)GOTO 25
      IF(LOOP-LW)25,18,18
   22 IF(IWEG)19,19,20
   19 WRITE(21,21)
   20 CONTINUE
      SAVE(JK)=WN
      SAVE(KK)=WC1
      FLOW(J,NF(2))=WWN
      JC=J-8
      WRITE(21,23)JC,PHI,0
      GO TO 17
   25 SAVE(JK)=WN
      SAVE(KK)=WC1
      FLOW(J,NF(2))=FLOW(J,NF(1))
```

AD-A042 979 SHEFFIELD UNIV (ENGLAND) DEPT OF CHEMICAL ENGINEERIN--ETC F/G 21/2
POLLUTANT MINIMISATION BY BLUE FLAME STAGED COMBUSTION.(U)
1977 D S PRIOR AF-AFOSR-2682-74
AFOSR-TR-77-0843 NL

UNCLASSIFIED

3 OF 3
AD
A042979

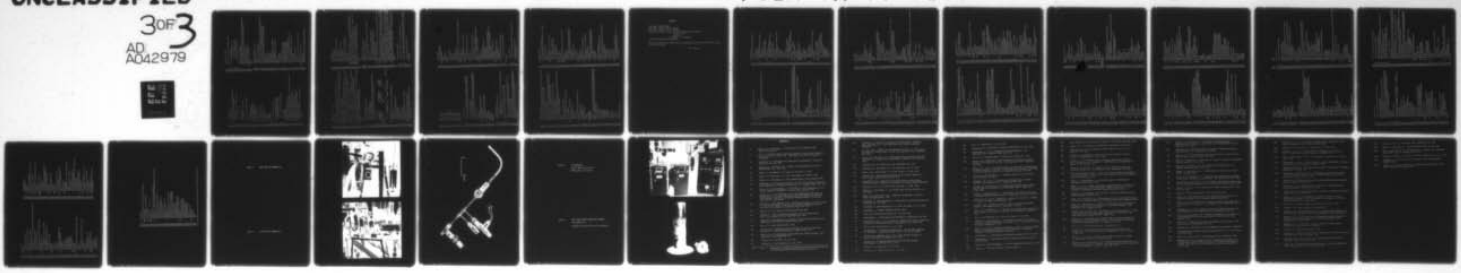

END
DATE
FILMED
9-77
DDC

```
      17 CONTINUE
         FLOW(8,NF(2))=0
         DO 27 J=9,JJ
      27 FLOW(8,NF(2))=FLOW(8,NF(2))+FLOW(J,NF(2))
         FLOW(25,NF(2))=FLOW(25,NF(1))
         WRITE(21,28)
         WRITE(21,29)(FLOW(J,NF(2)),J=1,JJ1)
C
C        RESET LOOP COUNTER
C
         LOOP=LOOP+1
         NL=NL-IFIX(UNIT(18,NU))-1
         GO TO 30
C
C        WEGSTEIN CONVERGENCE PROMOTER
C
      18 IWEG=1
         IF(WN-W0)31,39,31
      31 IF(W1-W2)32,39,32
      32 PHI=(W1-W2)/(WN-W0)
         IF(PHI-1)33,39,33
      33 Q=1./(1.-PHI)
         IF(Q-10.)35,35,34
      34 Q=10.
         GO TO 37
      35 IF(Q+10.)36,37,37
      36 CONTINUE
      37 WWN=Q*W1+(1.-Q)*WN
         GO TO 40
      39 WWN=WN
         Q=0
         PHI=0
         IWEG=-1
      40 GO TO 22
C
C        END OF WEGSTEIN ROUTINE
C
      30 FLOW(6,NF(2))=FLOW(6,NF(1))
         FLOW(7,NF(2))=FLOW(7,NF(1))
         IF(KPRINT(4).EQ.0) GO TO 44
C
C        PRINT INTERMEDIATE FLOW ANALYSIS
C
         WRITE(3,45)
         CALL WRITE1
      44 WRITE(21,8)LOOP
       8 FORMAT(1H0,' LOOP',I5)
       9 FORMAT(1H0,' END OF LOOP',I5)
      10 FORMAT(1H0,'FRACTIONAL CHANGE IN ITEM',I5,'IS',3X,F10.8)
      11 FORMAT(1H0,' ***CONVERGED***')
      12 FORMAT(1H0,' ***NOT CONVERGED***')
      16 FORMAT(1H0,T6,'J',T16,' PHI',T30,' Q')
      21 FORMAT(1H0,' WEGSTEIN FAILS')
      23 FORMAT(1H ,T6,I1,T10,F12.8,T24,F12.8)
      28 FORMAT(1H0,' NEW VALUE OF FLOW')
      29 FORMAT(1H ,6F12.4)
      45 FORMAT(1H0,'INTERMEDIATE FLOW ANALYSIS')
         RETURN
         END
```

```
         SUBROUTINE TEMPRES
C
C        SETS TEMPERATURE OR PRESSURE OR BOTH
C
C        UNIT J=1-14 STANDARD
C             J=15 -1 SET PRESSURE ONLY
C                   0 SET BOTH
C                  +1 SET TEMPERATURE ONLY
C             J=16 NEW TEMPERATURE VALUE
C             J=17 NEW PRESSURE VALUE
C
         COMMON/UNITS/UNIT(30,10)
         COMMON/FLOWS/FLOW(25,20)
         COMMON/PARAMS/LIST(10),JJ,LOOP,NIN,NOUT,NCALC,NFLOW,NCOMP,NU,
        1KPRINT(4),MLOOP,NF(10),IDCP(16),NL,INFLOW(20),NRUNS
         IF(UNIT(15,NU))1,1,2
       1 FLOW(7,NF(1))=UNIT(17,NU)
         IF(UNIT(15,NU))3,2,3
       2 FLOW(6,NF(1))=UNIT(16,NU)
       3 RETURN
         END

         SUBROUTINE WRITE1
C        PRINTS FINAL FLOW ANALYSIS
         REAL MDOTV
         COMMON/UNITS/UNIT(30,10)
         COMMON/FLOWS/FLOW(25,20)
         COMMON/PARAMS/LIST(10),JJ,LOOP,NIN,NOUT,NCALC,NFLOW,NCOMP,NU,
        1KPRINT(4),MLOOP,NF(10),IDCP(16),NL,INFLOW(20),NRUNS
         COMMON /SECOND/N,N1,NR,NT,IT,N2,KOUNT(10),NT1,K
         COMMON/PRINT/TAU(10),V(20),B(20,10),X(20),X0(20)
         V(17)='LIQF'
         WRITE(3,600)
         NCOMP1=NCOMP+1
         NT3=NCOMP+3
         DO 1 J=1,NFLOW
         WRITE(3,610) J
         WRITE(3,620) (FLOW(I,J),I=6,8)
         DO 2 I=1,NCOMP1
         WRITE(3,630) V(I),FLOW((I+8),J)
       2 CONTINUE
       1 CONTINUE
         WRITE(3,650)
         DO 3 I=1,NCALC
         NU=LIST(I)
         IF (UNIT(2,NU)-2.001) 4,4,3
       4 NTYPE=ABS(UNIT(2,NU)+0.001)
         NNIN=ABS(UNIT(5,NU)+0.001)
         NNOUT=ABS(UNIT(6,NU)+0.001)
         MDOTV=FLOW(8,NNIN)/UNIT(30,NU)
         WRITE(3,660) NU,NTYPE,NNIN,NNOUT,TAU(NU),
        *MDOTV,FLOW(6,NNOUT)
         WRITE(3,665)UNIT(26,NU),UNIT(16,NU)
         WRITE(3,670)
         DO 5 J=1,NT3
         IF(J.GT.3)GO TO 675
         JD=J+13
         WRITE(3,671)V(J),B(J,NU),V(JD),B(JD,NU)
         GO TO 5
       675 WRITE(3,672)V(J),B(J,NU)
         5 CONTINUE
         WRITE(3,680)
         WRITE(3,681)V(17),FLOW(25,NNOUT),UNIT(19,NU)
```

```
      WRITE(3,640) KOUNT(NU)
    3 CONTINUE
      V(17)='M'
  600 FORMAT(1H0,18X,'*****FINAL FLOW ANALYSIS*****',///)
  610 FORMAT(1H0,14X,'STREAM NUMBER  ',I2,/)
  620 FORMAT(1H0,8X,'SPECIES     FLOW RATE      TEMPERATURE ',F6.1,',K   P
     1RESSURE ',F4.2,' ATM.   TOTAL FLOWRATE ',1PE10.4,' MOLE/SEC',/)
  630 FORMAT(1H ,7X,A4,4X,1PE10.4)
  640 FORMAT(1H0,6X,'KOUNT=',I3,///)
  650 FORMAT(1H0,15X,'*****FINAL REACTOR ANALYSIS*****',///)
  660 FORMAT(1H0,5X,'MODULE NO. ',I2,' REACTOR TYPE ',I1,' INPUT FLOW ',
     1I2,' OUTPUT FLOW ',I2,/,5X,' RESIDENCE TIME ',E10.4,' SEC   MOOTV
     2',F1',4,' MOLE/SEC,CC   REACTOR TEMPERATURE ',F6.1,',K',//)
  665 FORMAT(1H ,5X,'HOMOGENEOUS FEED EQUIVALENCE RATIO',
     1F9.2,/,5X,' UNMIXEDNESS FACTOR TAU SD',F8.2)
  670 FORMAT(1H0,5X,'GASEOUS   PHASE',12X,'MIXED SPECIES   CONCENTRATION
     1 (MOLE/GM)',5X,'UNMIXED SPECIES   CONCENTRATION (MOLE/GM)')
  671 FORMAT(1H ,34X,A4,'=',8X,1PE10.4,22X,A4,'=',9X,1PE10.4)
  672 FORMAT(1H ,34X,A4,'=',8X,1PE10.4)
  680 FORMAT(1H0,/,5X,'LIQUID    PHASE',10X,'EXIT MASS FLOWRATE (GM/SEC)
     1',17X,'MEAN EVAPORATION RATE (GM/SEC)')
  681 FORMAT(1H ,35X,A4,'=',1PE10.4,34X,1PE10.4)
      RETURN
      END

      SUBROUTINE WRITE2
C     PRINTS INPUT FLOWS AND UNITS
      INTEGER UNNAME(15)
      DIMENSION NIF(20)
      COMMON/UNITS/UNIT(30,10)
      COMMON/FLOWS/FLOW(25,20)
      COMMON/PARAMS/LIST(10),JJ,LOOP,NIN,NOUT,NCALC,NFLOW,NCOMP,NU,
     1KPRINT(4),MLOOP,NF(10),IDCP(16),NL,INFLOW(20),NRUNS
C
C     MODULE NAMES
C
C    1. WSRFACTOR            2. PFREACTOR         3. MIXER
C    4. SPARE                5. RESET LOOP        6. SPARE
C    7. TEMPRESS             8. WEGSTEIN          9. COAN
C   10. PJET                11.
C   13.                      14.                  15.
C
      DATA UNNAME(1)/'WSR       PFR       MIXER                 RESET LOOP
     1          TEMPRES   TEST      COANDA    PJATOMISER
     2                                                        '/
      WRITE(3,100)
  100 FORMAT(1H0,18X,'***INITIAL FLOW ANALYSIS***')
      IPFLOW=0
      DO 10 I=1,NFLOW
      IF(FLOW(8,I).LT..00001)GOTO 10
      K=FLOW(1,I)+.001
      IPFLOW=IPFLOW+1
      NIF(IPFLOW)=K
   10 CONTINUE
      DO 20 I=1,IPFLOW
      WRITE(3,40)NIF(I)
   20 WRITE(3,50)(J,FLOW(J,NIF(I)),J=1,25)
      WRITE(3,300)
  300 FORMAT(1H0,'***UNIT INPUT DATA***')
   40 FORMAT(1H0,'STREAM NUMBER',I2)
   50 FORMAT(1H0,'FLOW ARRAY',/,5(I4,2X,F12,4))
      DO 1 I=1,NCALC
      NU=LIST(I)
      NIN=UNIT(3,NU)
      NOUT=UNIT(4,NU)
      NTYPE=UNIT(2,NU)
      WRITE(3,301)I,NU,UNNAME(NTYPE)
      WRITE(3,302)NIN
      DO 2 J=1,NIN
    2 WRITE(3,303)J,UNIT(J+4,NU)
      WRITE(3,304)NOUT
      DO 3 J=1,NOUT
    3 WRITE(3,305)J,UNIT(J+NIN+4,NU)
      WRITE(3,306)(J,UNIT(J,NU),J=1,30)
    1 CONTINUE
      WRITE(3,307)
  301 FORMAT(1H0,///,' MODULE ',I3,' UNIT',I4,5X,A10,2X,'ROUTINE')
  302 FORMAT(1H0,'INPUT FLOWS',15X,'NUMBER OF INPUT FLOWS = ',I3)
  303 FORMAT(1H ,10X,'INPUT',I3,' STREAM ',F3,0)
  304 FORMAT(1H0,'OUTPUT FLOWS',15X,'NUMBER OF OUTPUT FLOWS = ',I3)
  305 FORMAT(1H ,10X,'OUTPUT',I3,' STREAM ',F3,0)
  306 FORMAT(1H0,'UNIT PARAMETERS',/,5(I5,2X,F10,4))
  307 FORMAT(1H0,//,'****END OF INPUT DATA*****',//////)
      RETURN
      END

      SUBROUTINE WRITE3
C     PRINTS PER MODEL INFORMATION
      COMMON/UNITS/UNIT(30,10)
      COMMON/FLOWS/FLOW(25,20)
      COMMON /VAR1/FUEL,DDM,VSA,R(20),DEN1,AV1,MWSR,MSPM
      COMMON /BERP/XB,D6,QJ
      WRITE(3,201)
      WRITE(3,202)FLOW(6,1),UNIT(16,1),QJ,AV1
      WRITE(3,203)UNIT(15,2),DDM,VSA,D6,XB
      PHIOV=FLOW(25,4)*18,0/(168,3*FLOW(22,3))
      RECN=UNIT(15,MSPM)*100,0
      WRITE(3,204)PHIOV,RECN
  201 FORMAT(1H0,///,18X,'*****BLUE FLAME BURNER MODEL INFORMATION*****
     1)
  202 FORMAT(1H0,/,10X,'ESTIMATED AIR INLET TEMPERATURE      =',F9,3,'K
     1,/,10X,'AIR MANIFOLD PRESSURE',16X,'=',F9.3,'IN.HG',/,10X,'AIR FE
     2O FLOWRATE',20X,'=',F9,3,'LIT/MIN',/,10X,'COANDA INLET PLANE,MEAN
     3GAS VELOCITY =',F9,3,'M/SEC',//)
  203 FORMAT(1H ,9X,'FUEL INJECTION PRESSURE',14X,'=',F9,3,'PSIG',/,10X
     1,'ATOMISER FUEL MASS FLOWRATE',10X,'=',F9,3,'GM/SEC',/,10X,'SPRAY
     2INITIAL MEAN VELOCITY',10X,'=',F9,3,'M/SEC',/,10X,'SPRAY INITIAL
     3IZE DISTRIBUTION ',/,17X,'ROS,RAM. EXPONENT',13X,'=',F9,3,/,17X,
     4'ROS,RAM.   MEAN',15X,'=',F9,3,'MICRON',///)
  204 FORMAT(1H ,9X,'ESTIMATED BURNER OVERALL EQUIVALENCE =',F9,3,/,
     110X,'DEGREE OF INTERNAL RECIRCULATION     =',F9,3,'%',///)
      RETURN
      END

      SUBROUTINE MODULE(NT)
C
C     IDENTIFIES UNIT TYPE AND CALLS REQUIRED MODULE
C
C     IF A FURTHER MODULE IS REQUIRED ADD APPROPRIATE CALL CARD AND
C     VERIFY THAT CONTROL NUMBER IS CONSISTENT WITH COMPUTED GO TO.
C
      GO TO(1,2,3,4,5,6,7,8,9,10),NT
    1 CALL WSR
      GO TO 50
```

```
      2 CALL PFR
        GO TO 50
      3 CALL MIXER
        GO TO 50
      4 GO TO 50
      5 CALL LOOP1
        GO TO 50
      6 GO TO 50
      7 CALL TEMPRES
        GO TO 50
      8 CALL TEST
        GO TO 50
      9 CALL COAN
        GO TO 50
     10 CALL PJET
        GO TO 50
     50 RETURN
        END

        SUBROUTINE LOOP1
C
C     RESET LOOP AND NCYCLE AFTER SOLVING THE 1ST RECYCLE LOOP
C     ACCORDING TO WHETHER OR NOT FURTHER RECYCLE IS REQUIRED
C
        COMMON/UNITS/UNIT(30,10)
        COMMON/FLOWS/FLOW(25,20)
        COMMON/PARAMS/LIST(10),JJ,LOOP,NIN,NOUT,NCALC,NFLOW,NCOMP,NU,
       1KPRINT(4),MLOOP,NF(10),IDCP(16),NL,INFLOW(20),NRUNS,NCYCLE
        NCYCLE=0
        DO 70 J=1,NCALC
        J1=J+1
        J2=LIST(J)
        IF(IFIX(UNIT(2,J2))-8)70,80,70
     80 DO 90 I=J1,NCALC
        I2=LIST(I)
        IF(IFIX(UNIT(2,I2))-8)90,100,90
    100 NCYCLE=1
        LOOP=1
        GO TO 105
     90 CONTINUE
     70 CONTINUE
    105 RETURN
        END

        SUBROUTINE MIXER
C     STREAM MIXER/SPLITTER ROUTINE
C
C     UNIT J=1-14 STANDARD
C          J=15-14+NOUT FRACTION OF TOTAL INPUT IN 1ST,2ND--NOUT TH
C            OUTPUT FLOW
C     THE FIRST  OUTPUT FRACTION IS IN UNIT J=15
C     THE SECOND OUTPUT FRACTION IS IN UNIT J=16
C     ETC
C     THE LIQUID PHASE IS FRACTIONED AS FOR THE GASEOUS PHASE
        DIMENSION TOTAL(20),CCP(20),HMI(20),DCPDT(20)
        COMMON /UNITS/UNIT(30,10)
        COMMON /FLOWS/FLOW(25,20)
        COMMON /PARAMS/LIST(10),JJ,LOOP,NIN,NOUT,NCALC,NFLOW,NCOMP,NU,
       1KPRINT(4),MLOOP,NF(10),IDCP(16),NL,INFLOW(20),NRUNS,NCYCLE,K
        COMMON /SECOND/ N,NI,NR,NT,IT,N2,KOUNT(10),NT1
        LL=NIN+1
        NN=NIN+NOUT
        IF (K.NE.0) GOTO 20
        READ(29,100)N,IT,NR
    100 FORMAT(3I5)
        N1=N+1
        N2=N+2
        NT1=NCOMP+1
     20 FST=0
        FS=0
        DO 1 J=1,NCOMP
        TOTAL(J)=0
        CCP(J)=0
      1 CONTINUE
        NIN1=NIN-1
        IF (NIN-1)30,35,30
     30 DO 31 I=1,NIN1
        IF (ABS(FLOW(6,NF(I))-FLOW(6,NF(I+1))).GT.10)GOTO 33
     31 CONTINUE
     35 DO 32 J=1,NCOMP
        DO 32 I=1,NIN
        TOTAL(J)=TOTAL(J)+FLOW(J+8,NF(I))
     32 CONTINUE
        T=FLOW(6,NF(1))
        CALL PB3(T,NCOMP,HMI,CCP,DCPDT,K)
        GOTO 34
     33 DO 2 I=1,NIN
        T=FLOW(6,NF(I))
        CALL PB3(T,NCOMP,HMI,CCP,DCPDT,K)
        DO 2 J=1,NCOMP
        TOTAL(J)=TOTAL(J)+FLOW(J+8,NF(I))
        FST=FST+FLOW(J+8,NF(I))*CCP(J)*FLOW(6,NF(I))
      2 FS=FS+FLOW(J+8,NF(I))*CCP(J)
        T=FST/FS
     34 DO 3 I=LL,NN
        II=15+I-LL
        FLOW(6,NF(I))=T
        FLOW(7,NF(I))=FLOW(7,NF(1))
        FLOW(8,NF(I))=0
        DO 3 J=1,NCOMP
        FLOW(J+8,NF(I))=TOTAL(J)*UNIT(II,NU)
      3 FLOW(8,NF(I))=FLOW(8,NF(I))+FLOW(J+8,NF(I))
C       NPHAZ=0,HOM/=1,HET      FLOW MIXING
        NPHAZ=UNIT(30,NU)
        IF(NPHAZ-1) 150,140,150
    140 TOTLQ=0.0
        DO 40 I=1,NIN
     40 TOTLQ=TOTLQ+FLOW(25,NF(I))
        DO 43 I=LL,NN
        II=15+I-LL
     43 FLOW(25,NF(I))=TOTLQ*UNIT(II,NU)
C
        IF(NU.EQ.6)FLOW(6,8)=UNIT(29,6)
C
    150 RETURN
        END

        SUBROUTINE WSR
C
C     WSR SOLUTION ROUTINE ADAPTED FROM I.T.OSGERBY
C
        LOGICAL PLUG,PLUG1,PLUG2
        REAL MDOTV,M1,M2
```

```
      DIMENSION A (240)
      DIMENSION XØ(20),X(20),W(20),B(20),BB(20),HM(20),Y(20),DCP(20),AD
     *(20),TAU(10),BB(20,10),V(20),CPM(20),YØ(20)
      COMMON /PLPARS/PLV(8),PLUG,PLUG1,PLUG2,BØ,B
      COMMON/UNITS/UNIT(30,10)
      COMMON/FLOWS/FLOW(25,20)
      COMMON/PARAMS/LIST(10),JJJ,LOOP,NIN,NOUT,NCALC,NFLOW,NCOMP,NU,
     *KPRINT(4),MLOOP,NF(10),IDCP(16),NL,INFLOW(20),NRUNS,NCYCLE,K
      COMMON /SECOND/N,N1,NR,NT,IT,N2,KOUNT(10),NT1
      COMMON/PRINT/TAU,V,BB,X,XØ
      COMMON/RGAS/RG,RR,IK,AA(20,20),CC(20),JENT,TØ,WØ
      COMMON /EQLF/(20),DF(20)
      COMMON/RRCON/ICR,NR2,NR3,NR4
      COMMON /VAP2/PHYF,UFF,UNF,UOF,UF,UN,UO,RFF,RNF,ROF,RCSF(16),TSD,
     1VOLUM,M1,ETA1,M2,ETA2,PHY,FFD,PUO,W
C     IT=1  TEMPERATURE  CONSTANT
      ICR=4Ø
      JJ=2
      FLOW(7,NF(2))=P=FLOW(7,NF(1))
      VOLUM=UNIT(3Ø,NU)
      IF(NCYCLE.EQ.1.AND.LOOP.GT.15)GO TO 9Ø
      TØ=FLOW(6,NF(1))
   9Ø WRITE(3,11Ø)TØ
  11Ø FORMAT(1H ,'   TØ=',F10.2)
      TSD=UNIT(16,NU)
      ETA1=FLOW(25,NF(1))
      NT=NCOMP
      NT3=NT+3
      DO 12 J=1,NT
      XØ(J)=FLOW((J+8),NF(1))/FLOW(8,NF(1))
   12 CONTINUE
      IF (K.NE.Ø) GOTO 2Ø
      READ(29,1)N,IT,NR
    1 FORMAT(3I5)
C     COMPUTE  SPECIES
      N1=N+1
      N2=N+2
      NT1=NT+1
   2Ø RR=1.98726
      RG=82.Ø567
      DATA
     1V/'H','N','O','OH','H2O','KERO','CO','NO','N2O','CO2','H2','O2',
     2'N2'/,   W/1.Ø,14.Ø,16.Ø,17.Ø,18.Ø,168.3,28.Ø,3Ø.Ø,2*44.Ø,2.Ø,32.Ø,
     328.Ø/,JENT/Ø/,JW/Ø/
      IF(JW.NE.Ø)GO TO 14
      DO 16 I=1,2Ø
      DO 16 J=1,1Ø
   16 BB(I,J)=Ø.Ø
      W(14)=W(12)
      W(15)=W(13)
      W(16)=W(6)
      V(14)=V(12)
      V(15)=V(13)
      V(16)=V(6)
      JW=1
   14 CONTINUE
      ENTRY WSR.
      XX=Ø.Ø
      HØ=Ø.Ø
      WW=Ø.Ø
      WØ=Ø.Ø
      DO 4 I=1,NT
C     CALCULATE  MOLEC. WT.
      WØ=WØ+XØ(I)*W(I)
    4 CONTINUE
      CALL BB3 (TØ,NT,HM,CPM,DCP,K)
C     CALCULATE  FEED VALUES OF SPECIES AND ENTHALPY
C     INITIALISE EVAP
      M1=FLOW(6,NF(1))*WW
      FFF=Ø.Ø
      DO 5Ø L=1,3
   5Ø FFF=FFF+(FLOW(21+L,NF(1))*W(13+L))
      PHYF=FFF/M1
      UFF=FLOW(24,NF(1))*W(16)/FFF
      UOF=FLOW(22,NF(1))*W(14)/FFF
      UNF=1.Ø-UFF-UOF
      IF(PHYF-1.Ø)64,66,66
   6Ø DO 62 J=1,NT3
   62 RCSF(J)=Ø.Ø
      GO TO 66
   64 DO 52 J=1,NT3
   52 RCSF(J)=FLOW((8+J),NF(1))*W(J)/(M1-FFF)
   66 CONTINUE
      RFF=RCSF(6)
      ROF=RCSF(12)
      RNF=RCSF(13)
      IF(NCYCLE.EQ.Ø.AND.LOOP.EQ.999) GO TO 24
      IF(NCYCLE.EQ.1.AND.LOOP.EQ.1) GO TO 24
      T=UNIT(15,NU)
      P=UNIT(21,NU)
      TAU(NU)=UNIT(22,NU)
      DO 26 J=1,NT
      B(J)=BB(J,NU)
   26 CONTINUE
      GO TO 28
   24 TGESS=T=1500.Ø
      R=Ø.3Ø1/T
      TAU(NU)=5.Ø*VOLUM*R/(6.Ø*M1)
   28 CONTINUE
      CALL EVAP(JENT,T,TAU(NU),R,BØ,WØ)
      DO 3Ø I=1,NT
      HØ=HØ+HM(I)*BØ(I)
   3Ø CONTINUE
      IF (NCYCLE.EQ.1.AND.LOOP.EQ.1) GOTO 3
      IF (NCYCLE.EQ.Ø.AND.LOOP.EQ.999) GOTO 3
      DO 32 I=1,NT
   32 WW=WW+B(I)
      WW=1.Ø/WW
      GOTO 5
    3 CALL BB1(AA,CC,BØ)
      EQR=3*CC((N+1))/(2*CC((N+3)))
   97 IEQ=1
      CALL EQUILB(W,P,FLOW(6,1),BØ,EQR,T,B,WW,IEQ)
      DO 55  I=1,NT3
   55 B(I)=B(I)*(1.Ø-PHY)
      B(14)=BB(14)
      B(15)=BB(15)
      B(16)=BB(16)
    5 CONTINUE
      DO 11 I=1,NT
      X(I)=B(I)*WW
   11 XX=XX+X(I)
   18 CALL BB3  (T,NT,HM,CPM,DCP,K)
C     CHECK FOR NON-CONVERGED SOLUTION OR BLOW OUT
      IF (KOUNT(NU).EQ.15Ø) GO TO 22
      DO 21 J=N1,N2
```

ERRATUM

Line 884:- Add ZPP(2θ)
Line 921:- Replace ZPP by ZPP(J)
Line 922:- Replace ZPP by ZPP(J)
Before Line 923:- Insert

```
      IF (YS(J)/Yθ(J).LT.-1) GOTO 775
      ZPP(J) = θ.37
      GOTO 777
775   ZPP(J) = θ.37/ZPP(J)
```

Line 928:- Replace ZP by ZPP(J)

This correction gives satisfactory convergence for all stoichiometries tested (from θ.5 to 2.θ).

P.G. Felton.

```
      IF(BB(J)) 22,22,34
   34 YB(J)=B(J)/BB(J)
      IF (ABS(YB(J)-1.0)-5.0E-3) 22,22,23
   21 CONTINUE
   22 DO 36 I=1,NT
   36 B(I)=X(I)/WW
C     ESTIMATE REACTOR DENSITY
   23 RHO  /(82.0567*T)*WW
      CALL COMP (B,BB,P,T,R,Y,H,H0,CP,TAU(NU),WW,XX,BD,A,N,N1,NU)
      UNIT(15,NU)=FLOW(6,NF(2))*T
      R0=P*W0/(82.0567*T0)
      FLOW(25,NF(2))=ETA2
      FLOW(8,NF(2))=H2/WW
      UNIT(17,NU)=PHYF
      UNIT(18,NU)=PHY
      UNIT(19,NU)=FEED
      UNIT(20,NU)=PUO
      UNIT(21,NU)=R
      UNIT(22,NU)=TAU(NU)
      UNIT(23,NU)=UF
      UNIT(24,NU)=UO
      UNIT(25,NU)=UN
      UNIT(26,NU)=EQR
      DO 2 J=1,NT
      XB(J)=BB(J)*W0
      X(J)=B(J)*WW
      BB(J,NU)=B(J)
      FLOW((J+8),NF(2))=X(J)*FLOW(8,NF(2))
    2 CONTINUE
  101 RETURN
      END

      SUBROUTINE COMP(B,BB,P,T,R,Y,H,H0,CP,TAU,WW,XX,BD,D,NX,MY,NU)
      DIMENSION B(20),BB(20),D(NX,MY),A(20,20),C(20),DHDB(20,20),DBDT(20
     *),   DBDR(20),   BD(20),HM(20),CPM(20),DCPT(20),DP(20),Y(20),YB(20
     *),YS(20)
      COMMON /SECOND/N,N1,NR,NT,IT,IDUM(1),KOUNT(10),MDUM(1)
      COMMON/RGAS/RG,RR,IK,A,C,JENT,T0,W0
      KUNT=1
      NT3=NT-3
      ICT=0
      IEV=1
      DELTL=0.0
      DO 6 KK=1,150
      KOUNT(NU) =KK
C     CALCULATE PARTIAL DERIVATIVES
      CALL BB4(B,T,P,R,DHDB,DBDT,DBDR,BD,NU)
C     CALCULATE MATRIX COEF.
      DO 1 J=1,N
      DO 1 I=1,N
      ZB=0.0
      DO 2 L=N1,NT3
      ZB=ZB+(DHDB(J,L)-DBDR(J)*R*WW-HD(J)*WW)*A(I,L)
    2 CONTINUE
      D(J,I)=-TAU*(DBDB(J,I)-DBDR(J)*R*WW-BD(J)*WW+ZB)
    1 CONTINUE
      DO 4 I=1,N
      D(I,I)=1.0+D(I,I)
    4 D(I,MY)=BB(I)-H(I)+TAU*BD(I)
C     SOLVE MATRIX
      CALL CHOLES (D,NX,MY,0)
   28 IF(NX) 12,13,13
   12 WRITE(21,14)
   14 FORMAT(1H ,3X,15HSINGULAR MATRIX)
      NX=N
      GO TO 100
   13 DO 16 J=1,N
      YB(J)=B(J)
   16 YS(J)=D(J,MY)
C     TEST FOR CORRECTIONS TOO LARGE
      ZPX=0.0
      DO 777 J=1,N
      ZPP=ABS(YS(J)/YB(J))
      IF (ZPP.GT.ZPX) ZPX=ZPP
  777 CONTINUE
      ZP=0.37/ZPX
      IF(ZP.GT.1.0) ZP=1.0
C     CORRECT SPECIES CONCENTRATIONS
      DO 15 J=1,N
   15 Y(J)=YB(J)+YS(J)*ZP
      DO 17 I=1,N
      B(I)=Y(I)
   17 Y(I)=(B(I)-BB(I))/(TAU*BD(I))-1.0
      DO 10 J=N1,NT3
      YB(J)=B(J)
      B(J)=Y(J)
      BD(J)=0.0
      Y(J)=0.0
      JJ=J-1
      DO 9 I=1,JJ
      BD(J)=BD(J)+A(I,J)*BD(I)
    9 B(J)=B(J)+A(I,J)*B(I)
      IF (BD(J).EQ.0.0)  GO TO 667
      Y(J)=(B(J)-BB(J))/(TAU*BD(J))-1.0
  667 CONTINUE
      IF (BB(J))  37,38,37
   37 YB(J)=B(J)/BB(J)
      GO TO 39
   38 YB(J)=1.0
   39 IF (B(J))  40,10,10
   40 B(J)=1.0E-10
   10 CONTINUE
      WW=0.0
      DO 18 I=1,NT
   18 WW=WW+B(I)
      WW=1.0/WW
      ROLD=R
      R=P*WW/(RG*T)
C     ITERATION CONTROL
      DO 32 J=N1,NT3
      IF (ABS(YB(J)-1.0)-1.0E-05) 32,32,7
   32 CONTINUE
      GO TO 20
    7 IF (ZP-1.0)  49,50,50
   50 IF (IT-1)  52,49,52
   52 IF(IEV.GT.10)GO TO 505
      CALL EVAP(JENT,T,TAU,R,B0,W0)
      CALL BB3(T0,NT,HM,CPM,DCPT,KUNT)
      CALL BB1(A,C,B0)
      B(14)=B0(14)
      B(15)=B0(15)
      B(16)=B0(16)
      IEV=IEV+1
      H0=0.0
```

```
      DO 500 I=1,NT
      HR=HR+HM(I)*BB(I)
  500 CONTINUE
  505 CALL BB3(T,NT,HM,CPM,DCPT,KUNT)
      H=0.0
      CP=0.0
      DO 53 I=1,NT
      H=H+HM(I)*B(I)
   53 CP=CP+CPM(I)*B(I)
C     TEMPERATURE  CONTROL
      IF (ICT-0)  54,55,54
   55 DELT=(HR-H)/CP
      IF (DELT*DELTL) 56,56,57
   57 T=T+DELT*0.83
      GO TO 54
   56 T=T+DELT*0.38
   54 ICT=1
      ICT=ICT-1
      DELTL=DELT
      IF (T-5000.0)  58,58,59
   59 T=5000.0
      GO TO 60
   58 IF (T-300.0)  61,60,60
   61 T=300.0
C     TEMP  WITHIN  1 DEG  K
   60 IF (ABS(HR-H)-CP)  49,49,6
C     CHECK P,S,R, EQUATION
   49 DO 8 I=1,N
      IF( ABS(Y(I)       )-1.0E-4) 8,8,6
    8 CONTINUE
      GO TO 20
    6 CONTINUE
   20 IF(KOUNT(NU).EQ.150) WRITE(3,99)
      WRITE(3,200)KK,T
  200 FORMAT(1HO,3HKK=,I5,F10.2)
      XX=0.0
      H=0.0
      CP=0.0
      CALL BB3(T,NT,HM,CPM,DCPT,KUNT)
      DO 3 I=1,NT
      XX=XX+B(I)*WW
      H=H+HM(I)*B(I)
    3 CP=CP+CPM(I)*B(I)
      IF(KOUNT(NU).NE.150)JENT=2
  100 RETURN
   99 FORMAT(1HO,28H NO CONVERGENCE IN 150 STEPS)
      END

      SUBROUTINE BB1 (A,C,B)
      DIMENSION  A(20,20),B(20),C(20)
      DIMENSION NS(20,5),SC(20,5),J(5)
      COMMON/SECOND/N,N1,NR,NT
      COMMON/PRINT/TAU(10),V(20)
      DATA KTP/0/
      IF (KTP) 3,3,4
    3 N1=NT-N+3
      READ (29,98) (J(I),I=1,NL)
      DO 1 I=1,NL
      JJ=J(I)
      READ (29,99) ( NS(K,I),SC(K,I) ,K=1,JJ)
    1 WRITE(21,999)( V(NS(K,I)),SC(K,I) ,K=1,JJ)
  999 FORMAT(1HO,8(4X,A4,'*',F5.1))
    4 DO 6 I=1,20
      C(I)=0.
      DO 6 K=1,20
    6 A(I,K)=0.
      DO 5 I=1,NL
      II=N+I
      C(II)=0.
      JJ=J(I)
      DO 2 K=1,JJ
      L=NS(K,I)
      C(II)=C(II)+B(L)*SC(K,I)
      A(L,II)=-SC(K,I)
    2 A(II,II)=0.0
    5 CONTINUE
   98 FORMAT(5I5)
   99 FORMAT(5(I3,E10.4))
      KTP=1
      RETURN
      END

      SUBROUTINE BB3(T,NT,HMI,CPMI,DCPTMI,K)
      DIMENSION HMI(NT),CPMI(NT),DCPTMI(NT)
      DIMENSION COE(14),C(14,20)
      DIMENSION CC(6),TT(5)
      COMMON /VAP3/PO(20)
      COMMON /EQL/F(20),DF(20)
      RG=1.98726
      TTLN = ALOG(T)
      TLN = 1.-TTLN
      IF (K) 4,7,4
    7 WRITE (21,103)
  103 FORMAT (1H1,3X,34H THERMO  DATA  CHECK  DATA  AT  TO)
      READ (29,70)((C(I,KK),I=1,14),KK=1,NT)
   70 FORMAT(2(E14.8,4E15.8,/),E14.8,3E15.8)
C     KK=6==UEL:=13=N2
      DO 90 I=1,5
      I1=I+5
      I2=I1+5
      I3=I2+5
      PO(I)=C(I,6)
      PO(I1)=C((7+I),6)
      PO(I2)=C(I,13)
   90 PO(I3)=C((7+I),13)
    4 TE=T
      IF (TE-300.)10,20,20
   10 WRITE(21,80) T
   80 FORMAT(1H1,51HTEMPERATURE IS OUT OF RANGE OF CURVE FIT TABLES T =,
     1E17.5)
      CALL WRITE1
      CALL EXIT
   20 IF (TE-1000.)30,40,40
   30 KL=0
      GO TO 60
   40 IF (TE-3000.) 50,50,10
   50 KL=7
   60 CONTINUE
      TT(1)=T
      DO 1      M=2,4
    1 TT(M)= TT(M-1)*T
      TT(5)=1./T
      DO 100 KK=1,NT
      DO 5 J=1,14
    5 COE(J)=C(J,KK)
      CC(1)= COE(KL+1)
      DO 3 J=2,6
      KKK=(KL+J)
```

```
      3 CC(J)= COF(KKK)*TT(J-1)
        H=            CC(1)+.5*CC(2)+CC(3)/3.+.25*CC(4)+.2*CC(5)+CC(6)
        FX  =(CC(1)*TLN )-.5*CC(2)-(CC(3)+.5*CC(4))/6.-.05*CC(5)+CC(6)-
       *COF(KL+7)
        CP  =                 (CC(1)+CC(2)+CC(3)+CC(4)+CC(5))
        DCP=CC(2)+2.*CC(3)+3.*CC(4)+4.*CC(5)
C       SPECIES ENTHALPY
        HMI(KK)=H*RG*T
C       SPECIES HEAT CAPACITY
        CPMI(KK)=CP*RG
C       SPECIES HEAT CAPACITY DERIVATIVE
        DCPTMI(KK)=DCP*RG/T
C       SPECIES FREE ENERGY
        F(KK)=FX
C       SPECIES FREE ENERGY DERIVATIVE
        DF(KK)=-H/T
        IF(K.EQ.0) WRITE (21,71) HMI(KK),CPMI(KK),F(KK),DF(KK)
     71 FORMAT(1H ,4E17.5,//)
    100 CONTINUE
        K=1
        RETURN
        END

        SUBROUTINE BB4 (B,T,P,R,DBDB,DBDT,DBDR,BD,NU)
        DIMENSION DBDR(20,20),BD(20),DBDT(20),DBDR(20),B(20),DC(4)
        COMMON/SECOND/N,N1,NR,NT,IT,IDUM(1),KOUNT(10),NT1
        COMMON/RATE/TT,FF(40),BB(40),DFF(40),DBB(40)
        DIMENSION D(40,18),I1(40,7),ER(40,7),KS(40,7),IE(40),IC(40)
        COMMON /RRATE/A(40),EX(40),TEX(40),KK(40,4),ITR(40),ITP(40),
       1IB(40)
        COMMON/RGAS/RG,RR,IK
        COMMON/PRINT/TAU(10),V(20)
        DATA KRD/0/
        IF (KRD) 1,1,2
      1 NT1=NT+1
        NT2=NT+2
        NT3=NT+3
        KRD=1
        V(14)='M'
        B(NT1)=1.
        READ (29,99) IK
        DO 10 IR=1,NR
        READ (29,99) ITR(IR),ITP(IR),(KK(IR,I),I=1,4),A(IR),EX(IR),
       *TEX(IR),IF(IR),IC(IR),IB(IR)
        IF(IK.EQ.1.AND.IR.EQ.1)GO TO 900
        GO TO 910
    900 V(12)='6O2'
        V(11)='12H2'
        V(7)='12CO'
    910 CONTINUE
        WRITE (3,999) IR,(V(KK(IR,I)),I=1,4),A(IR),FX(IR),TEX(IR),IF(IR),
       *IC(IR),IB(IR)
        V(12)='O2'
        V(11)='H2'
        V(7)='CO'
    999 FORMAT(1H ,I5,2X,A4,'+ ',A4,'= ',A4,'+ ',A4,4X,3E15.6,4X,3I5)
     12 IF (IE(IR)) 11,11,14
     14 L=IE(IR)
        READ (29,98) (I1(IR,I),ER(IR,I),I=1,L)
        WRITE (21,997) (I1(IR,I),ER(IR,I),I=1,L)
    997 FORMAT(1H ,5(I10,E17.6))
     11 DO 16 I=1,4
     16 KS(IR,I)=KK(IR,I)
        IF (IC(IR)) 10,10,17
     17 M=IC(IR)
        READ (29,97) (KS(IR,I),I=1,M)
        WRITE (21,97 ) (KS(IR,I),I=1,M)
     10 CONTINUE
        V(14)='O2'
      2 CONTINUE
        TT=T
        BS=0.
        DO 18 I=1,NT
     18 BS=BS+B(I)
        IF (KOUNT(NU).GT.1.AND.IT.EQ.1)  GO TO 888
        CALL RATES
    888 CONTINUE
        DO 100 IR=1,NR
        DO 19 I=1,NT
     19 D(IR,I)=0.
        K1=KK(IR,1)
        K2=KK(IR,2)
        K3=KK(IR,3)
        K4=KK(IR,4)
        IF (ITP(IR)-ITR(IR))  30,20,20
     20 IF(IR.EQ.1.AND.IK.EQ.1) GOTO 25
        GOTO 21
C       QUASI-GLOBAL HYDROCARBON KINETICS (IK=1
     25 D(1,K1)=FF(1)*B(K2)*0.5/(P**(0.825))
        D(1,K1)=D(1,K1)/SQRT(R(K1))
        D1=D(1,K1)*2.0*B(K1)
        D(1,K2)=D1/B(K2)
        D(1,NT1)=D1
        D(1,NT2)=D1*DFF(1)
        D(1,NT3)=D(1,NT1)
        GO TO 100
C       EVALUATE TYPE  A+B=C+D
     21 CONTINUE
        D(IR,K1)=FF(IR)*B(K2)
        D1=D(IR,K1)*B(K1)
        D(IR,K2)=FF(IR)*B(K1)+D(IR,K2)
        D(IR,K3)=-BB(IR)*B(K4)
        D2=D(IR,K3)*B(K3)
        D(IR,K4)= -BB(IR)*B(K3)+D(IR,K4)
        D(IR,NT1)=D1+D2
        D(IR,NT2)=D1*DFF(IR)+D2*DBB(IR)
        D(IR,NT3)=D(IR,NT1)
        GO TO 100
C       EVALUATE TYPE  A+A+M=A2+M
     30 BSUM=BS
        IF (IE(IR)) 311,311,31
     31 K=IE(IR)
        DO 35 J=1,K
     35 BSUM=BSUM+ER(IR,J)*B(NT3)
    311 D1=FF(IR)*B(K1)*B(K2)*R
        D2=-BB(IR)*B(K3)
        D(IR,K1)=FF(IR)*B(K2)*BSUM*R
        D(IR,K2)=FF(IR)*B(K1)*BSUM*R +D(IR,K2)
        D(IR,K3)=-BB(IR)*BSUM
        DO 32 J=1,NT
     32 D(IR,J)=D(IR,J)+D1+D2
        IF (IF(IR)) 36,36,34
     34 DO 33 J=1,K
        LL=I1(IR,J)
     33 D(IR,LL)=D(IR,LL)+(D1+D2)*ER(IR,J)
     36 D(IR,NT1)=(D1+D2)*BSUM
```

```
      D(IR,NT2)=(D1*DFF(IR)+D2*DBB(IR))*BSUM
      D(IR,NT3)=(2.*D1+D2)*BSUM
  100 CONTINUE
C     CALCULATE PARTIAL DERIVATIVES
      DO 49 J=1,NT3
      DO 49 I=1,NT
   49 DBDB(I,J)=0.
      DO 50 IR=1,NR
      K=ITR(IR)
      L=ITP(IR)+K
      M=K+1
      IF (IR.EQ.1.AND.IK.EQ.1) GOTO 44
      GOTO 42
   44 DC(1)=1.0
      DC(2)=6.0
      DC(3)=12.0
      DC(4)=12.0
      GOTO 45
   42 DO 48 KO=1,4
   48 DC(KO)=1.0
   45 CONTINUE
      DO 50 J=1,NT3
      DO 51 I=1,K
      LL=KS(IR,I)
   51 DBDB(LL,J)=DBDB(LL,J)-(D(IR,J)*DC(I))
      DO 52 I=M,L
      LL=KS(IR,I)
   52 DBDB(LL,J)=DBDB(LL,J)+(D(IR,J)*DC(I))
   50 CONTINUE
      DO 72 K=1,N
      DO 71 J=1,NT
   71 DBDB(K,J)=DBDB(K,J)*R
      BD(K)=DBDB(K,NT1) *R
      DBDT(K)=DBDB(K,NT2) *R
      DBDR(K)=DBDB(K,NT3)
   72 CONTINUE
   99 FORMAT(6I5,3E12.6,3I3)
   98 FORMAT(5(I5,F17.6))
   97 FORMAT (10I5)
      RETURN
      END

      SUBROUTINE CHOLES(A,N,M,MATSYM)
      DIMENSION  A(N,M)
      IF(A(1,1).NE.0.0) GO TO 47
      DO 37 J=2,N
      IF(A(J,1).EQ.0.0) GO TO 37
      IFLIP=J
      GO TO 27
   37 CONTINUE
      GO TO 54321
   27 DO 57 K=1,M
      TEMP=A(IFLIP,K)
      A(IFLIP,K)=A(1,K)
      A(1,K)=TEMP
   57 CONTINUE
   47 DO 2 J=2,M
      A(1,J)=A(1,J)/A(1,1)
    2 CONTINUE
      DO 6 I=2,N
      DO 7 J=2,M
      IF(MATSYM.EQ.0)GO TO 49
      IF(I-J)69,68,67
   49 IF(J.GT.I)GO TO 69
   68 K=J-1
      SUM=0.0
      DO 3 IR=1,K
      SUM=SUM+A(I,IR)*A(IR,J)
    3 CONTINUE
      A(I,J)=A(I,J)-SUM
      GO TO 7
   69 K=I-1
      SUM=0.0
      DO 4 IR=1,K
      SUM=SUM+A(I,IR)*A(IR,J)
    4 CONTINUE
      IF(A(I,I).EQ.0.0) GO TO 54321
      A(I,J)=(A(I,J)-SUM)/A(I,I)
      GO TO 7
   67 A(I,J)=A(J,I)*A(J,J)
    7 CONTINUE
    6 CONTINUE
      DO 52 K=2,N
      I=N+1-K
      SUM=0.0
      LL=I+1
      DO 51 IR=LL,N
      SUM=SUM+A(I,IR)*A(IR,M)
   51 CONTINUE
      A(I,M)=A(I,M)-SUM
   52 CONTINUE
      GO TO 12345
54321 N=-1
12345 RETURN
      END

      SUBROUTINE RATES
      COMMON/RATE/ T,FR(40),BR(40),DFR(40),DBR(40)
      COMMON/RGAS/RR,R,IK
      COMMON /EQL/F(20),DF(20)
      COMMON /PRATE/A(40), E(40),TEX(40),KK(40,4),ITR(40),ITP(40),
     1IR(40)
      COMMON/SECOND/N,N1,NR,NT,IDUM(12),NT1
      COMMON/RRCON/ICR,NR2,NR3,NR4
      RT=1./T
      RTT= RT/T
      RRT=1./(RR*T)
      DRRT=-1./T
      F(NT1)=0.
      DF(NT1)=0.
    7 DO 100 IR=1,NR
      DBR(IR)=0.
       BR(IR)=0.
      DFR(IR)=0.
       FR(IR)=A (IR)
      IF (E(IR)) 1,2,1
    1 FR(IR)=FR(IR)*EXP(-E(IR)*RT)
      DFR(IR)=E(IR)*RTT
    2 IF (TEX(IR)) 3,4,3
    3 TEMP=T**TEX(IR)
      FR(IR)=FR(IR)*TEMP
      DFR(IR)=DFR(IR)+TEX(IR)/T
    4 IF (IR(IR)) 5,100,5
    5 K=KK(IR,1)
      L=KK(IR,2)
      J=KK(IR,3)
```

```
      I=KK(IR,4)
      EQ=F(I)+F(J)-F(K)-F(L)
      IF (EQ+70.) 100,9,9
    9 DEQ=DF(I)+DF(J)-DF(K)-DF(L)
      EQ=EXP(EQ)
      IF (IR(IR)) 11,100,10
   10 BR(IR)=FR(IR)*EQ
      DBR(IR)=DFR(IR)*DEQ
      IF  (ITP(IR)-ITR(IR)) 8,100,100
    8 BR(IR)=BR(IR)*RRT
      DBR(IR)=DBR(IR)+DRRT
      GO TO 100
   11 B=FR(IR)/(EQ*RRT)
      DB=DFR(IR)-DEQ-DRRT
      BR(IR)=FR(IR)
      DBR(IR)=DFR(IR)
      DFR(IR)=DB
      FR(IR)=B
  100 CONTINUE
   13 RETURN
      END

      SUBROUTINE EQUILB(W,P,T0,B0,EQR,T,B,WW,IEQ)
C     INITIAL GUESS = EQUILIBRIUM COMPOSITION  \ C12H24
      DIMENSION V(7),R(7),ST(7),AK(7),B0(15),B(15),W(15)
      DATA V /-11.84810,-12.85260,-14.13725,-10.68009,-12.11305,
     1-5.62023,-19.72111/, R /1.21520,1.09197,1.24664,0.97691,
     21.10236,0.39284,1.32315/, ST /-0.035275,-0.031336,-0.035112,
     3-0.027232,-0.030898,-0.011081,-0.029936/
      IF(IEQ.NE.1)GO TO 20
      XL1=(-0.0002676*T0)+0.97688
      XL2=(0.0002744*T0)+1.08108
      IF(XL2-EQR) 300,300,302
  302 IF(XL1-EQR) 304,304,306
  300 XM2=(0.24372*T0)-811.40762
      XC2=(0.31694*T0)+2843.37848
      T=(XM2*EQR)+XC2
      GO TO 20
  304 XC1=(0.39992*T0)+1683.944
      T=(247.8*EQR)+XC1
      GO TO 20
  306 XC0=(0.80176*T0)+209.032
      T=(1767.0*EQR)+XC0
   20 DO 36 J=1,7
      GT=(T-1500.0)/100.0
      AK(J)=V(J)+R(J)*GT+ST(J)*GT*GT
      AK(J)=EXP(AK(J))
   36 CONTINUE
      VOL2=B0(7)+B0(10)+12.0*B0(6)
      VOL3=B0(1)+B0(4)+24.0*B0(6)+2.0*(B0(5)+B0(11))
      VOL4=B0(3)+B0(4)+B0(5)+B0(7)+B0(8)+B0(9)+2.0*(B0(10)+B0(12))
      VOL5=B0(2)+B0(8)+2.0*(B0(9)+B0(13))
      LL=1.0
      IF(18.0*B0(6)+0.5*B0(11)+0.5*B0(7)-B0(12)) 200,202,202
  200 WZ=0.01
      AM=0.12
  206 IF(18.0*B0(6)+0.5*B0(11)+0.5*B0(7)-B0(12)) 207,103,103
  207 PH20=AM
      P02=W7
      PH2=PH20*AK(2)/SQRT(P02)
      GO TO 104
  202 WZ=0.002
      AM=0.07
  103 PH20=AM
      PH2=W7
      P02=(PH20*AK(2)/PH2)**2.0
  104 POH=PH20*AK(3)/SQRT(PH2)
      PH=AK(4)*SQRT(PH2)
      P0=AK(5)*SQRT(P02)
      E=2.0*(PH20+PH2)+POH+PH
   77 PC0=E*VOL2
      X=(1.0+SQRT(P02)/AK(1))*VOL3
      PC0=PC0/X
      PC02=PC0*SQRT(P02)/AK(1)
   68 QQ=VOL5*E/(2.0*VOL3)
   65 RR=SQRT(QQ)*(AK(7)+AK(6)*SQRT(P02))
      RR=RR+2.0*QQ-(E*VOL5/VOL3)
      DR=(0.5*(AK(7)+AK(6)*SQRT(P02))/SQRT(QQ))+2.0
      IF(ABS(RR/DR)-0.0001) 63,63,64
   64 QQ=QQ-RR/DR
      GO TO 65
   63 PN2=QQ
      PNO=AK(6)*SQRT(P02*PN2)
      PN=AK(7)*SQRT(PN2)
   67 AL=PC0+PC02+PH+PH2+P0+P02+PH20+POH+PN+PN2+PNO
      BE=(2.0*P02+P0+PH20+POH+PNO+PC0+2.0*PC02)/E
      BE=BE*VOL3/VOL4
      IF(LL-1) 81,81,41
   81 IF(ABS(AL-1.0)-0.0001) 62,41,41
   62 IF(ABS(BE-1.0)-0.0001) 18,41,41
   41 IF(LL-2) 46,45,50
   46 W1=WZ
      AM1=AM
      AL1=AL
      BE1=BE
      WZ=WZ*0.9
      GO TO 50
   45 W2=WZ
      AM2=AM
      AL2=AL
      BE2=BE
      AM=AM*1.1
   50 LL=LL+1
      IF(LL-4) 206,51,51
   51 WA=(W1-W2+W2*AL1-W1*AL2)/(AL1-AL2)
      AMC=(AM-AM2+AM2*BE-AM*BE2)/(BE-BE2)
      WB=(W1-WZ+WZ*AL1-W1*AL)/(AL1-AL)
      AMB=((WB-W2)*(AM1-AM)/(W1-W2))+AM
      AMD=(AM1-AM+AM*BE1-AM1*BE)/(BE1-BE)
      WD=((AMD-AM)*(W1-W2)/(AM1-AM))+W2
      G1=(WD-W2)/(AMD-AMC)
      G2=(WB-WA)/(AMB-AM1)
      C1=(AMD*W2-WD*AMC)/(AMD-AMC)
      C2=(AMB*WA-WB*AM1)/(AMB-AM1)
      AM=(C2-C1)/(G1-G2)
      WZ=(G1*C2-G2*C1)/(G1-G2)
      LL=1.0
      IF(AM) 26,26,27
   26 AM=0.005
   27 IF(WZ) 28,28,206
   28 WZ=0.001
      GO TO 206
   18 B(1)=PH
      B(2)=PN
      B(3)=P0
      B(4)=POH
      B(5)=PH20
      B(6)=0.0
```

```
      B(7)=PCO
      B(8)=PNO
      B(9)=0.0
      B(10)=PCO2
      B(11)=PH2
      B(12)=PO2
      B(13)=PN2
      WW=0.0
      DO 320 J=1,13
      WW=WW+B(J)*W(J)
  320 CONTINUE
      DO 330 J=1,13
      B(J)=B(J)/WW
  330 CONTINUE
      B(9)=B(8)/20.0
      B(6)=B(12)/20.0
      IFQ=1
      RETURN
      END

      SUBROUTINE PFR
      LOGICAL PLUG,PLUG1,PLUG2
      COMMON/UNITS/UNIT(30,10)
      COMMON/FLOWS/FLOW(25,20)
      COMMON/PARAMS/LIST(10),JJ,LOOP,NIN,NOUT,NCALC,NFLOW,NCOMP,NU,
     *KPRINT(4),MLOOP,NF(10),IDCP(16),NL,INFLOW(20),NRUNS
      COMMON/PRINT/TAU(10),V(20),BB(20,10),X(20),X0(20)
      COMMON /SECOND/N,N1,NR,NT,IT,N2,KOUNT(10),NT1
      COMMON /PLPARS/PLV(8),PLUG,PLUG1,PLUG2,B0(20),B(20)
      UNIT(30,NU)=UNIT(30,NU)/10
      PLUG=.TRUE.
      PLUG1=PLUG2=.FALSE.
      TR=K1=0
      PLV(1)=1
      PLUG1=.TRUE.
      CALL WSR
      PLUG1=.FALSE.
      TR=TR+PLV(5)
      K1=K1+PLV(4)
      PLV(2)=PLV(3)=PLV(6)*FLOW(6,NF(2))
      DO 1 I=1,NCOMP
    1 X0(I)=X(I)
      PLV(1)=2
      PLUG2=.TRUE.
      CALL WSR1
      PLUG2=.FALSE.
      TR=TR+PLV(5)
      K1=K1+PLV(4)
      DO 100 I=1,8
      PLV(1)=I+2
      PLV(2)=FLOW(6,NF(2))*2-PLV(3)
      PLV(3)=FLOW(6,NF(2))
      DO 2 J=1,NCOMP
      B(J)=B(J)*2-B0(J)
    2 X0(J)=X(J)
      CALL WSR1
      TR=TR+PLV(5)
      K1=K1+PLV(4)
  100 CONTINUE
      TAU(NU)=TR
      KOUNT(NU)=K1
      PLUG=.FALSE.
      UNIT(30,NU)=UNIT(30,NU)*10
      RETURN
      END

      SUBROUTINE PJET
C
C     PRESSURE JET ATOMISER ROUTINE
C
      DIMENSION X(20),A(20)
      COMMON /UNITS/UNIT(30,10)
      COMMON /FLOWS/FLOW(25,20)
      COMMON /VAR1/PFUEL,DDM,VSA,R(20),DEN1,AV1,MWSR,MSPM
      COMMON /BERR/XB,D6,QJ
C     EVALUATE ATOMISER FUEL MASS FLOWRATE LB/HR,GM/SEC
      PFUEL=UNIT(15,2)
      DD=(0.8475*SQRT(PFUEL))*(0.02738*PFUEL)+1.71
      DDM=DD*453.59/3600.0
C     INITIALISE STREAM 4
      DO 20 J=2,25
      FLOW(J,4)=0.0
   20 CONTINUE
      FLOW(6,4)=300.0
      FLOW(7,4)=FLOW(7,2)
      FLOW(25,4)=DDM
C     EVALUATE ATOMISER SPRAY INITIAL MEAN VELOCITY,M/SEC
      VU=0.05638+(0.000123*PFUEL)+(0.011739*SQRT(PFUEL))
      VS=4.1787*VU*SQRT(PFUEL)
      VSA=0.981*VS
C     ROSIN RAMMLER EVALUATION CORRELATIONS
      D1=DD/(7.914*SQRT(PFUEL))
      DB= 2.7000+(0.2162*D1)
      D2= EXP(2.3026*DB)
      D3= 0.3358-(0.02427*D1)
      XB= D2/(PFUEL**D3)
      D4= 0.3712-(0.02589*D1)
      SMD=413.4/(PFUEL**D4)
C     CORRECT XB,SMD (= TO LASER MIMENTS)
      XB=XB*(0.81189+0.0011*PFUEL)
      SMD=SMD*(0.81189+0.0011*PFUEL)
      D5=XB/SMD
C     POLYNOMIAL GAMMA FUNCTION APPROXIMATION
      M=1
      A1=0.5748646
      A2=0.9512363
      A3=0.6998588
      A4=0.4245549
      A5=0.1010678
      D6=2.721
   80 D7=1.0-(1.0/D6)
      GAM=1.0-A1*D7+A2*(D7**2.0)-A3*(D7**3.0)+A4*(D7**4.0)-A5*(D7**5.0)
      D8=GAM/D7
      IF((D5-D8).LE.0.0001) GO TO 100
      D6=D6-0.001
      IF(M-500)70,1000,1000
   70 M=M+1
      GO TO 80
  100 CONTINUE
      DO 120 K=1,20
      X(K)=12.0*FLOAT(K)
      A(K)=(X(K)/XB)**D6
      R(K)=100.0/EXP(A(K))
  120 CONTINUE
 1000 RETURN
      END
```

```
      SUBROUTINE COAN
C
C     COANDA INTERNAL RECIRCULATION UNIT ROUTINE
C
      COMMON /UNITS/UNIT(30,10)
      COMMON/FLOWS/FLOW(25,20)
      COMMON /VAP1/PFUEL,DDM,VSA,R(20),DEN1,AV1,MWSR,MSPM
      COMMON /REAP/XB,D6,QJ
      COMMON/PARAMS/LIST(10),JJ,LOOP,NIN,NOUT,NCALC,NFLOW,NCOMP,NU,
     1KPRINT(4),MLOOP,NF(10),IDCP(16),NL,INFLOW(20),NRUNS,NCYCLE,KK
      DATA PC,SW,D1,DS,D2,PI/730.0,0.0,0.0254,3.02,3.7,2.94,3.142/
C     SKEWNESS AND EFFICIENCY FACTORS
      Y1=1.045
      Y2=1.153
      EF=0.39
C     INITIALISE STREAM 3
C
C     TAIR=ESTIMATED COANDA SLIT AIR TEMPERATURE  ( FLOW(6,1)   )
C     TROT=MEASURED ROTAMETER AIR TEMPERATURE     ( UNIT(17,1)  )
      QJ=UNIT(15,1)
      PCC=UNIT(16,1)
      TAIR=FLOW(6,3)=FLOW(6,1)
      TROT=UNIT(17,1)
      RJ=0.465*(PC+25.4*PCC)/TROT
      RJ1=RJ*TROT/TAIR
      QJ=QJ*SQRT(1.227/RJ)
      QJ1=FLOW(8,3)=QJ*RJ/1740.0
      FLOW(7,3)=FLOW(7,1)
      FLOW(22,3)=0.21*QJ1
      FLOW(23,3)=0.79*QJ1
      MWSR=UNIT(30,1)
      MSPM=UNIT(29,1)
      GO TO 1000
      ENTRY COAN1
C     COMPUTE MEAN GAS VEL.,RECIRCULATION RATIO
      IF(NCYCLE.EQ.1.AND.LOOP.EQ.1)GO TO 70
      IF(NCYCLE.EQ.0.AND.LOOP.EQ.999)GO TO 70
      R1=UNIT(21,NU)*UNIT(15,NU)*1000.0/UNIT(29,6)
      GO TO 80
   70 R1=341.0/UNIT(29,6)
   80 MM=1
      Z=(R1/RJ1)*(D2**2.0)/(2.0*DS*SW)
      FI1=SQRT(Z/((2.0*Y2)-Y1))
   30 Z1=((RJ1/R1)-1.0)*(1.0/FI1)+1.0
      Z2=(1.0-(1.0/FI1))**2.0
      FI=SQRT(Z/((2.0*Y2/Z1)-(Y1*Z2)))
      IF(ABS(FI-FI1).LE.0.0001)GO TO 20
      FI1=FI
      IF(MM-200)40,1000,1000
   40 MM=MM+1
      GO TO 30
   20 FI=FI*EF
      W1=(FI-1.0)*RJ*QJ*(1.0E-04)/6.0
      D1M=D1*1.0E-02
      AV1=4.0*W1/(R1*PI*(D1M**2.0))
      RCN=UNIT(15,MSPM)=1.0-(1.0/FI)
      UNIT(16,MSPM)=1.0-RCN
 1000 RETURN
      END
      SUBROUTINE EVAP(JENT,T,TTAU,DEN,B0,W0)
C
C     EVAPORATION AND MIXING ROUTINE
C
C     JENT=ENTRY CONTROL PARAMETER
C     NSR=NO OF PREVIOUS CONVERGED REACTOR
C     NSRN=NUMBER OF CONVERGED REACTORS ALREADY PASSED THROUGH
C     FOR THE CURRENT LOOP
C     LOOPY=INITIALISATION CONTROL PARAMETER
C     NCYCY=NETWORK CONTROL PARAMETER
C     MWSR=NUMBER OF REACTORS IN RECYCLE PATH
C     MSPM=THE UNIT NUMBER OF THE RECYCLE SPLITTER
C
      LOGICAL PLUG,PLUG1,PLUG2
      REAL M1,M2
      DIMENSION B0(20),RCS(16),D(21),EM(21),RF(21),VR(21),V(21),S(21),
     1EMF(21),TB(21),S1(21),Z(21),CD(21),CD1(21),AA(21),DV(21),DM(21),
     2EMD(21),EMN(21),DN(21)
      DIMENSION PUR(5,21),SR(5,21),DR(5,21),VRR(5,21),RFR(5,21),
     1EMR(5,21)
      COMMON /VAP1/PFUEL,DDM,VSA,R(20),DEN1,AV1,MWSR,MSPM
      COMMON /VAP2/PHYF,UFF,UNF,UOF,UF,UN,UO,RFF,RNF,ROF,RCSF(16),TSD,
     1VOLUM,M1,ETA1,M2,ETA2,PHY,FED,PUO,W(20)
      COMMON /VAP3/PO(20)
      COMMON/PARAMS/LIST(10),JJ,LOOP,NIN,NOUT,NCALC,NFLOW,NCOMP,NU,
     1KPRINT(4),MLOOP,NF(10),IDCP(16),NL,INFLOW(20),NRUNS,NCYCLE,KK
      COMMON /PRINT/TAU(10)
      COMMON/UNITS/UNIT(30,10)
      COMMON /PLPARS/PLV(8),PLUG,PLUG1,PLUG2
      DATA IPROP,NCYCY,LOOPY/3*0/
C     HAS ALL FUEL EVAPORATED ?
      IF(ETA1-0.0)5,10,20
   20 IF(ABS(ETA1/DDM)-0.0001)10,10,30
    5 ETA1=0.0
   10 FED=W.0
      UNIT(29,NU)=1001
      GO TO 804
   30 IF(NCYCLE-1)50,40,50
   40 IF(LOOP.EQ.1)LOOPY=1
      IF(LOOP-LOOPY)50,50,45
   45 LOOPY=LOOP
      JENT=0
   50 IF(JENT.EQ.0)GO TO 400
      IF(JENT-2)500,600,500
C     JENT=0: K=0 FOR 1ST NSR
  400 IFLAPS=0.0
      NSR=NU
      NSRN=0
      JENT=1
      IF(NCYCLE.EQ.1.AND.LOOP.EQ.1)NCYCY=1
      TINC=1.0E-04
      FL=3.0E+02
C     IPROP=0 FOR REGION B PROPS.
      AMW=W(13)
      AMU=1.141
      TCRIT=126.2
C     JENT=1 OR 3;K>0 FOR 1ST OR SUBSEQUENT NSR
  500 VI=(2.08*(3.97*(T-273.0)/1600.0))*(1.0E-05)
      PH=T-493.0
      PHM=(T+493.0)*0.5
      IF(PHM-1000.0)520,540,540
  520 NN=0
```

```
      GO TO 550
  540 NN=5
  550 CPK=0.0
      IF(IPROP.EQ.0)NN=NN+10
      DO 560 N=1,4
      CPK=CPK+(PO(NN+N+1)*PHM**(N))
  560 CONTINUE
      CPK=(CPK+PO(NN+1))*1.98726
      ED=CPK*4.187/AMW
      TK=(CPK/AMU)*(((14.52*PHM/TCRIT)-5.14)**(2.0/3.0))*4.187E-07
      REV=ED*PR/FL
      EN=6.283*TK*ALOG(1.0+REV)/ED
      IF(JENT.GE.2)GO TO 700
      DEN1=DEN
      IF(NCYCLE.EQ.1.AND.LOOP.GT.15)GO TO 565
      CALL COAN1
  565 VRELI=ABS(AV1-VSA)
      DO 500 J=1,21
      D(J)=((12.0*FLOAT(J))-6.0)*(1.0E-06)
      EM(J)=EN*D(J)
      RE(J)=VRELI*D(J)*DEN*1000.0/VI
      VR(J)=VRELI
      V(J)=0.524*D(J)**3.0
      S(J)=0.0
  500 CONTINUE
      FE=0.0
      TTIME=0.0
      TT=0.0
      PU0=100.0
      GO TO 1000
C     JENT=2 IK=0 FOR SUBSEQUENT NSR
  600 TELAPS=TELAPS+TAU(NSR)
      NSRN=NSRN+1
      JENT=3
      PUR(NSRN)=PU
      DO 608 J=1,21
      SR(NSRN,J)=S(J)
      DR(NSRN,J)=D(J)
      VRR(NSRN,J)=VR(J)
      RER(NSRN,J)=RE(J)
      EMR(NSRN,J)=EM(J)
  608 CONTINUE
      GO TO 500
  700 CONTINUE
C     SET PARAMETERS TO PREVIOUS NSR EXIT VALUES
      FE=0.0
      TT=0.0
      TTIME=TELAPS
      IF(NCYCLE.EQ.0.AND.NCYCY.EQ.1)GO TO 720
      NNN=NSRN
      GO TO 750
  720 NCYCY=0
      NNN=NSRN-MWSR
      IF(MWSR.EQ.0)GO TO 750
      DO 730 I=1,MWSR
  730 TTIME=TTIME-TAU(NSR-I-1)
  750 PU0=PUR(NNN)
      DO 758 J=1,21
      D(J)=DR(NNN,J)
      VR(J)=VRR(NNN,J)
      RE(J)=RER(NNN,J)
      EM(J)=EMR(NNN,J)
      S(J)=SR(NNN,J)
  758 CONTINUE
      NSR=NU
C     EVAPORATION CALCULATION
 1000 IF(NU.GT.MSPM.AND.NCYCY.EQ.1)GO TO 101
      GO TO 102
  101 DDMX=DDM*UNIT(15,MSPM)
      GO TO 1005
  102 IF(NU.GT.MSPM.AND.NCYCY.EQ.0)GO TO 103
      DDMX=DDM
      GO TO 1005
  103 DDMX=DDM*UNIT(16,MSPM)
 1005 TT=TT+TINC
      TTIME=TTIME+TINC
      DO 55 J=1,21
      EMF(J)=EM(J)*(1.0+0.242*SQRT(RE(J)))
      TR(J)=(414.0*D(J)**3.0)/EMF(J)
      IF(TR(J)-TTIME)52,52,53
   52 S1(J)=0.0
      GO TO 54
   53 S1(J)=EMF(J)*TINC/790.0
      S(J)=S(J)+S1(J)
      GO TO 55
   54 S(J)=V(J)
   55 CONTINUE
      Z(1)=S(1)*(100.0-R(1))/V(1)
      DO 110 J1=2,20
  110 Z(J1)=S(J1)*(R(J1-1)-R(J1))/V(J1)
      Z(21)=S(21)*(R(20))/V(21)
      VB=0.0
      DO 125 J2=1,21
  125 VB=VB+Z(J2)
      PU=100.0-VB
      FE=FE+((200.0-PU-PU0)*TINC*DDMX/200.0)
      PU0=PU
      IF(TT.GE.TTAU)GO TO 2000
      DO 200 J=1,21
      CD(J)=RE(J)**(1.0/1.1764706)
      CD1(J)=(28.0/CD(J))+0.48
      AA(J)=(0.949*DEN*CD1(J)*(VR(J)**2.0))/D(J)
      DV(J)=AA(J)*TINC
      DM(J)=EMF(J)*TINC
      EMD(J)=414.0*(D(J)**3.0)
      IF(EMD(J)-DM(J))160,160,170
  160 D(J)=0.000001
      GO TO 200
  170 EMN(J)=EMD(J)-DM(J)
      DN(J)=(EMN(J)/414.0)**(1.0/3.0)
      D(J)=DN(J)
      IF(VR(J)-DV(J))180,180,190
  180 VR(J)=0.000001
      GO TO 195
  190 VR(J)=VR(J)-DV(J)
  195 RE(J)=VR(J)*D(J)*DEN*1000.0/VI
      EM(J)=EN*D(J)
```

```
  200 CONTINUE
      GO TO 1005
C     COMPUTE INTERMEDIATE CONCENTRATIONS (NIC 251)
 2000 FED=FF/TTAU
      IF(FED-(0.99*ETA1))804,132,132
  132 FED=0.99*ETA1
      WRITE(3,135)
  135 FORMAT(1H ,'   EVAP ***')
  804 M2=M1*FED
      ETA2=ETA1-FED
      IF(LOOPY.LE.1)WRITE(3,77)NCYCLE,LOOP,T,TTAU
   77 FORMAT(1H ,'  -EVAP-  NCYCLE=',I5,'LOOP=',I5,'TEMP=',F10.3,E11.3)
      BETA=FED/M2
      TTAU=VOLUM/((M2/DEN)*(ETA2/0.791))
      BM=PHYF*(1.0-BETA)
      PHY=(BM+BETA)/(1.0+TSD)
      UF=((BM*UFF)+BETA)/(BM*BETA)
      UN=BM*UNF/(BM*BETA)
      UD=1.0-UF-UN
      RRR=(1.0-BETA)*(1.0-PHYF)
      RRN=RRR*(1.0+TSD)
      RRS=TSD*BM
      RF=(RRN*RFF)+(RRS*UFF)*(TSD*BETA)
      RF=RF/(RRR+TSD)
      RO=((RRN*ROF)+(RRS*UOF))/(RRR+TSD)
      RN=((RRN*RNF)+(RRS*UNF))/(RRR+TSD)
      DO 800 I=1,NCOMP
      IF(I.EQ.6)GO TO 800
      IF(I.GE.12)GO TO 800
      RCS(I)=RRN*RCSF(I)/(RRR+TSD)
      RO(I)=RCS(I)*(1.0-PHY)/W(I)
  800 CONTINUE
      RO(6)=RF*(1.0-PHY)/W(6)
      RO(12)=RO*(1.0-PHY)/W(12)
      RO(13)=RN*(1.0-PHY)/W(13)
      RO(14)=UD*PHY/W(14)
      RO(15)=UN*PHY/W(15)
      RO(16)=UF*PHY/W(16)
      WO=0.0
      DO 802 I=1,NCOMP
  802 WO=WO+RO(I)
      WO=1.0/WO
      RETURN
      END
```

****

PLATE 1. FRONT VIEW OF BURNER RIG.

PLATE 2. SIDE VIEW OF BURNER RIG.

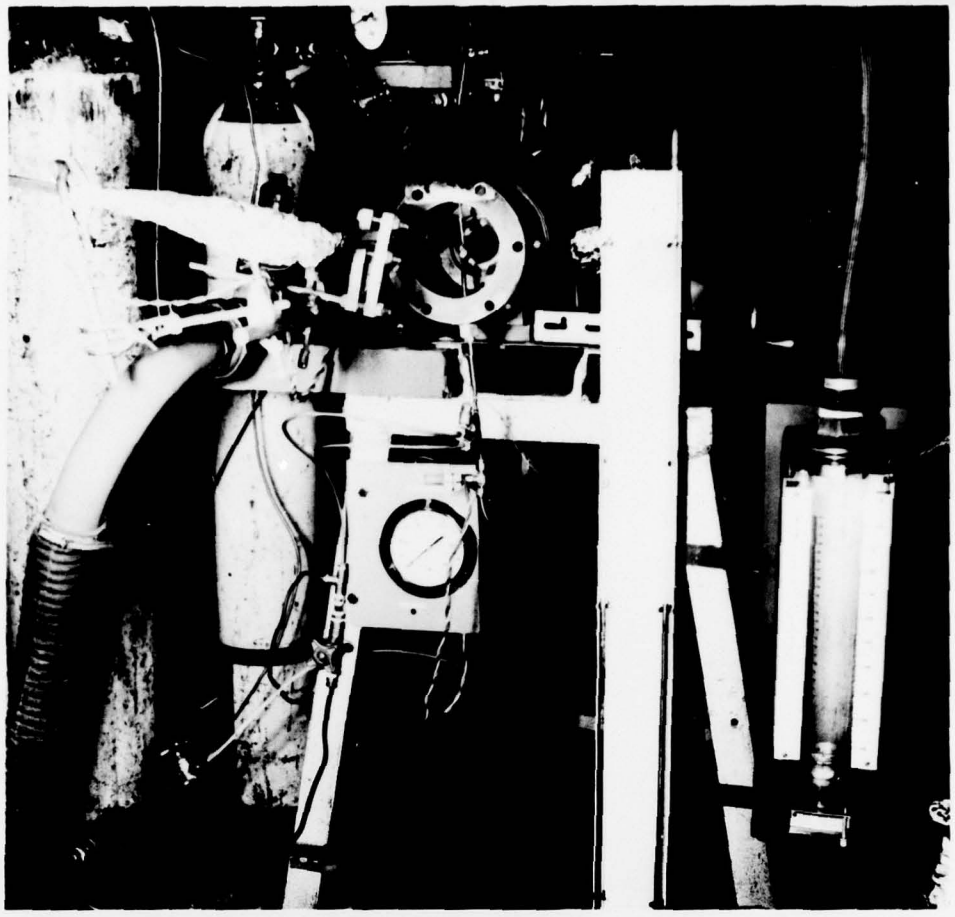

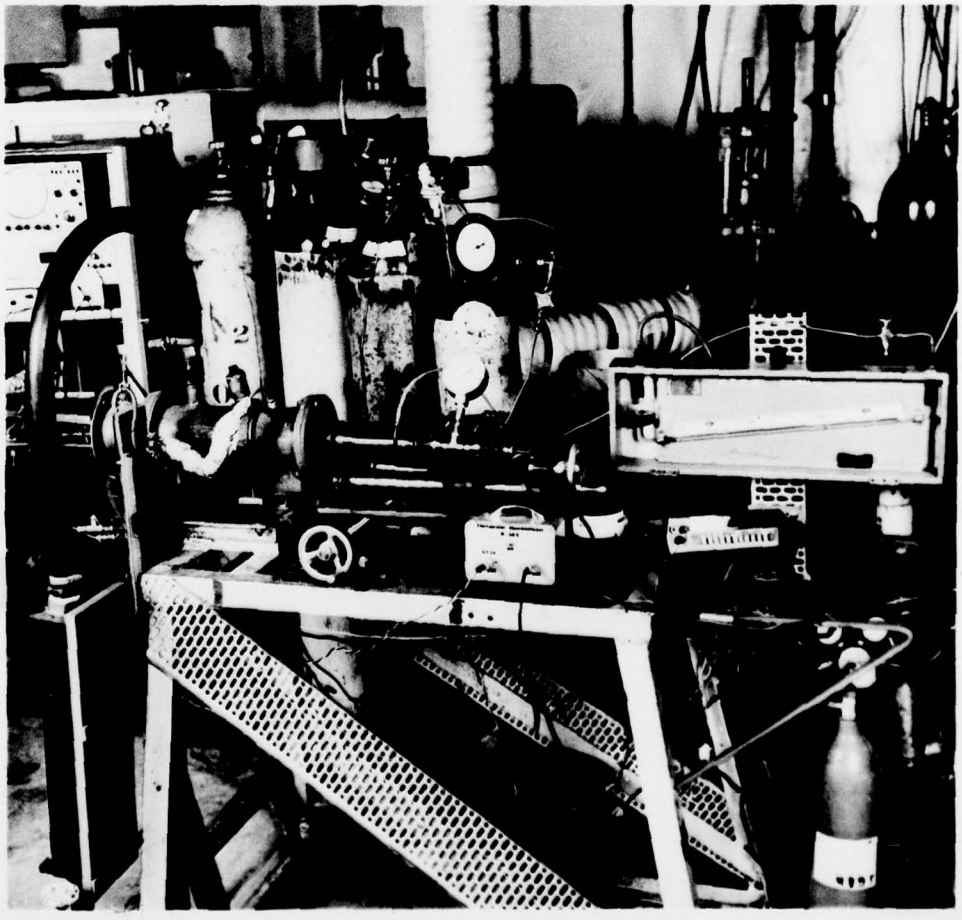

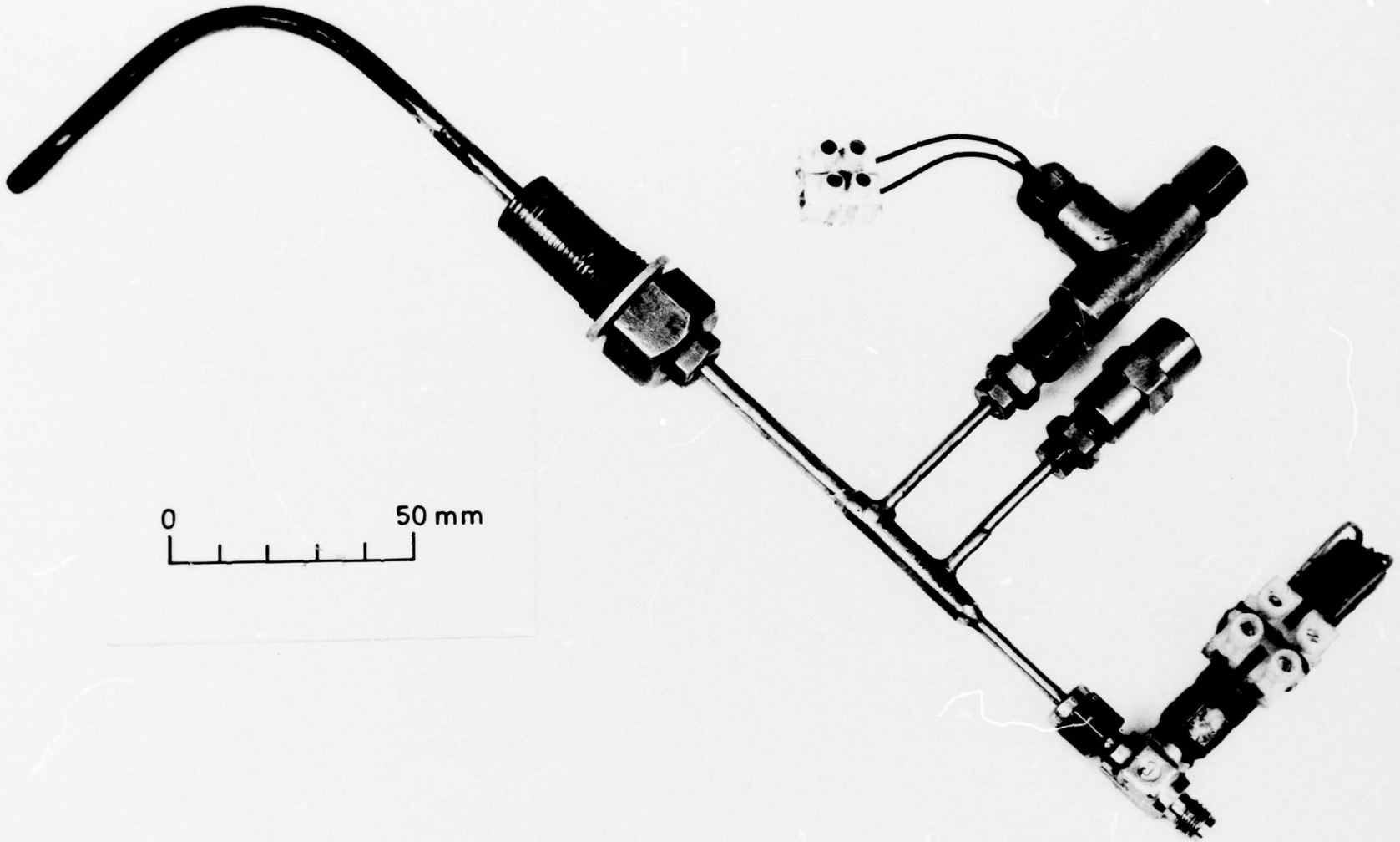
0
50 mm

PLATE 4. GAS ANALYSERS.

CO_2,CO IRGAs on the left,

NO/NO_x CLA to the right.

PLATE 5. BLUE FLAME BURNER COMBUSTION CHAMBER AND COANDA UNIT.

Components removed after tests completed.

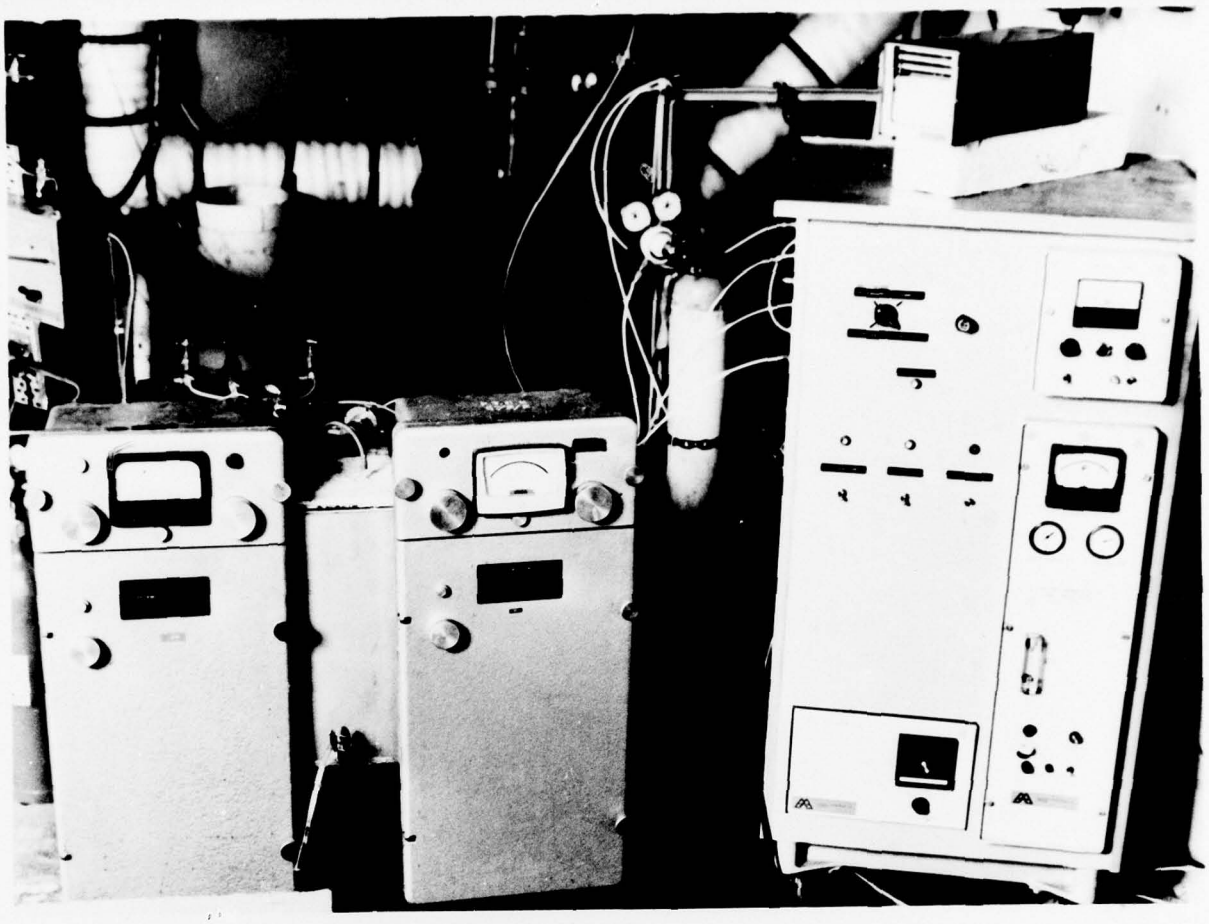

REFERENCES

1) Hinze, J.O., "Turbulence. An Introduction to its Mechanism and Theory", McGraw Hill.

2) Poll, I., "Chemical Reactor Modelling applied to Gas Turbine Combustors", A.R.C. Report No. 35 883, 1975. (Very many other useful references presented.)

3) Eisenklam, P., "Atomisation of Liquid Fuel for Combustion", Journal of Inst.Fuel, 243, 130, 1961.

4) Mugele, R.A., and Evans, H.D., "Droplet Size Distribution in Sprays", Ind.Eng.Chem., 43, 1317, 1951.

5) Rosin, P., and Rammler, E., Journal of Inst.Fuel, 7, 1933.

6) Bowen, I.G., and Joyce, J.R., Shell Tech.Report No. ICT/17, 1948.

7) Watkins, S., and Opdyke, S., AVCO Lycoming Report No.D12-b-085-74,1974.

8) Macfarlane, J., "Liquid Fuel Atomisers for use in Gas Turbine Combustion Model Experiments", Cranfield Symposium No.11 - Pergamon Press, 327, 1971.

9) Felton, P., and Swithenbank, J., "The Effect of Fuel Preparation on Gas Turbine Combustor Performance", HIC 232 (see footnote), 1975.

10) Hunter, S.C. et al, "Advanced, small, High Temperature-Rise Combustor program, Vol.1, Analytical Model Derivation and Combustor Element Rig Tests (Phases I and II)", Air Research Manufacturing Co. of Arizona, USA, Report No. AD-778-766.

11) Prakash, S., and Sirignano, W.A., "Preliminary Analysis of a Fuel Droplet in a Convective Field", Joint Meeting of Central and Western States Sections of the Combustion Institute, Texas, USA, 1975.

12) Mellor, R., Ph.D. Thesis, Sheffield University, 1969.

13) Sjögren, A., "Soot Formation by Combustion of an Atomised Liquid Fuel", 14th Combustion (Int.) Symposium, 919, 1973.

14) Gaydon,A.G.,and Wolfhard,H.G., "Flames, their Structure, Radiation and Temperature, 2nd Edition, Chapman & Hall, 1960.

15) Poll, I., Private Communication, 1975.

16) Ohta,Y. et al, "Vapourisation and Combustion of Single Liquid Fuel Droplets in a Turbulent Environment", JSME, 18/115, 1975.

17) Emmons, H.W., "Fluid Mechanics and Combustion", Plenary Lecture, 13th Combustion (Int.) Symposium, 1971.

18) Probert, R.P., Phil.Mag., 34, 94, 1946.

19) Goldsmith, M., Jet Propulsion, 26, 172, 1956.

NB. HIC ≡ University of Sheffield, Department of Chemical Engineering and Fuel Technology, High Intensity Combustion Report.

20) Williams, A., "Combustion of Droplets of Liquid Fuels: A Review", Comb. and Flame, 21, 1, 1973 (Very many other useful references presented).

21) Godsave, G.A.E., "Studies of the Combustion of Drops of a Fuel Spray - the Burning of Single Drops of Fuel", 4th Combustion (Int.) Symposium, 818, 1953.

22) Faeth, G.M., and Lazar, R.S., "Bipropellant Droplet Burning Rates and Lifetimes in a Combustion Gas Environment", NASA Report No. CR-72622, 1969.

23) Spalding, D.B., 4th Combustion (Int.) Symposium, 847, 1953.

24) Goldsmith, N., and Penner, S.S., Jet Propulsion, 24, 245, 1954.

25) Kassoy, D.R., and Williams, F.A., AIAA Journal, 6, 1961, 1968.

26) Vincent, M.W., "Fuel Spray Evaporation in Gas Turbine Combustors", Ph.D. Thesis, Sheffield University, 1973.

27) Brzustowski, T.A., "Chemical and Physical Limits on Vapour Phase Diffusion Flames of Droplets", Can.Journal of Chemical Engineering,1965.

28) Agafanova, F.A., et al, Soviet Phys.Tech.Phys., 2, 1689, 1958.

29) Kotake, S., and Okazaki, T., Int.Journal Heat and Mass Transfer, 12, 595, 1969.

30) Beer, J.M., and Chigier, N.A., "Combustion Aerodynamics", Applied Science Publishers Ltd., 1973.

31) Frössling, N., "The Evaporation of Falling Drops", Gerlands Beitrage Zur Geophysik, 52, 170, 1938.

32) Eisenklam, P., and Arunachalam, S.A., Comb. and Flame, 10, 171, 1966.

33) Rosenhead, L., "Laminar Boundary Layers", (ed.) .

34) Zahm, A.F., NACA Technical Report No. 253, 520, 1926.

35) Swithenbank, J., "The Unknown Fluid Mechanics of Combustion", HIC 220.

36) Nuruzzaman, A.S.M., et al, "The use of a Simplified Model for Prediction of Burnout of Non-Uniform Sprays", Chem.Eng.Sci., 26, 1635, 1971.

37) Mellor, A.M., Comb.Sci.Tech., 8, 101, 1973.

38) Swithenbank, J., "Combustion Fundamentals", HIC 150 (Also available as: AD.710321 - U.S.Def.Doc.Center; and as USAFOSR 70/2110TR).

39) Gosman, A.D., Spalding, D.B., et al, "Heat and Mass Transfer in Recirculating Flows", Academic Press, 1969.

40. Harsha, P.T., "A General Analysis of Free Turbulent Mixing", AFOSR Report No. AEDC-TR-73-177, 1974.

41) Heywood, J.B., AIAA Paper 71-712, 1971.

42) Couldin, F.C., Comb.Sci.Tech., 7, 33, 1973.

43) Katz, S., Chem.Eng.Sci., 9, 250, 1958.

44) Rosenweig, R.E., Can.Journal of Chemical Engineering, 44, 255, 1966.

45) Swithenbank, J., et al, "Combustor Design Fundamentals", 14th Combustion (Int.) Symposium (HIC 180), 1973.

46) Vulis, L.A., "Thermal Regimes of Combustion", McGraw Hill, 1963.

47) Golden, D.M., "Estimation of Rate Constants of Elementary Processes. A Review of the State of the Art," 14th Combustion (Int.) Symposium, 121, 1973.

48) Baulch, D.L., et al, "Critical Evaluation of Rate Data for Homogeneous, Gas-Phase Reactions of Interest in High Temperature Systems", Department of Physical Chemistry Reports 1-4, University of Leeds, 1968-69.

49) Green, E.H., and Toennies, G.P., "Chemical Reaction in Shock Waves", Arnold, London, 314, 1969.

50) Williams, G.C., et al, "The Combustion of Methane in a Jet-Mixed Reactor", 12th Combustion (Int.) Symposium, 913, 1969.

51) Edelman, R., and Fortune, O., "A Quasi-global Chemical Kinetic Model for the Finite Rate Combustion of Hydrocarbon Fuels", AIAA Paper 69-86, 1969.

52) Odgers,J., and Kretschmer, D., "Modelling of Gas Turbine Combustors - A Convenient Reaction Rate Equation", Journal Eng. for Power, 173,1972.

53) Zeldovich, Y.B., et al, "Oxidation of Nitrogen in Combustion", Academy of Sciences of USSR, Inst.Chem.Phys., 1947.

54) Fenimore, C.P., "Formation of Nitric Oxide in Premixed Hydrocarbon Flames", 13th Combustion (Int.) Symposium, 373, 1971.

55) Pratt, D.T., and Malte, P.C., "The Role of Energy-Releasing Kinetics in NO_x Formation: Fuel Lean, Jet Stirred CO-Air Combustion", Comb.Sci. Tech.

56) Levy, A., and Merryman, E.L., Comb. and Flame, 9, 229, 1965.

57) Edelman, E., and Economos, C., "A Mathematical Model for Jet Engine Combustor Pollutant Emissions", AIAA Paper 71-714, 7th Propulsion Joint Specialist Conference, U.S.A.

58) Baker, R.J., et al, "Detailed Measurements of Flow in the Recirculation Region of an Industrial Burner by Laser Anemometry", Combustion (European) Symposium, Sheffield, 583, 1973.

59) Swithenbank, J., "Measurement in Combustion Processes", HIC 230, 1975.

60) Swithenbank, J., "Analogue and Digital Storage and Display Systems", HIC 231, 1975.

61) Prior, D.S., and Swithenbank, J., HIC 247 (Company Confidential), 1975.

62) Bugler, J., "Polluting Britain", Pelican ISBN 0 14.

63) Royal Commission on Environmental Pollution: 1st Report, Cmnd 4585, 1971.

64) Elkins, H.B., "The Chemistry of Industrial Toxicology", Wiley, 1959.

65) "Nationwide Air Pollutant Emissions Trends 1940-70", U.S.A. E.P.A. Report No. 115, 1973.

66) Sawyer, R.F., "Atmospheric Pollution by Aircraft Engines and Fuels. A Survey", AGARD Report No. AR-40, 1973.

67) Bartok, W. et al, "Systems Study of Nitrogen Oxide Control Methods for Stationary Sources - Volume II", Esso Research and Engineering Co. Report No. PB 192 789, 1969.

68) Solymosi, F., and Kiss, J., "Removal of NO_x Pollutant by Catalytic Combustion Reactions", 15th Combustion (Int.) Symposium, 1233, 1974.

69) Air Pollution Control Office, U.S.A. E.P.A. Report (Contract CPA 22-69-147), "The Federal R. and D. Plan for Air Pollution Control by Combustion Process Modification", 1971.

70) Lawton, J., and Weinberg, F., "Electrical Aspects of Combustion", Clarendon (Oxford) Press, 1969.

71) Pagni, P.J., et al, "Smoke Suppressant Additive Effects on Particulate Emissions from Gas Turbine Combustors", AGARD Conf.Proc.No. 125 on Atmospheric Pollution by Aircraft Engines, Section 28, 1973.

72) Pompeii, F., and Heywood, J.B. "The Role of Mixing in Burner generated Carbon Monoxide", Comb.Sci.Tech.

73) Pratt, D.T., and Malte, P.C., "Measurement of Atomic Oxygen and Nitrogen Oxides in Jet-stirred Combustion", 15th Combustion (Int.) Symposium, 1974.

74) Pratt, D.T. and Crowe, C.T., "Effects of Turbulent Mixing and Chemical Kinetics on Nitric Oxide Production in a Jet-stirred Reactor", 14th Combustion (Int.) Symposium, 1972.

75) Eberius, K.H., and Just, Th., "NO Formation in Fuel Rich Flames: A Study of the Influence of the Hydrocarbon Structure," 41st Meeting of the AGARD Propulsion Energetics Panel, London, 1973.

76) Myerson, A.L., "The Reduction of Nitric Oxide in Simulated Combustion Effluents by Hydrocarbon-Oxygen Mixtures", Corp.Research Labs.Report, Esso Research and Engineering Co., Linden, N.J., U.S.A.

77) Bracco, F.V., 14th Combustion (Int.) Symposium, 1973.

78) Tuttle, J.H., et al, "Emissions from and within an Allison J-33 Combustor II: The Effect of Inlet Air Temperature", Comb.Sci.Tech., 7, 125, 1973.

79) Hedley, A.B., "Factors affecting the Formation of Sulphur Trioxide in Flame Gases", Journal of Inst.Fuel, 1967.

80) Banchero, J.T., and Verhoff, F.H., "Evaluation and Interpretation of the Vapour Pressure Data for Sulphuric Acid Aqueous Solutions with application to Flue Gas Dewpoints", Journal of Inst.Fuel, 1975.

81) Chinitz, W., and Baurer, T., "An Analysis of Non-Equilibrium Hydrocarbon-Air Combustion", Paper 65-19, Fall Meeting Western States Section, U.S.A., 1965.

82) Lefebvre, A.H., "Pollution Control in Continuous Combustion Engines", 15th Combustion (Int.) Symposium, 1169, 1974.

83) Kamo, R., et al, "Recirculation and Fuel-Air Mixing as related to Oil Burner Design", API Publication 1723, 1964.

84) Hazard, H., "Reduction of NO_x by EGR in a Compact Combustor", ASME Annual Meeting, Detroit, U.S.A., 1973.

85) Saxton, D.J. and Lane, E.R., "The Ventres Blue Flame Burner", API Research Conference Paper 61-10, 1961.

86) Reman, G.H., and Verkoren H., "A High Intensity Combustor for Liquid Fuels", Pergamon, 1964.

87) Cooper, P.W., and Marek, C.J., "Design of Blue Flame Burners utilising Vortex Flow or Attached-Jet Entrainment", API Publication 1723-A, 1965.

88) Torborg, R.H., and Janssen J.E., "Performance and Radiation Studies with The API Prototype Blue Flame Burner", API Conference Paper CP66-9, 1966.

89) Nagey, T.F., et al., "A Low Emission Gas Turbine Passenger Car?", Mech. Eng., 14, 1974.

90) Reeve, M., "The Clean Combustion of Oil", HIC 198, 1973.

91) Hedley, A.B., and Jackson, E.W., "The Influence of Recirculation in Combustion Processes", API Conference Paper CP66-8, 1966.

92) Wendt, J.L., et al, "Reduction of Sulphur Trioxide and Nitrogen Oxides by Secondary Fuel Injection", 14th Combustion (Int.) Symposium, 897, 1973.

93) Yamagashi, K., et al, "A Study of NO_x Emission Characteristics in Two Stage Combustion", 15th Combustion (Int.) Symposium, 1157, 1974.

94) Bolt, J.A., and Locklin, D.W., "Recent Developments in Oil Burners for Space Heating and Industrial Applications", 7th World Petroleum Congress, 119.

95) Myers, P.S., "Combustion Problems in Automotive Air Pollution", 14th Combustion (Int.) Symposium, 871, 1973.

96) Derwent, R.G., and Stewart, H.N.M.,"Atmospheric Environment",7,385,1973.

97) "Nationwide Air Pollutant Emission Trends 1940-70" U.S.A. E.P.A. Report No. AP116, 1973.

98) Beer, J.M., and Lee, K.B., 10th Combustion (Int.) Symposium, 1966.

99) Hammond, D.C., Jnr., and Mellor, A.M., "Analytical Calculations for the Performance and Pollutant Emissions of Gas Turbine Combustors", AIAA/SAE 7th Propulsion Joint Specialist Conference, AIAA Paper No. 71-711, 1971.

100) Roberts, R., et al., "An Analytical Model for NO_x Formation in a Gas Turbine Combustor", AIAA Journal, 10, 820, 1972.

101) Edelman, R., and Economos, C., AIAA Paper No. 71-714, 1971.

102) Anasoulis, R.F., et al, "Development of a Combustor Flow Analysis, Part 1: Theoretical Studies", Report No. AFAPL-TR-73-98.

103) DISA Technical Course 1C1 "Hot Wire Anemometry", Lecture Notes Volume, April, 1974.

104) Swithenbank, J. et al, "A Laser Diagnostic for the Measurement of Droplet and Particle Size Distribution", HIC 245, 1976.

105) Lengelle and Verdier, "Gas Sampling and Analysis in Combustion Phenomena", AGARD Report No. 168, 1973.

106) Halstead, C.J. and Munro, A.J.E., "The Sampling, Analysis and Study of the Nitrogen Oxides formed in Natural Gas/Air Flames", I.G.T./A.G.A. Conference, Chicago, U.S.A., 1971.

107) Sievert, R.M., "Hydrogen Interference in Chemiluminescent NO_x Analysers", Comb. and Flame, 25, 273, 1975.

108) Zwolinski, J.B., "Selected Values of Properties of Hydrocarbons and Related Compounds", API Project 44, 1952.

109) Souders, M., et al, "Entropy and Heat of Formation of Hydrocarbon Vapours", Ind.Eng.Chem., 41, 1048, 1949.

110) McBride, B.J. et al, "Thermodynamic Properties to 6000 K for 210 Substances involving the first 18 elements", NASA Report No. SP-3001, Lewis Research Centre, U.S.A., 1963.

111) Perry, R.H., "Chemical Engineers Handbook", McGraw Hill, 1950.

112) McAdams, W.H., "Heat Transmission", McGraw Hill.

113) Andersen, O.K., "Time Resolution Power in Correlation Measurements with DISA Type 55A01 Hot Wire and Hot Film Anemometers", DISA Information.

114) Andersen, O.K., "On the Distortion of Measured Correlation Functions - Caused by the Frequency Response of the Measuring System", DISA Information No. 3, 21, 1966.

115) Osgerby, I.T., "An Efficient Numerical Method for Stirred Reactor Calculations", AEDC Report No. TR-72-164.

116) Burdett, N., Private Communication, 1975.

117) Spiers, H.M., "Technical Data on Fuel", 6th Edition, The British National Committee World Power Conference, 1962.

118) Hastings, C.Jnr.,"Approximations for Digital Computers", Princeton University Press, U.S.A., 255, 1955.

119) Tipler, W., "The Measurement and Significance of Fuel Spray Momentum", Shell Technical Report No. APD 202/62M, 1962.

120) Wise, H., et al, 5th Combustion (Int.) Symposium, 132, 1955.

121) Misic, D., and Thodos, G., Journal Chem.Eng. Data, 8, 540, 1963.

122) Mon, G., and Ping Pao H., "Two dimensional, incompressible, Turbulent Curved Wall Jets", H. Diamond Labs., U.S.A.

123) Burgess, G., Robson, P. & Wells, G., Private Communication, Aug., 1975.

124) Bradshaw, P., "An Introduction to Turbulence and its Measurement", Pergamon Press.

125) Coates, M., "Chemical Synthesis in a Turbulent Plasma Reactor", Ph.D. Thesis, Sheffield University, 1971.